Optimisation of the ozone pre-treatment of agricultural residues and conversion to platform chemicals.

by

Hafsat Hussaini Ibrahim

A thesis submitted to Newcastle University for the Degree of Doctor of Philosophy

School of Engineering

Newcastle University

United Kingdom

July 2022

Abstract

Biomass in the form of agricultural residues offers clear potential for conversion into energy, especially the use of processing residues such as corn cob and rice husk etc, due to their abundance/availability and high carbohydrate content. Depending on the conversion process, pre-treatment allows easier access to the carbohydrate components (cellulose and hemicellulose) for conversion to advanced generation biofuels and platform chemicals such as 5-hydroxymethyl furfural, furfural etc. leaving lignin as a low-value residue which is often burnt to provide parasitic energy for the conversion process. The conversion of lignin into high-value platform chemicals will increase the profitability and sustainability of the biorefinery process. However, to achieve complete utilisation of the lignin, it must be of high purity and lack extensive modifications. Ozone pre-treatment is recently gaining attention as a promising green alternative for cellulose isolation. However, the drawback of using ozone for large-scale industrial applications is the high costs for generating ozone *in-situ* as it cannot be stored due to its short lifetime and high reactivity.

This study aims to pre-treat and fractionate the agricultural processing residues (corn cob and spelt husk) and convert the carbohydrate components to chemical platforms (5-hydroxymethyl furfural and furfural) that can be used in several applications i.e medicines, diesel, fuel additives and plastics.

The first stage of this study developed an energy-efficient surface two-zone plasma ozone generator consisting of two stainless-steel mesh electrodes and a dielectric of quartz glass. The design offered good temperature control, which produced 2.5 times higher concentration and quantity of ozone at the same power input than a conventional single-zone plasma reactor. A maximum ozone concentration of 140g m^{-3} and 90g $(kWh)^{-1}$ productivity was obtained from the two-zone system, comparable to commercial ozone generators but with 30 – 40% lower power consumption (11kWh kg^{-1} O_3). Hence mitigating the drawbacks with the use of ozone in industrial applications caused by large energy demand.

Optimisation of the ozone pre-treatment process was achieved by incorporating ultrasound which enhanced lignin separation by 38.5%. Following organosolv fractionation at low temperature (80ºC), about 90% and 94% of lignin with high purity (95%) were recovered for corn cob and spelt husk respectively with guaiacyl-syringyl lignin the major fraction from corn cob and guaiacyl lignin from spelt husk. In addition, 84 - 85% cellulose was recovered with

78% purity. The recovered cellulose had its crystallinity decreased by 19% and its degree of polymerisation (DP) decreased by 17%.

In a microwave reactor, corn cob and spelt husk (untreated and pre-treated) were reacted in a DMSO-H_2O media to produce HMF and furfural. HMF and furfural yields of untreated corn cob were higher than those from spelt husk due to a difference in their morphology with increased porosity of corn cob allowing easy access to cellulose. Pre-treatment led to a 58% and 74% increase in HMF yield for corn cob and spelt husk respectively, while a 10% and 66.7% increase in furfural. Reacting fractionated cellulose from corn cob and spelt husk yielded a similar HMF yield of 40mg g^{-1} irrespective of the feedstock used. Overall, HMF and furfural yields were influenced by changes in cellulose properties following pre-treatment such as fibre size, increased surface area, decrease in the degree of polymerisation and decrease in lignin content following lignocellulose pre-treatment.

The economic efficiency and competitiveness of the conversion process for large scale co-production of HMF, furfural and lignin from spelt husk was determined. The proposed approach was compared with process where HMF and furfural were co-produced without lignin. Co-production with lignin yielded a profit of $213,657 higher than without lignin for a plant size of 100 tonnes per day of spelt husk due to extra revenue obtained from lignin sales, meaning fractionation of lignin had a positive effect on the process economics than its utilisation for heat or boiler fuel.

Thus, the improved pre-treatment and quality separation of biomass components enhanced downstream conversion to value-added products, thereby improving the sustainability and cost-effectiveness of the ozone pre-treatment process and conversion to HMF and furfural. In addition, the co-production of lignin will offset the cost of production of platform chemicals, thereby increasing the economics of a biorefinery.

Dedication

Dedicated to
My parents, Husband, Son, Daughter, Nephew and Siblings.

Acknowledgement

I would like to thank Allah for his grace and mercy in my life. My sincere gratitude goes to my supervisors: Dr. Anh Phan and Dr. Paul Bilsborrow for their extraordinary support, enthusiasm and guidance provided during this research project.

I would like to thank my sponsor, Petroleum Technology Development Fund (PTDF) Nigeria for their financial support without which this research would not have been possible.

Special thanks to the staff within School of Engineering especially Dr. Kui Zhang, Rob Dixon, Ashley Craig, Kevin Brown, and entire staff of mechanical workshop for their technical assistance in the laboratory and fabrication of equipment used in this study.

I wish to extend my sincere gratitude to my parents (Prof. H. D. Ibrahim and Hajiya Amina Ibrahim), mother-in-law (Hajiya Hassana Abdullahi), Husband (Abubakar), Son (Sultan Hussain), Daughter (Hawwa), Nephew (Yusuf Emaad), Sister (Aisha) and brothers (Ibrahim, Imraan and Abdullahi) for their patience, understanding, encouragement and unending support during my research.

Table of Contents

List of publications

1. Ibrahim, H. H., Bilsborrow, P. E. & Phan, A. N. (2021) Intensification of pre-treatment and fractionation of agricultural residues. *Chemical Engineering and Processing - Process Intensification,* 159**,** 108231.

2. Ibrahim, H. H., Bilsborrow, P. E., Phan, A. N. & Zhang, K. Energy efficient cold plasma ozone generator: development, characterisation, and application in cellulose hydrolysis. (Under review for publication by the journal of Chemical Engineering and Processing – Process Intensification).

External conference

1. Poster presentation at " 29^{th} European Biomass Conference and Exhibition (EUBCE), 2021 held in Marseille, France" titled "Ultrasound-assisted ozone pre-treatment and fractionation of residual lignin from Biomass to value added Products"

List of figures

List of tables

List of abbreviations

BET	Brunauer-Emmett-Teller (Surface area analysis)
CI	Crystallinity Index
DBD	Dielectric Barrier Discharge
DP	Degree of polymerisation
FTIR	Fourier Transform Infrared Spectroscopy
GC	Gas Chromatography
GVL	γ – valerolactone
HMF	5-Hydroxymethyl furfural
IL-1	1-(-4-sulfonic acid) butyl-3-methyl imidazolium.
LA	Levulinic acid
SEM	Scanning Electron Microscopy
[BMIM]Cl	1-Buthyl-3-methylimidazolium chloride
[EMIM]Cl	1-Ethyl-3-methylimidazolium chloride

Chapter 1: Introduction

1.1 Background

One of the key challenges of any nation is energy generation as rapid economic growth has led to increased demand for energy and platform chemicals (Makhubela and Darkwa, 2018). World energy consumption is expected to increase by 50% between 2005 and 2030 with demands rising from 11.4 billion tons of oil equivalent to 17.7 billion (World Energy Outlook, 2019). Currently, fossil fuels provide more than three-quarters of the world's energy (Fig 1.1) and about 90% of materials and chemicals (World Energy Outlook, 2020). This growth in demand, combined with depleting fossil fuel reserves, environmental pollution associated with the use of fossil fuels and price volatility necessitates the search for renewable alternatives to fossil fuels (Li et al., 2018)

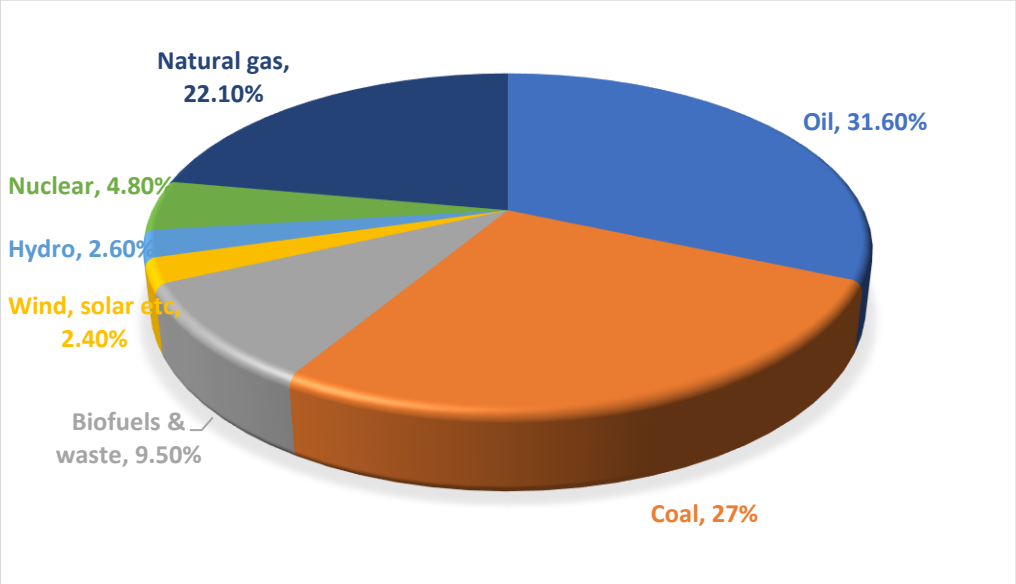

Fig 1.1: Total world energy consumption in 2020 (www.iea.org/statistics)

The utilisation of renewable sources of energy (biomass, solar, wind, geothermal, hydro and tidal) is increasing rapidly (~2.3% per year) globally to provide sustainable, cost-effective and environmentally friendly alternatives to fossil fuels (World Energy Outlook, 2019). Amongst these renewable sources, biomass is the only renewable source that has the potential to produce all forms of primary energy (transportation fuel, heat and electricity) and value-added chemicals, as it is the only carbon & hydrogen-rich source available on earth besides fossil fuels. To fulfil this growth in energy demand, it is important to have efficient and cost-effective technologies and pathways to produce energy and platform chemicals.

Biomass such as food crops (corn, sugarcane etc.) was projected to meet 30% of the growing energy demand but has a drawback as it requires large areas of arable land which in turn will lead to competition with food for the growing population (Demirbaş, 2001a). To overcome these drawbacks, the utilisation of waste from these food crops, forest residues and aquaculture (algae and seaweeds) need to be exploited to generate energy and chemicals as it is estimated to meet 14% of the total energy supply globally (World Bioenergy Association, 2019).

Lignocellulose biomass such as agricultural residues, wood and wood waste containing 10 – 25% lignin, 20 -30% hemicellulose and 40 – 50% cellulose (Brémond et al., 2018) are easily accessible renewable sources that are widely available throughout many regions of the world. Agricultural processing residues such as corn cob, cereal straw, spelt husk, sugarcane bagasse etc offer clear potential that avoids the development of extensive collection systems for these low-density high-volume feedstocks (Kumar et al., 2018).

The most rigid component of plant cell walls is lignin, which is a 3-dimensional cross-linked aromatic polymer that covers/protects cellulose and hemicellulose obstructing their biodegradation due to its resistance to chemical and enzymatic degradation (Travaini et al., 2016). Cellulose and hemicellulose obtained from biomass can be hydrolysed with catalysts (homogenous or heterogeneous) to form sugars that can further be processed into chemical platforms such as furfural and 5-hydroxymethyl furfural (HMF) (Fig 1.2) (Taherzadeh and Karimi, 2008).

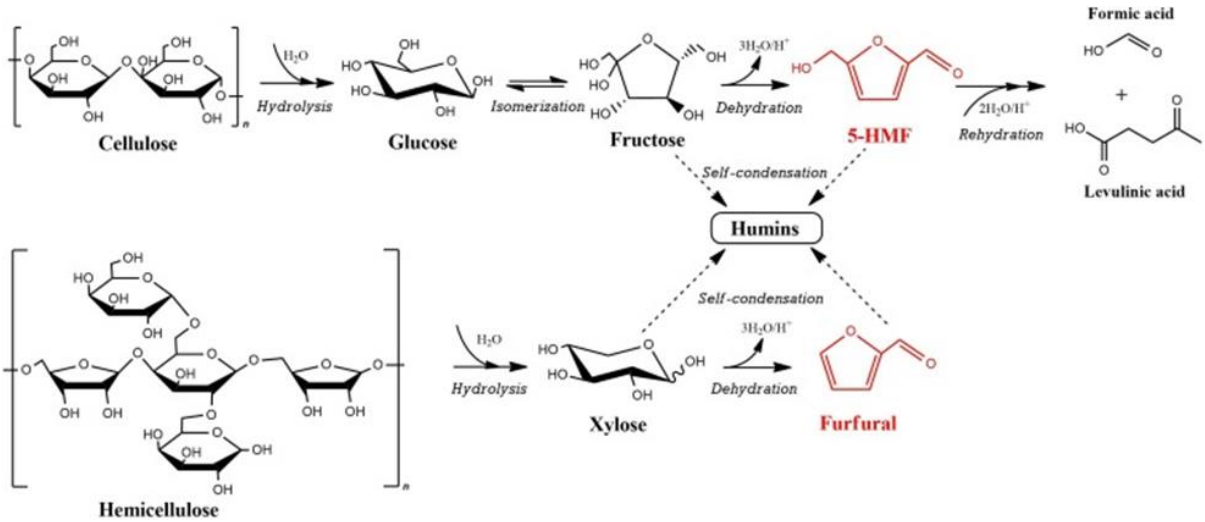

Fig 1.2: Lignocellulose biomass conversion to HMF and Furfural (Slak et al., 2022).

Platform chemicals are chemical intermediates that are able to produce a broad range of derivatives with diverse final applications (Bomtempo et al., 2017). Currently, over around 80

vol% of crude oil processed is converted into energy and fuels, of which less than 20 vol% is used for bulk chemicals, polymers and pharmaceuticals (Strassberger et al., 2014), hence the need to explore this area.

Production of the top 10 platform chemicals (furfural, glutamic acid, HMF, itaconic acid, citric acid, xylitol, succinic acid, malic acid, 2,5 furan dicarboxylic acid and glycerol) listed by the US Department of Energy is necessary due to its potential to replace petroleum-based building blocks for polymer industries (plastics), fuel and speciality chemicals (Menegazzo et al., 2018). The global demand for plastics in 2011 was 280 metric tonnes, of which 70% are made of petro-based polyvinyl chloride (PVC), polyethylene terephthalate (PET) and polyolefins (Louwerse and Rothenberg, 2012). The major problem with these petroleum-based plastics is that they are non-biodegradable and recyclable making plastic waste management one of the biggest problems facing mankind (Zheng et al., 2005). Biobased plastics are emerging slowly and promising as they can be recycled to monomers by hydrolysis or thermal depolymerisation.

Amongst these top 10 chemicals, HMF (Fig 1.3) is referred to as the "sleeping giant" due to its broad versatility as it contains aldehyde and ketone functional groups and a furanic ring system which when broken down leads to the formation of 175 product derivatives as well as 20 different high-performance polymers (Lauren, 2017). For example, the substitution of polyethylene (used for food packaging and soft drink bottles) by HMF derived compounds will reduce health-related problems as it is toxin-free. The aldehyde group and hydroxyl methyl groups in HMF make it suitable for many chemical reactions such as esterification, dehydration, hydrolysis, and halogenation due to its potential in synthesising compounds such as medicines, diesel, fuel additives and plastics (Yu et al., 2017). Currently, the production of HMF depends on extracted sugar syrups from energy crops (sugarcane) as an alternative to fossil fuel sources (Kläusli, 2014), although this can have a significant effect on global food security. The first commercial-scale HMF plant was developed in Switzerland in 2014 by AVA Biochem (a subsidiary of AVALON industries) with a capacity of 300 tons yr^{-1} annual production of HMF from fructose (Thoma et al., 2020). In 2019, they announced the plan to scale up HMF production to 5000 – 10,000 tonnes yr^{-1} (Thoma et al., 2020) but to date, no large-scale commercial HMF plant is in operation due to the high price of HMF (\$6000 kg^{-1}) (Slak et al., 2022). As such, more sustainable, cost-effective and efficient commercial manufacturing is to target cheap biomass sources such as plant and agricultural wastes.

Furfural (Fig 1.3) has the potential to be transformed into almost 100 different chemicals that can be utilised as solvents, fuels, resins or lubricants (Dashtban et al., 2012). Furfural contains a heteroaromatic furan ring with an aldehyde functional group making it suitable for typical aldehyde reactions such as acetalisation, decarbonylation and reduction to alcohols to produce solvents such as furfuryl alcohol, resins, and nylon 6,6 (Mariscal et al., 2016). Current large-scale commercial production of furfural was developed by central Romana corporation located in the Dominican Republic with a capacity of 35,000 tons yr^{-1} obtained from sugarcane bagasse (Slak et al., 2022) and 20,000 tons yr^{-1} capacity produced in South Africa (Mariscal et al., 2016) . Furfural production is estimated to have a market value of 630 million EUR by 2024 with a plant capacity of 300,000 tons yr^{-1} using agricultural residues as feedstocks (Slak et al., 2022).

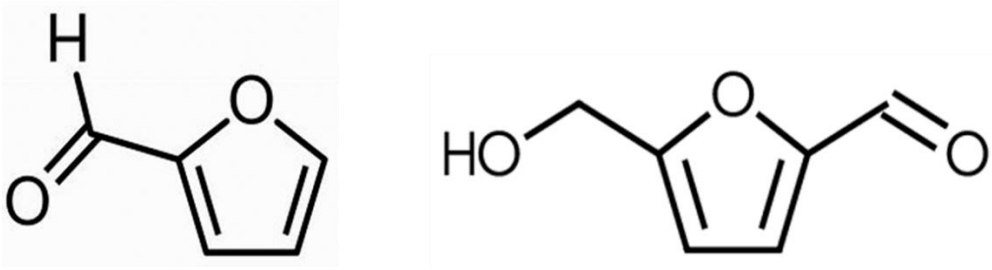

Furfural **5-hydroxymethyl Furfural (HMF)**

Fig 1.3: Chemical structure of furfural and HMF.

1.2 Project significance

Globally about 140 giga tonnes of biomass wastes are produced annually with 66% derived from cereal crops (wheat, rice, corn, oat, sorghum, barley) (Tripathi et al., 2019), of which 60% of these residues are produced in low-income countries (Smil, 1999) with about 517 Mt of cereal crop residue unexploited globally. Particularly in developing countries such as China, India and Africa, most agricultural residues are not utilised but burned in open fields producing particulate and smokes that affect people's health particularly the respiratory system or are allowed to decompose naturally, which promotes increased greenhouse gas emissions. Global cereal yield is predicted to increase by 0.9% per annum between 2007 and 2050 equating to a further increase of 1 billion tonnes of residue (Tripathi et al., 2019) hence making it a consistent by-product from agricultural production. Recycling these residues will play a vital role to reduce environmental problems. However, using them as feedstock for chemical and biological processes needs pre-treatment to disrupt the complex structure (lignin – carbohydrate complex)

and allow increased accessibility and easy conversion of the carbohydrate content to platform chemicals (Satari et al., 2019). The lignin-carbohydrate bonds create an obstacle to successful fractionation and selective isolation of individual components from lignocellulose biomass (Balakshin et al., 2011).

The main stages (Fig 1.4) involved in the conversion of lignocellulose biomass into platform chemicals are (i) lignin separation and hydrolysis of cellulose/hemicellulose into monomers (sugars) and ii) conversion of monomers in the presence of a catalyst(s) into chemical platforms.

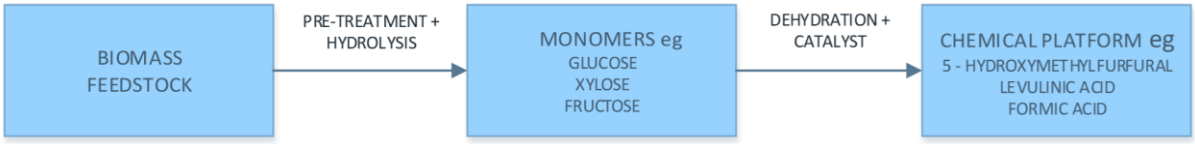

Fig 1.4: Stages involved in the conversion of biomass waste to platform chemicals.

Currently, most bio-refineries focus on exploitation of the carbohydrate portion of biomass to produce advanced generation biofuels e.g. cellulosic ethanol (Matsakas et al., 2019) and platform chemicals such as 5-hydroxymethyl furfural (HMF) and furfural (Zhang et al., 2017a). Lignin left as a residue is considered of low value and often burned as low-grade fuel or dumped as waste which causes environmental pollution (Yuan et al., 2013). Conversion of lignin into high-value chemicals that can be used to produce low-cost carbon fibres, thermoplastic elastomers, polymeric foams alongside the utilisation of carbohydrate counterparts for biofuel production is important to increase the profitability and sustainability of the bio-refinery process. However, to achieve complete utilisation of all biomass components to value added products, it is important that the lignin recovered is of high purity (Ragauskas et al., 2014) and to achieve this, it is necessary to isolate the lignin at an early stage i.e. pre-treatment to prevent irreversible adsorption of hydrolytic enzymes and lignin degradation (Saini et al., 2016).

Recovered lignin can be converted through oxidation, hydrocracking and hydrodealkylation to produce high value aromatics such as syringaldehyde, phenol and benzene which are valuable starting material for the petrochemical and pharmaceutical industries (Strassberger et al., 2014). Currently, 95% of phenol production occurs through partial oxidation of cumene (isopropylbenzene) through the Hock process. Phenols market price is between 800 – 1000 $

tonne^{-1} (Khanal et al., 2021), Producing it from lignin not only serve as substitute for fossil fuel sources but can generate more revenue for the biorefinery process.

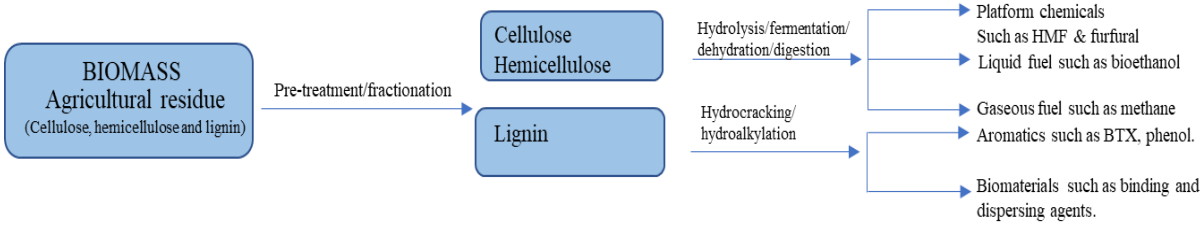

Fig 1.5: Biomass conversions to value added materials.

In addition, since pre-treatment is expected to disrupt biomass structure, it is important to understand how these changes affect the production of HMF and furfural. As pre-treatment is considered the most costly component of the biorefinery process representing up to 30% of production costs (Panneerselvam et al., 2013b), effective pre-treatment is required to reduce production costs and be able to compete with fossil fuel derived counterparts.

Ozone assisted pre-treatment has recently gained attention due to its high reactivity at ambient temperature and pressure without decomposing the cellulose and hemicellulose fractions. In addition, ozone is generated *in-situ* and can be easily broken down, therefore, eliminating further high-cost separation/purification steps resulting in a cost-effective and environmentally friendly process (Travaini et al., 2016). To date, ozone pre-treatment has largely focused on the conversion of the cellulose and hemicellulose fractions to biofuels, leaving lignin as a residue. However, only using hemicellulose/cellulose for ethanol or platform chemical production is not economic due to the high energy cost for the generation of ozone (Travaini et al., 2016). Therefore, integrating lignin valorisation with biofuel and platform chemical production is needed to increase the profitability and sustainability of the bio-refinery process.

The development and implementation of a biorefinery is important for the establishment of a biomass-based economy, whereby the co-production of platform chemicals and fuels will increase the profitability and sustainability of the process. Bio-industries can combine their material flow (residue from one bio-industry becomes a starting material for another) to achieve a complete utilisation of the biomass thereby creating opportunities for several small-scale businesses. Also, national reliance of many countries on imported fossil fuels will be reduced as biomass is readily available in many countries (Cherubini *et. al*, 2008).

1.3 Aim and Objectives

This research aims to convert agricultural residues into chemical platforms (HMF and furfural) via intensified ozone pre-treatment. This will be achieved through the following objectives:

1. Develop an energy-efficient ozone generator to reduce the costs associated with ozone generation.
2. Optimise the pre-treatment of agricultural residues (corn cob and spelt husk) using ozone coupled with ultrasound (sonication).
3. Fractionate and recover lignin as a co-product in the process.
4. Evaluate the effect of pre-treatment on cellulose structure and its effect on conversion yields to furfural and HMF.
5. Evaluate the techno-economic potential of the co-production of lignin, furfural and HMF.

1.4 Thesis layout

Chapter 1 provides background information about energy, biomass, platform chemicals as well as project significance followed by the aim and objectives of the project; **Chapter 2** provides a review of literature for ozone generation, ozone pre-treatment of biomass, HMF and furfural production from biomass; **Chapter 3** provides information regarding material and their sources, as well as a detailed description of the procedure and analytical instruments used; **Chapter 4** describes the design and characterisation of an energy-efficient two-zone plasma ozone generator; **Chapter 5** describes and compare the oxidative pre-treatment of agricultural residues (corn cob and spelt husk) as well as lignin fractionation and their effects on the structure of the fractionated components (lignin, holocellulose). **Chapter 6** describes the acid catalysed production of HMF and furfural as well as effects of changes on cellulose/biomass structure (caused by pre-treatment) on the yield of HMF and furfural; **Chapter 7** describes the techno-economic potential of the co-production process (lignin, HMF and furfural); **Chapter 8** provides a general discussion on the results obtained from this study and its relevance to industry and research community. Finally, **Chapter 9** gives a conclusion from the results obtained and recommendation for future work.

Chapter 2: Literature Review

2.1 Overview of lignocellulose biomass.

Lignocellulose biomass consists of waste and residues obtained from forest, agriculture, municipal solid waste, wood processing and paper waste which constitutes more than 60% of the total plant biomass (Arora et al., 2020). This abundantly available renewable resource serves as an alternative to petroleum resources for the production of biofuels, platform chemicals and polymers with the potential to negate the environmental and economic issues concerning the use of petrochemicals (Lucia, 2008).

Lignocellulose biomass offers a wide range of opportunities with the biorefinery concept with the potential to produce a variety of products such as transport fuels, polymers, platform chemicals and speciality chemicals (Mountraki et al., 2011). Biorefinery bears similar analogy to petroleum refining converting biomass into different range of products (Kokossis and Yang, 2010).

2.1.1 Cellulose

Cellulose, found in the cell wall of the upper part of plants (Medronho and Lindman, 2015) is a linear polymer consisting of β-D-glucopyranose units connected via β-(1-4) glycosidic bonds (Fig 2.1). Cellulose fibres are made up of 20 – 300 microfibrils connected by strong hydrogen bonds and Van der Waal forces (Medronho and Lindman, 2015). Hydrogen bonds inside the microfibrils are responsible for the linearity of the polymer, while hydrogen bonds between the microfibril chains are responsible for the crystallinity/amorphous structure of cellulose (Arora et al., 2020). Thus, cellulose is not regarded as a single crystal but rather a less structured collection of non-uniform crystalline fragments accompanied by amorphous parts laterally displaced (Himmel et al., 2007).

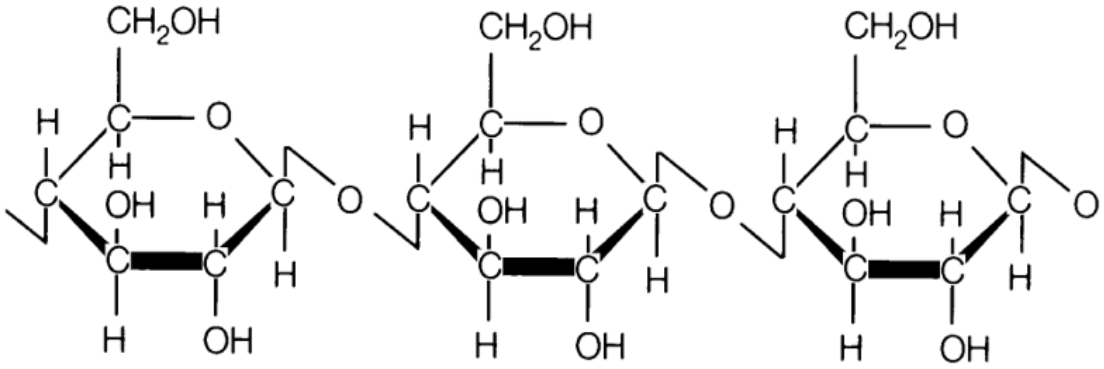

Fig 2.1: Structure of cellulose (Medronho and Lindman, 2015).

Cellulose is used as a substrate in the manufacture of biofuels and chemicals due to its high energy efficiency and low cost compared to other sources. Cellulose is utilised for biofuel and platform chemical production by breaking down its polymeric structure by enzymes or chemicals to monomeric sugars (glucose) before further conversion to the desired fuel (Medronho and Lindman, 2015). However, a key challenge with the utilisation of cellulose is its dissolution. Cellulose does not melt or dissolve in aqueous and common organic solvents due to its partial crystalline structure and a high degree of polymerisation (Kennedy and Hasamudin, 1995, Hudson and Cuculo, 1980).

2.1.2 Hemicellulose

Hemicellulose is a branched polymer of pentosan, hexosans and acetylated sugars. Hemicellulose (Fig 2.2) provide the major link between lignin and cellulose and are covalently linked to a phenolic residue (Takkellapati et al., 2018). Unlike cellulose, hemicellulose is amorphous with a low degree of polymerisation. In addition, its structure is more open due to considerable side branch groups, thus making it easier to hydrolyse than cellulose under mild reaction conditions (Arora et al., 2020).

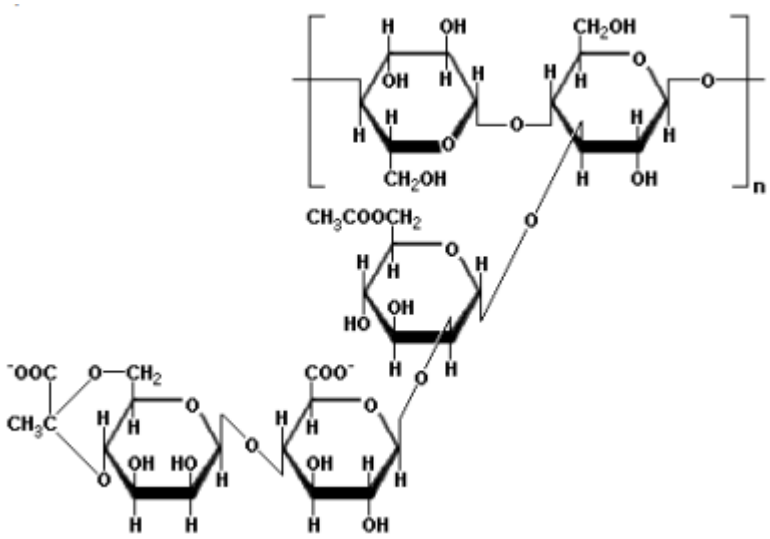

Fig 2.2: Structure of hemicellulose (Takkellapati et al., 2018).

2.1.3 Lignin

Lignin is the most abundant naturally existing aromatic, which constitutes a substantial portion of the cell wall of vascular plants providing rigidity to plants (Melro et al., 2018). Lignin (Fig 2.3) is a three-dimensional amorphous aromatic polymer formed by the polymerisation of three main precursors, i.e. sinapyl, coniferyl and coumaryl alcohols linked together by alkyl-alkyl, alkyl-aryl and aryl-aryl ether linkages (Arora et al., 2020). Each of these precursors gives rise to different lignin units such as P-hydroxyphenyl, guaiacyl and syringyl (Yuan et al., 2013).

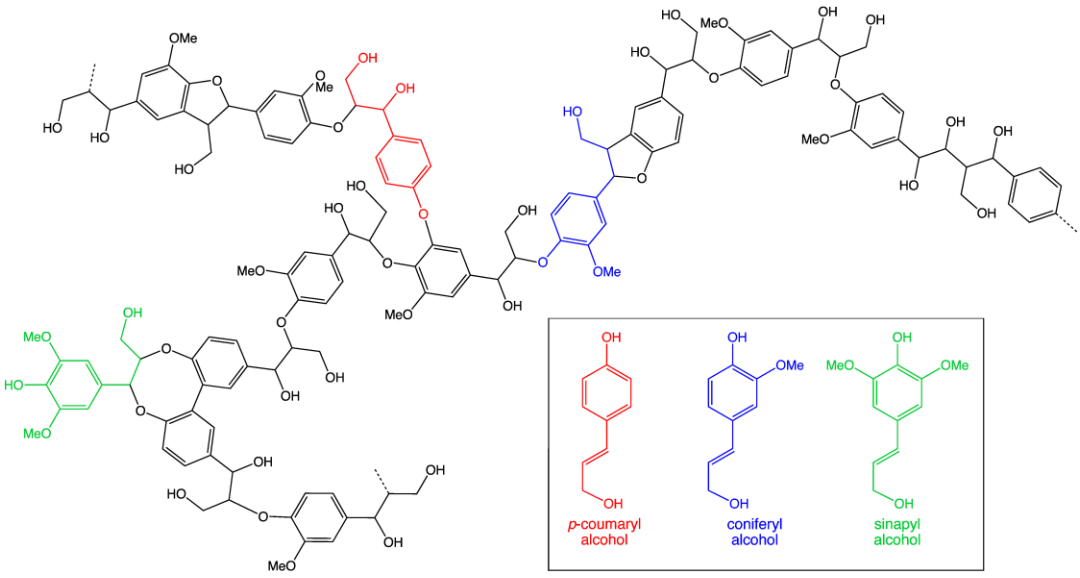

Fig 2.3: Three primary lignin precursors and lignin structural units (Yuan et al., 2013).

Lignin is commonly used for low value applications such as boiler fuel, dust suppressant, and cement additives (Lora, 2008, Strassberger et al., 2014) despite having advantages such as thermal stability, antioxidant activity and containing phenolic derivatives such as phenols, vanillin, guaiacol etc (Lucia, 2008, Bozell, 2010). However, its use is still minimal due to limited separation techniques, which result in low extraction yields, undesired chemical modification and extensive degradation (Tilman et al., 2006, Lucia, 2008).

Currently, in a biorefinery, cellulose and hemicellulose are the most utilised components to produce biofuels and platform chemicals due to their high carbohydrate content. However, these carbohydrates aren't easily accessible by chemicals and enzymes due to the lignin covering/protecting the carbohydrate fractions. Lignin limits cellulose hydrolysis in two ways: firstly, by forming a physical barrier that prevents chemical/enzyme access and secondly by non-productive binding to chemicals and enzymes (Pan et al., 2005). These limits must be overcome to explore biofuels and platform chemicals from lignocellulose materials economically and efficiently (Arora et al., 2020); hence often the requirement for a pre-treatment step.

2.2 Biomass pre-treatment

Pre-treatment of lignocellulose biomass disrupts lignin and the crystalline structure of cellulose making it easy for subsequent hydrolysis of cellulose into its respective monomers (glucose and fructose). Therefore, effective pre-treatment methods must maximise lignin removal, prevent loss of hemicellulose/cellulose fractions and limit the formation of by-products/inhibitors (Kumar et al., 2018).

There are various options available for the pre-treatment of biomass, such as physical, biological, chemical and physio-chemical. Physical pre-treatment such as ball milling, grinding, extrusion, and chipping are employed to increase the biomass's surface area, pore size, and decrease the crystallinity of cellulose. However, drawbacks are that the methods employed are high energy-consuming making it economically infeasible (Behera et al., 2014, Zhu et al., 2010).

Biological pre-treatment involves the addition of microorganisms such as fungi which produce enzymes that degrade lignin, hemicellulose, and cellulose. These methods seem promising due to the low energy requirements and environmental friendliness. However, prolonged incubation time (usually days) is needed for the fungi to degrade lignin completely and

substantial hemicellulose and cellulose loss remains a problem with this pre-treatment method (Zheng et al., 2014, Saritha et al., 2012, Behera et al., 2014).

Physio-chemical pre-treatment involves a combination of both physical and chemical processes. Some of the physio-chemical processes such as ammonia fibre explosion, CO_2 and steam explosion involve subjecting the biomass to very high temperature (160-270°C) and pressure (20-50 bar) for a period of time in the presence of ammonia, CO_2 or hot water, this leads to digestion of the lignocellulosic matrix due to shearing and autohydrolysis of the glycosidic bonds of lignin. However, drawbacks with this method are the high cost of equipment, high energy usage and volatile fatty acid production from the dissolution of lignin, hemicellulose and sugars (Chandra et al., 2007, Hendriks et al., 2009).

Chemical pre-treatment involves using chemicals such as acids, alkaline, ionic liquids and oxidising agents to cleave the lignin-carbohydrate linkages. Pre-treatment methods investigated by various researchers in recent times indicate that chemical pre-treatment is the most promising as it is conducted at low temperature and pressure, yields high delignification with a short pre-treatment time. Amongst these, ozone pre-treatment seems to be the most attractive in terms of lignin's selective degradation without affecting the biomass's cellulose and hemicellulose fractions (Travaini et al., 2016, Agbor et al., 2011, Elgharbawy et al., 2016).

Ozonolysis, ionic liquids, DES (deep eutectic solvent), steam explosion and organosolv methods are considered green pre-treatment methods. Green pre-treatment methods are defined as those methods that require a minimum amount of heating, pressure and chemical reagents to disrupt the structure of the lignocellulose biomass (Ab Rasid et al., 2021). Steam explosion and ionic liquids are relatively well established (especially where it has been widely investigated and used for cellulosic ethanol production) and has the highest number of recent publications in the literature between the years 2018–2021(Fig. 2.4) while ozonolysis and deep eutectic solvent are relatively new technologies in the pre-treatment of biomass and limited to a very few studies (Fig 2.4) (Ab Rasid et al., 2021). However, DES is shown as the most widely researched pre-treatment amongst the two with its effect on the structural changes in the lignocellulose biomass established (Pan et al., 2017) hence, it is not considered here.

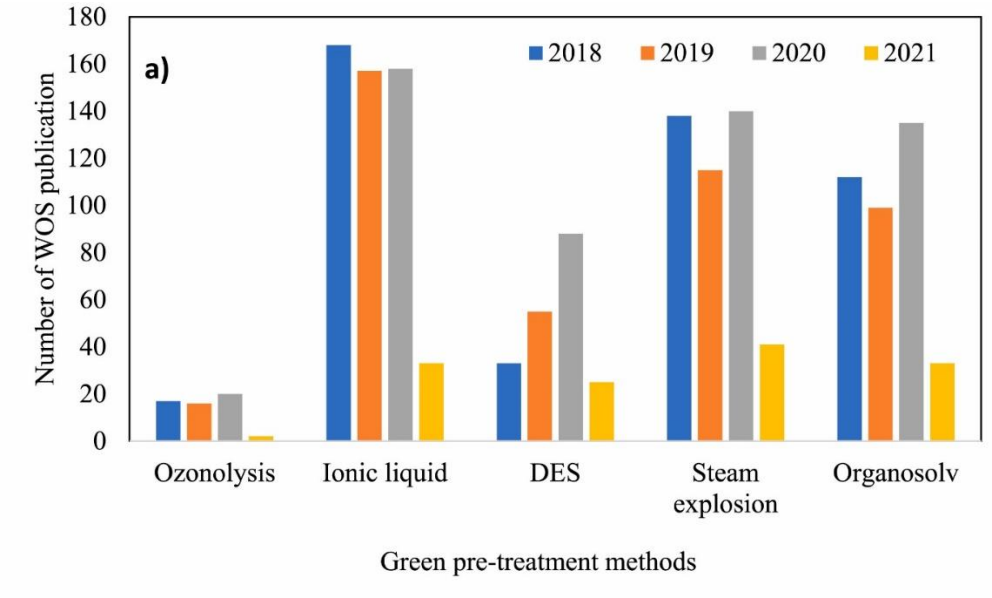

Fig 2.4: Recent publications of green pre-treatment methods for biomass derived from Web of Science (WOS) search engine (Ab Rasid et al., 2021).

2.3 Ozone pre-treatment.

2.3.1 Ozone generation

Ozone pre-treatment was first introduced in 1970 but has since been very much neglected due to the high costs of ozone generation (Ab Rasid et al., 2020). However, it is recently gaining attention due to recent developments for ozone generation via cold plasma technology. Ozone can be generated with 30% less energy via cold plasma technology compared to previous methods, thereby prompting a new wave of exploration for biomass pre-treatment (Schultz-Jensen et al., 2011a).

Currently, three techniques have generally been used to generate ozone, i.e. the electrolysis of water, the use of high energy sources such as UV light and electrical discharge between a dielectric barrier (cold plasma technology). However, due to the high investment costs for ozone generation, an efficient ozone generator needs to produce the highest ozone concentration with the smallest power consumption possible.

2.3.1.1 Ozone generation through electrolysis of water.

The electrolytic system consists of an anode and cathode separated by a solid polymer membrane. Water is fed into the anode side and it is dissociated at the interface between the

anode and the membrane by passing direct current splitting it into the two basic elements (oxygen and hydrogen) and then converting part of the liberated oxygen into ozone while the hydrogen ions migrate to the cathode (Fig 2.5). To produce as much as possible ozone, it is important that the anode has a potential difference above the decomposition and ozone reaction potential (Bruce, 2004). However, this method of ozone generator suffers drawbacks of high electrical consumption and the production of toxic chemicals (resulting from the precipitation of charged ions such as Ca^{2+} and Mg^{2+} present in water to hydroxides or carbonates) which are difficult to dispose of (Manning, 2000)

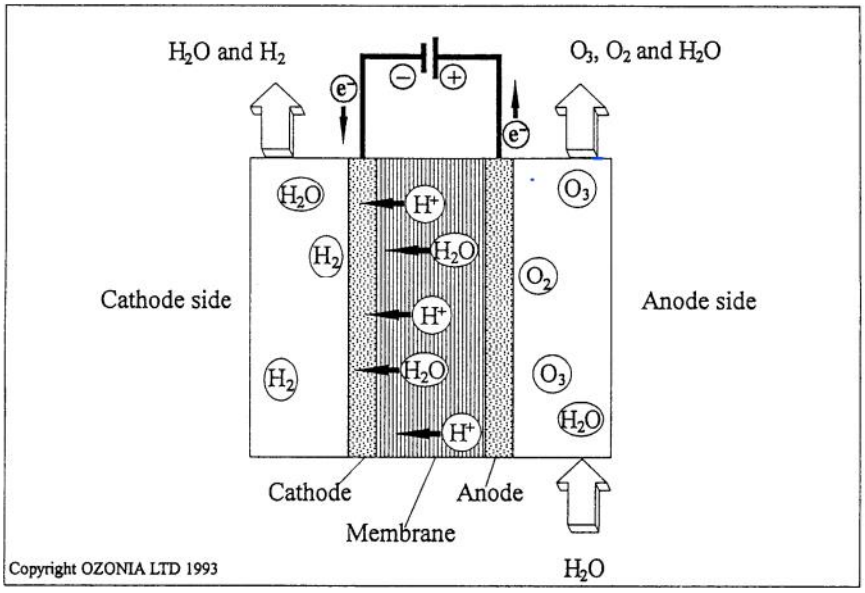

Fig 2.5: Ozone generation via the electrolysis of water (Bruce, 2004).

2.3.1.2 Ozone generation using Ultraviolet (UV) light.

Ultraviolet light is the light that has a higher frequency than visible light, i.e. a wavelength in the range of 100 – 380nm. Ozone is formed from the photo-dissociation of oxygen by a UV lamp creating valent oxygen atoms which then combine with oxygen to form ozone (Fig 2.6). The main advantage of this ozone generation method is that the system is cost-effective and simple to construct. However, drawbacks are that the resultant ozone is usually of low concentration which can't be used for large-scale commercial applications (Eliasson and Kogelschatz, 1991).

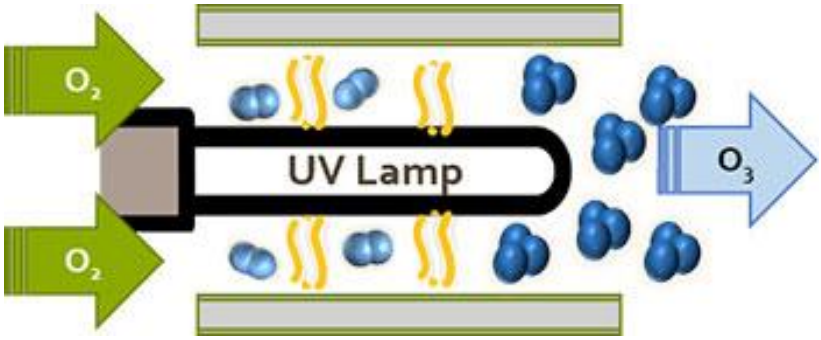

Fig 2.6: Ozone generation via ultraviolet light (Eliasson and Kogelschatz, 1991)

2.3.1.3 Ozone generation using dielectric barrier discharge

This ozone generation method involves using an electrical discharge between two electrodes with at least one dielectric barrier between them to convert oxygen to ozone. An AC voltage in the range of 10 – 30 kV (depending on reactor configuration) induces a displacement current which causes a high electric field outside the dielectric leading to an electrical discharge to occur (plasma field) causing ionisation of oxygen gas or air and recombination to form ozone (Ollegott et al., 2020). The function of the dielectric barrier is to limit the flow of current from one electrode to the other. The dielectric materials used are mainly glass, quartz, ceramics and polymers (Ollegott et al., 2020).

Amongst the three-techniques used, the dielectric barrier discharge (DBD) method is considered the most efficient method suitable for large-scale commercial applications as it produces a high concentration of ozone with no toxic chemicals (Pekárek, 2012, Jenei et al., 2007). Different DBD designs and geometries have been reported in the literature, but all have similar characteristics with two electrodes connected to a high AC generator and separated by at least one layer of a dielectric material (Siemens, 1857, Pekárek, 2012). Two main categories exist (volume and surface DBD) depending on the configuration of the set-up.

Volume dielectric barrier discharge

The volume DBD involves two electrodes arranged in parallel or coaxial with one of the electrodes covered by the dielectric (Fig 2.7). The discharge occurs between the dielectric and ground electrode. The cylindrical setup is usually used for industrial-scale ozone generation for applications such as waste-water treatment and air disinfection (Miao and Yun, 2011). Boonduang et al. (2012) developed a cylinder-cylinder volume DBD ozone generator with a

glass dielectric which generated a maximum ozone yield of 14 g h^{-1} and ozone concentration of 80 g m^{-3} at an oxygen flow rate of 12L min^{-1} consuming 480w of power.

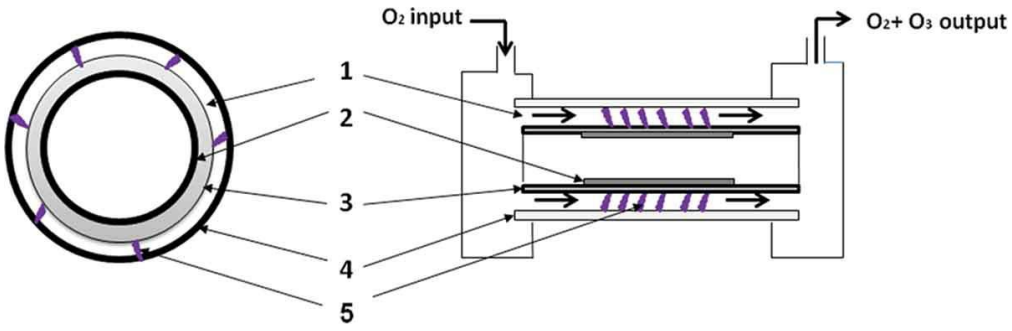

Fig 2.7: Volume DBD including the following components; (1) Discharge gap, (2) HV mesh electrode, (3) Glass tube, (4) Ground electrode and (5) Plasma (Nassour et al., 2016).

Surface dielectric barrier discharge

Surface DBD involves two electrodes in contact with either side of the dielectric (Fig 2.8) (Nassour et al., 2016). The dielectric fills the gap between the electrodes and causes the discharge to only occur at the surface, changing the shape of the electric field lines, thus enhancing the electric field by reducing the voltage breakdown. Offerhaus et al., (2017) designed a surface DBD with two conducting metal grids on both sides of an Al_2O_3 plate (dielectric) and observed a homogenous plasma along the electrode for all tested conditions. Masuda et al., (1988) designed a surface DBD ozone generator using parallel strip-like electrodes with high purity alumina ceramic as a dielectric layer to produce a high ozone concentration of 100,000 ppm ozone from oxygen with an energy efficiency of 170g $(kWh)^{-1}$.

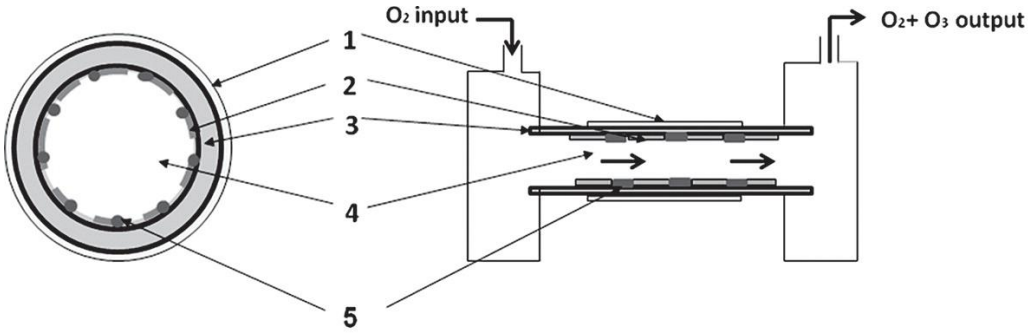

Fig 2.8: Surface DBD including the following components; (1) Ground electrode, (2) HV mesh electrode, (3) Glass tube (dielectric), (4) Gas flow and (5) Plasma (Nassour et al., 2016).

The surface DBD is gaining increasing attention due to its advantages over volume DBD with higher energy efficiency achieved from increased electron discharge due to contact between the two electrodes on either side of the dielectric (Li et al., 2018a). The surface DBD also has a free gas space where ozone can accumulate without being decomposed by its interaction with objects (Li et al., 2018a). Nassour et al., (2016) did a comparative study between volume and surface DBD reactors and found that the latter had 2.5 times higher ozone generation due to the formation of a more uniform density of micro-discharges. In addition, surface DBD was more energy efficient as the volume DBD consumed 40% more power (53W vs 38W) at 6kV. To enhance the local electric field, a parking material with high dielectric constant is normally used (Palma et al., 2020).

Packed bed dielectric barrier discharge reactor

The packed bed reactor is like the DBD (surface or volume) reactor with pellet/packing materials in the gap between the barrier and the electrode. The main characteristic of the packed bed reactor is the simultaneous occurrence of volume and surface plasma. Volume plasma happens between the voids of the pellets while the surface plasma happens on the surface of the pellets as well as the point of contact between the pellets and electrodes (Al-Abduly et al., 2020). The presence of the pellets provide turbulence to the flow of gas (oxygen or air) and increase contact with the plasma zone. In addition, the pellets can be catalysed to obtain a synergistic effect between plasma and catalyst hence improving the process efficiency. Liang Chen et al., (2006) observed a maximum ozone concentration, ozone production rate and energy yield of 61g m^{-3}, 3.7g h^{-1} and 173g $(kWh)^{-1}$ respectively for a packed bed reactor with Al_2O_3 (2mm diameter) as packing material and had about 12 times energy yield compared to DBD without packing material. Both ozonisers were constructed using stainless steel rod electrodes and a glass dielectric. However, a key drawback with the packed DBD reactor configuration is the heating up of the dielectric barrier during continuous use, leading to a decrease in ozone output and concentration due to ozone decomposition with increasing temperature in the reactor (Jodpimai et al., 2015). Hence, a cooling medium is needed to dissipate the energy.

2.4 Mechanism of ozone generation

Ozone is generated from the reaction between three oxygen atoms (Porto et al., 2020). Ozone is generated *in-situ* due to its highly reactive, unstable nature and is often generated using pure oxygen or air as feedstock. The use of air as feedstock is particularly favourable from an economic point of view as it is freely available (Eliasson and Kogelschatz, 1991). However, challenges occur with the use of air in the formation of NOx species which consume the oxygen needed for ozone generation and compete with oxygen for energetic electrons and hence lower the rate of oxygen dissociation leading to a low concentration of ozone produced (Al-Abduly et al., 2020). In addition, the concentration of ozone produced from air does not exceed 3% w/w due to the low oxygen content (21%) of dried air (Wang and Chen, 2013). Therefore, pure oxygen is the preferred feedstock for ozone generation due to the absence of side reactions caused by the presence of nitrogen hence leading to a higher concentration of ozone produced (Eliasson and Kogelschatz, 1991).

Ozone generation from pure oxygen involves the reaction of oxygen species with high energy electrons in a plasma field. Collisions between the electrons and oxygen molecules split the oxygen into oxygen atoms (O (^{3}P) and O (^{1}D)) where ^{3}P and ^{1}D represent ground and excited states respectively (Equation 2.1 & 2.2). One oxygen atom (either O (^{3}P) or O (^{1}D)) then recombines with an oxygen molecule in a three-body collision reaction to form ozone where M= O, O_2, O_3 and neutrals (Equation 2.3 & 2.4) (Chen et al., 2008)

$$e + O_2 \longrightarrow O(^3P) + O(^3P) + e \qquad \text{Equation 2.1}$$

$$e + O_2 \longrightarrow O(^3P) + O(^1D) + e \qquad \text{Equation 2.2}$$

$$O(^3P) + O_2 + M \longrightarrow O_3 + M \qquad \text{Equation 2.3}$$

$$O(^1D) + O_2 + M \longrightarrow O_3 + M \qquad \text{Equation 2.4}$$

However, the reverse reaction of ozone formation occurs simultaneously leading to decomposition of ozone (Equation 2.5). Equation (2.5) is an exothermic process and increase in the reactor temperatures (>25^{o}C) arising from heat generated during the collision of electrons with oxygen molecules and ozone formation results in the conversion of unstable ozone back to oxygen (Chen et al., 2008).

$$O_3 + M \longrightarrow O + O_2 + M \qquad \text{Equation 2.5}$$

Furthermore, increased concentration of oxygen radical can lead to decomposition of ozone converting it oxygen (Equation 2.6). This happens when the relative concentration of O/O_2 is higher than 0.3 – 0.5% (Eliasson and Kogelschatz, 1991).

$$O + O_3 \longrightarrow 2O_2 \qquad \text{Equation 2.6}$$

Ozone is used for several industrial applications such as disinfection (Morrison et al., 2021), food processing (Pandiselvam et al., 2017), bleaching of paper pulp, waste-water treatment (Perkowski et al., 1996) etc. However, its application for biomass pre-treatment has been limited to only a few studies (Sulfahri et al., 2020). Hence, the focus of this thesis is on the application of ozone for biomass pre-treatment.

2.5 Ozone for biomass pre-treatment

Ozone is a strong oxidising agent produced *in-situ* from oxygen or air (Baig et al., 2015) which has gained attention as a pre-treatment method to selectively remove lignin (electron-deficient ozone attacks electron-rich lignin) from lignocellulose material at ambient temperature and pressure without degrading the cellulose and hemicellulose fractions. Furthermore, ozone can be easily decomposed, eliminating separation/purification steps resulting in a cost-effective and environmentally friendly process (Travaini et al., 2016).

Ozone has been used to pre-treat various biomass feedstocks such as cereal straw, wood pulp, sugarcane bagasse, cotton stalk, energy grass, sawdust etc. (Ben'ko et al., 2013, Panneerselvam et al., 2013, Li et al., 2015, García-Cubero et al., 2009). Up to 60% lignin was removed from wheat straw at 95% moisture content using ozone treatment at an oxygen flow rate of 1L min^{-1} for 25 hours (Binder et al., 1980) and 75% glucose was obtained via enzymatic hydrolysis. However, the process was considered impractical due to the long reaction time and lignin and cellulose were found to oxidise concurrently during pre-treatment. Similarly, Schultz-Jensen et al., (2013) obtained 60% delignification from ozone pre-treated wheat straw with 50% moisture content at an oxygen flow rate of 0.01 Ls^{-1} at a much shorter reaction time of 60 min and observed that ozone did not oxidise the cellulose fraction. They concluded that oxidation of cellulose in the work of Binder et al., (1980) was probably due to the formation of carboxylic acid arising from the oxidation of lignin following the longer pre-treatment time (25 hours) which in turn degraded some of the carbohydrates i.e. cellulose and hemi-cellulose. The longer reaction time was probably due to the high moisture content (95%) of the wheat straw.

Kaur et al., (2012) obtained 42% lignin reduction and 53% glucose yield when cotton stalk was ozone pre-treated at an oxygen flow rate of 0.37 L min^{-1} for 150 min, compared to 46.6% lignin reduction and 56% glucose yield when the cotton stalk was pre-treated with 4% NaOH for 60 min at 121°C. It was suggested that NaOH pre-treatment increased porosity through swelling of the biomass coupled with saponification of inter-molecular ester bonds of lignin.

Panneerselvam et al., (2013a) pre-treated four energy grasses with ozone at an oxygen flow rate of 0.25 L min^{-1} for 2 hours and observed 59.9% lignin reduction with little impact on cellulose. In addition, there was no enhanced sugar yield of the ozone pre-treated samples during enzyme hydrolysis due to enzyme inhibition caused by degradation products. However, many researchers have widely reported that ozone pre-treatment does not produce inhibitory compounds, which concluded that degradation products obtained from ozone pre-treatment depend on the type of biomass and its interaction with ozone (Quesada et al., 1999, Schultz-Jensen et al., 2011, Travaini et al., 2013).

Up to 66% decrease in acid-insoluble lignin with 92% recovery of cellulose and xylan was obtained when sugarcane bagasse was ozone pre-treated at an air flow rate of 1L min^{-1} for 1 hour (Travaini et al., 2013). In addition, they observed that an increase in ozone concentration from 3.07% to 3.44% decreased ozonation time from 195min to 120 min. Ozone concentration affected the reaction rate, influencing the type and concentration of oxidants available for reactions in the aqueous phase. Thus, a higher ozone concentration increases the concentration of oxidants available for reaction with lignin and therefore the speed of the reaction.

2.5.1 Factors affecting ozone efficiency

Various authors have reported that ozone pre-treatment efficiency depends on several factors such as reactor design, moisture content, particle size, time, ozone concentration and ozone/air flow rate (Travaini et al., 2016, Baig et al., 2015, Neely, 1984).

2.5.1.1 Reactor design

This is one of the essential parameters in ozonolysis as it provides information on the ozone concentration profile, which influences ozone consumption. A suitable reactor should provide maximum contact between ozone and the substrate for the oxidation reactions (Vidal and Molinier, 1988). Different reactor design options such as fixed-bed, batch, rotatory, drechsel trap, cylindrical, multi-layer fixed-bed and bubble-column have been used for various studies.

At the same oxygen flow rate of 1 L min^{-1}, up to 50% delignification of wheat straw was obtained after 5 hours in a batch reactor (Binder et al., 1980) whereas 34% delignification was obtained in a fixed-bed reactor (García-Cubero et al., 2009). The fixed-bed reaction consumed 100% ozone whereas the batch reactor only consumed 30% of the ozone fed in due to insufficient ozone contact with the substrate. About 66% lignin degradation was obtained when Vidal and Molinier, (1988) ozone pre-treated sawdust in a fixed-bed reactor at an oxygen flow rate of 1 L min^{-1} and electrical power supply of 33kV (ozone production of 65 mg L^{-1}) for 2 hours compared to 22.5% reduction in a semi-batch reactor. This is because fixed- bed reactors provide effective contact between ozone and the substrate due to multiple gas (ozone) inlets in the reactor (reactor configuration).

Cesaro and Belgiorno, (2013), ozonised municipal solid waste at an air flow rate of 10 L min^{-1} for 120 min in a drechsel trap and bubble column reactor. The bubble column reactor was found to be more effective as a higher amount of ozone (0.7g min^{-1}) reacted with the substrate and a smaller amount of ozone was left in the reactor due to effective contact between the oxidant and substrate compared to (0.2 g min^{-1}) in a drechsel trap reactor. Most recently, Shamjuddin et al., (2021) developed a diffusion-reaction model of empty fruit bunch inside a well-mixed novel Ribbon mixer reactor (QzBIONY) and obtained 78% delignification due to enhanced contact between the substrate and ozone achieved in the reactor.

2.5.1.2 Moisture content

Moisture content of biomass acts as a transport medium in ozonolysis, transferring ozone from the gas phase into solid biomass pores via free water-bonded water-biomass (Choi et al., 2002, Li et al., 2015a). However, the optimal moisture content (saturation point of biomass) depends upon the nature of the biomass (Neely, 1984). At a moisture content below the saturation point of the biomass, ozone mass transfer is limited and cannot react with all of the biomass substrate. On the other hand, at moisture contents above the saturation point, a thick film of water blocks the biomass pores leading to large residence time of ozone which enhances ozone decomposition into hydroxy radicals leading to excessive ozone consumption as the reaction favours other non-selective pathways (Mamleeva et al., 2009, Vidal and Molinier, 1988).

Souza-Corrêa et al., (2013) ozonised sugarcane bagasse at different moisture contents (10%, 25%, 50% and 75% w/w) at an oxygen flow rate of 0.6 L min^{-1} for 6 hours and observed that 80% lignin was removed at 50% moisture content compared to 45% and 50% delignification obtained at 10% and 75% moisture content respectively with no change in cellulose content.

Similarly, Travaini et al., (2013) achieved 66.8% lignin removal from sugarcane bagasse at 40% moisture content whereas only 9.6% delignification was obtained at 80% moisture content. From these findings, it can be concluded that water protects lignin from the oxidation reaction with ozone resulting in low delignification.

It was reported by Ben'ko et al., (2013) that the optimum moisture content for agricultural residue is higher than that of wood due to their ability to bond water. Neely, (1984) found the optimum moisture content for ozone pre-treatment of red oak sawdust to be 25-35%, 40-50% for Japanese cedar (Sugimoto et al., 2009) and 20-40% for wood meal (*Quercus serrata*) (Ueda et al., 2014).

2.5.1.3 Particle size

The particle size of biomass is important because the ozone pre-treatment process is a surface reaction (Shi et al., 2015). An optimum particle size needs to be determined because mechanical pre-treatment will increase the process costs. For particle sizes above 2mm, ozone consumption is decreased due to a reduced surface area, leading to low delignification (Schultz-Jensen et al., 2013). Reducing particle size from 2mm to 0.08mm increased delignification efficiency of sugarcane bagasse but only from 75% to 80% (Souza-Corrêa et al., 2013). Neely, (1984) observed a four-fold reduction in reaction time when particle size was reduced from 1000 to 106 μm. However, Vidal and Molinier, (1988) observed no significant variation when working with particle sizes of 1 and 2mm for poplar sawdust which is likely due to the close similarity in sizes used. Hence, the effect of particle size on ozonolysis depends on the type of biomass feedstock and the moisture content.

2.5.1.4 pH

During ozonolysis, the pH decreases due to the formation of organic acids from degradation reactions. Lignin bonded to carbohydrates are favoured in alkaline media. However, pH > 4 causes ozone destruction and reactive species are generated that attack carbohydrates. García-Cubero et al., (2009) studied the ozone pre-treatment of wheat and rye straw in 20% sodium hydroxide solution in a fixed-bed reactor. Carbohydrate degradation and lower delignification (19.6% and 22.6%) for wheat and rye straw, respectively were observed due to the increased alkalinity of the medium. Yu et al., (2017) observed a higher delignification (14%) of green liquor of mixed wood chips when pre-treated at pH 2 than compared to a neutral medium.

2.5.1.5 Pre-treatment time, ozone consumption and oxygen/air flow rate.

Ozone consumption is directly dependent on the pre-treatment time, ozone concentration and oxygen/air flow rate. For all types of biomass, ozone consumption varies with reaction time in a similar way. At the start of pre-treatment, ozone consumption is fast due to the preferential reaction between ozone and lignin leading to highest delignification. After this time is a stabilisation period where ozone consumption quickly decreases and delignification increases only slowly (Binder et al., 1980, García-Cubero et al., 2009, Schultz-Jensen et al., 2013)

Ozone consumption increases with an increase in oxygen/air flow rate leading to reduced reaction time. This is due to excess ozone being available for reactions providing constant ozone concentrations in the reactor. Neely, (1984) obtained 60% delignification using an oxygen flow rate of 17 L min^{-1} for 10 min compared to 65% obtained at an oxygen flow rate of 0.5L min^{-1} for 90 min. Although working with a high flow rate (> 1L min^{-1}) was thought to be uneconomical as a higher amount of ozone is generated and consumed, making the process expensive. Also, more side reactions occur as more ozone is available to react with the already degraded lignin and carbohydrate fractions (Neely, 1984, Schultz-Jensen et al., 2011b).

Table 2.1: Summary of studies from the literature on ozone pre-treatment of biomass.

Biomass feedstock	**Reactor design**	**Moisture content (%)**	**Flow rate (Lh^{-1})**	**Particle size (mm)**	**Ozone concentra-tion (%)**	**Time (h)**	**Delignifi-cation (%)**	**Reference**
Empty fruit bunch	Ribbon mixer	40	2	0.3	4.65	1	78	Shamjuddin et al., 2021
Sugarcane bagasse	Glass columns	50	N/a	3	N/a	1	25	Perrone et al., 2021
Aspen woodchip	Fixed-bed	40	0.167	0.6 - 1	2.8	1.67	-	Ben'ko et al., 2013
Wheat straw	Batch	95	1	<0.2	0.44	5	50	Binder et al., 1980
	Fixed-bed	50	1	3 -5	2.7	2.5	34	García-Cubero et al., 2009
	Fixed-bed	40	0.6	1	0.6	3	60	Schultz-Jensen et al., 2013
Rye straw	Fixed-bed	60	1	3 - 5	2.7	2.5	45	García-Cubero et al., 2009
Cotton stalk	Fixed-bed	35	0.37	2	2.1	2.5	42.3	Kaur et al., 2012
Maize stover	Fixed-bed	60	1	<0.053	2.8	1	78	Li et al., 2015a
Sugarcane bagasse	Fixed-bed	40	1	3 - 5	3.44	1	66.8	Travaini et al., 2013
	Batch	50	0.6	0.08	-	6	80	Souza-Corrêa et al., 2013
Energy grass	Fixed-bed	30	0.25	<2	1.9	2	59.9	Panneerselvam et al., 2013b

Coastal bermuda grass	Rotary	30	1	<2	25	1	31	Lee et al., 2010
Red oak	Cylindrical	50	0.5	0.106	3.37	2	60	Neely, 1984
Poplar sawdust	Semi-batch	75	1	2	1.63	2	22.5	Vidal and Molinier, 1988
	Fixed-bed	75	1	2	1.63	2	66.6	
Spent culture media	Rotary	40	0.05	<5	6	1	47	Ueda et al., 2014

2.6 Production of 5-hydroxymethyl furfural (HMF)

The production of HMF from cellulose based renewable sources has attracted increasing attention due to the depletion of fossil fuel reserves (Lynd and Wang, 2003). Production of HMF (Table 2.2) from cellulose is challenging due to its crystal structure and industrial application of HMF is limited due to the high costs of production. Therefore, to efficiently utilise the industrial application of HMF, a high yielding and low energy process needs to be developed (Zhang et al., 2017).

The yield of HMF from cellulose largely depends on the catalyst and reaction media used. Cellulose is converted to HMF through a series of chemical reactions. Firstly, cellulose is depolymerised and hydrolysed to glucose, then the glucose is isomerised to fructose and finally, the fructose undergoes dehydration to produce HMF (Zhang et al., 2016) (Fig 2.9).

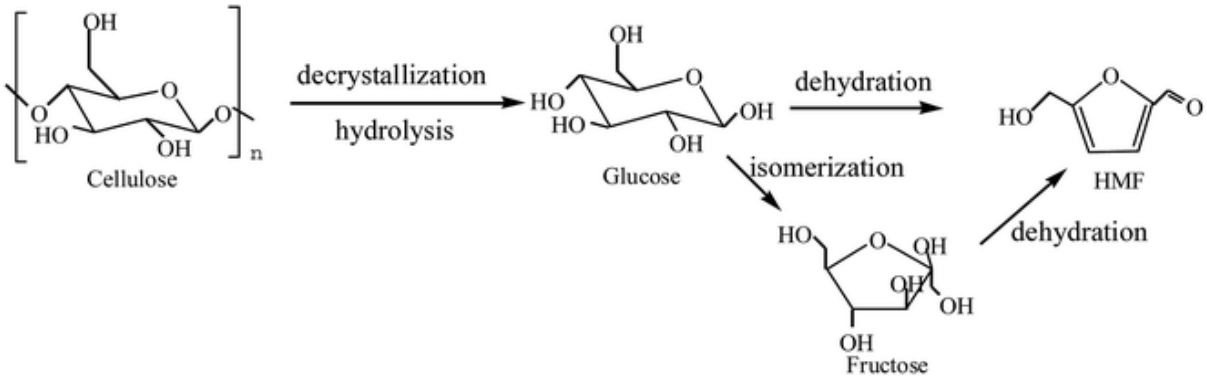

Fig 2.9: Schematic conversion of cellulose to HMF (Zhang et al., 2016)

2.6.1 Catalysts

Catalysts play a major role in the yield and selectivity of HMF produced. Catalyst active sites, pore size and surface area determine the selectivity towards HMF (De et al., 2011). All the studies described below used conventional mode of heating such as oil bath and hot plates. Up to 33% HMF yield from glucose was achieved in the presence of a Bronsted acid catalyst (Amberlyst-70) compared to only 8% without catalyst (Morales et al., 2014). Jia et al., (2014) achieved HMF yield of 67% from fructose at 130°C in DMSO without the addition of a catalyst while Wang et. al, (2011) achieved a higher yield of 90% HMF in the presence of Glu-TsOH catalyst (carbon-based acid) under similar conditions.

Bronsted acid catalysts such as HCl, H_2SO_4, glycolic acid, salicylic acid etc have been used due to their low cost and easy accessibility, with 20.7% HMF obtained from cellulose in water and HCl as catalyst at 300°C for 30 min and 2.1% HMF obtained with maleic acid as catalyst

and glucose in water at 140°C for 24 min (Zhang et al., 2016). Although most of the studies done with Bronsted acids have utilised fructose as substrate.

Catalysts such as $CrCl_3$, $AlCl_3$, $ZnCl_2$, $CuCl_2$ have been used extensively to increase selective formation of HMF. The chloride ion in the metal-halide catalysts promotes isomerisation of glucose through the 1,2-hydride shift pathway and also increases the dehydration of fructose (Li et al., 2018c) while the metal forms a co-ordination complex with sugars (Wang et al., 2015a, Yu et al., 2017). The first validation that metal salt can catalyse HMF production from glucose was reported by Zhao et al., (2007), who found out that 70% HMF was obtained from glucose using $CrCl_2$ as catalyst in ionic liquid ([BMIM] Cl) solvent at 100°C for 3 hours. The authors observed that chromium catalyst was effective for converting glucose to HMF but inactive in converting cellulose to HMF.

Furong et al. (2010) used $FeCl_2$ as catalyst in 1-(4-sulfonic acid) butyl-3-methylimidazolium hydrogen sulphate (IL-1) to hydrolyse cellulose at 150°C for 5hours and obtained 33.81% yield of HMF and 5.93% Levulinic acid. Wei et al., (2011) used $IrCl_3$ as catalyst in [BMIM]Cl at 120°C for 30 min and obtained 89 % yield of HMF. In addition Su et al., (2009) combined $CrCl_2$ with other metal chlorides such as $CuCl_2$ and $FeCl_2$ and noted an increased HMF yield. They observed that reacting cellulose with a combined $CrCl_2$ and $CuCl_2$ catalyst in 1-ethyl-3-methylimidazolium chloride ([EMIM] Cl) at 120°C for 8 hours yielded 57.5% HMF.

The degradation of cellulose with metal halide catalyst in ionic liquid solvent provided a high HMF yield although catalyst recovery, utilisation and a long reaction time are still challenges to be overcome. As such, solid catalysts were used in studies to overcome the above drawbacks. Solid catalysts (bifunctional catalyst) with a combination of Lewis and Bronsted acid sites are reported to minimise by-products such as levulinic acids, humins, levoglucosan (Rout et al., 2016).

Otomo et al., (2015) reported 42% HMF yield (high for heterogenous reaction systems) from microcrystalline cellulose using β-zeolite as a catalyst in DMSO/THF at 180°C for 3 hours. It was observed that the catalytic performance increased with increasing pore size.

Nandiwale et al., (2014) converted microcrystalline cellulose over bimodal H-ZSM5 Zeolites in H_2O at 170°C for 4 hours and obtained 46% yield of HMF. However, the catalytic activity decreased with four runs due to its low hydrothermal stability. In the search for a heterogenous catalyst with high hydrothermal stability, Li et al., (2018b) achieved 53.3% HMF yield from microcrystalline cellulose at 170°C for 8hours using Nb/C catalyst in THF/H_2O.

2.6.2 Solvents

Apart from the catalyst, the yield of HMF is also affected by the type of solvent used. Solvents serve various roles during the conversion process: enhanced dissolution of substrate and catalyst, higher product yield through stabilisation of the substrate, intermediates and products, lastly, by acting as a catalyst to improve reaction kinetics. In addition, solvents increase the purity and ease of separation of HMF. Thus, they substantially impact the process both environmentally and economically (Yu et al., 2017). The recyclability and performance of a solvent depends on their partition co-efficient, boiling point and thermal stability (Saha and Abu-Omar, 2014).

Over the years, studies have focused on the use of organic solvents such as dimethyl sulfoxides (DMSO), Ionic Liquids (IL), N, N-dimethylformide (DMF), methyl isobutyl ketone (MIBK) and tetrahydrofuran (THF) as reaction media to produce HMF because of their high efficiency in the dissolution of cellulose due to their moderate polarity with no acidic hydrogen (Yu et. al, 2017).

Jia et al., (2014) achieved HMF yield of 67% from fructose at 130°C in DMSO without the addition of a catalyst while Morales et al., (2014) achieved a higher yield of 90% HMF in the presence of a Amberlyst-70 resin catalyst (having sulfonic acid sites) under similar conditions. This was achieved due to the preferential interaction of fructose to the sulfonyl oxygen of DMSO via hydrogen bonding. About 52% HMF yield was obtained from glucose in a THF/water mixture in the presence of $AlCl_3$ as catalyst at 120°C (Yang et al., 2012). Roman-Leshkov et al., (2006) obtained a 55% HMF yield from fructose in methyl isobutyl ketone (MIBK)/H_2O using HCl as catalyst. However, these organic solvents have limitations for large-scale use as the cost of separation from the HMF product is expensive due to their high boiling points.

Ionic liquids such as [BMIM]Cl and [C4MIM]Cl refer to salts in liquid state. They have been used extensively in converting cellulose to HMF by providing enhanced cellulose solubility by disrupting the polysaccharide macrostructure through hydrogen bonding. A yield of 40% HMF was achieved with cellulose in [BMIM]Cl with cellulose derived carbonaceous catalyst (CCC) at 160°C for 15 min. A yield of 70% HMF was obtained from glucose using $CrCl_2$ as catalyst in ionic liquid ([BMIM]Cl) solvent at 100°C for 3 hours. Also, ionic liquids have demonstrated a reduction in activation energy as 62% HMF was obtained from glucose at 100°C when compared to higher temperature (>120°C) used in most studies in a mixture of $[C_2OHmim]Cl$/MIBK with $CrCl_2$ for 2hrs (Siankevich et. al, 2016). However, the drawback of

using ionic liquids is the high price, toxicity, and difficulty in separating HMF due to their high viscosity and boiling point. To efficiently utilise these solvents, more research needs to be done to improve the product separation process.

For a more environmentally friendly process, water was considered as an alternative to organic solvents. Möller et al., (2013) obtained 12% HMF from microcrystalline cellulose (74% CI) using water at 270°C for 1hr without a catalyst. In the presence of $ZnCl_2$ at a temperature of 145°C, 20-32% HMF was obtained from fructose using water as the reaction medium (Zhu et al., 2005). A yield of 19% HMF was obtained when Seri et al., (2002) converted cellulose in water at 250°C with $LaCl_3$. These low HMF yields were reported to be due to rapid rehydration of HMF products in water to levulinic (LA) and formic acids (FA).

Another green solvent explored was γ-valerolactone (GVL), a biomass derived solvent which showed improved performance as a solvent compared to water. Zhang et al., (2017) observed 27.1% HMF from reacting untreated corn cob in GVL with SPTPA (acidic polymer catalyst) at 175°C for 60 min. A yield of up to 60% HMF was achieved when a GVL/water mixture was used as the solvent with $AlCl_3$ catalyst. Catalyst proton solvation in GVL made it more reactive than in water, thus providing faster hydrolysis of cellulose to glucose.

Different approaches have been used to minimise side reactions, such as biphasic systems in which water and water-immiscible organic solvents (e.g MIBK/H_2O, DMSO/H_2O) are used. Organic solvents continuously extract HMF from the aqueous phase (Fig 2.10) and as a result HMF yields improve as it is continuously separated from the aqueous phase thereby preventing rehydration reactions that lead to by-product formation (Yu and Tsang, 2017).

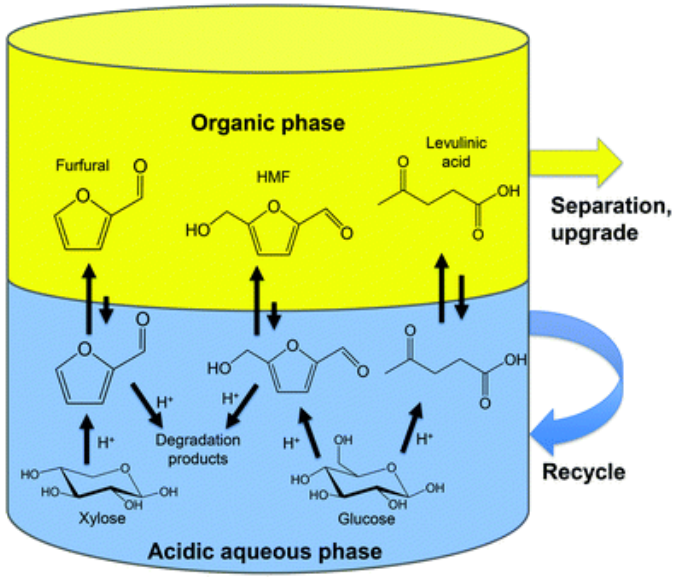

Fig 2.10: Biphasic systems for producing platform chemicals from lignocellulosic biomass (Luterbacher et al., 2014)

Román-Leshkov and Dumesic, (2009) converted glucose to HMF using HCl as catalyst, DMSO/H_2O as the reactive phase and MIBK-2 butanol as the extractive phase at 180°C and achieved 76% HMF yield with 85% selectivity. Saha and Abu-Omar, (2014) reported 68% HMF yield from H_2O-NaCl/ SBP biphasic solvents at 170°C with HCl/$AlCl_3$ catalyst. However, drawbacks with this method is that it requires the use of a large amount of solvent due to high HMF water solubility and poor partitioning into the organic phase (Román-Leshkov and Dumesic, 2009).

Table 2.2: Summary of studies from the literature for HMF production from cellulose and glucose with various catalysts and solvents.

Feedstock	**Catalyst**	**Solvent**	**Temp (°C)**	**Time (min)**	**HMF yield (%)**	**References**
Cellulose	HCl	MIBK/H_2O	200	20	25.8	Wang et al., 2020)
Cellulose	HCl	MIBK/2-butanol	180	12	76	Dumestic et al., 2007
Cellulose	$AlCl_3$	DMSO	150	540	20.5	Xiao et al., 2014
Cellulose		DMSO/[BMIM]Cl			54.9	
Cellulose	Beta-Cal750	H_2O/DMSO	180	180	42	Otomo et al., 2015
Cellulose	CrCl2	EMIMCl/H_2O	220	360	89	Ding et al., 2012
Cellulose	ATP-SO_3H-Cr_3	EMIMCl	120	120	31.2	Zhang et al., 2014
Cellulose	$CrCl_3$/$CuCl_2$	EMIMCl	120	480	57.5	Su et al., 2009
Cellulose	HCl	H_2O	300	30	20.7	Yin et al., 2011
Cellulose	LPSnP-1	H_2O	150	20	32	Dutta et al., 2014
Cellulose	$NaHSO_4$/$ZnSO_4$	THF/H_2O	160	60	53.2	Shi et al., 2013
Cellulose	[C2OHMIM]Cl	$CrCl_2$	140	240	38	Siankevich et al., 2016
Glucose	Amberlyst - 15	[BMIM]Cl	140	30	25.6	Hu et al., 2013
Glucose	$CrCl_3$	DMSO	140	15	54	Rasrendra et al., 2012
	$AlCl_3$				52	
Glucose	$AlCl_3$	DMSO/H_2O	140	20	25	Yu et al., 2016
Glucose	$RuCl_3$	H_20	120	5	32	Saha et al., 2013
	$Zr(O)Cl_2$				39	
Glucose	H-ZSM5 Zeolite		195	30	42	Wrigstedt et al., 2016
Glucose	LPSnP-1	H_20/MIBK	150	20	50	Dutta et al., 2014
Glucose	CCC	[BMiM]Cl	160	15	46.4	Siankevich et al., 2016

Different biomass substrates (sugarcane bagasse, corn cob, pine wood, wheat straw and bamboo fibre) have been used to produce HMF (Table 2.3). HMF yield from lignocellulose feedstocks depends on the interaction between cellulose, hemicellulose and lignin thus making its conversion more challenging than model cellulose. Sun et al., (2015) compared the activity of the NH_2SO_3H catalyst in THF/H_2O at 180°C for 40 min on pine wood, bamboo fibre and cotton and achieved 31%, 52% and 10% HMF yield from the respective feedstocks. Low yield in cotton was due to the dense and regular crystal structure of cellulose which restricted catalyst accessibility. Also, 27.1% HMF was achieved when Zhang *et al.,* (2017) reacted corn cob with SPTPA in GVL (γ – valerolactone). They reported that GVL disrupted cellulose crystallinity and inhibited re-precipitation of lignin by-products that otherwise limits the accessibility of cellulose. However, catalyst and solvent systems are important in the efficient conversion of biomass to HMF. All studies described in Table 2.3 utilised untreated biomass feedstocks whereby HMF yield could be increased through the pre-treatment of biomass to improve accessibility and decrease the crystallinity of cellulose.

Table 2.3: Summary of operational conditions from the literature on the conversion of different biomass feedstocks to HMF.

Feedstock	**Catalyst**	**Solvent**	**Temp (°C)**	**Time (min)**	**HMF (%)**	**Reference**
Sugarcane bagasse	$Zr(O)Cl_2$, $CrCl_3$	LiCl/[BMIM]Cl	120	5	42	Dutta et al., 2012
Corn cob	SPTPA	GVL	175	45	21.4	Zhang et al., 2017
Corn Stover	Fe_2Cl_3	THF/H_2O	170	80	45	Cai et al., 2014
Maple wood	H_2SO_4		170	40	21	
Poplar sawdust	$AlCl_3.6H_2O$	THF/H_2O	180	30	26	Yang et al., 2012
Wheat Straw	HCl	H_2O	146	30	3.4	Yemis and Mazza, 2012
Barley husk	Sulphanilic acid	H_2O/2-butanol/MIBK	150	60	41	Mirzai and Karimi, 2016

2.6.3 Microwave heating

In recent years, Microwave irradiation is increasingly gaining attention for its rapid heating, high efficiency (faster start up and shut down times) and easy operation as compared to conventional heating such as oil bath or hot plates. Microwave enhances dissolution of cellulose thereby increasing HMF and furfural yield by reducing the reaction time. It provides more rapid and efficient thermal energy via an electromagnetic field that penetrates the centre of reactants and generate uniform heat throughout the volume than conventional heating that relies on the diffusion of heat from the heating surface to the reactant, hence microwave heating provides energy savings of up to 85-fold (Yu et al., 2017). Only a few researchers have used this technology for HMF production. Li et al., (2009) used microwave irradiation at 400W for 1 min to convert cellulose and glucose with 3.6% $CrCl_3$ in [C4MIM]Cl at 100ºC and achieved 60% and 90% HMF yield respectively. In contrast, the above reaction with the same conditions was carried out using an oil bath at 100ºC for 60 min and 17% yield of HMF was achieved. It was noted that the high yield resulting from using microwave heating was due to rapid thermal energy transfer resulting in low activation energy where the [C4MIM]Cl acted as a water scavenger by dilution thus preventing HMF decomposition. In another study, Liu et al., (2013a) made a direct conversion of cellulose to HMF using microwave heating at 400W for 3.5 min using $ZrCl_4$ as a catalyst in [BMIM]Cl and achieved HMF yield of 51.4%.

Similarly, various researchers used lignocellulosic feedstock for HMF production, Zhang and Zhao, (2010) converted corn stalk, rice straw and pine wood in the presence of $CrCl_3$ in [C4MIM]Br under microwave irradiation at 100ºC, and 400 W for 3 min and 45%, 47% and 52% HMF yields were achieved for the respective feedstocks. Also, Sun et al., (2015) converted bamboo fibre to HMF using solid organic catalyst (NH_2SO_3H) in a THF/H_2O biphasic system at 180ºC for 40 min with 500Hz microwave heating and achieved 52.2% HMF yield. They showed that addition of sodium chloride (NaCl) to the reaction increased HMF yield due to the ability of NaCl to continuously separate HMF from the water phase into the organic phase. They also achieved lower HMF yields of 25% and 31% HMF yield from pine wood powder and polar wood powder respectively due to their high lignin content. Ching et al., (2017) converted microcrystalline cellulose (MCC) in water with dilute acid catalyst (H_2SO_4) using microwave irradiation at 120°C for 10 min and obtained 46% HMF yield. Addition of isopropanol (70%v/v) as a co-solvent increased HMF yield by 7%. Wrigstedt et al., (2016) reacted cellulose in a biphasic system of GVL/H_2O using HCl as catalyst at 160°C for 3 min using microwave irradiation and achieved 74% HMF yield. Sweygers et al., (2018)

converted cellulose in a biphasic solvent comprising of methyl isobutyl ketone (MIBK) and H_2O using HCl as catalyst at 177°C for 98 min under microwave at 800W and obtained 43.2% HMF yield. They validated the above biphasic system using Bamboo as lignocellulose feedstock under the same reaction conditions and achieved 42.44% HMF yield. As such, the proposed biphasic system could be used for a variety of lignocellulose feedstocks. Previous studies using microwave irradiation to produce HMF are summarized in Table 2.4

Table 2.4: Summary of studies using microwave heating to produce HMF.

Feedstock	Catalyst	Solvent	Time (min)	Temp (°C)	HMF (%)	References
cellulose	HCl	MIBK/H_2O	98	177	43.2	Sweygers et al., 2018
cellulose	H_2SO_4	H_2O/C_3H_8O	40	120	46	Ching et al., 2017
cellulose	HCl	γGVl/H_2O	3	160	74	Wrigstedt et al., 2016
cellulose	$CrCl_3.6H_2O$	$[C_4MIM]Br$	3	100	52	Zhang and Zhao, 2010
cellulose	$ZrCl_4$	[BMIM]Cl	3.5	220	51	Liu et al., 2013
cellulose	NH_2SO_3H	THF/H_20	40	180	52.2	Sun et al., 2015
cellulose	$CrCl_3.6H_2O$	BMIMCl	1	80	60	Li et al., 2009

2.7 Production of furfural

Furfural is a biomass derivative that has great potential for manufacturing solvents, plastics, and fuels (Hui et al., 2019). The hydrolysis of hemicellulose produces furfural in the presence of a catalyst to xylose which then undergoes subsequent dehydration to furfural (Fig 2.11)

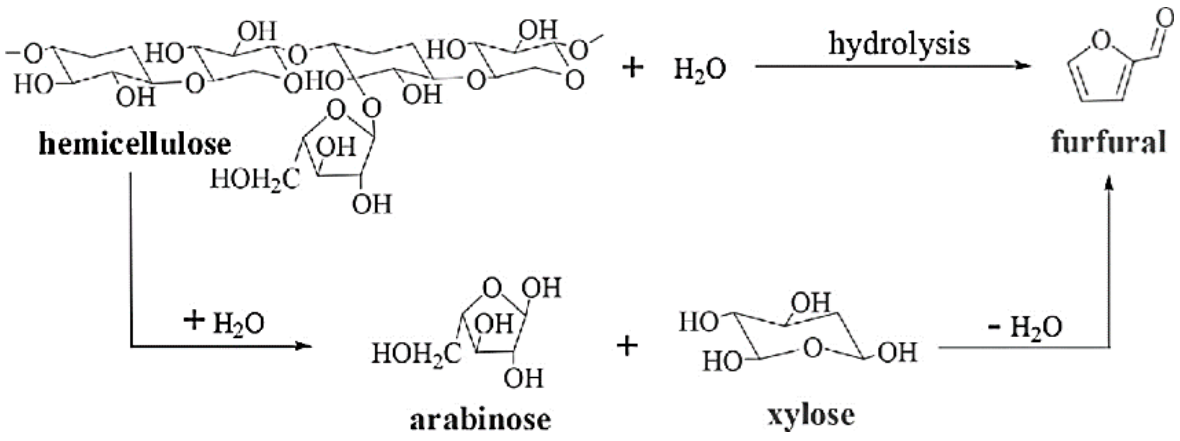

Fig 2.11: Hydrolysis of hemicellulose to furfural (Hui et al., 2019)

Most of the early research used xylose as a model compound to produce furfural (Lange et al., 2012). Catalysts serve an important role in hemicellulose conversion to furfural as it helps promote bond cleavage providing access to xylose thus facilitating its dissolution and conversion (Holm et al., 2010). Several homogenous catalysts such as H_2SO_4, HCl, $FeCl_3.6H_2O$, $AlCl_3.6H_20$, $Al_2(SO_4)_3$ and $SnCl_4$ have been used for furfural production. Marcotullio and De Jong, (2010) used 50mM HCl to convert xylose in aqueous solution at 170^{o}C and obtained 81.3 mol% furfural with 90% selectivity. Gallo et al., (2013) obtained an 80% furfural yield from xylose with a mixture of 10 % wt water and GVL as solvents using sulfuric acid catalyst at 160^{o}C for 40 min. Wang et al., (2015b) obtained 78.1% furfural yield at 150^{o}C for 120 min using $SnCl_4$ as a catalyst in a MTHF/H_20 solvent. Yang et al., (2017) reacted a variety of metal salts such as $SnCl_4$, $AlCl_3$, $CrCl_3$, $CuCl_2$, $CuSO_4$, $FeCl_3$ in a GVL/H_20 solvent at 130^{o}C for 30 min and observed the highest furfural yield of 87% using HCl. Amongst the catalysts used, those with a chloride ion were found to be the most effective in xylan conversion. The chloride ions (Cl^-) stimulate the formation of 1,2-enediol from xylose and its subsequent dehydration to furfural (Marcotullio and De Jong, 2010). However, drawbacks with the use of homogenous catalysts arise due to difficulty in catalyst recovery as it is dissolved in the reaction media. Hence, heterogenous catalysts having benefits of easy separation and recovery were investigated. Li et al., (2015b) reacted xylose at 180^{o}C using a Sn-MMT (montmorillonite with tin) catalyst for 30 min and obtained 76.8% furfural yield in SBP/NaCl-DMSO-H_2O media. Gallo et al., (2013) reacted xylose with H-Beta catalyst at 170^{o}C for 30 min in GVL solvent and obtained 70% furfural yield. The co-existence of Bronsted and Lewis acid functionalities on the catalyst showed a high selectivity resulting in high furfural yields. Gürbüz et al., (2013) used H-M (H-mordenite) catalyst to convert xylose at 175^{o}C for 40 mins obtaining 80% furfural yield in GVL water solvent mixture (10 wt% water). Furfural yields were higher at lower concentration of water in the solvent mixture due to reduced furfural degradation.

Various solvents such as MIBK, THF, DMSO, GVL and H_2O have been used for furfural production. Gallo et al., (2013) found that a higher yield of furfural (70%) was achieved in GVL than water (55% furfural yield) when using xylose with H-Beta catalyst at 170^{o}C for 30 min and explained due to the dehydration reaction occurring faster in GVL hindering the subsequent degradation of furfural. Yang et al., (2017) found that under the same reaction conditions (130^{o}C, 30min) in the presence of different solvents such as MIBK, THF and GVL, the highest furfural yield of 87.8% from xylose using a mixture of GVL/water (ratio of 8:2

vol/vol) was obtained. Addition of water to the GVL led to increased furfural yield as furfural products were continuously extracted into the organic phase to prevent the formation of by-products. Mellmer et al., (2014) studied the effect of solvents on reaction kinetics of the acid catalysed conversion of xylose into furfural and found that the solvent GVL had the highest reaction rate and highest furfural selectivity (value) as GVL lowered the activation energies of the reaction.

Like HMF, rapid heating, reduction in reaction time and higher yields was observed from microwave assisted heating for furfural production. Choudhary et al., (2012) observed a 53% furfural yield from xylan in the presence of sodium molybdate/HCl catalyst using microwave heating at 150ºC for 5 mins. Whereas, using a conventional heating, a 36% furfural yield was observed using same reactants and temperature for 30 mins. Similarly, Xiouras et al., (2016) made a comparison between conventional and microwave heating from xylose and observed a higher yield of 76% furfural yield at 7 mins, 200ºC for microwave heating as compared to 60% yield for conventional heating.

Table 2.5: Summary of solvents and catalysts used in furfural production.

Feedstock	**Catalyst**	**Solvent**	**Temp (ºC)**	**Time (min)**	**Furfural yield (mol%)**	**Reference**
Xylose	HCl	H_2O	200	30	81	Marcotullio and De Jong, 2010
Xylose	H_2SO_4	GVL-H_2O	170	30	80	Gallo et al., 2013
Xylan	$SnCl_4$	2-MTHF-H_2O	150	120	78	Wang and Chen, 2013
Xylan	$Al_2(SO_4)_3$	GVL-H_2O	130	30	87	Yang et al., 2017
Xylose	NaCl-Sn-MMT	SBP-H_2O-DMSO	180	30	76	Li et al., 2015b
Xylose	H-M	GVL-H_2O	175	40	80	Gürbüz et al., 2013
Xylose	H_2SO_4	GVL	175	60	75	Mellmer et al., 2014

The conversion of xylose or hemicellulose to furfural has provided a valuable understanding of the mechanism of furfural formation. However, it was not deemed to be economically viable to produce furfural from xylose or hemicellulose as this needed to be obtained in pure form from biomass (Luo et al., 2019). Hence, a number of studies on the production of furfural from different biomass feedstocks have been carried out by researchers (Table 2.6). Furfural yields from biomass depends on the interaction between hemicellulose, cellulose and lignin making its conversion more challenging than for the model compound xylose. Hemicellulose is always accompanied by the dissolution of cellulose or lignin, hence why most researchers have concentrated on the simultaneous conversion of the three major components (Luo et al., 2019). Luo et al., (2017) obtained a furfural yield of 33.6% (based on hemicellulose weight in *pubescens)* from *pubescens* at 160^{o}C for 4h in a GVL-water media. Water was found to promote the cleavage of chemical bonds between the hemicellulose, cellulose, and lignin fractions with GVL dissolving lignin and hemicellulose leaving cellulose. Li et al., (2014) obtained 66.3 mol% furfural and 44.3% levulinic acid from hemicellulose and cellulose simultaneously by reacting sugarcane bagasse in a THF-water solvent (2:1) at 200^{o}C for 20 min, leaving lignin as a precipitated solid residue. Li et al., (2017) reacted corn stover with a strong acid catalyst (SC-CaC_t-700) at 200^{o}C for 40 min in GVL and obtained 93% furfural yield. There was no furfural produced without the addition of a catalyst and 55% furfural yield was obtained when water was used as solvent in the presence of the same catalyst. This can be concluded that both catalyst and solvent were important in furfural production.

Table 2.6: Furfural production from different lignocellulose feedstocks.

Feedstock	**Catalyst**	**Solvent**	**Temp (^{o}C)**	**Time (min)**	**Furfural yield (Mol%)**	**Reference**
Pubescens	-	GVL/H_2O	160	240	33.6	Luo et al., 2017
Bagasse	HCl	THF-H_2O	200	20	66.3	Li et al., 2014
Corn Stover	SC-CaC_t-700	GVL	200	40	93	Li et al., 2017
Corn cob	H_2SO_4	H_2O	160	45	71	Wang et al., 2014
Wheat straw	SAPO-44	H_2O-Toluene	170	120	93	LaxmikantáDhepe, 2014

Even though a large volume of research has been done on the effect of catalyst and solvents on HMF and furfural yields from biomass, the relationship between the structure of the biomass such as cellulose crystallinity, degree of polymerisation, surface area of cellulose and hemicellulose acetylation on the HMF and furfural yields are scarce. As pre-treatment is expected to disrupt biomass structural and compositional features, it is important to understand how these changes affect the HMF and furfural yields. In addition, the improved biodegradability of ozone pre-treated biomass during enzymatic hydrolysis to bioethanol has been proven by previous studies (Binder et al., 1980, Neely, 1984, Kumar et al., 2009, Souza-Correa et al., 2013, Garcia-Cubero et al., 2009), no study has shown any relationship between ozone pre-treated biomass to production of platform chemicals.

2.8 Techno-economic analysis of ozone pre-treatment

Techno-economic analysis of a process is the analysis carried out to evaluate the economic feasibility of a new technology or process. It evaluates the technical performance and economic feasibility of a new technology and helps decision makers with regards to investment or research and development (Kuppens et al., 2015). Currently, the amount of literature (papers) on the techno-economic analysis or economic evaluation of ozone pre-treatment technology for production of platform chemicals or biofuels is almost non-existent. This indicates that economic feasibility studies are not currently the main concern of researchers. Since the technology is still relatively new for production of biofuels or platform chemicals, focus is on further technological development. Fernández-Delgado et al., (2019) carried out a comparison on an economic evaluation of three pre-treatment scenarios namely: alkaline, peroxide and ozone pre-treatments to produce biobutanol from a plant capacity of 1ton/day of brewer's spent grains (BSG). They estimated the cost of ozone production as 1.8 € kg^{-1} of O_3 and total capital cost of €341,250 and reached a conclusion that ozone pre-treatment had 3 times more total capital cost than alkaline (€113,750) and peroxide pre-treatment (€136,500) due to specific equipment needed for ozone generation increasing the total cost of equipment. Although no detailed calculation was provided.

2.9 Summary

Although ozone pre-treatment has been extensively researched, further investigation is necessary to tackle the challenges posed by the high costs of ozone generation and the high level of ozone consumption in the process. Cold plasma technology has proved that ozone can be generated with 30% less energy than other methods, thereby prompting the design of an ozone generator that produces a high ozone concentration with low power consumption possible which would be suitable for the pre-treatment of biomass.

A large volume of research has been carried out on the effects of catalyst and solvents on HMF and furfural yields from biomass but an understanding of the effects of structure and composition of the biomass on HMF and furfural yields is scarce. As pre-treatment is expected to make the holocellulose more accessible, it is important to understand how these changes can affect the HMF and furfural yields. Furthermore, microwave assisted heating will be used for this work due to advantages it offers over conventional heating.

Chapter 3: Materials and Methodology

This chapter describes the materials, equipment, experimental procedures, analytical and characterisations methods used for this work. The agricultural residues used for this work are corn cob and spelt husk. Corn cob represents an abundant agricultural processing residue which has attracted considerable attention in recent years for the production of biofuels and platform chemicals as it is obtained from the most abundant (850 million tons annually) grain crop globally (Wang et al., 2019). Corn cob is used in this study to represent a low lignin feedstock with high moisture content while spelt (an ancient grain) is attracting considerable interest for improved human nutrition and health (Bonafaccia et al., 2000) and the residual protective husk represents a medium lignin feedstock with low moisture content.

3.1 Materials

3.1.1 Chemicals

The chemicals used for this study all purchased from sigma Aldrich are listed in Table 3.1 and analytical standards listed in Table 3.2 except for oxygen gas which was purchased from BOC Ltd (UK, purity of 99.9%).

Table 3.1: List of chemicals used.

S/N	Chemicals	CAS Number	Purity
1	α – Cellulose	9004-34-6	99.9%
2	Oxygen gas	7782-44-7	99.9%
3	Aluminium chloride	231-206-1	97%
4	Sodium thiosulfate	CHE 3 566	99.50%
5	potassium iodide	7681-11-0	99%
6	Sulfuric acid	33-97-41	99.99%
7	Toluene	108-88-3	99.80%
8	Ethanol	64-17-5	99.80%
9	Dimethyl sulfoxide	67-68-5	99.98%
10	2-propanol	67-63-0	99.90%
11	Sodium Chlorite	7758-19-2	80%
12	Sodium Hydroxide	1310-73-2	97%
13	Hydrochloric acid	7647-01-0	37%
14	Hydrogen Peroxide	7722-84-1	30%
15	Iron (III)chloride	7705-08-0	97%
16	Copper (II) chloride	7447-39-4	99%
17	Calcium Chloride	10043-52-4	99.99%
18	Manganese (II) Chloride	7773-01-5	99%
19	Choline Chloride	67-48-1	99%
20	Urea	57-13-6	99%

Table 3.1 (contd): List of chemicals used

S/N	Chemicals	CAS Number	Purity
21	3,5-dinitrosalicylic acid (DNS)	609-99-4	98%
22	Bis-(Ethylenediamine)copper (II) hydroxide solution	14552-35-3	-

Table 3.2: List of standards used.

S/N	Chemicals	CAS Number	Purity
1	5-Hydroxymethyl Furfural (HMF)	67-47-0	99%
2	Furfural	98-01-1	99%
3	Levulinic acid	123-76-2	98%
4	D (+) - Glucose	50-99-7	99.5%
5	Oxalic acid	144-62-7	98%
5	Acetic acid	64-19-7	99.9%
6	Formic acid	64-18-6	96%
7	Glycolic acid	79-14-1	99%
8	L (+) - Fructose	7776-48-9	97%
9	L (+) - Arabinose	5328-37-0	99.5%
10	D (+) - Xylose	58-86-6	99%

3.1.2 Feedstocks

Corn cobs (Figure 3.1a) were harvested at stage R3 (milk stage) of maturity across a range of countries i.e. United States of America, South Africa, United Kingdom, France, Spain, Morocco, Germany, Greece and Senegal (thereby representing a typical agricultural processing residue) followed by storage at 0-5°C for 1–25 days. Waste corn cobs were kindly provided by Barfoots of Botley Ltd, UK. They were stored in a cold room at 6°C prior to use to prevent decay. The cobs were cut into pieces < 5mm and blended (HGBTWTS3 laboratory blender 8010 ES) for 3 minutes to obtain a particle size of ~2.0mm (which was the minimum particle size achievable due to the high moisture content of the fresh cobs (i.e. 72%) as finely ground or powdered biomass is not required for an efficient ozonation process (Wan Omar and Amin, 2016). Corn cob was used in its natural undried state as moisture is needed for ozone pre-treatment as well as to save operational costs of drying.

Spelt husks (Figure 3.1b) obtained from Gilchesters Organics (Stamfordham, UK) were ground (HGBTWTS3 laboratory blender), sieved to 2.0mm and stored at room temperature prior to use.

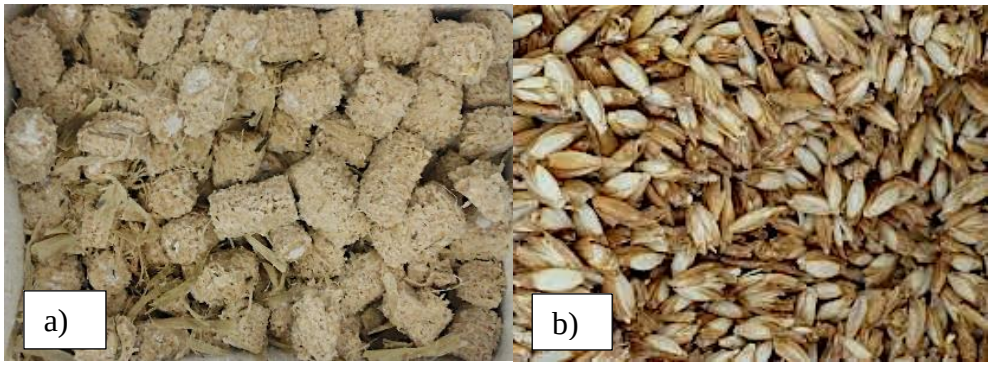

Fig 3.1: The feedstocks used; a) corn cob and b) spelt husk.

3.2 Feedstock analysis

3.2.1 Lignin analysis

Acid insoluble lignin (AIL) was determined by treating approximately 1g of oven dried sample with 15mL 72% (w/v) sulphuric acid for 2 hours at 20^{o}C with constant stirring at 170 rpm to facilitate dispersion of sample in the acid (TAPPI T-222). After complete disintegration, the solution was transferred to a 1L round bottom flask, diluted to 3% sulphuric acid solution to a total volume of 575mL and refluxed for 4h maintaining a constant volume. The insoluble material was allowed to settle overnight, and the supernatant collected for acid soluble lignin (ASL) analysis. The acid insoluble lignin was filtered and washed to neutrality (pH 7) with hot water, dried at 105^{o}C to a constant weight and gravimetrically determined, prior to ignition at 850^{o}C for 45 mins to obtain lignin ash. The lignin ash was subtracted from the lignin to give the % of ash-free lignin according to the method developed for the pulp and paper industry (TAPPI T-222) while the ASL was determined from the filtrate according to TAPPI method UM 250. Approximately 1mL of filtrate (from acid insoluble lignin determination) was placed in a UV-Vis spectrophotometer to measure the absorbance at 205nm. Acid soluble lignin was calculated using the following formula.

$$\text{ASL} = \frac{\text{Abs} \times \text{volume} \times \text{dilution}}{\text{a} \times \text{W} \times \text{pathlength}} \text{ X } 1000 \text{ mg g}^{-1}$$

Where Abs = absorbance at 205nm,

volume = volume of filtrate (l)

Dilution factor

a= molar absorptivity of lignin at 205 nm (110 $Lg^{-1}cm^{-1}$) (Schoning, 1965)

W= weight of sample (g)

Pathlength (cm)

3.2.2 Holocellulose (hemicellulose and cellulose) determination

According to the method developed by Wise et al., (1946), holocellulose content was determined by suspending approximately 5g of oven dried sample in 150mL of distilled water at 75°C at a stirring speed of 170 rpm followed by the addition of 10 drops of glacial acetic acid and 1.5g of sodium chlorite. After 1 hour, the same amount of reagent was again added, and the reaction was continued for a further 3 hours. The solution was cooled in an ice bath, filtered and washed with distilled water until neutrality (pH 7), then quickly rinsed with acetone and dried at 105°C to a constant weight. The holocellulose was estimated gravimetrically.

3.2.3 Cellulose content

Cellulose content was estimated according to TAPPI T203os-61. Approximately 2g of holocellulose sample was weighed in a beaker suspended in a water bath at 20^{o}C and 15mL of 17.5% sodium hydroxide (w/v) solution added and stirred for 1 min. A further 10mL 17.5% sodium hydroxide solution was added to the mixture and stirred for another 1 min. This was repeated again, and the resultant solution allowed to swell for 3 min. After this, an additional 10mL of sodium hydroxide solution was added and the content mixed for another 3 min and the resultant solution was allowed to stand for a further 30 min. After 30 min, 100mL of distilled water was added and the solution filtered. The residue was washed with a further 25mL of sodium hydroxide solution and 650mL of cold distilled water to remove any trace of residual acid from the sample prior to drying in an oven at 105^{o}C to a constant weight. The cellulose content was estimated gravimetrically.

3.2.4 Moisture, Ash and Extractives

Moisture, ash and extractives of both feedstocks were determined according to ASTM D3173, ASTM D3174 and ASTM E1690 respectively (Appendix A2). All analyses were repeated thrice and the mean values presented. The composition of the agricultural residues used are

presented in Table 3.3, the moisture content of the corn cob and spelt husk were 72.1% and 11.2% respectively.

Table 3.3: Chemical composition (%) of raw corn cob and spelt husk feedstocks expressed on a dry weight basis.

Properties	**Corn cob**	**Spelt husk**
Acid insoluble lignin (AIL)	5.1 ± 0.3	16.03 ± 0.1
Acid soluble lignin (ASL)	2.97 ± 0.16	3.96 ± 0.26
Cellulose	43.2 ± 0.2	31.8 ± 0.5
Hemicellulose	37.8 ± 0.2	29.1 ± 0.1
Ash	3.2 ± 0.01	8.4 ± 0.04

3.3 Experimental set-ups and procedures.

3.3.1 Ozone generator set-up

The ozone generator (Fig 3.2) consisted of a plasma ozone generator with an inlet connected to an oxygen cylinder via a flow meter (50 – 300 mL min^{-1}) to regulate the amount of oxygen fed into the reactor. The reactor outlet was connected to a wash bottle containing 200mL of 2% potassium iodide solution (KI) where the amount of ozone generated can be quantified using iodometric titration (Yulianto et al., 2019).

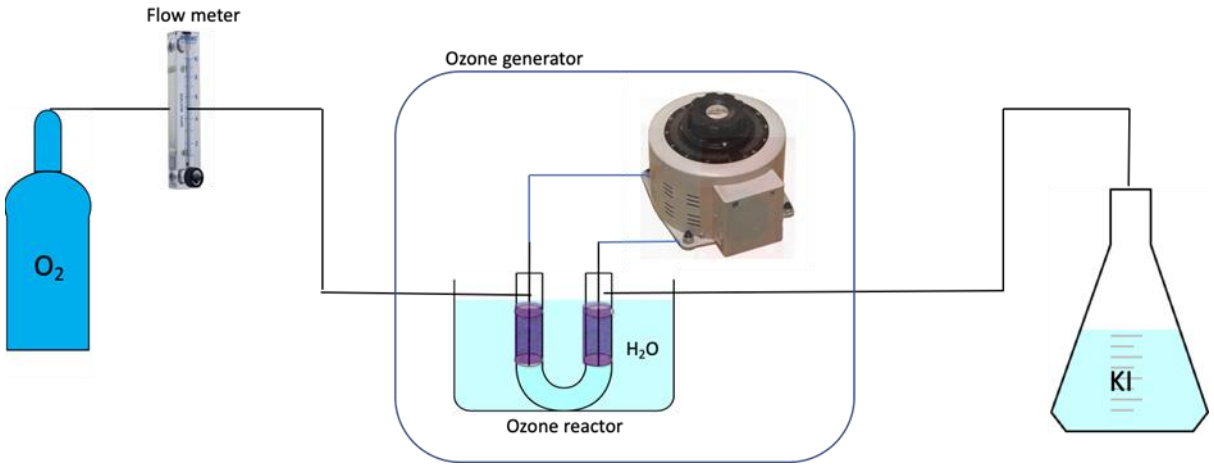

Fig 3.2: Experimental set-up of the ozone generator.

Using iodometric titration, the amount of ozone was determined based on reaction of iodide (I^-) with O_3 to give Iodine (I_2) (Equation 3.1) which is evident from the colour change of KI solution from clear to amber indicating oxidation of KI with O_3 as one mole of O_3 yields one mole of I_2.

Hence, the number of moles of I_2 was determined by titrating with sodium thiosulfate (Equation 3.2) until the amber colour turned clear and the volume of sodium thiosulfate consumed recorded.

$$O_3 + 2I^- + H_2O \longrightarrow I_2 + 2OH^- + O_2 \qquad \text{Equation 3.1}$$

$$I_2 + 2Na_2S_2O_3 \longrightarrow 2NaI + Na_2S_4O_6 \qquad \text{Equation 3.2}$$

Using the volume of sodium thiosulfate recorded, ozone concentration was calculated using Equation 3.3.

$$C = \frac{24 \times V_t \times M \times 1000}{F_R \times t} \qquad \text{Equation 3.3}$$

Where C is the ozone concentration (g m^{-3}), V_t is the volume (L) of titrant ($Na_2S_2O_3$), M is molar concentration of titrant (M), F_R is oxygen flow rate ($Lmin^{-1}$) and t is time (min) (Yulianto et al., 2019).

Average gas temperature (T_{avg}) in the u-tube reactor was calculated using Equation 3.4.

$$T_{avg} = \frac{P/A}{\alpha \times K} \times d_g + T_w \qquad \text{Equation 3.4}$$

Where T_{avg} is average gas temperature of oxygen in the reactor (°C), T_w is the wall/cooling medium temperature (°C), K is the thermal conductivity of oxygen gas (Wm^{-1} $°C^{-1}$), P is discharge power of the reactor (W), A is electrode surface area (cm^2), d_g is discharge gap width (cm) and α is 12 for two-sided cooling (Brueggemann et al., 2017).

The ozone production rate and energy efficiency were calculated using the following formula;

Ozone produced (mg h^{-1}) = ozone concentration (mg L^{-1}) × Flow rate (L h^{-1}) Equation 3.5

Ozone generator efficiency (g $kW^{-1}h^{-1}$) = ozone produced (g h^{-1}) × power (kW) Equation 3.6

3.3.2 Ozone pre-treatment

Ozone pre-treatment setup (Fig 3.3) consisted of a cold plasma ozone generator connected to a gas inlet controlled via a 250 mL min^{-1} flow meter (error: ±0.10 mL min^{-1}) yielding an ozone

output of 0.44 g h^{-1} and concentration of 2.02% w/w (Section 4.3). The outlet of the reactor was connected to a 250 mL batch reactor placed in a Branson 2510 ultrasonic bath set at a frequency of 40 kHz (maximum frequency needed to enhance mass transfer) to enhance mixing of ozone with the biomass substrate, while ice was added to maintain the temperature to 25°C. The unreacted ozone was then passed through 2wt% potassium iodide solution (KI) and was quantified using the iodometric titration method. The experiments were repeated thrice.

The relationship between oxygen flow rate and cold plasma input as well as ozone production was established (Chapter 4, Section 4.3). Ozone of concentration of 2% w/w was injected into the reactor containing a known amount of feedstock over a range of reaction times i.e. 15 – 90 min. An ozone concentration of 2wt% was sufficient for optimum lignin separation from biomass (Ben'ko et al., 2013, Panneerselvam et al., 2013b, Li et al., 2015a, García-Cubero et al., 2009). Moisture content of corn cob was varied from 72. % to 42.9% by drying down the feedstock in an oven at 105^{o}C for different times. Whereas moisture content for spelt husk was varied from 11% to 100% (wet basis) by adding water. Wet feedstock with moisture contents adjusted to the desired moisture were used to reduce the overall energy cost of the process.

The pre-treated materials were washed with 100mL distilled water and filtered. The solid residue was dried in the oven at 105°C to a constant weight prior to compositional analysis. While the filtrate (liquid) were analysed for ozone pre-treatment degradation products using high performance liquid chromatography (HPLC) as described in Section 3.4.4.

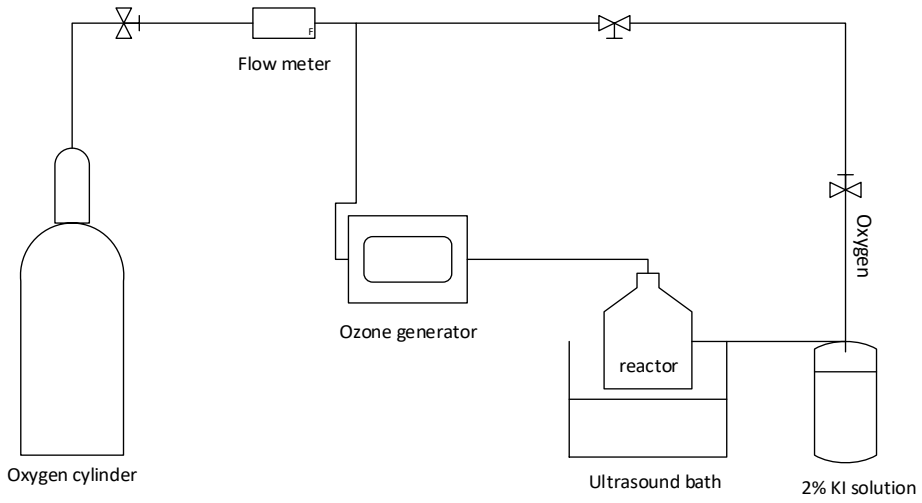

Fig 3.3: Ultrasound/ozone pre-treatment set-up.

3.3.3 Biomass fractionation.

Fractionation was carried out by weighing approximately 30g of feedstock (raw or ozone pre-treated) into a 250mL round bottom flask and 50mL of toluene added and refluxed for 2 hours to remove fatty acids. The mixture was cooled to room temperature, filtered and the residue dried overnight in an oven. The residue (toluene extracted) was subjected to mild (70-80°C) ethanol extraction by weighing 12.5g of dried residue into a 250mL round bottom flask, 100mL of ethanol:water (60:40 v/v) was added to obtain a solid-liquid ratio of 1:8. Thereafter 2mL of 37% HCl was added to enhance the hemicellulose hydrolysis. The mixture was refluxed for 1-4hrs, cooled to room temperature, filtered, and washed 4 times with 25mL ethanol to remove any lignin present (Fig 3.4). The residue (cellulose pulp) was dried while the solvent from the filtrate (lignin and hemicellulose) was evaporated at 40°C and 150 mbar using a rotary evaporator. 15mL of acetone was added to dissolve the resultant solid and lignin precipitated by adding 100mL of water leaving mainly the hydrolysed hemicellulose (xylose and arabinose) and lignin degradation products as water soluble fractions. The mixture was filtered, washed 4 times with 25mL of water and the lignin residue dried (Au - Zijlstra et al., 2019).

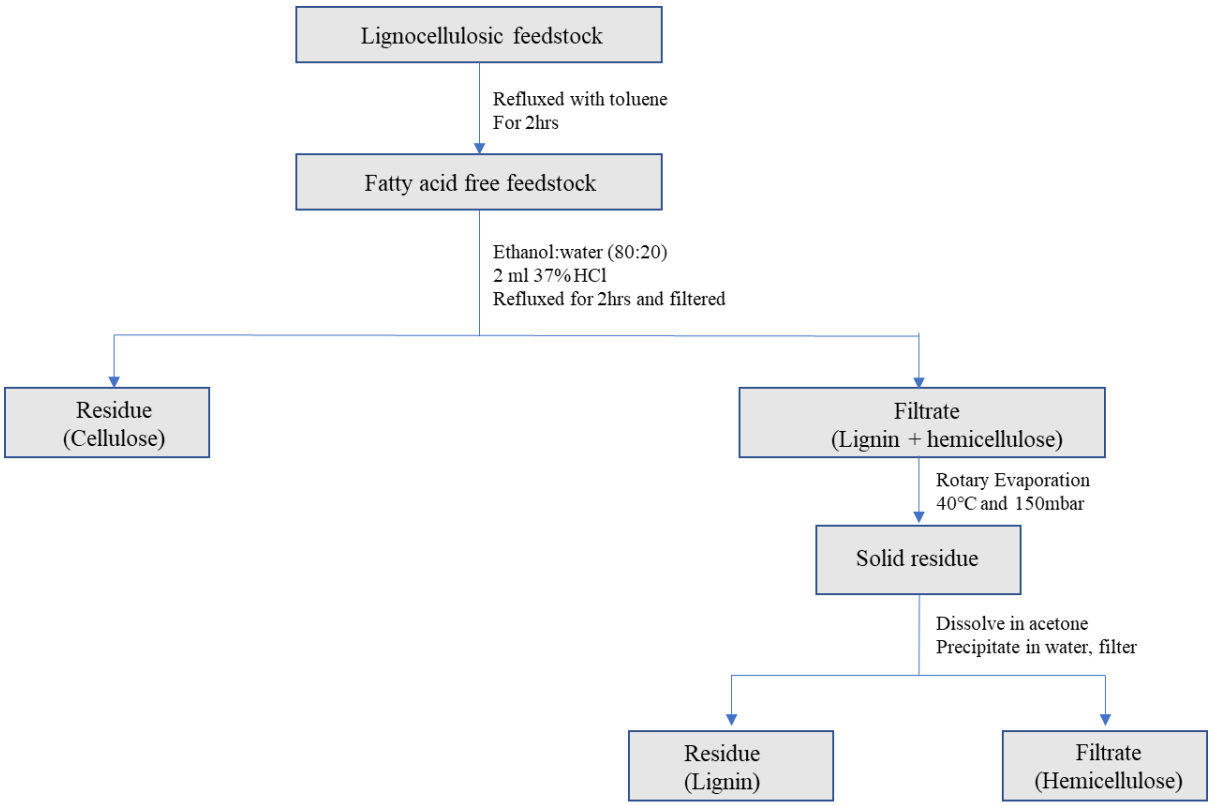

Fig 3.4: Fractionation of lignocellulosic biomass (agricultural residues).

3.3.4 Alkaline hydrogen peroxide pre-treatment.

About 1g of dried feedstock was placed into a beaker containing 20 mL of 1% (w/w) hydrogen peroxide solution with pH adjusted to 11.5 with addition of 5M sodium hydroxide. The mixture was incubated in a water bath at 120°C at different reactions times (30-240 min). After completion of the pre-treatment, the mixture was filtered, washed thoroughly until the pH became neutral (Ayeni et. al., 2017). The residue was oven dried at 60°C and liquid analysed using High Performance Liquid Chromatography (HPLC) as described in Section 3.4.4.

3.3.5 Microwave assisted production of 5-Hydroxylmethyl furfural (HMF) and Furfural.

The microwave digestion system set-up (Fig 3.5) consisted of a 250mL round bottom flask placed onto the magnetic stirrer equipped in the Ethos microwave digestive system. A double condenser connected to a water bath set at 5^{o}C was attached to the flask to prevent vapour loss due to evaporation from the reaction. A known volume of mixed solvent (DMSO and water) was added to a known amount of cellulose to obtain 5 - 20 wt% and 0.1 wt % of $AlCl_3$ and 1 wt% HCl as catalyst to generate a total volume of 20mL. The microwave power was set to obtain a desired temperature (160°C – 180°C) over a set of reaction times (2-15 min) and optimum condition for highest HMF and furfural yield obtained (Chapter 6, Section 6.3). After completion of the reaction, the solution was allowed to cool and then the sample was filtered, the filtrate containing solvents, HMF, furfural, levulinic acid was collected, analysed using the GC as described in Section 3.4.2 and, the total reducing sugar content was analysed using the DNS method (Section 3.4.9). While, the residue was washed with water, dried at 105°C and weighed to determine the amount of unreacted cellulose. The reactions were repeated in triplicate for reproducibility.

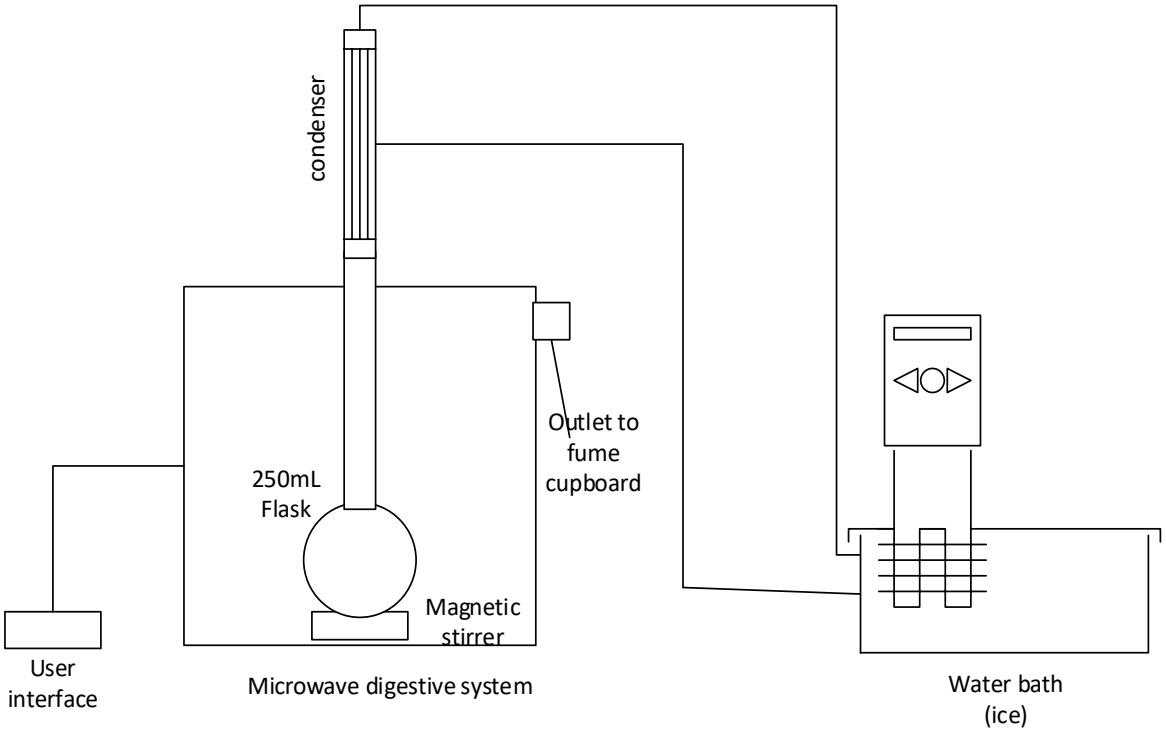

Fig 3.5: Microwave assisted synthesis set-up.

3.4 Analytical methods.

3.4.1 Fourier Transform Infrared Spectroscopy (FTIR)

Fourier Transform Infrared Spectroscopy (FTIR) was used to identify the functional group present in solid samples such as the untreated biomass as well as identify functional group changes in the pre-treated and fractionated biomass. The FTIR analysis was performed using the Agilent Technology Cary 630 FTIR spectrometer. The method used transmittance with a spectra range of 4000 to 550 cm^{-1} with 10 scans at $2cm^{-1}$ resolution. The background signal was taken and the sample was added to cover the diamond ATR (Attenuated Total Reflection). The cap was screwed down to lock the sample to the diamond ATR and the spectrum taken. The background signal was subtracted from the sample spectrum to obtain results for that solid.

3.4.2 Gas chromatography (GC)

The filtrate from microwave digestion (1 μL) was injected using a micro syringe into an Agilent 7890A gas chromatograph equipped with a flame ionisation detector set at 250°C. A Restek Rtx-1701 capillary column of 60m length, 250μm internal diameter and 0.25μm thickness was

used, with helium as carrier gas. The initial oven temperature was set at 45°C with 10 min hold time at a heating rate of 3°C min^{-1} while final oven temperature was set at 250°C with 5min hold time (NREL, 2016). The area ratios were obtained for HMF, furfural and levulinic acid with 1-octanol as internal standard and concentrations obtained from calibration plots (Appendix A3). The yields of HMF, Furfural and Levulinic acids were calculated as follows according to Goswami et al., (2016). To confirm the identity of each identified peak, GC-MS analysis (Appendix A4) was performed on selected runs and no inconsistencies observed.

Mass of product (mg) = [product concentration (mg mL^{-1}) × [volume of reaction mixture (mL)]

$$\text{Product yield } (mg\ g^{-1}) = \frac{\text{Mass of Product (mg)}}{\text{Mass of cellulose (g)}} \qquad \text{Equation 3.7}$$

3.4.3 Hydrogen Nuclear magnetic resonance (H^1NMR)

Hydrogen Nuclear magnetic resonance (H^1NMR) is used to determine the structure of a molecule with respect to hydrogen nuclei. H^1NMR is the most widely used for lignin structural analysis as it provide comprehensive information about linkages and composition of H/G/S (hydroxylphenyl, guaiacyl and syringyl) units in lignin (Lu et al., 2017). H^1NMR spectra of lignin was generated using a Bruker Avance – 300 spectrometers operating at a frequency of 300 mHz using 50mg of fractionated lignin dissolved in 0.5mL deuterated dimethyl sulfoxide (DMSO-d6).

3.4.4 High performance liquid chromatography (HPLC)

Water soluble fractions such as monomeric sugars and carboxylic acids were measured from the ozone pre-treatment filtrate by HPLC (Perkin Elmer Flexar series 200) using an Aminex HPX-87H column at 65ºC with a refractive index (RI) detector at 0.6 mL min^{-1} flow rate for 30 min and 0.005M H_2SO_4 as mobile phase adapted from (Fang et al., 2018). Samples were filtered through a 0.45µm filter paper to remove any suspended solid particles from the hydrolysates prior to injection in the HPLC. The concentrations of each component were calculated based on standard calibration curve (HPLC peak area vs Concentration) (Appendix A5) from the analytical standards (Table 3.2) of each component.

3.4.5 Scanning Electron Microscopy (SEM)

Scanning Electron Microscopy (SEM) is a method used to view the surface morphology of a material at a higher magnification (x40 – 100,000) than conventional microscope (Mikmekov et al., 2011). The surface morphology of the untreated and pre-treated corn cob, spelt husk and model cellulose was analysed using a TM3030 Hitachi microscope operating with accelerating voltage of 15kV. The sample was mounted on a conductive carbon tape prior to imaging. The sample holder was then mounted on the stage, scanned at different magnification (x250 – 4000) and images taken for all samples to show structures at different scales and allow accurate comparison between the samples (Mikmekov et al., 2011).

3.4.6 Thermogravimetric Analysis (TGA)

Thermogravimetric Analysis (TGA) was used to determine the change in thermal stability of the biomass materials caused by pre-treatment through monitoring of the weight change in sample versus temperature at a fixed heating rate in an inert environment. The thermogravimetric (TGA) analysis was done using Netzsch TG 209 thermogravimetric analyser with ~10mg of sample heated from 25°C to 800°C at a rate of 10°C min^{-1} in an atmosphere of helium (flow rate of 20 mL min^{-1}) and resulting thermogram is obtained showing a melting peak, followed by a degradation peak at different temperatures.

3.4.7 X-ray diffraction (XRD)

X-ray diffraction (XRD) analysis was used to further characterise the structure of cellulose (untreated, fractioned and model cellulose) and provide an understanding into its crystal structure and measure its crystallinity. The analysis was carried out with an 18 KW D/Max-2500PC diffractometer at a 2θ range of 5º- 45º with a scan speed of 0.6º 2θ per minute using copper K-α radiation and results plotted based on signal and angle. The crystallinity index (CI) of cellulose was calculated using peak height method as follows;

$$\text{CrI } \% = \frac{I_{002} - I_{amp}}{I_{002}} \times 100 \qquad \text{Equation 3.8}$$

I_{002} and I_{amp} are the intensity of the crystalline and amorphous region of cellulose obtained at 2θ of 22.5°C and 18°C respectively.

3.4.8 Degree of polymerisation of cellulose

Degree of polymerisation of untreated and pre-treated cellulose was analysed using Matrix-assisted laser desorption/ionisation time of flight (MALDI-TOF) according to methods described by Kosyakov et al., (2018) using DMF as solvent and α-cyano-4-hydroxycinnamic acid as matrix. Once cellulose was dissolved in the solvent and loaded into the instrument, the laser ionised the cellulose molecules into ions with alkali metals (mostly present as impurities in the sample) such as MLi^+, MK^+, MNa^+. The ions are then pulled into the mass analyser area of the instrument where the molecules are separated based on their mass to charge ration. The separated molecules are accelerated by high-voltage current and fly through the tube before reaching the detector. Smaller molecules reach the detector faster than larger molecules. However, drawbacks encountered with use of this technique was that larger molecular weight ions were not detected giving rise to very low (DP 17) degree of polymerisation of cellulose. In addition actual mechanism of the cationisation process still remains unclear in the literature (Tuma, 2003).

Hence, the standard industrial method for determination of the degree of polymerisation of cellulose through viscometry was used for subsequent analysis of cellulose in this work. It offered clear advantage as higher DP of cellulose was achieved in addition to it being a relatively quick method requiring less technical expertise. Average viscometric degree of polymerisation (DPv) of cellulose was obtained using the Ostwald capillary viscometry and Cupriethylene-diamine solution (Cuen) as solvent. The efflux time of solution containing 250 mg of cellulose sample dissolved in 25mL of Cuen solvent and 25mL of distilled water was determined using the capillary viscometer according to TAPPI T230 and DPv calculated using the following Mark-Houwink-Sakurada equation: $DPv^{0.905}=0.75\ [\eta]$ (Mishra et al., 2012).

Where DPv is the average viscometry degree of polymerisation and η is the intrinsic viscosity.

3.4.9 Total reducing sugar (TRS) analysis using 3,5-dinitrosalicylic acid (DNS)

The filtrate from microwave assisted reaction was diluted to 250 times and 3mL of diluted sample was reacted with 3ml of 3,5-dinitrosalicylic acid solution in a test-tube by heating in a boiling water for 5mins. A colour change from light yellow to dark red is observed because of glucose reacting with DNS to form 3-amino-5-nitrosalicylic acid and gluconic acid. The intensity of the red colour increases as the glucose concentration in the sample increases. After

the reaction, the mixture is allowed to cool for 2 mins and the absorbance of the mixture measured at a wavelength of 485nm using a UV-Vis spectrophotometer (Zhou et al., 2013).

3.4.10 UV-Vis Analysis

A UV-Vis spectrophotometer was used to quantify the total reducing sugars (TRS) from the filtrate obtained from microwave reaction (after undergoing DNS reaction) by measuring the absorption or reflection of the material as a function of wavelength. A UV-Vis spectrophotometer (model 7310) was used to scan the filtrate at different wavelength and a peak absorbance of TRS was observed at wavelength of 485nm. DNS solution was used as a blank. The sample from microwave filtrate was diluted to obtain absorbance range of 0.1 - 3.0. The TRS concentration was calculated based on a standard calibration curve obtained with glucose (Appendix A7), concentrations calculated using the Beer Lambert's law and the yield calculated as follows;

Mass of TRS (mg) = TRS concentration in sample (mg mL^{-1}) × Volume of reaction mixture (mL) × dilution factor

$$\text{TRS yield } (mg\ g^{-1}) = \frac{\text{Mass of TRS (mg)}}{\text{Mass of cellulose (g)}} \qquad \text{Equation 3.9}$$

3.4.11 Brunauer-Emmett-Teller (BET)

Brunauer-Emmett-Teller (BET) method was used to determine the surface area and pore volume of the untreated and pre-treated biomass. The sample (90mg) was first degassed overnight at 95ºC under vacuum (10^-6 Pa). The analysis was carried out using the NOVA-2200 BET surface analyser Quantachrome where the degassed sample was injected into the BET measurement unit and cooled down to 77K, followed by nitrogen injection at different pressures (6-point pressure measurement) to determine the nitrogen displacement (Contescu et al., 2018). Quantification of the surface area and pore volume was done using the instrument's software (NOVAWin).

3.5 Energy consumption of equipment

The energy consumed by the ultrasound equipment used for pre-treatment was calculated using equation 3.10 (Patil et al., 2012)

$$E_{\text{sonication (kWh } kg^{-1})} = \frac{\text{power consumed by equipment(kW)} \times \text{Pre-treatment time (h)}}{\text{Volume } (m^3) \times \text{total solid concentration (kg } m^{-3})} \quad \text{Equation 3.10}$$

Energy consumed by the microwave reactor is calculated from microwave power and running time (heating up time and holding time) using Joules's law (Equation 3-11) (Shao et al., 2019)

$$Input\ energy\ (MJ) = P \times (t_1 + t_2) \times 0.6 \quad \text{Equation 3.11}$$

Where P is power (W), t_1 is heating up time (min), t_2 is holding time (min) and "0.6" is a conversion factor considering the units of input energy, power and time.

Energy consumed by equipment such as reactor, evaporator, rotary vacuum dryer were calculated using the heat energy equations (Equation 3.12)

$$Q = mC_p\Delta T \quad \text{Equation 3.12}$$

Where Q= heat energy (J), m= mass (Kg), Cp= specific heat capacity (J $kg^{-1}{}^{o}C^{-1}$), ΔT = change in temperature (^{o}C).

3.6 Economic analysis

The capital and operating costs of co-production of HMF, furfural and lignin from spelt husk against co-production of HMF and furfural without lignin were examined and a cost-effectiveness analysis was conducted to analyse the economic performance of the system. A plant size of 100metric tonnes per day of spelt husk was considered for a working period of 320 days per year of production, 40 days per year for plant maintenance and an operating period of 20 years.

The techno-economic analysis reported is based on the n^{th}-plant economics assumptions (Table 3.4) meaning the process technologies used in the design have been successfully established in industries. The depreciation of the process equipment was calculated using the linear method (León et al., 2020) and income tax rate of 21% was considered for United Kingdom in accordance with UK corporation tax (Grasham et al., 2022).

Table 3.4: General economic assumptions (n^{th}-plant assumptions) and cost factors

Variable	**Assumptions**
Financing	100% equity
Plant life	20 years
Plant depreciation period	6 years
Discounted rate	5%
Start-up time: Revenue (% of normal) Variable cost (% of normal) Fixed cost (% of normal)	0.5 years 50% 75% 100%
Construction period: First 12 months expenditure (%) Second 12 months expenditure (%) Last 12 months expenditure (%)	3 years 8% 60% 32%
Income tax rate	21%
Working capital	15% of fixed cost
Land purchase	6% of total purchased equipment cost
Plant availability	320 days per year

3.6.1 Total capital cost

The total capital investment cost is the sum of all direct costs (including installed equipment cost, piping, electricals, instrumentation etc) indirect costs (engineering, supervision, legal expenses and contingency) and working capital (León et al., 2020).

The individual cost of equipment was obtained from the internet (www.matches.com), chemical engineering textbooks (Peters and Timmerhaus, 1991) and the literature (Gholami et al., 2021, Jiang et al., 2020, Kim et al., 2020, Davies et al., 2020). The total equipment cost was estimated using equations 3-13 and 3-14 (Ng and Martinez-Hernandez, 2020). This cost was then multiplied by lang factor for solid-liquid processing plants to determine the total capital cost.

The purchased equipment cost for the current plant capacity was estimated by using costs and capacity obtained from the literature and converting it to cost of present plant capacity (Equation 3.13).

$$\frac{\text{COST}_{\text{size 2}}}{\text{COST}_{\text{size 1}}} = \left(\frac{\text{Size}_2}{\text{Size}_1}\right)^{\text{R}}$$ Equation 3.13

Where; Size_1 is the old capacity, Size_2 is the new capacity, $\text{COST}_{\text{size1}}$ is the cost of the old capacity, $\text{COST}_{\text{size2}}$ is the cost of the new capacity, R is the scaling factor, taking as 0.6 (six-tenth-factor rule)

The purchased equipment cost was converted to present year (Equation 3.14) using the chemical engineering plant cost index (CEPCI)

$$\text{C}_\text{p} = \text{C}_\text{o}\left(\frac{\text{I}_\text{p}}{\text{I}_\text{o}}\right)$$ Equation 3.14

Where; C_p is the present cost of equipment, C_o is the original cost of equipment, I_p is the present plant index value, I_o is the original index value.

3.6.2 Total production cost

The total production cost consists of variable and fixed operating cost. The variable operating cost was calculated from raw material cost and utility cost. While, the fixed cost was calculated from operating labour cost, general safety engineering, plant maintenance and general overhead.

Raw material cost

Raw material usage was obtained from the material balance of the process which was then multiplied by the individual prices of the individual raw materials to obtain the total annual raw material cost. The individual raw material prices were obtained from the internet (www.Alibaba.com) and from the literature (Kim et al., 2020, Jiang et al., 2020, Yan et al., 2020).

Utility cost

Utility cost for this work were electricity and waste-water treatment. Electricity costs were obtained by multiplying the total energy consumption of the equipment by the electricity cost per kWh (\$0.06 kW h^{-1}) While the waste-water treatment was assumed to be 35% of maintenance costs (León et al., 2020).

Operating labour cost:

The operating labour for the plant was calculated from Equation 3.15

$N_{OL} = (6.29 + 31.7P^2 + 0.23N_{np})^{0.5}$ Equation 3.15

Where N_{OL} is the number of operators in every shift, P is the number of processing steps including solid handling such as transport, particle size reduction etc. and N_{np} is the number of processing steps including compression, heating, cooling, mixing, separation etc. for the process, 320 days of annual operation was used with employee pay of 19.8USD/employee hour (León et al., 2020).

3.6.3 Annual revenue calculation

The annual revenue (Equation 3.16) was calculated from production rate of the products per year multiplied by current market prices obtained from Kuznetsov et al., (2020), van Putten et al., (2013), Kim et al., (2021). Once the revenue was obtained, the annual profit (Equation 3-17) was calculated by subtracting the total production cost from annual revenue (Gómez Millán et al., 2021, Hossain et al., 2019).

Revenue ($ yr^{-1}) = product yields (kg yr^{-1}) × current price of product ($ kg^{-1}) Equation 3.16

Annual profit ($ yr^{-1}) = Revenue – total production cost Equation 3.17

3.6.4 Minimum fuel selling price (MFSP)

The minimum selling price was obtained using Equation 3.18 (Ng and Martinez-Hernandez, 2020)

$$MFSP = \frac{(TOC+ACC)}{Annual\ product\ yield}$$ Equation 3.18

Where TOC = total operating cost and ACC = annualised capital cost.

Annualised capital cost was calculated using Equation 3.19 (Ng and Martinez-Hernandez, 2020)

ACC = TCI * CRF Equation 3.19

Where TCI = total capital cost and CRF = capital recovery factor.

Capital recovery factor was calculated using equation 3-20 (Ng and Martinez-Hernandez, 2020)

$$CRF = \frac{r(1+r)^n}{(1+r)^n - 1}$$ Equation 3.20

Where r = the discounted rate and n = plant life span

3.6.5 Sensitivity analysis

Sensitivity analysis of the impact of economic parameters such as feedstock price, variable operating costs, furfural yield, total capital investment and DMSO price were included in the analysis. The MFSP was measured for 20% change in the value of each critical parameter while keeping the other variables constant.

Chapter 4: Design and characterisation of an energy efficient cold plasma ozone generator.

4.1 Introduction

The production of ozone is gaining increasing attention as it is used in many applications e.g. disinfection, food processing, bleaching of paper pulp, waste-water treatment (Pandiselvam et al., 2017) biomass pre-treatment (Ibrahim et al., 2021) etc. However, drawbacks with the use of ozone for large-scale industrial applications are associated with high energy demand and high costs for generating the ozone *in situ* as it cannot be stored due to its short life-time and high reactivity (Travaini et al., 2016). This drawback can be mitigated by creating an ozone generator that produces a high concentration of ozone with reduced energy consumption thereby reducing the overall running cost of the process. This chapter aims to design and characterise an energy efficient ozone generator using cold plasma technology on the basis that ozone can be generated with 30% less energy via cold plasma technology compared to previous methods, thereby prompting a new wave of exploration (Schultz-Jensen et al., 2011a). This chapter is in a paper submitted to journal of Chemical Engineering and Processing – Process Intensification.

4.2 Plasma reactor design

In a bid to develop a cost and energy efficient ozone generator, an ozone generator reactor (plasma DBD reactor) was developed using low-cost materials such as quartz glass and stainless-steel mesh. The dielectric material used to make the U-tube DBD reactor (Fig. 4.1) consists of quartz glass of 150mm length on both sides, width of 90mm, inner diameter of 20mm and outer diameter of 22mm. The electrodes (inner and outer) were made up of 316 stainless steel mesh with a diameter of 20mm and length of 60mm. The electrodes are in contact with either side of the dielectric material (quartz glass) causing a discharge to occur on the surface**.** High voltage wires were connected to a variable AC power supply of 0 – 240 volts providing a voltage of 1 – 10kV utilizing a power of 5 - 40 watts. The u-tube shaped ozone reactor was placed in a container with water/ice to regulate the temperature during ozone generation.

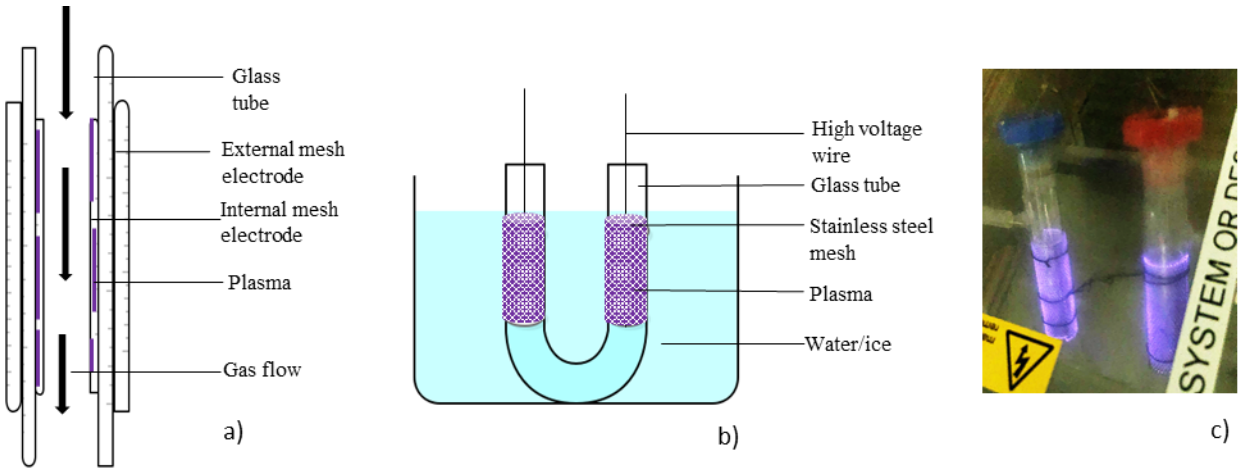

Fig 4.1: Double surface plasma zone u-tube ozone generator reactor a) 2-d configuration b) design c) picture of reactor.

4.2.1 Effect of power and reactor configuration

At a power of 8W the amount of ozone produced and concentration for the two-zone plasma (TZP) was 2.5 times higher (118.8 mgh^{-1} vs 324 mgh^{-1} and 19.8 gm^{-3} vs 51.4 gm^{-3} respectively) than for the single zone plasma (SPZ) reactor (Fig. 4.1 a&b). The two-zone plasma reactor provides an increased surface area for unreacted oxygen flowing through the first plasma zone thus enhancing the amount and concentration of ozone generated. In addition, at a fixed oxygen flow rate input (100 mL min^{-1}), the optimum rate of ozone production (118.8 vs 332 mgh^{-1}) and concentration (19.8 vs 58 g m^{-3}) for SZP and TZP were achieved at a power input of 8W and 13W, respectively. A further increase in power consumption (above 8W and 13W for SZP and TZP respectively) led to a rapid decrease in the amount and concentration of ozone produced (Fig. 4.1a&b). This is likely because increased heat obtained from the high energy electrons and dielectric heating (Saleem et al., 2019) produced at higher power level slows down ozone formation and results in the conversion of ozone back to oxygen. As ozone is very sensitive to temperature where it slowly decomposes (in minutes) at ambient temperature and rapidly (<1 second) at higher temperature (Salam et al., 2013), there is therefore the need for a cooling system for the ozone generator to mitigate the effect of increasing temperature.

It is important to note that at the same voltage, the power consumption of TZP was below two times the power consumption of SZP implying that the TZP was more energy efficient than SZP achieving 2.5 times increase in ozone concentration and amount generated. For example, at a voltage of 5kV the amount of power consumed by the TZP reactor was 1.7 times higher (17.7 vs 31.7 W) than for the SZP (Fig 4.1c).

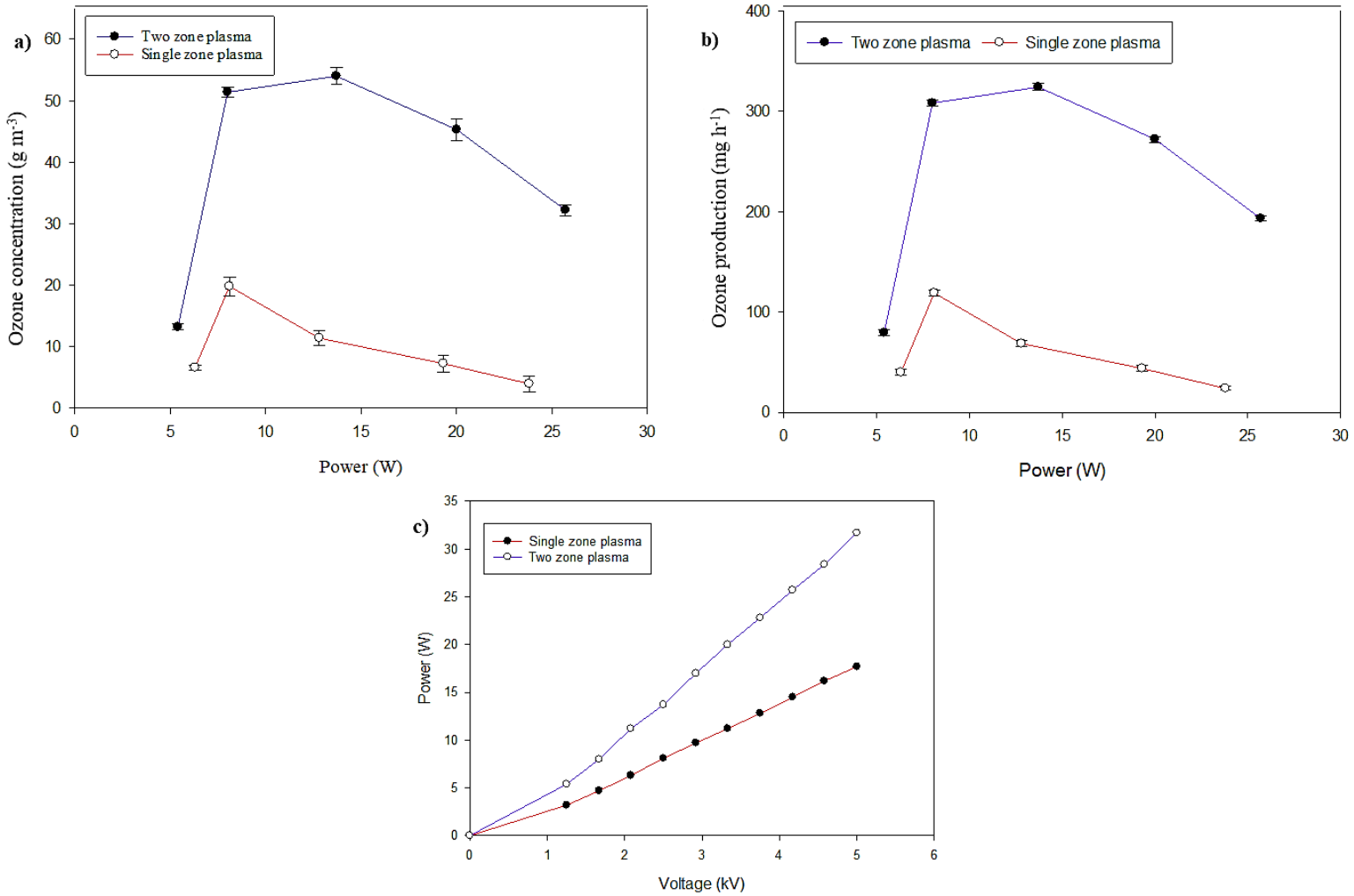

Fig 4.2: Comparison of single and two-zone plasma reactors for power consumption with respect to; a) ozone concentration, b) ozone production with a 0.1 L min^{-1} oxygen flow rate for 10 min without cooling and c) voltage applied.

In addition, higher ozone amount and concentration for the TZP was observed as unreacted oxygen and/or decomposed ozone from the first plasma zone passes through the second zone for recombination into ozone hence increasing ozone generation efficiency. Similarly, Li et. al. (2018) observed a higher ozone concentration of 56.2 g Nm^{-3} for double surface DBD having two plasma zones at the top and bottom of a horizontal reactor than 28 g Nm^{-3} ozone concentration for a single plasma zone of a horizontal reactor at a power of 3000 J L^{-1}.

4.2.3 Effect of cooling conditions.

To minimise the decomposition of ozone at high power input (> 13W) in the DPZ system, the U-shaped reactor was placed in either a water (18°C) or water/ice (0°C) bath to provide a cooling effect and maintain a steady reactor temperature. At high power input of 13W, the ozone concentration increased from 54.0 g m^{-3} (air) to 112.2 g m^{-3} (water) and 117.6 g m^{-3} (ice), and the amount of ozone generated increased from 324.0 mg h^{-1} (air) to 673.2 mg h^{-1} (water) and 705.0 mg h^{-1} (ice) (Fig 4.3). At power input >13W both the ozone concentration and amount generated stabilised because of constant removal of heat from the reactor by the cooling water or ice. According to Equations 2.3 & 2.4, (Section 2.4), every oxygen atom obtained from the splitting of an oxygen molecule by energetic electrons from the plasma field leads to formation of one ozone molecule, with an increase in input power, more ozone molecules are formed because of an increase in oxygen atoms. At a further increase in power input (above the optimum), the temperature increases, and rate of ozone formation slows down. Simultaneously, a strong micro discharge in the discharge gap takes place at increased power and the oxygen atoms reach an undesired concentration and start to destroy the already formed ozone molecules (Equation 2.5) (Chen et al., 2008, Jodpimai et al., 2015) and the ozone destruction reaction shows a strong temperature dependence (Chen et al., 2008, Brueggemann et al., 2017).

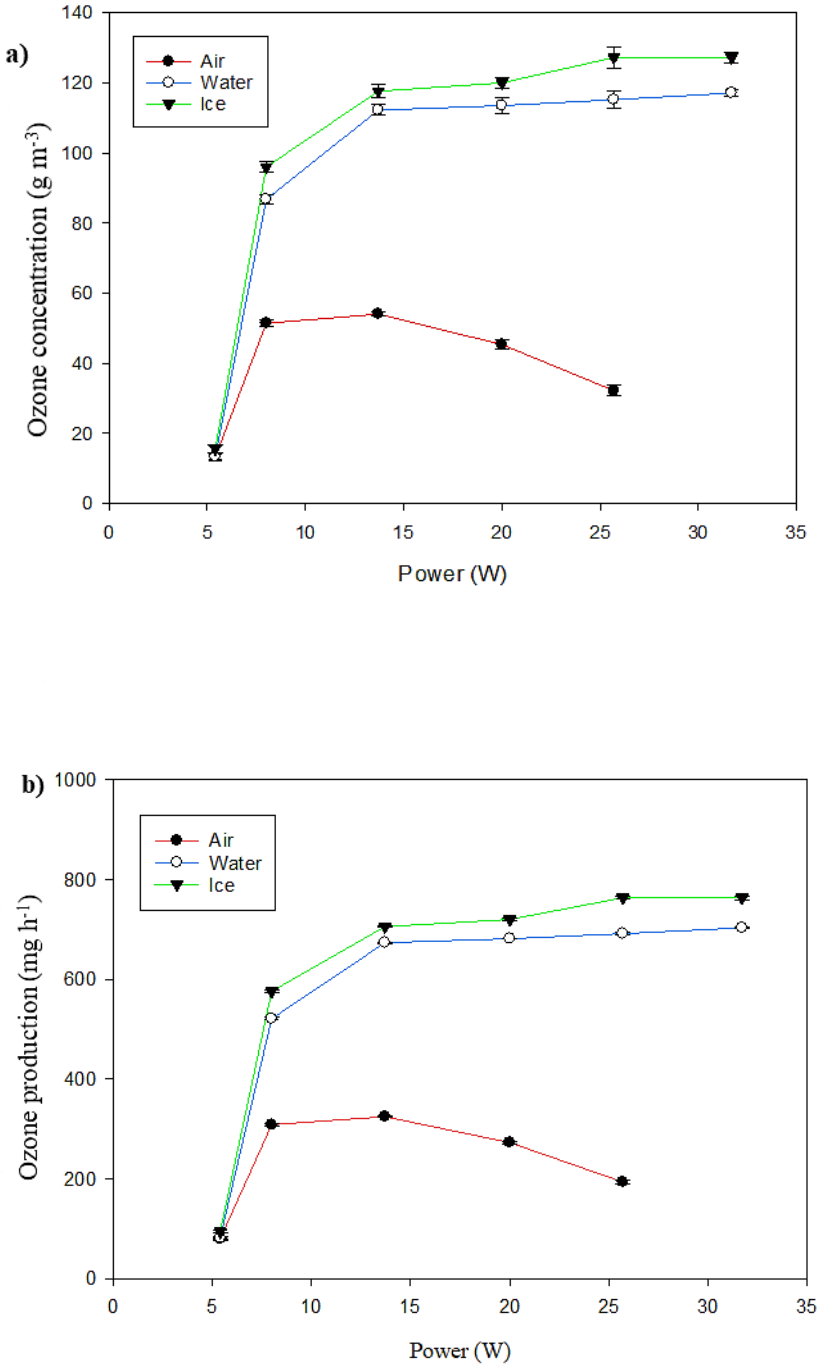

Fig 4.3: The effect of cooling with water and ice on; a) ozone concentration and b) ozone production for the double surface plasma (DSP) zone ozone reactor with a 0.1 L min^{-1} oxygen flow rate for 10 min.

The process of heat removal from the ozone reactor involves heat conduction from the discharge gap through the gas layer to the dielectric and stainless-steel mesh (electrode) and then to the cooling water (Brueggemann et al., 2017). Having measured the cooling water temperature or wall temperature (reaction without cooling) during ozone generation at varying power input levels. The average wall temperature when cooling was applied was 15 - 30°C lower than without cooling (Table 4.1) showing that removal of heat led to a lowering of the temperature in the tube thereby increasing the rate of ozone formation. When energy is introduced into the system for ozone generation, only about 10-20% of energy introduced into the system is utilised for ozone synthesis, the rest 80% is dissipated as heat (Fridman, 2008). To achieve ozone stability the heat should be removed rapidly. Without cooling, the temperature of the system increases favouring decomposition reaction of ozone, which is exothermic, this decomposition reaction becomes significantly faster than ozone formation reaction leading to a decrease in total ozone concentration. The reaction rate of ozone decomposition is 6 – 8 times faster than the dissociation rate of oxygen molecules (Fridman, 2008). Furthermore, when cooling is applied to the system, the temperature is maintained below ambient temperature (Table 4.1) and increase in power led to production of more oxygen radical to produce more ozone thus slowing down the ozone decomposition reaction thereby producing a relatively stable ozone concentration.

Table 4.1: Reactor wall temperature (T) and ozone produced in the two -zone ozone generator from oxygen at increasing power levels with and without cooling.

Power (W)	**T (°C) no cooling**	**T (°C) with cooling (water at 18°C)**	**Ozone produced (mg h^{-1}) without cooling**	**Ozone produced (mg h^{-1}) with cooling (water at 18°C)**
5.4	32.0	18.5	79.2	81.0
8	35.4	18.8	308.2	520.8
13.7	41.2	20.3	324.1	673.2
20	45.1	20.9	272.0	681.1
25.7	55.3	22.4	193.2	691.4

4.3.3 Effect of flow rate

At a constant power input of 8W in the TZP there was a decrease in ozone concentration as flow rate was increased from 0.05 to 0.25 $Lmin^{-1}$ (Fig 4.4a) likely due to reduced time available for collisions between oxygen atoms and electrons within the plasma zone (Brueggemann et al., 2017, Jodpimai et al., 2015). The greater the number of particles in an ionisation zone, the lower the energy of collision leading to reduced dissociation of oxygen and hence recombination to form ozone (Brueggemann et al., 2017).

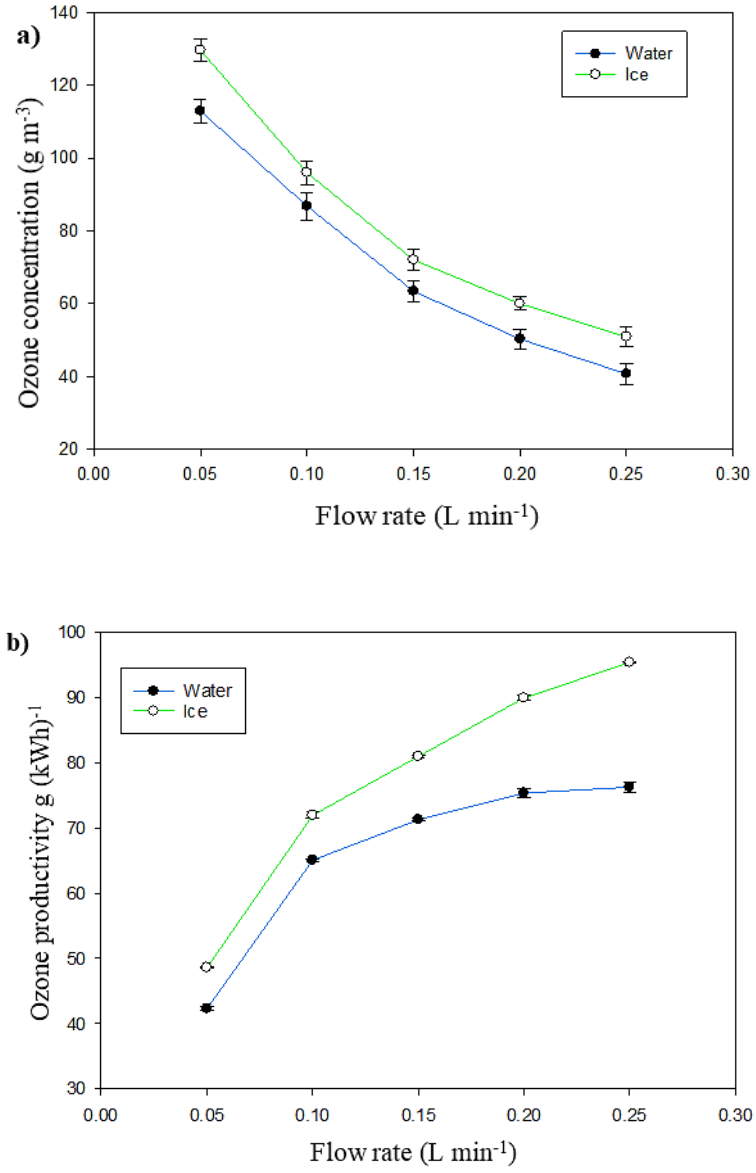

Fig 4.4: Effect of oxygen flow rate on; a) ozone concentration b) ozone production at a constant power input of 8W for 10min.

Plasma density is the concentration of ionised gas particles in each volume. At high plasma density, concentration of atomic oxygen is high. when the relative concentration of O/O_2 is higher than 0.3 – 0.5% (Eliasson and Kogelschatz, 1991), ozone production is reduced due to undesired three body recombination of the atomic oxygen to form molecular oxygen as well as destruction of already formed ozone.

4.3.4 Effect of packing material

Catalytic (TiO_2 and SiO_2 pellets) and non-catalytic (glass bead) packing materials were added to the reactor gap to provide turbulence to the flow of oxygen and increase the contact between oxygen and the plasma zone. In surface plasma, the reaction occurs on the surface between the electrode and dielectrics at a solid-gas interface, these increases the ionisation in the plasma due to interaction of plasma with the solid surface owing to additional electrons coming from the surface. The small glass beads led to an enhanced electric field near the contact points leading to more electrons available for collision with oxygen molecules to form oxygen atoms (the precursor for ozone formation) (Liang Chen et al., 2006), The addition of small glass beads (2.0mm) increased the ozone concentration by 20 g m^{-3} and rate by 100 mg h^{-1} because of a reduction in the active surface area thereby reducing the potential reaction between oxygen and the plasma surface. Furthermore, the addition of glass beads increased the surface area leading to enhanced ozone formation as the glass beads provide an additional surface for Equation 2.3 & 2.4 (Section 2.4). This in turn led to an increase in power efficiency by 18 g $(kWh)^{-1}$ with a higher concentration (120 vs 96 g m^{-3}) and amount of ozone (720 vs 576 mg h^{-1}) produced at the same power input when compared to the reactor without glass beads (Fig 4.5). In the reactor without packing material, more oxygen flows out of the plasma zone without reaction on the surface of the dielectric.

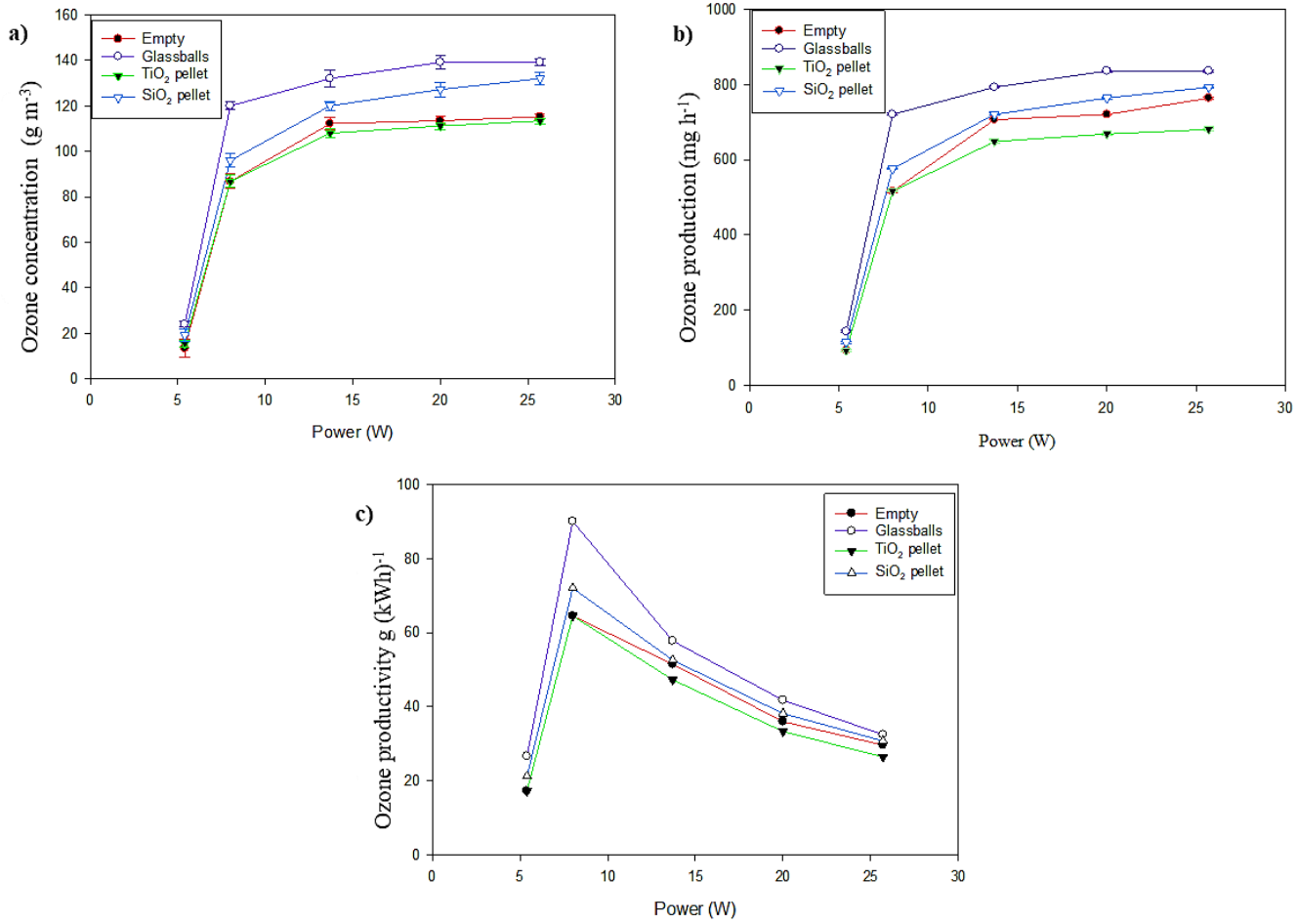

Fig 4.5: Glass bead packing material used together with effects of their addition on; a) ozone concentration, b) rate of ozone produced and c) ozone production. Conditions used were 0.1 L min^{-1} oxygen flow rate for 10 min with ice cooling.

It is known that the amount of nitrogen in the oxygen gas used for ozone generation can affect the catalytic activity of any photocatalysts used (Seok et al., 2015). UV light emitted in the discharge gap is due to the transition of nitrogen from a high energy state to a lower energy state. SiO_2 and TiO_2 used as packing materials in this work have high band gap energy of 8.9 and 3.2eV respectively which means they need a very high energy level to activate their photocatalytic activity. The oxygen gas used for this study had a purity of 99.9% with a very low nitrogen content (<500 ppm) thereby with little potential to cause inactivation of the photocatalytic effects of SiO_2 and TiO_2. The addition of SiO_2 increased the ozone concentration from 117 ± 1.50 to 120 ± 2.2 g m^{-3} when compared to the reactor without packing material while the addition of TiO_2 pellets resulted in a slight decrease to 108 ± 1.30 g m^{-3} (Fig 4.6). The slight decrease in ozone concentration in the case of TiO_2 can be attributed to its high dielectric constant (86) (Pekárek et al., 2016). A high dielectric constant causes an increase in the electric field with higher power input producing a localised heating that leads to the destruction of ozone. SiO_2 and glass beads with much lower dielectric constants of 3.9 (Wei et al., 2020) and 3.5 (Liang Chen et al., 2006) respectively exhibited the opposite effect resulting in a reduction in ozone formation and concentration. For each ozone reactor, there exists an optimum value of dielectric constant that favours ozone generation. Ogata et. al., (1991) observed that ozone production was minimal when $BaTiO_3$ pellets (of dielectric constant 660) were used as a packing material. Similarly, Holzer et. al. (2005) observed that higher ozone concentration (200 ppm) was achieved with a DBD reactor without packing material than for a reactor with $BaTiO_3$ pellets (with dielectric constant of 5000).

The size and shape of the glass bead, TiO_2 and SiO_2 used as packing materials had a significant effect on the ozone concentration and generation efficiency. Spherical 2 mm glass beads were used in comparison to the larger 3.18 mm diameter cylindrical shaped TiO_2 and SiO_2 pellets. The smaller the diameter of the substrate, the greater the surface area available which increases the possibility of a micro discharge and collisions between the oxygen molecules. In addition, Al-Abduly et al., (2020) packed an ozone generator with cylindrical aluminium pellets (2 and 3 mm), spherical glass beads (2 mm), spherical molecular sieve beads (2 mm) and spherical soda-lime beads (3 mm) and observed that irrespective of the size of the packing material, spherical packing material was more effective for ozone generation than cylindrical shaped materials. Chen et al., (2008) packed an ozone generator with glass beads (2, 3, and 5 mm) and Al_2O_3 pellets (2, 5 and 10 mm), and observed maximum ozone production with the smaller pellets i.e. 2 mm. Hence for the reactor used in this study, the maximum ozone concentration

140 g m^{-3} was achieved with 2mm glass beads at low power input of 8W and oxygen flow rate of 0.1 L min^{-1}. when compared with other literature (Table 4.2), the ozone generator used in this work will be suitable for many industrial applications due to the cost effectiveness of ozone generation with low oxygen and power consumption. A higher concentration of ozone means that a lower volume will be needed for industrial applications. Therefore, the scalability of the ozone generator is potentially attractive due to its ease of construction, and inexpensive materials used as it is a compact design that saves equipment space with multiple plasma zones arranged in parallel to generate a higher amount of ozone than a single zone with increased discharge length due to the synergistic effect of the multiple zones. For example, two zone generates 2.5 times more ozone (section 4.2.1) than doubling the length of a single zone plasma. Using a long length increases the residence time of ozone in the reactor thereby enhancing other side reactions that lead to ozone destruction thereby reducing the ozone concentration and efficiency.

Table 4.2: Comparison of different reactor configurations from the literature for ozone concentration and productivity.

Discharge	**Dielectric**	**Packing material diameter (mm)**	**Oxygen flow rate (L min^{-1})**	**Ozone conc. (g m^{-3})**	**Productivity (g $kw^{-1}h^{-1}$)**	**Voltage (KV)**	**Power (W)**	**Reference**
Cylinder -cylinder	Glass tube	-	0.12 (air)	8	46	8	5	Fang et al., 2008
Fence like copper foil (DSDBD)	Al_2O_3 plate	-	0.1	48.3	108.7	-	5	Li et al., 2018a
Cylinder-cylinder Packed with SiO_2 pellets	Glass tube	1.25	0.5	130	83.3	-	6.4	Schmidt-Szałowski et al., 1990
Cylinder – cylinder packed with Al_2O_3 pellets	Glass tube	2.00	1	61	173	15	15.6	Liang Chen et al., 2006
Cylinder – cylinder packed with glass beads	Glass tube	2.00	0.06	152	108	-	34.6	Al-Abduly et al., 2020
Cylinder-cylinder Packed with glass beads	Glass tube	2.00	0.1	140	90	2.5	8	Current study (our work)

4.4 Summary

Higher ozone concentration and amount (2.5 times) was achieved using a two-zone compared with a single- zone plasma reactor. A maximum ozone concentration of 140 gm^{-3} and 90 g $(kWh)^{-1}$ productivity were obtained from the two-zone system, which is comparable to commercial ozone generators but with 30 – 40% lower power consumption (11 kWh kg^{-1} O_3). Cooling of the generator led to a decrease in gas temperature in the reactor leading to an increase in ozone concentration at low power input. Mitigating the drawbacks of high cost of ozone generation associated with its industrial applications such as biorefineries, waste-water treatment and the textile industries, as high concentration of ozone is produced with lower power and oxygen consumption.

Chapter 5: Pre-treatment and fractionation of residual lignin from agricultural residues.

5.1 Introduction

Oxidative pre-treatment such as ozone assisted has recently gained attention due to its high reactivity at ambient temperature and pressure without decomposing the cellulose and hemicellulose fractions. To date, pre-treatment has largely focused on conversion of the cellulose and hemicellulose fractions to biofuels, leaving lignin as a residue. However, only using hemicellulose/cellulose for ethanol or platform chemical production is not economic due to the high energy and costs required to produce ozone. Therefore, integrating lignin valorisation with biofuel production is needed to increase the profitability and sustainability of the bio-refinery process.

The aim of this chapter is to evaluate the oxidative effect of intensified ozone pre-treatment and fractionation compared to alkaline hydrogen peroxide pre-treatment on agricultural residues. This will be achieved by:

- Intensifying ozone pre-treatment by incorporating ultrasound to improve ozone mass transfer.
- Subjecting ozone pre-treated spelt husk and corn cob agricultural residues to organosolv fractionation with the yield and purity of components assessed.
- Evaluate the structure and composition of the resultant lignin and cellulose for potential use in downstream chemical production.
- Compare the effect of ozone and hydrogen peroxide pre-treatment on cellulose composition and structure.
- Propose a mechanism for the pre-treatment and fractionation reaction.

Part of this chapter has been published in Chemical Engineering and Processing–process Intensification Journal, 159, 108231 (Appendix A1).

5.2 Intensification of ozone pre-treatment.

In addition to improving the economics of ozone pre-treatment through reduction of ozone production costs via the design of an energy-efficient ozone generator (Chapter 4), it is important to enhance sugar production for platform chemicals through increased lignin separation via ozonolysis. This could be achieved through increasing contact of ozone with

biomass particles to improve the ozone-lignin reaction (Wan Omar and Amin, 2016). Binder et. al., (1980) and Vidal and Molinier (1988) showed that a conventional magnetic stirrer was ineffective for adequate mass transfer leading to low ozone consumption which in turn leads to low lignin separation and low sugar recovery.

5.2.1 Ultrasound-assisted ozone pre-treatment.

Including ultrasound in the ozone pre-treatment of corn cobs enhanced the mixing between biomass and ozone, resulting in an increase in ozone consumption from 0.24 to 0.39g O_3 g^{-1} corn cob with a 38.5% decrease in the acid insoluble lignin concentration from 52 to 32 mg g^{-1} compared to using ozone only. This is because ultrasound increases the diffusion of ozone into the feedstock, most likely via the creation of a pressure difference resulting in pressure waves passing through the liquid leading to formation of bubbles. The bubbles grow and then collapse resulting in the re-distribution of molecules around the bubbles to other parts of the feedstock, this results in formation of microjets that penetrate/break cell walls and increase the surface area of the substrate (Bussemaker and Zhang, 2013). The results in this study are similar to other studies (Vidal and Molinier, 1988a, Neely, 1984, Cesaro and Belgiorno, 2013) in which the lowest acid insoluble lignin content was achieved by increasing the contact with ozone. Vidal and Molinier (1988) ozone pre-treated popolar sawdust, achieving 66% reduction in AIL using a fixed-bed compared to a 22.5% reduction using a stirred tank reactor. Similarly, Cesaro and Belgiorno (2013) treated municipal solid waste and observed that more ozone (0.7 $gmin^{-1}$) reacted with the waste when using a bubble column reactor compared (0.2 $gmin^{-1}$) when a drechsel trap reactor was used, as a result of more effective surface contact between ozone and the substrate. To the best of our knowledge, this is the first study where ultrasound has been incorporated with ozone pre-treatment of biomass in a batch reactor to improve surface contact between ozone and the substrate.

From SEM images (Fig 5), it can be seen that untreated corn cob exhibited compact fibrillary morphology (Fig 5.1i) with intertwined fibres covering the cellulose while ozone pre-treatment alone (Fig 5.1ii) showed a looser fibrous network and disorganised morphology likely due to disruption of the cell wall structure. The fibre network following ozone with ultrasound pre-treatment (Fig 5.1iv) was more collapsed and separated with greater exposure of the inner part (cellulose) thereby accounting for the lower lignin content. Similar structural changes were

observed when sugarcane bagasse was treated with ozone (Souza-Corrêa et al., 2013, Travaini et al., 2013) and ozone-alkali mix (Bi et al., 2016)

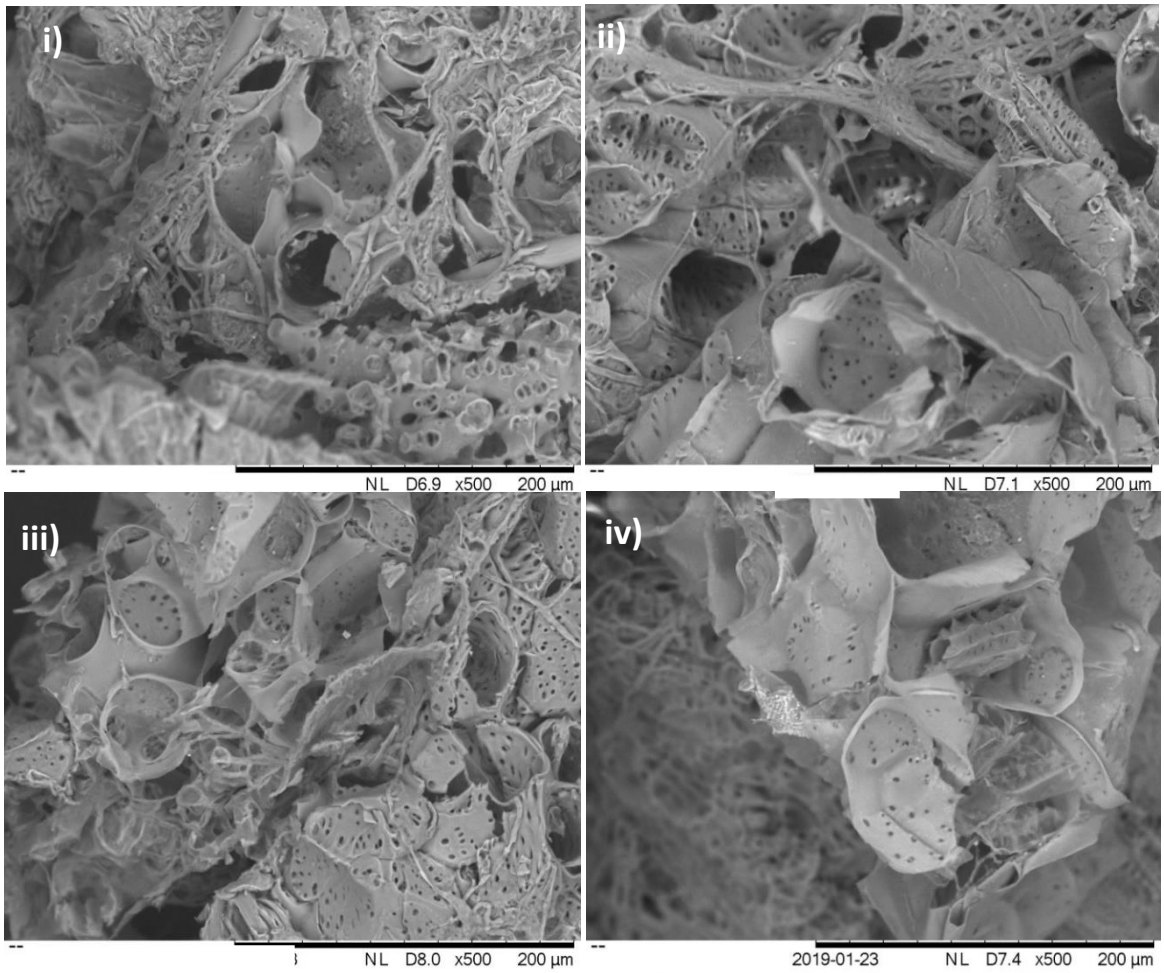

Fig 5.1: SEM images of corn cob; i) untreated, ii) pre-treated with ozone, iii) pre-treated with ultrasound and iv) pre-treated with ultrasound and ozone at ozone concentration of 2 wt % and pre-treatment time of 30 min.

Furthermore, the effect of pre-treatment on the surface area and pore volume of corn cob determined by Brunauer-Emmett-Teller (BET) analysis (Table 5.1) showed that all three pre-treatments resulted in both an increase in surface area and pore volume of corn cob. Ozone pre-treatment in combination with ultrasound showed the highest surface area and pore volume of 17.5 m^2g^{-1} and 0.0065 cm^3g^{-1} respectively due to increased lignin-carbohydrate link disruption within the lignocellulose matrix. A similar increase in surface area and pore volume was

obtained for ozone pre-treated waste (magazine paper) from 70 m^2g^{-1} and 0.1 cm^3g^{-1} to 95 m^2g^{-1} and 0.125 cm^3g^{-1} respectively (Kojima and Yoon, 2008).

Table 5.1: Surface area and pore volume of untreated and pre-treated corn cob.

Sample of corn cob	**Surface area (m^2g^{-1})**	**Pore volume (cm^3g^{-1})**
Untreated	9.8	0.0037
Ozone pre-treated	15	0.0056
Ultrasound pre-treated	11	0.0042
Ozone/ultrasound pre-treated	17.5	0.0065

5.2.2 Effect of pre-treatment time

Pre-treatment time above 30 min for both ozone and ultrasound had a negligible effect on total lignin (acid insoluble + acid soluble lignin) recovery. From the reaction mechanism (Reaction 5.1, Section 5.7) electron deficient ozone can access the electron rich aromatic bonds of lignin as long as ozone can penetrate the biomass which in this case was aided by the use of ultrasound. After this initial reaction the available aromatic bonds decline leading to a small and non-significant decrease in acid insoluble lignin and increase in acid soluble lignin content. Incorporation of ultrasound in the pre-treatment led to a shorter peak reaction time (30 min) compared with 360 min for poplar sawdust (Vidal and Molinier, 1988b) 150 min for wheat and rye straw (García-Cubero et al., 2009) and 120 min for sugarcane bagasse (Travaini et al., 2016) when using ozone alone in a fixed-bed reactor.

5.2.3 Effect of moisture content

Feedstock moisture content has been reported as the most important character influencing ozone pre-treatment (Neely, 1984, García-Cubero et al., 2009, Mamleeva et al., 2009, Travaini et al., 2016) because it serves as a medium to aid ozone movement within the feedstock as well as affecting the concentration of ozone and of generated radicals. However, optimum moisture content (MC) is feedstock specific. Feedstocks of varying moisture content (corn cobs 42.9%-100% and spelt husk 11%-100%) were pre-treated and showed that acid insoluble lignin

decreased (up to 66% MC for corn cob and 40% MC for spelt husk) with moisture content but then increased thereafter (Table 5.2). Acid soluble lignin (ASL) increased following reaction with ozone likely due to the insertion of hydrophilic groups from the lignin-carbohydrate complex (LCC) converting acid insoluble lignin (AIL) to acid soluble lignin (García-Cubero et al., 2009, Yu et al., 2011).The highest acid soluble lignin of 44.6 and 42.1 mg g^{-1} was achieved at 66% and 40% moisture content for corn cob and spelt husk corresponding to a total lignin recovery of 50.4 and 73.6% respectively (Table 5-2).

Table 5.2: Lignin fractions following ultrasound/ozone pre-treatment of spelt husk and corn cob with varying moisture content at an ozone concentration of 2 wt% for 30 mins.

Feedstock	**Moisture content (%)**	**Acid insoluble lignin (mg g^{-1})**	**Acid soluble lignin (mg g^{-1})**	**Total lignin (mg g^{-1})**	**Lignin recovery (%)**	**Glucose (mg g^{-1})**
Spelt husk	0	160.3 ± 0.1	32.7 ± 0.16	193.0	-	-
	11	84.0 ± 0.44	34.3 ± 0.05	118.3	61.1	1.23
	30	60.2 ± 0.28	38.9 ± 0.78	99.2	51.4	0.85
	40	55.2 ± 0.71	42.1 ± 0.54	97.3	50.4	1.41
	50	58.2 ± 0.88	39.5 ± 0.34	97.7	50.6	1.52
	70	61.6 ± 0.49	37.8 ± 0.29	99.4	51.5	1.17
	80	64.4 ± 0.13	36.9 ± 0.05	101.3	52.5	1.09
	100	70.0 ± 0.32	35.0 ± 0.34	105.0	54.4	1.00
Corn cob	0	51.0 ± 0.3	29.8 ± 0.49	80.8	-	-
	42.9	31.5 ± 0.08	34.8 ± 0.05	66.3	82.1	[1]ND
	51.7	22.2 ± 0.12	38.6 ± 0.41	60.8	75.2	ND
	57.98	15.3 ± 0.67	42.7 ± 0.12	58.0	71.8	ND
	66.02	14.9 ± 0.95	44.6 ± 0.17	59.5	73.6	<0.1
	72.02	16.7 ± 0.10	42.5 ± 0.54	59.2	73.3	ND
	82	21.3 ± 0.16	38.8 ± 0.77	60.1	74.4	ND
	100	35.3 ± 0.3	32.0 ± 0.42	67.3	83.3	ND

[1] ND means not detected

The loss of lignin during pre-treatment is likely due to the oxidation to low molecular weight compounds such as phenolics and carboxylic acids such as acetic acid, oxalic acid, formic acid and glycolic acid (lignin degradation products) (Fig 5.2). At a moisture content below the saturation point of the biomass (66% and 40% for corn cob and spelt husk respectively), there is a limited mass transfer of ozone which results in reduced reactivity with the substrate. However, at moisture contents above the saturation point, the biomass pores are blocked by a thick film of water leading to large residence time of ozone, therefore more ozone is decomposed without any positive contribution to the pre-treatment (Vidal and Molinier, 1988b, Mamleeva et al., 2009). The optimum moisture content for increasing the ozone reactivity is feedstock specific, e.g. 40-50% for Japanese Cedar sawdust (Sugimoto et al., 2009) 160% for Aspen sawdust (Nadezahda *et al*., 2009) and 90% for cotton stalk (Silverstein et al., 2007). Therefore, the saturation point of biomass/feedstock should be identified when using ozone assisted pre-treatment. Furthermore, it can be seen that at the moisture saturation point of biomass, the concentration of lignin degradation products is lowest (Fig 5.2) which is evident that lignin was solubilised rather than degraded. In contrast, at a higher moisture content there are competing reactions as reactive OH radicals are generated due to the excess moisture degrading lignin more than solubilizing it (Hoigne and Bader,1983: Traviani *et al.,* 2013). Mamleeva et. al., (2009) showed that oxidation of lignin (degradation of lignin) led to generation of oxyaromatics that are transformed into short chain aliphatic acids. The major degradation products generated from spelt husk were acetic, formic, glycolic and oxalic acids with the same acids generated for corn cob with the exception of glycolic acid, this may be due to differences in the type of lignin present in the feedstocks. Acetic, formic and oxalic acids were the major degradation products identified for ozonated wheat straw (Binder *et al.,* 1980) while for ozonated wood chips, acetic, formic, oxalic, tartaric and glyoxalic acids were identified (Ben'ko et al., 2013).

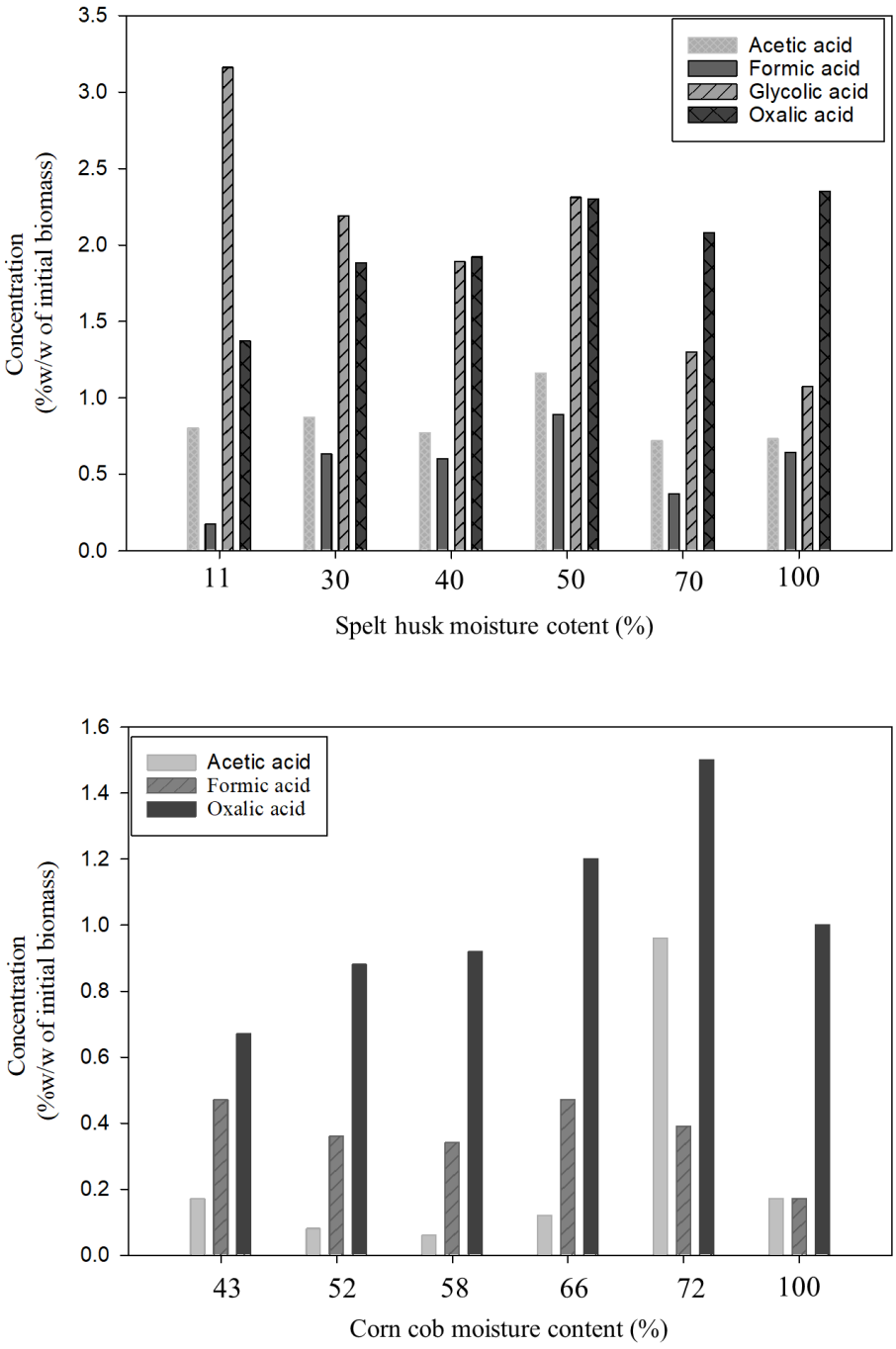

Fig 5.2: Major lignin degradation products obtained from; (a) ozonated spelt husk and (b) corn cob. At different moisture contents.

Furthermore, a low concentration of glucose (<2% wt/wt of the initial biomass) remained in the wash water with no trace of xylose, HMF and furfural detected (Table 5.2) indicating that only a small amount of cellulose was hydrolysed during pre-treatment. Therefore, it can be concluded that ozone assisted pre-treatment provides an approach where the cellulose and hemicellulose remain relatively intact (Schultz-Jensen *et al.*, 2013). This is one of the unique advantages of ozone pre-treatment over commercial pre-treatment alternatives such as steam explosion where substantial amounts (30-37%) of cellulose and hemicellulose are lost/solubilised in the process due to high temperature (200°C -220°C) and pressure (1 – 1.5 MPa) producing inhibitory products such as HMF and furfural which hinder subsequent hydrolysis (Nges *et al.*, 2016).

The SEM images of raw spelt husk (Fig 5.3 Ai) show a more densely packed structure than that of raw corn cob (Fig 5.3 Bi) which has a more loosely packed fibrous structure likely due to a higher lignin content. Following pre-treatment, SEM images of both feedstocks showed a more porous structure with an increased surface area resulting from the breakage of lignin bonds. The images with the widest pores ~15mm (Fig 5.3 A & B (iii)) correspond to the lowest acid insoluble lignin content showing a more open porous structure. A similar behaviour was also shown by Barros *et al.*, (2013) for ozone pre-treated sugarcane bagasse and straw.

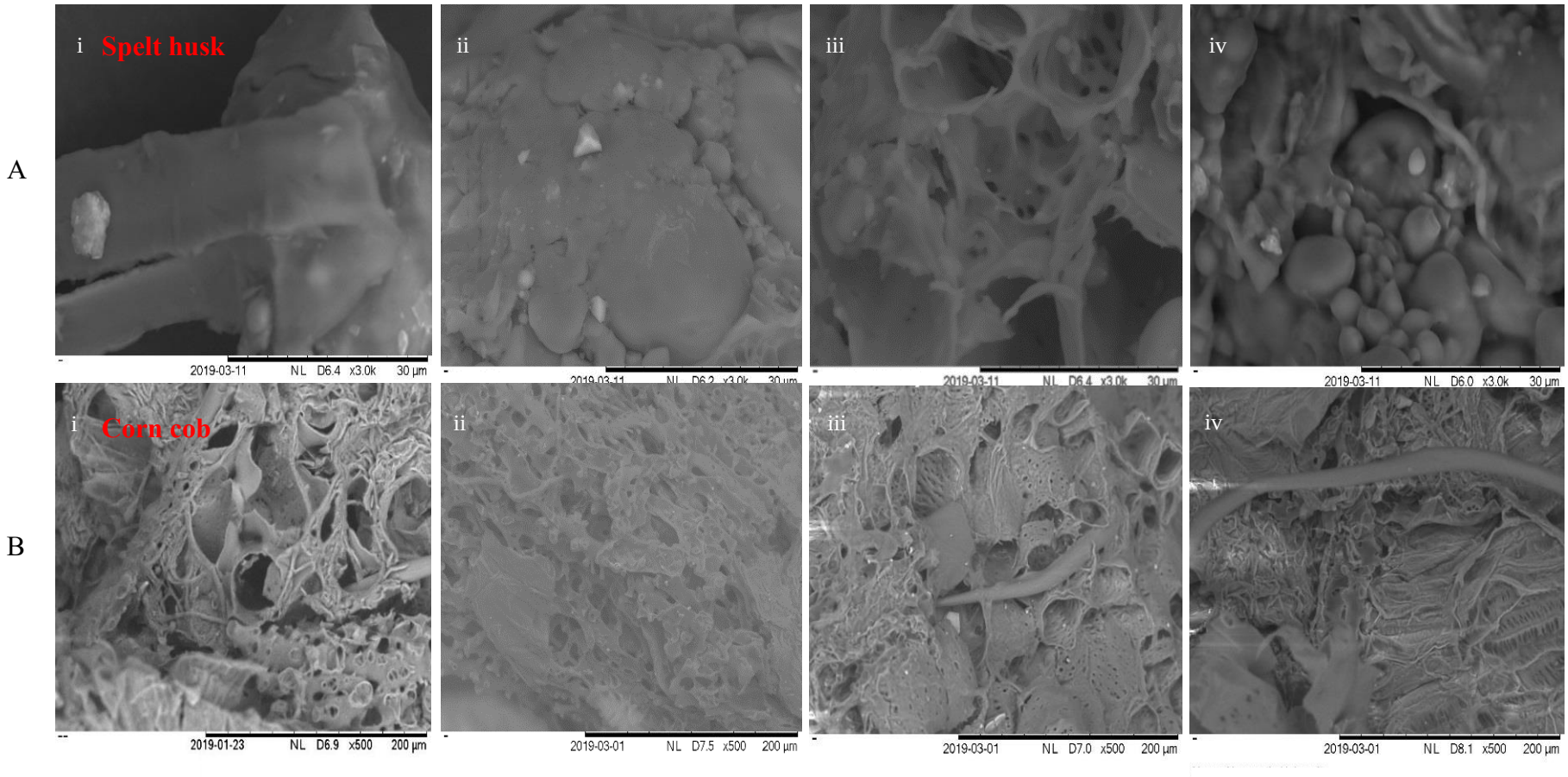

Fig 5.3. SEM images of; (A) spelt husk and (B) corn cob following ozone/ultrasound pre-treatment for 30 min at an ozone concentration of 2% mol mol^{-1} with varying feedstock moisture content: (i) raw, (ii) 11%, (iii) 40% and (iv) 50% for spelt husk and (i) raw, (ii) 42.91%, (iii) 66.02% and (iv) 100% for corn cob.

5.3 Fractionation of ozone pre-treated agricultural residues.

Typically, after pre-treatment, the resultant solid containing remainder of lignin, cellulose and hemicellulose is subjected directly to enzymatic or catalytic hydrolysis for further downstream processing to produce bioethanol or platform chemicals, leaving a low-quality lignin residue at the end of the process (Ragauskas et al., 2014). The low-quality lignin obtained due to irreversible adsorption of enzymes and fermentation components during enzymatic hydrolysis is often used as boiler fuel (Bozell, 2010) to improve the energy balance of the process.

Therefore, recovering high-quality lignin and converting it into high-value chemicals alongside the utilisation of cellulose and hemicellulose for biofuel and platform chemical production is of importance from an economic and sustainable perspective. Lignin, 15 – 25 wt% of lignocellulosic biomass, composing of aromatic compounds, can be used to produce low-cost carbon fibre (Baker and Rials, 2013) which can replace steel in the body of automobiles, used as a substitute for polymeric materials such as polyurethane foams, phenolic powder resins (Inone-Kauffmann, 2009) and a precursor for green diesel production through hydrogenation (Yuan et al., 2013). However, to achieve complete utilisation of all three structural components of the biomass to value-added products, it is necessary to simultaneously convert lignin alongside cellulose to phenolic derivatives or fractionate high quality lignin prior to the hydrolysis stage to prevent irreversible adsorption of hydrolytic enzymes, the breakdown of lignin, formation of unwanted by-products that deteriorates the properties of final product (Saini et al., 2016).

Conventional organosolv fractionation utilises mixture of organic solvents such as ethanol, acetic acid, methanol, formic acid etc. and water at a temperature of 150-200°C in the presence or absence of catalyst to separate individual biomass component (Matsakas et al., 2018, Sun et al., 2018). Ethanol is proven to be the most effective organosolv solvent to fractionate lignin due to its ease of recovery and low cost (Arato et al., 2005, Matsakas et al., 2018). Many previous studies have used an ethanol/water concentration of 60:40 for conventional organosolv pre-treatment at a temperature range of 150-200°C, 1% acid catalyst (HCl /H_2SO_4), 1-1.5MPa pressure to optimise carbohydrate and lignin recovery (Zhang et al., 2016a, Wildschut et al., 2013).

5.3.1 Effect of fractionation temperature and time

Ethanol fractionation of pre-treated biomass at a temperature above boiling point (80°C) and below boiling point (70°C) of ethanol in contrast to temperature range of 150-200°C (conventional organosolv) at different reaction times were examined to determine the best conditions for lignin and cellulose recovery as well as hemicellulose recovery from the liquid fraction. The goal was to fractionate at a low temperature to improve process cost and safety.

Ozone pre-treated feedstock at saturation moisture content (40% MC for spelt husk and 66% MC for corn cob) containing 55.2 and 14.9 mg g^{-1} of acid insoluble lignin respectively were fractionated with ethanol:water (60:40) at 80°C.

Cellulose pulp as a term used in this study refers to residual solid containing cellulose, hemicellulose, extractives, proteins, and remnant of lignin obtained after organosolv fractionation and filtration.

Increasing the reaction time from 60 to 180 min (Fig 5.4a), resulted in a greater lignin recovery from 35.1 - 41.7 mg g^{-1} (63.5 - 75.5%) and from 39.7– 51.8 mg g^{-1} (71.9 - 94%) for 70°C & 80°C temperatures respectively but then decreased to 26.7 and 46.9 mg g^{-1} (48.4 and 85%) respectively at 240 min. Cellulose pulp yields were slightly decreased from 60 to 180min from 779.5– 701.2 mg g^{-1} (91.5 to 82.3%) and then increased to 86.2% at 240min and 70^{o}C, while cellulose pulp yields decreased from 736.9– 695.2 mg g^{-1} (86.5 - 81.6%) with increasing reaction time from 60 – 180 min at 80^{oo}C. The increase in cellulose pulp yield at 240 min reaction time might be because of a re-polymerisation or recombination of reaction intermediates such as HO_2 radicals forming more solid residue hence leading to a pseudo-increased cellulose yield and decreased lignin recovery at the extended reaction time of 240 min. Furthermore, an increase in temperature from 70°C to 80°C led to an increase in lignin recovery and decrease in cellulose pulp yield because of increased hemicellulose hydrolysis at the higher temperature which shows that the concentration of water-soluble fractions increased 2 fold (Fig 5.4b)

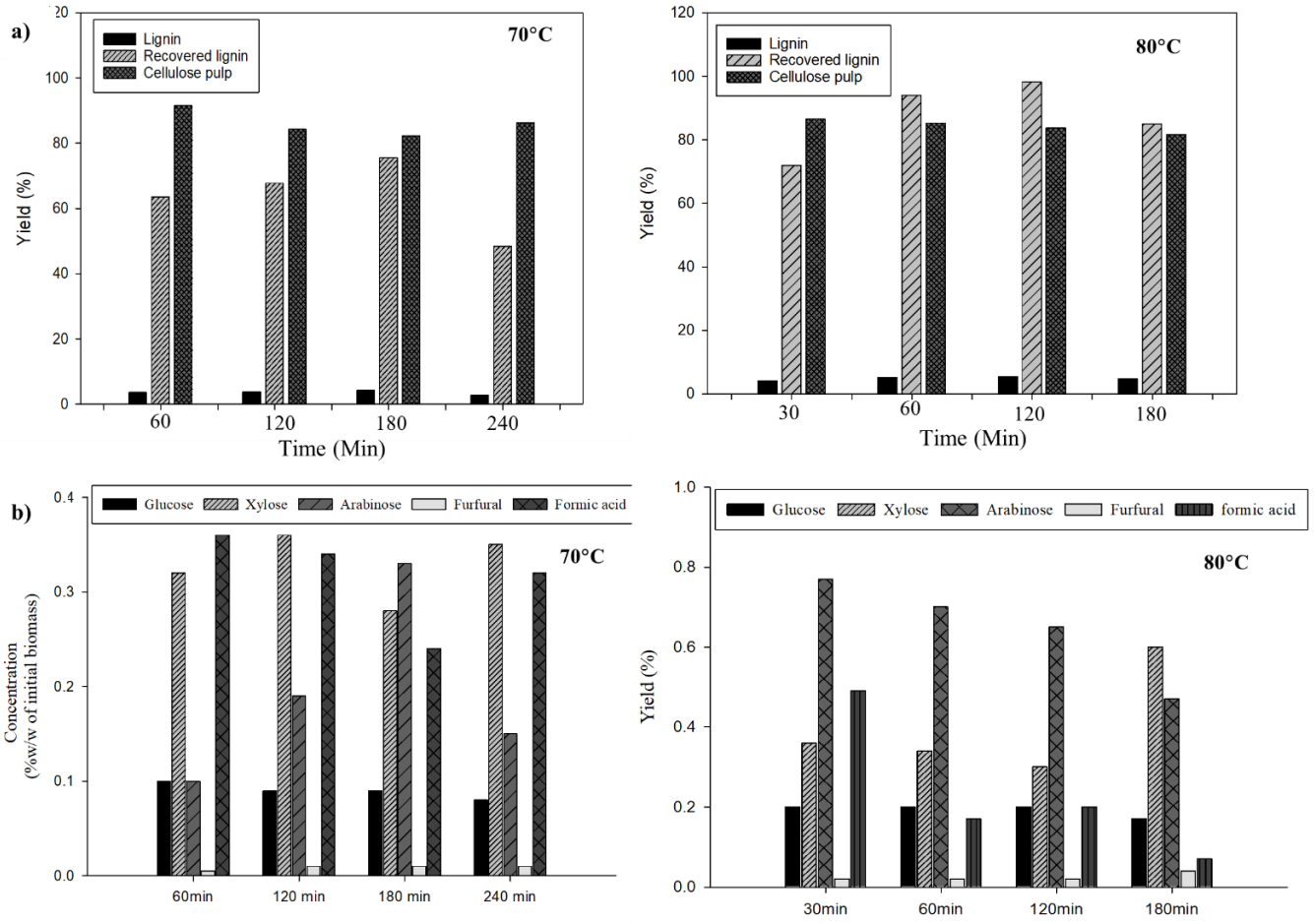

Fig 5.4: Effect of fractionation temperature and time on; (a) lignin and cellulose pulp recovery and (b) water soluble fractions.

A small amount of water-soluble hemicellulose (xylose and arabinose) of 1.13% from spelt husk and 1.04% from corn cob was also obtained (Fig 5.4b). The high lignin recovery of >90% for spelt husk and corn cob were higher than the 85% achieved using the ethanol/ organosolv for raw corn cob and spelt husk. This higher lignin recovery is likely because of increased disruption and opening of the lignocellulose matrix following ozone pre-treatment as the lignin-hemicellulose bonds are already disrupted making it easier to solubilise using the organic solvent at mild temperatures. In addition, the hemicellulose water soluble fraction of ozone pre-treated feedstock was much lower (<2.0%) than that obtained using conventional organosolv for raw corn cob and spelt husk (7-8%). High hemicellulose water soluble fractions (7-8%) as reported with the use of conventional organosolv are likely due to increased hydrolysis of the hemicellulose which occurs at the higher temperature of 150 – 200ºC and pressures in the presence of an acid needed to chemically break ether bonds in the lignin (Duff and Murray, 1996, Matsakas et al., 2019). In this study increased lignin (>90%) and cellulose recovery (85%) were both obtained at a relatively mild temperature of 80ºC and atmospheric pressure reducing the risks (such as safety, equipment corrosion) associated with operation at high temperature and pressures. Matsakas et al., (2018) pre-treated spruce biomass using a hybrid organosolv-steam explosion pre-treatment, post the steam explosion, organosolv fraction was done using 65% ethanol at 200ºC for 60 min which achieved 79% lignin recovery with 95.7% purity, 72% cellulose pulp yield and 5% water soluble fraction. Shui et al., (2016) fractionated corn stalk with a mixture of acetic acid/formic acid/water (3:6:1 v/v/v) at 90ºC for 180 min and achieved 38% lignin yield with 44% purity and 53% cellulose pulp yield.

Similar to organosolv fractionation is ionosolv fraction, which involves the use of an ionic solvent at temperatures of 120 - 160ºC and atmospheric pressure to dissolve lignin and hemicellulose leaving cellulose as a filterable solute and lignin is recovered using an anti-solvent (Brandt-Talbot et al., 2017). However, problems with this fractionation method is that more aggressive changes are observed with regenerated lignin as well as drawbacks with the use of an ionic liquid as solvent due to high cost, low thermal stability and high affinity for water (low tolerance to moisture) (Usmani et al., 2020). Verdía et al., (2014) fractionated Miscanthus giganteus with an ionic liquid (1-butylimidazolium hydrogen sulphate) at 120ºC for 4h and recovered 82% of cellulose and 70% lignin, although the cellulose was found to be contaminated with the ionic liquid while alterations in lignin structure were observed as a result of cross linking and formation of water insoluble pseudo-lignin. Similarly Lara-Serrano et al.,

(2019) fractionated barley straw with an ionic liquid (1-ethyl-3-methylimidazolium acetate) at 105 ^{o}C for 3.5h and recovered 80% cellulose and 70% lignin.

5.3.2 Effect of catalyst on fractionation.

The effect of catalyst addition to organosolv fractionation at 80^{o}C of untreated and pre-treated spelt husk for 120 min was determined. The addition of 1 wt% HCl increased lignin recovery from 3.31 – 23.1 mg g^{-1} (6 to 41.8%) and from 4.58– 51.9 mg g^{-1} (8.3 to 94%) for untreated and pre-treated spelt husk respectively (Fig 5.5b). It can be explained due to the increased solubilisation of lignin and hemicellulose. It is noteworthy that the lignin recovery from fractionation without acid was very low (6-8%) due to the low temperature (80^{o}C) used in this study, for self-catalysis to occur during fractionation it needs a higher temperature (>180^{o}C) to cause acetylation of hemicellulose leading to release of acetic acid that catalyses the reaction (Nitsos et al., 2018). However, the addition of acid (1 wt% HCl) enhanced hemicellulose hydrolysis leading to increase in water soluble fraction from a total of 1 to 3% w/w and 1.2 to 2.4% w/w for untreated and pre-treated spelt husk respectively (Fig 5.5a). Cellulose pulp yield decreased from 800– 634.7 mg g^{-1} (94 to 74.5%) and 789.8– 695.2 mg g^{-1} (92.7 to 81.6%) respectively indicating the enhanced solubilisation of lignin and hemicellulose with a cellulose rich pulp obtained. This also led to a colour change and saturation of filtrate after the organosolv fractionation (Fig 5.5C). Nitsos et al., (2016) observed an increased solubilisation yield from 30 - 55% from Spruce biomass was pre-treated with 1% HCl, 60:40 (ethanol:water) at 185^{o}C for 60 min. Shui et al., (2016) observed an increase in lignin yield from 35.0 to 38.3% when 1% HCl was added to corn stalk pre-treatment with acetic acid/formic acid/water (3:6:1 v/v/v) at 90^{o}C for 180 min.

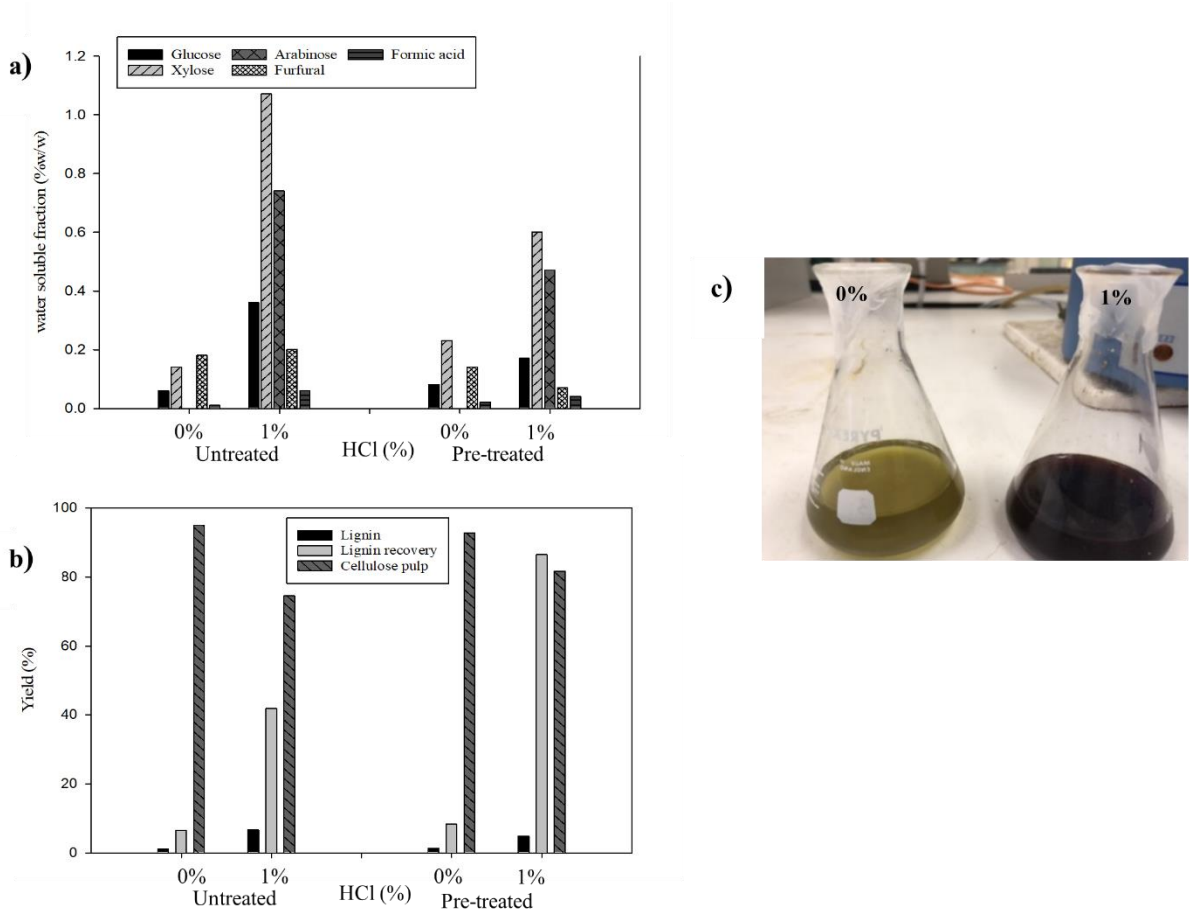

Fig 5.5: Effect of acid on (a) water soluble yields (b) lignin andcellulose recovery and (c) picture of filtrate after organosolv fractionation with ethanol:water (60:40) at 80^{o}C for 2h.

5.4 Fractionated lignin properties

Fractionated lignin FTIR (Fig 5.6) in comparison to untreated and pre-treated feedstocks shows the absence of O-H bands at 3450 cm^{-1} which is a characteristic of cellulose. Increased intensities at 2926 and 2831 cm^{-1} corresponds to C-H vibrations of aliphatic hydrocarbons and CH_3O groups respectively (Yan et al., 2015), which is a characteristic of lignin bonds. In addition, aromatic vibrations of C=C observed at 1610 and 1517 cm^{-1} and C-O vibrations at 1274 and 1033 cm^{-1} corresponds to lignin (Yan et al., 2015). This shows that lignin was successfully fractionated from the lignocellulose feedstock (corn cob and spelt husk).

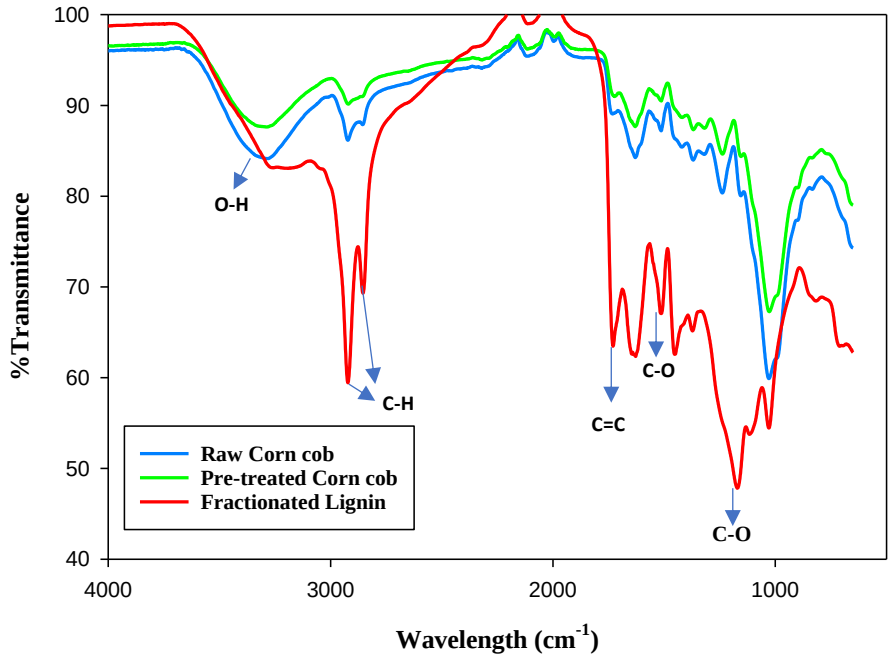

Fig 5.6: FTIR of fractionated lignin compared to untreated and pre-treated corn cob.

The lignin fractionated from raw spelt husk showed small micron particles agglomerated to form clusters (Fig 5.7) while the lignin following pre-treatment showed a smooth and increased surface area due to collapse of the internal structure as well as breakage of chemical bonds such as β-O-4 and 4-O-5. Similar changes were observed for switch grass (*Panicum Virgatum*) (Long et al., 2014) with a smooth surface for lignin treated with hot compressed water at 180°C compared to loose agglomerated particles in the raw feedstock. Stewart *et al.*, (2014) also observed small and dense micron particles when lignin from *Salix purpurea* was precipitated using water at 40°C. Fractionated lignin from raw corn cob in the current study showed a loosely packed agglomeration of micron particles compared to that of raw spelt husk; This can be due to the lower lignin content (5 wt%) of corn cob.

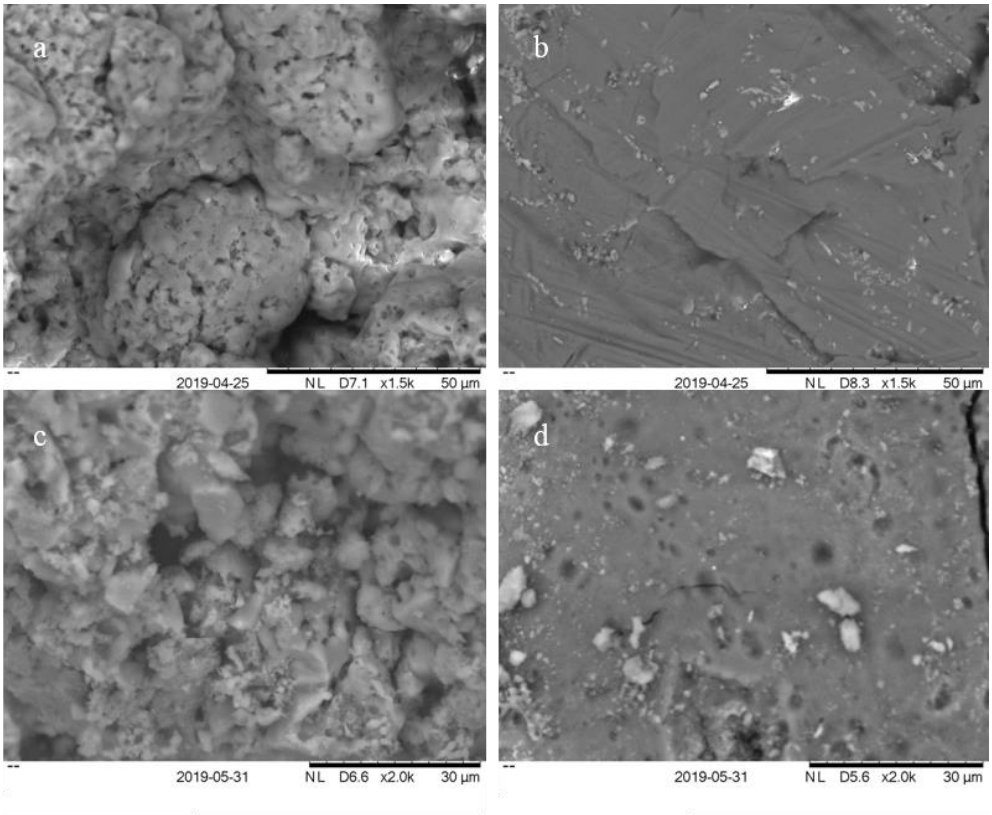

Fig 5.7: SEM images of fractionated lignin at 80°C with 1% HCl catalyst for 120min: (a) untreated, (b) ozone pre-treated spelt husk (c) untreated and (d) ozone pre-treated corn cob.

Furthermore, a decreased ^{1}H NMR spectral intensity in the aromatic region of ozone pre-treated lignin (Fig 5.8) was observed compared to the untreated feedstock, suggesting increased reactivity of ozone with the aromatic components of lignin which was also showed in other studies (Ben'ko et al., 2013, Bule et al., 2013). ^{1}H NMR spectra (Fig 5.8) of corn cob showed that the lignin consists of H, G and S units of monomers while spelt husk spectra is made up of H and G monomers with no peak in the S region of the spectra. Hence, the type of lignin obtained from corn cob is classified as guaiacyl-syringyl while that from spelt husk is guaiacyl lignin. This is in agreement with Sun, (2010) that the unit of monomers that make up a lignin polymer differ between different feedstocks and this influences its suitability for value added product and platform chemical production.

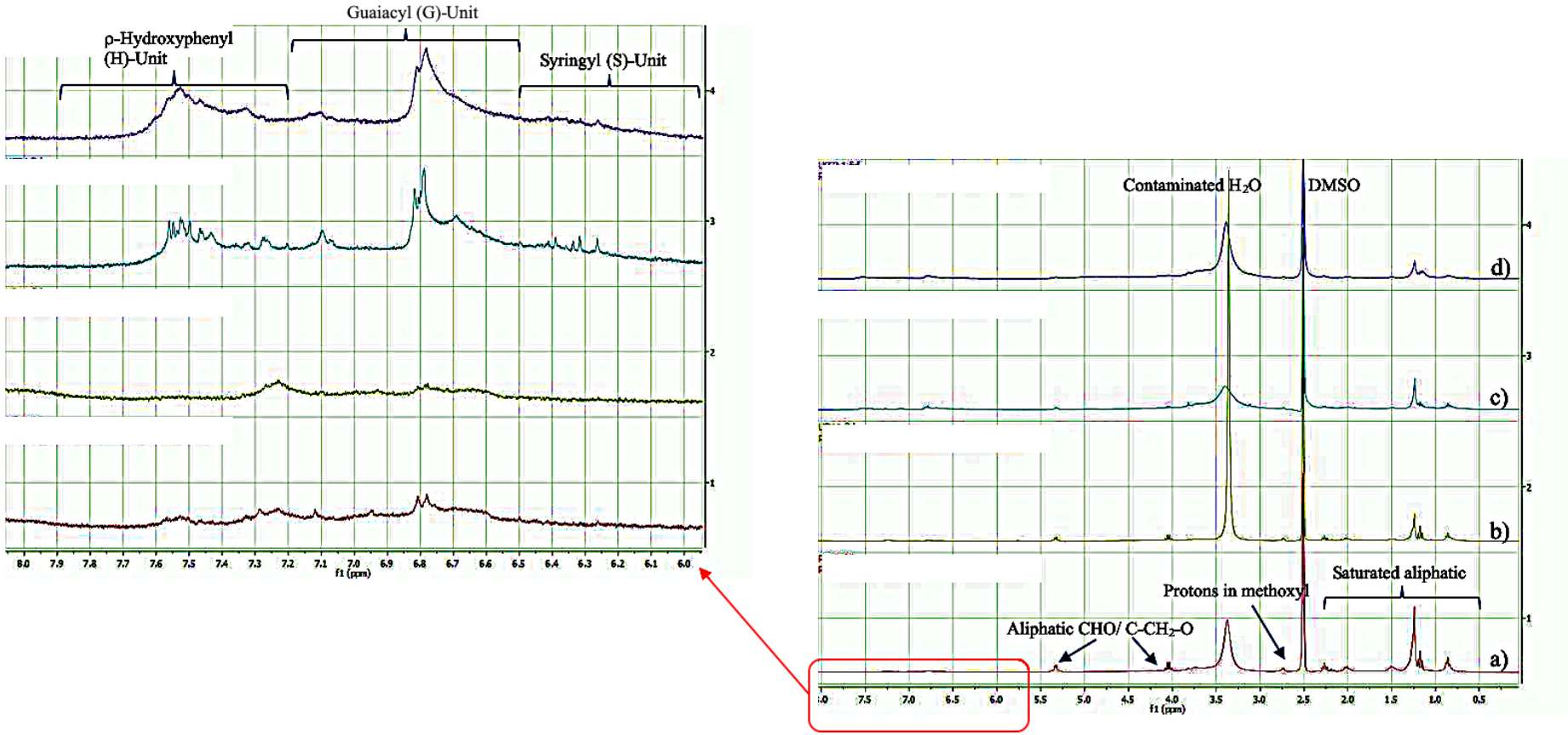

Figure 5.8. ^{1}H NMR spectra of ethanol fractionated lignin from: (a) ozone pre-treated spelt husk, (b) untreated spelt husk, (c) untreated corn cob and (d) ozone pre-treated corn cob.

The purity of the extracted lignin was determined by measuring the amount of sugars arising from cellulose and hemicellulose hydrolysis as well as ash content of the lignin. This is important as purity is the major factor that determines the use of lignin for advanced applications (Matsakas *et al.*, 2019). About 95% pure lignin was achieved for both ozone pre-treated spelt husk and corn cob with ash content and total carbohydrate impurities both below 2%. Furthermore, the hemicellulose impurities and ash contents were higher for untreated spelt husk (2.00%) compared to ozone pre-treated spelt husk (1.35%) which can be attributed to poor hydrolysis of lignin-hemicellulose bonds leading to isolation of lignin with hemicellulose as it remains attached to the lignin. Similarly, Matsakas et al., (2019) recovered 79.4% lignin with 96% purity from spruce biomass using ethanol as solvent and 1% HCl at 200^{o}C for 60 min. Li et al., (2020) recovered 59% lignin with 55% purity from pine sawdust using ethanol as solvent and 15% H_2SO_4 at 180^{o}C for 60 min.

5.5 Fractionated cellulose properties.

The FTIR of fractionated cellulose compared to untreated and pre-treated feedstocks (Fig 5.9) shows absence of bands at 2920 and 2870 cm^{-1} that correspond to C-H vibrations of the methyl and methylene groups in lignin. In addition, absence of bands at 1610 and 1274 cm^{-1} corresponding to aromatic vibrations of C=C and C-O of lignin were observed (Yan et al., 2015). Hence, bands at 3400,1057, and 897cm^{-1} corresponding to aliphatic O-H groups, C-O-C pyranose skeletal vibrations and β-glycosidic linkages respectively (Chen et al., 2018) show that cellulose was effectively fractionated from both lignocellulose feedstocks (corn cob and spelt husk).

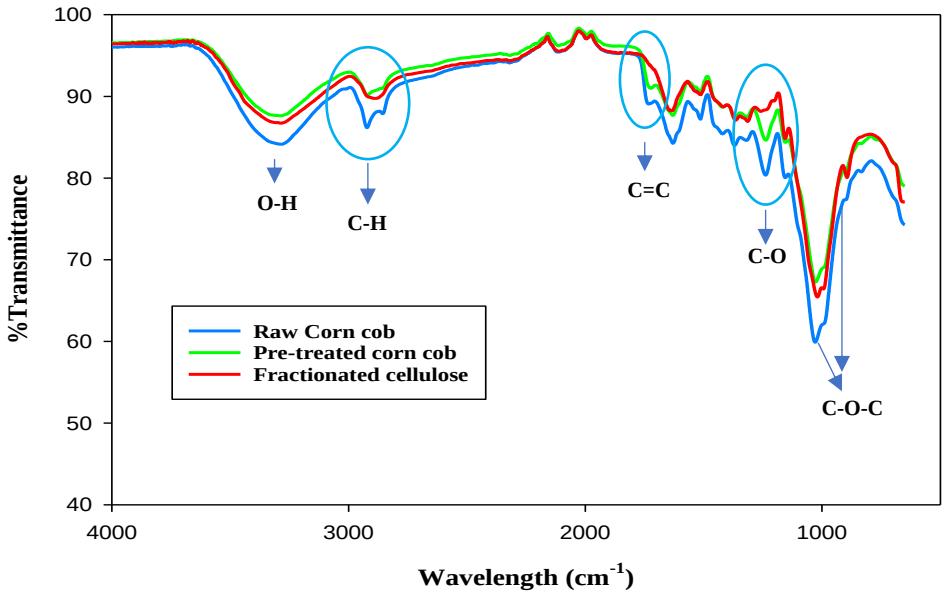

Figure 5.9: FTIR of fractioned cellulose compared to untreated and pre-treated corn cob.

The raw corn cob and spelt husk feedstocks showed a compact organised and rigid cellulose structure (Fig 5.10). It is due to strong hydrogen bonding between the glucose monomers. However, the ozone pre-treated cellulose showed a more disorganised surface morphology with a loosening of the structure likely due to partial oxidation/depolymerisation of the cellulose as suggested by Mamleeva et al., (2009). This more disorganised structure will potentially enhance the solubility of cellulose and aid its conversion into platform chemicals and biofuels (Ben'ko et al., 2013).

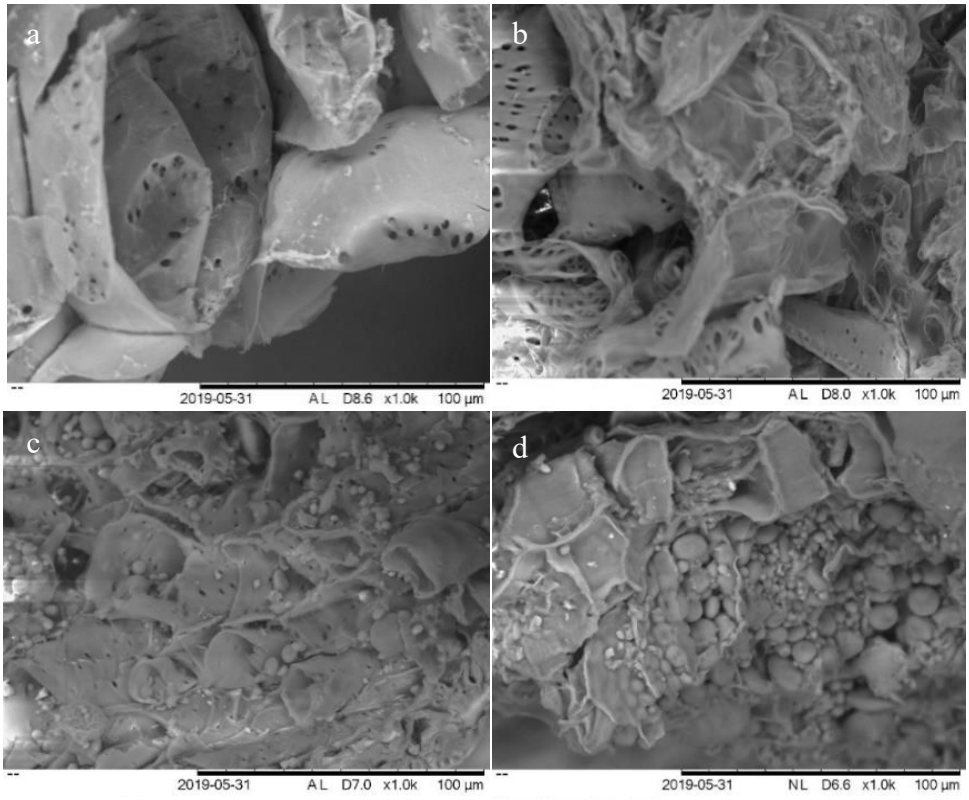

Figure 5.10: SEM of fractionated cellulose at 80°C, with 1% HCl for 120 min from: (a) untreated, (b) ozone pre-treated corn cob, c) untreated spelt husk and d) ozone pre-treated spelt husk.

X-ray diffraction (XRD) spectra of the cellulose showed signal peaks at 2θ of 16.5, 22.1 and 34.4° (Fig 5-11I) corresponding to the lattice plane of cellulose I crystals (Park et al., 2010, Liu et al., 2019). Cellulose crystallinity index (CI) is the ratio of amount of crystalline cellulose to total amount of sample containing both crystalline and amorphous cellulose (Nges et al., 2016). The CI of raw corn cob (45.5%) was higher than spelt husk (30.2%). It is due to the lower

lignin content of corn cob (5.1 wt%). Ozone pre-treatment led to a decrease in the CI values of corn cob and spelt husk from 45.5 to 36.8% and 30.2 to 28.3% respectively due to increased disorder and amorphisation of the cellulose (Fig 5.11I). A similar decrease in the CI of aspen sawdust cellulose was reported as a result of loosened structure and reduced crystal size caused by partial oxidative depolymerisation of cellulose by ozone (Ben'ko *et al.*, 2013).

The thermal stability of the fractionated cellulose from untreated and ozone pre-treated feedstock (Fig 5-11II) showed a rapid loss of mass at a temperature of 350ºC because of cellulose and hemicellulose degradation (Liu et al., 2019, Cheng et al., 2012). The TGA thermograms (Fig 5.11II) showed mass loss in three steps. The first step occurred at 100ºC which showed moisture loss from the sample, the second stage at 280ºC corresponds to organic extractives such as fats, alkaloids, terpenoids and the third stage at 350ºC correspond to cellulose degradation (Mothé and de Miranda, 2009). Ozone pre-treated cellulose showed a higher decomposition rate compared to untreated feedstock. A slow degradation of cellulose in the raw feedstock at temperatures > 300ºC could be due to stronger cellulose intermolecular forces, together with the presence of lignin and ash impurities. The peak degradation temperature (350ºC) in the DTG curves remained the same for both untreated and pre-treated feedstocks which shows that ozone pre-treatment did not affect the thermal stability of cellulose. A slight shoulder appeared in the untreated spelt husk at 350ºC due to presence of lignin and hemicellulose while its absence in the pre-treated sample shows removal of this component (Perrone et al., 2016).

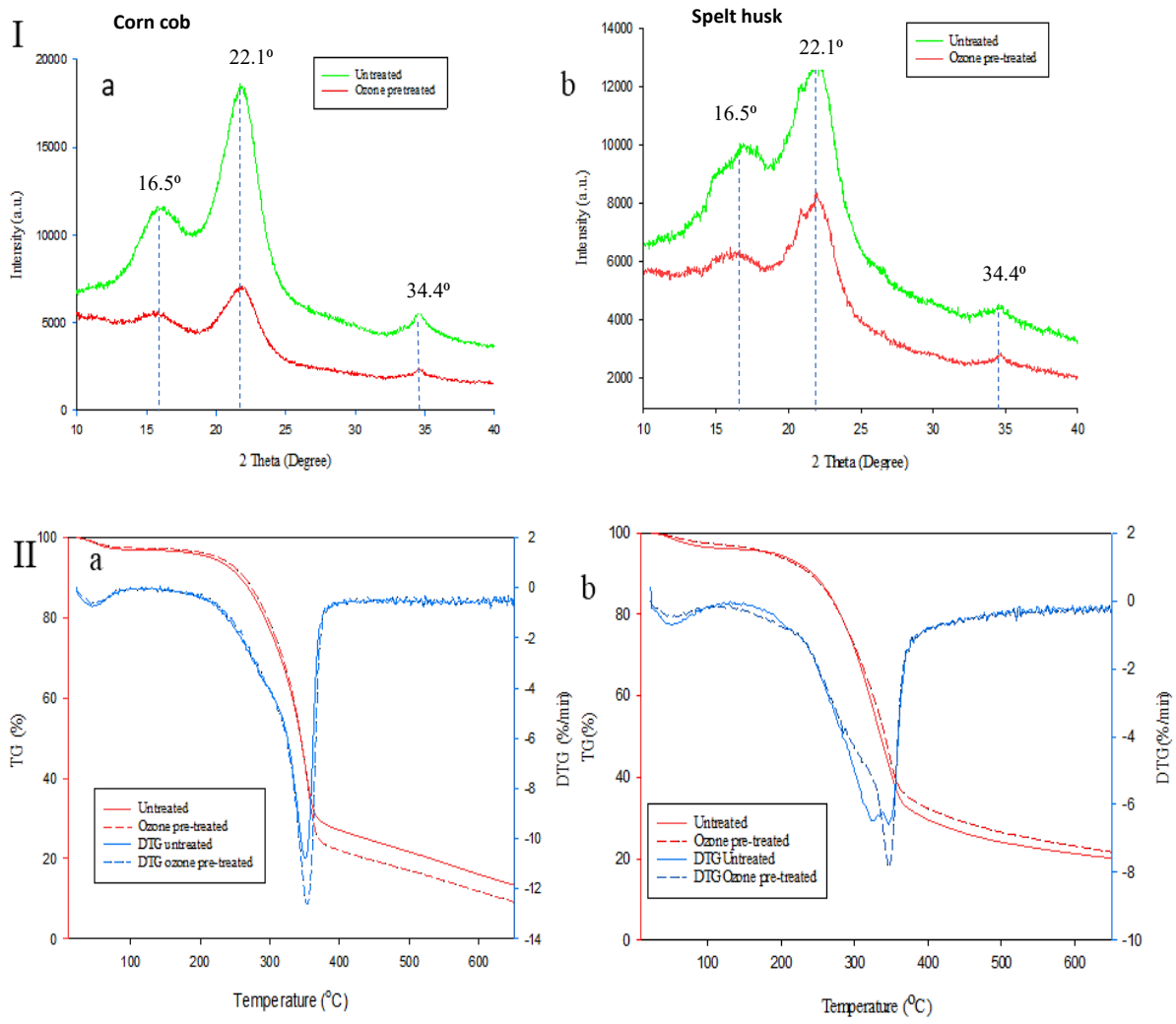

Fig 5.11: (I) XRD and (II) TG and DTG curves of recovered cellulose from untreated and ozone pre-treated; (a) corn cob and (b) spelt husk.

Subsequently, the effect of ozone pre-treatment on degree of polymerisation (DP) of cellulose was determined using matrix-assisted laser desorption/ionisation time of flight (MALDI-TOF) analysis. The degree of polymerisation of both untreated spelt husk and corn cob were 17 containing glucosyl monomer with one potassium adduct having a m/z of 2812 and from the spectra observed (Fig 5.12), the difference in mass between adjacent signals was 162 m/z corresponding to one glucosyl unit ($C_6H_{10}O_5$) (Jung *et al.*, 2010). In addition, a decrease in intensity was observed at higher m/z, this is because cationisation from adduct formation of bigger molecules are unfavourable making it difficult to reach the mass spectrometer and generate a signal (Brasseur *et al.*, 2014). The DP of spelt husk remained unchanged after ozone

pre-treatment while that of corn cob decreased to DP 14 (m/z 2309.712) having a glucosyl monomer with one sodium adduct. However, very low degree of polymerisation (17) was obtained for corn cob and spelt husk due to limitations from the MALDI-TOF technique used as larger molecular weight ionised molecules resulting from adduct formation are difficult to detect. Hence, average viscometry degree of polymerisation (DPv) of corn cob and spelt husk were obtained from its intrinsic viscosity in cupriethylenediamine hydroxide (Cuene) solution to obtain a definite degree of polymerisation. Untreated corn cob and spelt husk had DPv of 290 and 88.7 respectively. Ozone pre-treatment led to a decrease in DPv to 235 and 58.2 respectively. This decrease in DP of ozone pre-treated corn cob can be due to the lower content of lignin in the raw feedstock enabling the partial oxidation of cellulose. Hubbell *et al.*, (2010) also determined the DP of Avicel PH-101 cellulose with varying amounts of lignin after acid chlorite pre-treatment and observed a significant reduction in the degree of polymerisation of cellulose at lower lignin levels.

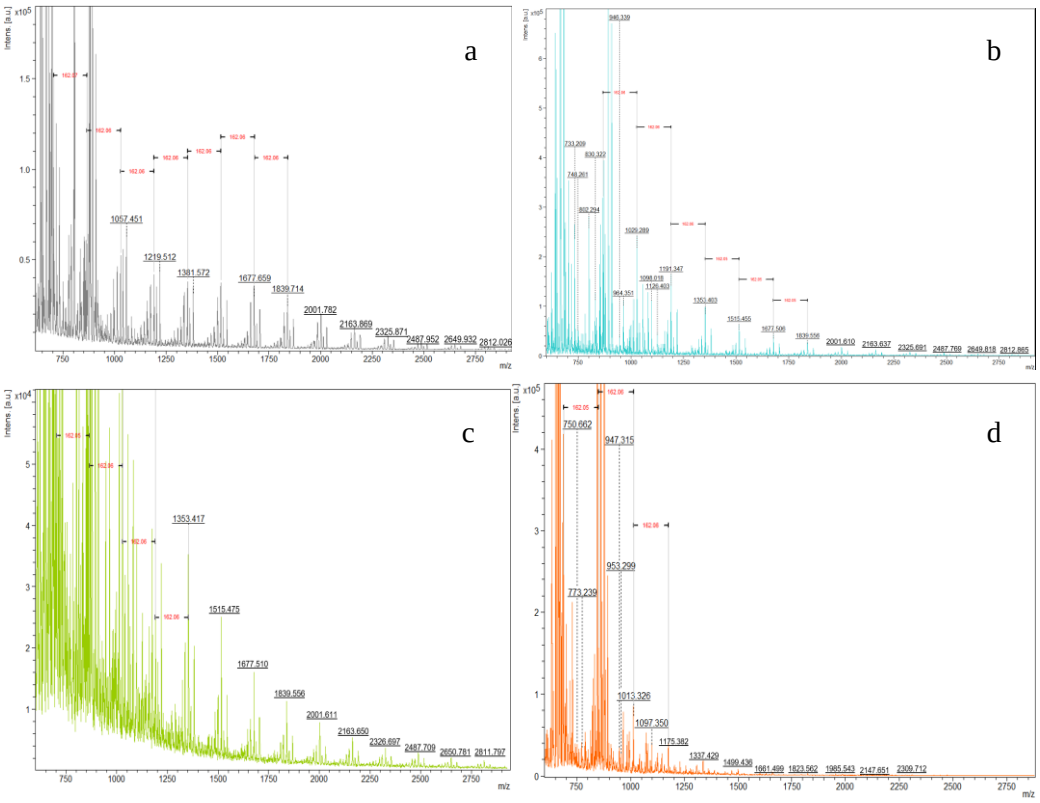

Figure 5.12: MALDI-TOF spectra of fractionated cellulose from: (a) untreated spelt husk, (b) ozone pre-treated spelt husk, (c) untreated corn cob and (d) ozone pre-treated corn cob.

Cellulose purity is defined by the percentage of holocellulose (hemicellulose and cellulose) content in the cellulose pulp. 78% purity was achieved for ozone pre-treated spelt husk with 591.2 mg g^{-1} (69.4%) cellulose and 74.1 mg g^{-1} (8.7%) hemicellulose as compared to 73% purity of untreated spelt husk with 505.2 mg g^{-1} (59.3%) cellulose and 116.7 mg g^{-1} (13.7%) hemicellulose content. The higher purity achieved for pre-treated cellulose pulp is because of greater lignin (increased lignin recovery) and hemicellulose solubilisation compared to that of un-treated spelt husk. It is worth mentioning that the impurities in the cellulose pulp are due to the existence of other components such as extractives, proteins and the remainder of the lignin retained in the cellulose pulp.

5.6 Hydrogen peroxide pre-treatment.

The evaluation of pre-treatment efficiency of biomass feedstock with an oxidant (hydrogen peroxide) other than ozone was examined (detailed comparison of the two methods in section 5.8). Hydrogen peroxide pre-treatment is most efficient with highest carbohydrate recovery of approximately 90%) and highest lignin separation of approximately60%) when the pH of the solution is 11.5 (Gould, 1984, Yang et al., 2002). At pH 11.5, the dissociation of hydrogen peroxide occurs to produce a hydroperoxyl anion (HOO^-) (mechanism shown in Section 5.9.3) which is responsible for the oxidative reaction of carbonyl and ethylene groups in lignin as well as an initiator for radical formation (Ho et. al., 2019). As such, the addition of sodium hydroxide was used to obtain a pH of 11.5 during pre-treatment.

Alkaline hydrogen peroxide pre-treatment of corn cob and spelt husk was carried out at different pre-treatment times and the solid residue characterised (Table 5.3). The cellulose portion increased for the first 60 min for corn cob from 33.35 to 76.15% and spelt husk from 23.9 to 53.37% (Table 5.3) while lignin decreased from 5.0 to 1.25% for corn cob and from 16.03 to 5.47% for spelt husk respectively. Beyond 60 min the cellulose content of the residue decreased which implies a degradation of carbohydrate as low amount of lignin is present that could react with the generated radicals, as such an optimum pre-treatment time of 60 min was chosen for subsequent pre-treatments. Similar results were reported by Martinez-partino et. al., (2017) and Fernandez-delgado et. al., (2019) in their study of alkaline hydrogen peroxide pre-treatment of olive tree and brewers spent grains respectively for bioethanol production.

Table 5.3: Hydrogen peroxide pre-treatment of corn cob and spelt husk with 1% (w/w) H_2O_2, pH 11.5, 120°C with variation in reaction time from 15-90 mins.

Feedstock Pre-treatment time (min)	**Recovered solid (%)**	**Cellulose (mg $g^{-1)}$**	**Hemicellulose (mg g^{-1})**	**Lignin (mg g^{-1})**
Corn cob				
untreated		432.4 ± 1.0	378.2 ± 1.2	50.1 ± 0.1
15	90.5 ± 0.8	333.5 ± 0.2	221.0 ± 1.0	30.2 ± 0.1
30	68.1 ± 1.4	498.3 ± 0.8	307.9 ± 0.8	26.2 ± 0.5
45	64.3 ± 1.7	620.7 ± 1.5	183.9 ± 1.5	17.3 ± 0.7
60	61.4 ± 0.6	761.5 ± 1.7	124.3 ± 1.3	12.5 ± 0.5
90	57.3 ± 1.3	469.3 ± 0.3	317.7 ± 1.5	28.3 ± 0.2
Spelt husk				
untreated		318.5 ± 0.8	291.3 ± 1.3	160.3 ± 0.3
15	64.9 ± 1.1	239.7 ± 0.8	208.4 ± 0.3	84.1 ± 0.3
30	47.9 ± 1.6	470.7 ± 0.3	235.0 ± 0.8	66.3 ± 0.4
45	31.4 ± 1.7	499.1 ± 1.5	209.7 ± 1.0	54.7 ± 0.8
60	23.3 ± 0.8	533.7 ± 1.5	94.7 ± 1.6	58.2 ± 0.7
90	27.2 ± 0.5	318.9 ± 1.2	131.3 ± 1.5	68.5 ± 0.8

The liquid separated after pre-treatment was analysed and the major product obtained from spelt husk and corn cob was formic acid with traces of acetic acid (Fig 5.13). Furthermore, similar to Section 4.3.0, glycolic acid was obtained from spelt husk and absent for corn cob, which is due to differences in the type of lignin present in both feedstocks. Highest concentration (~12% wt/wt of initial biomass) of the degradation products (Fig 5.13) was obtained at 60 min which corresponds to the pre-treatment conditions with the highest lignin

removal (Table 5.3). Higher concentrations (3 fold) of the lignin degradation products were obtained from alkaline hydrogen peroxide pre-treatment than from ozone pre-treatment which shows that the reactive peroxide degrades the lignin rather than solubilises it. However, this could be recovered to value added chemicals but will increase the process costs and energy due to additional separation and purification to individual chemicals.

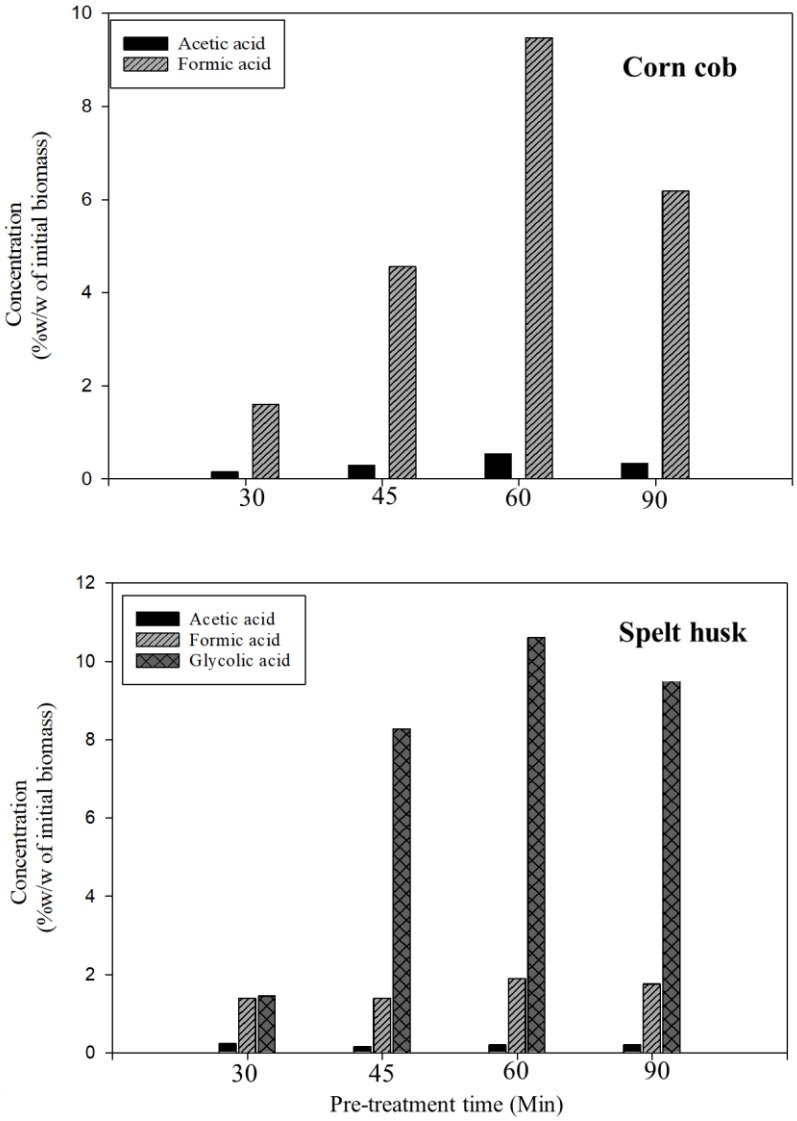

Figure 5.13: Major alkaline peroxide lignin degradation products from corn cob and spelt husk.

5.7 Mechanism of ozone and hydrogen peroxide pre-treatment and organosolv fractionation.

5.7.1 Ozone treatment mechanism

Ozone reacts with biomass in 3 consecutive stages; firstly, ozone solubilisation in water where ozone bonds with water in the biomass. The formation of reactive species mainly ozone and hydroxyl radicals occurs depending on the reaction conditions, but other radicals such as hydrogen peroxide can also be generated. Secondly, ozone selectively reacts with aromatic bonds (carbon double bonds) due to their high electron density leading to opening of the lignin structure. Ozone reacts with aromatic bonds through hydroxylation of the aromatic ring after an initial electrophilic attack. Followed by 1,3-cycloaddition to open olefinic double bonds (Reaction 5.1) by the Criegee mechanism (Criegee, 1975). For aromatics, an initial hydroxylation is necessary to destabilise and increase its reactivity toward electrophilic substitution reactions, unlike alkenes where it reacts right away (Sixma and Wibaut, 2010).

Finally, ozone reacts with the carbon double bonds through 1,3-dipolar cycloaddition to produce the 1,2,3-trioxolane intermediate (Reaction 5.1) which then decomposes to *syn* and *anti* isomers of carbonyl oxides (Zwitterions) and a carbonyl compound (Reaction 5-2).

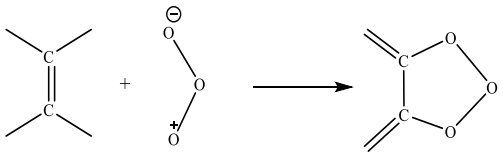

Reaction 5.1

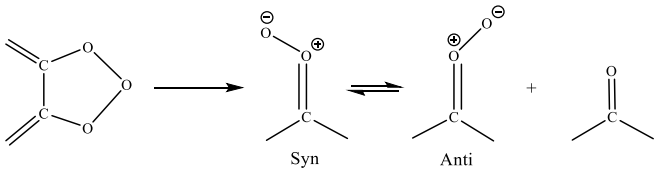

Reaction 5.2

Depending on reaction conditions, a number of different products can be formed. The *syn* and *anti* isomers of zwitterions can combine with carbonyl compounds to form ozonoide (Reaction 5.3). Alternatively, the *syn* and *anti* isomers of zwitterions can react with solvents such as water to form other carbonyl compounds liberating hydrogen peroxide (Reaction 5.4) or can polymerise to form diperoxides or polymeric peroxides (Reaction 5.5).

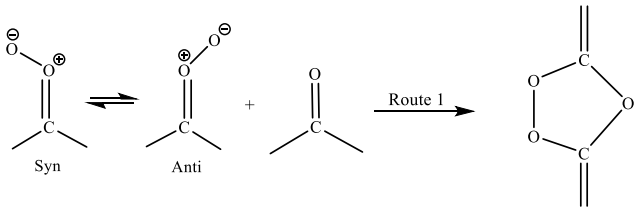

Reaction 5.3

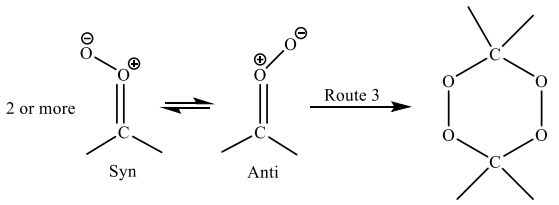

Reaction 5.4

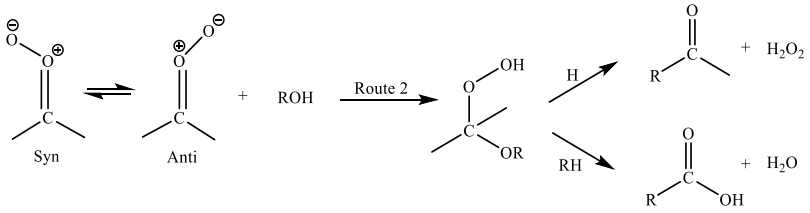

Reaction 5.5

Depending on reaction conditions, resulting radicals (such as OH, H), peroxide and ozone may react with lignin degradation products to form low molecular weight fragments such as HCOOH, although the reaction mechanism between ozone and lignin is not completely understood (Souza-Corrêa *et al.*, 2013b). Apart from reacting with the carbon double bonds of the lignin aromatics, ozone undergoes reactions with carbon-hydrogen and carbon - oxygen bonds leading to cleavage of β-O-4 bonds and methoxyl groups of the lignin polymer (Ragnar *et al.,* 1999). The reaction between ozone and carbon double bonds occurs at a very fast rate leading to faster lignin degradation and high initial ozone consumption. Carbohydrates (carbon single bonds) are more resistant to ozone and their reaction is 10^6 times slower than lignin (Travaini *et al.*, 2016). Ozone reacts directly with carbohydrates to form carboxyl groups or reacts with water to generate hydroxyl radicals, which then react with the carbohydrate components leading to unsystematic cleavage of the glycosidic bonds with the production of acetic, formic, oxalic, glycolic and other dicarboxylic acids.

5.7.2 Organosolv fractionation

Conventional organosolv fractionation of biomass occurs by breakdown of ether bonds in lignin to fragments small enough to dissolve in the organic solvent. α-ether bonds are the main linkages broken as these are weaker than the β-ether linkages. β-ether linkage cleavage only occurs in a highly acidic medium (>1M conc) of organic acid and at relatively high temperatures (>150°C) (McDonough, 1992).

Two consecutive processes occur during organosolv fractionation, the first process involves splitting of lignin into smaller fragments. This can occur through hydrolysis at the benzylic position of α-ether bonds in the presence of an acid through the formation of an intermediate (quinone methide) to form an S_{N2} nucleophilic substituted compound (Reaction 5.6) or direct splitting of the ether bonds forming a reactive stabilised carbocation (Reaction 5.7) which can undergo unwanted condensation reactions with other molecules to form compounds containing a single carbon bond (McDonough, 1992).

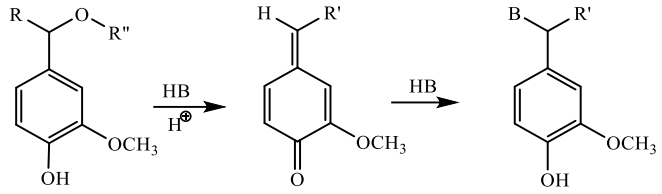

Reaction 5.6

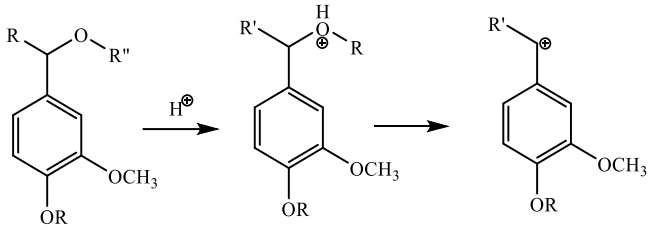

Reaction 5.7

The second process involves hydrolysis of lignin-carbohydrate ether linkages (glucosidic bonds) by acid to separate the lignin and carbohydrate fractions (Reaction 5.8). This fractionated lignin solubilises in the solvent/mixture of solvents, yielding a cellulose rich solid fraction and a liquid fraction containing lignin fragments and hydrolysed carbohydrates (McDonough, 1992).

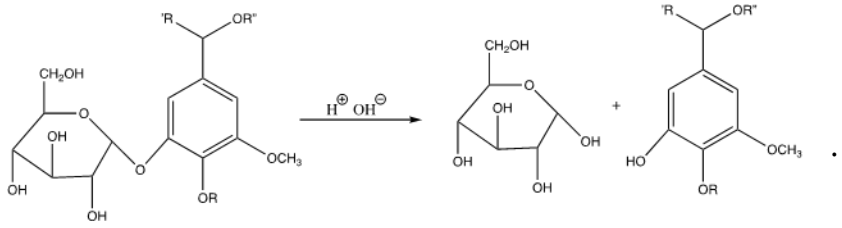

.

Reaction 5.8

Therefore, the use of ozone prior to organosolv pre-treatment leads to disruption and opening of the biomass structure which makes it easier for the hydrolysis and breakage of the lignin–carbohydrate bonds. These bonds weaken during pre-treatment with increased solubilisation of lignin at mild temperatures and atmospheric pressure leading to high lignin, cellulose and hemicellulose recovery while for organosolv alone, higher extraction temperatures (120°C - 180°C) and pressure of about 2MPa are needed to accelerate lignin-lignin bond (ether bond) as well as lignin-carbohydrate bond (glycosidic bonds) breakage and solubilisation. These

conditions (high temperature and pressure) cause increased hydrolysis of the hemicellulose and cellulose fractions leading to a reduced recovery.

5.7.3 Mechanism of hydrogen peroxide pre-treatment.

Chemical addition of a base such as sodium hydroxide to increase the pH to 11.5 is very important in hydrogen peroxide pre-treatment as the concentration of the main lignin reacting species (HOO^-) generated is optimum at that pH (Gould, 1984).

At a pH of 11.5, hydrogen peroxide dissociates to a hydroperoxyl anion (HOO^-) (Reaction 5.9) which reacts further with hydrogen peroxide to form hydroxyl ions (OH^-) (Reaction 5.10). The (HOO^-) and (OH^-) are the main reacting species that react with lignin degrading it to low molecular weight oxidation products such as carboxylic acids. However, (OH^-) reacts with the carbohydrate components leading to unsystematic cleavage of the glycosidic bonds with the production of acetic, formic, oxalic, glycolic and other dicarboxylic acids. When compared to ozone pre-treatment, more (OH^-) is produced leading to a higher fraction of degraded carbohydrate during pre-treatment. In the absence of any other reactants, the (HOO^-) and (OH^-) recombine to form oxygen and water (Reaction 5.11).

$$H_2O_2 \rightleftharpoons HOO^- + H^+ \qquad \text{Reaction 5.9}$$

$$H_2O_2 + HOO^- \longrightarrow OH^- + O_2 + H_2O \qquad \text{Reaction 5.10}$$

$$OH^- + O_2 + H^+ \longrightarrow O_2 + H_2O \qquad \text{Reaction 5.11}$$

$$H_2O_2 + HOO^- + H^+ \longrightarrow O_2 + H_2O \qquad \text{Reaction 5.12}$$

5.8 Comparison between ozone and alkaline hydrogen peroxide pre-treatments.

1. Cellulose recovery was higher following ozone pre-treatment (98% cellulose recovery) as ozone was more selective to lignin degradation than alkaline hydrogen peroxide (70% cellulose recovery). During hydrogen peroxide pre-treatment, hydrogen peroxide dissociates to produce the hydroperoxyl anion (HOO^-) which further reacts with hydrogen peroxide to produce hydroxyl ($HO^{\cdot}$) and superoxide anion radicals ($O_2^{-\cdot}$). These generated radicals then react with lignin depolymerising it to low molecular

weight fragments. Although, when compared to ozone pre-treatment, more hydroxyl radicals ($HO^{\cdot}$) are generated from hydrogen peroxide dissociation leading to reactions with the carbohydrate fraction of the biomass causing undesired cellulose degradation (Ho *et. al.*, 2019).

2. Ozone pre-treatment involves operation at ambient temperature and pressure with a pre-treatment time of 30 min while one-hour was needed for alkaline hydrogen peroxide pre-treatment at a temperature of 120°C. In addition, utilisation of hydrogen peroxide at ambient temperature for a safer and greener process will need a much longer residence time of 6 hours or more.
3. Ozone pre-treatment does not require a chemical additive whereas the addition of an alkali such as sodium hydroxide is needed to maintain alkalinity at a a pH of 11.5 during hydrogen peroxide pre-treatment which leads to a subsequent washing or neutralisation with acid to ensure the suitability of the biomass for further processing. Consequently, the addition of an acid will lead to the generation of a high amount of salts which could act as an inhibitor to further downstream processing as well as increased process and chemical costs.
4. No product dilution occurs during ozone pre-treatment due to the absence of a liquid phase while hydrogen peroxide pre-treatment requires separation of the solid and liquid fractions and excessive washing to maintain a neutral pH generating water waste that need to be treated.
5. Mass (pre-treated solid) loss after ozone pre-treatment was 5% for corn cob and 7% for spelt husk. In addition, organosolv fractionation was needed for separation into individual components, whereas using hydrogen peroxide led to a much higher mass loss of 31% for corn cob and 68% for spelt husk, respectively. This is as a result of greater solubilisation and hydrolysis of the components (hemicellulose and lignin) during hydrogen peroxide pre-treatment (Su et al., 2015).

Chapter 6: Effects of pre-treatment on cellulose properties and its conversion to platform chemicals such as HMF and furfural.

6.1 Introduction

Cellulose conversion to platform chemicals has gained increasing attention as cellulose is an abundant renewable material containing a high amount of monomeric glucose units linked by β-(1,4)-glycosidic bonds with strong intra- and inter-molecular hydrogen bonds and Van der Waals forces. Production of HMF from cellulose is challenging due to its crystal structure and high degree of polymerisation limiting its solubility in reaction solvents (Zhang et al., 2017). Cellulose undergoes various physico-chemical changes during processing due to lignocellulose materials having to undergo various forms of pre-treatment in a bid to change the recalcitrant structure and make cellulose accessible for further conversion. The aims of Chapter 6 are to study changes in the cellulose properties arising from pre-treatment and evaluate its effect on the rate of conversion to HMF and furfural. This will be achieved by:

- Using model cellulose (α-cellulose) to study the effects of ozone, ultrasound, and ozone/ultrasound pre-treatments on cellulose properties.
- Evaluate how changes in the cellulose properties affect the rate of conversion to HMF and Furfural.
- To evaluate the effect of different catalysts and solvents on HMF and Furfural yield
- Investigate the chemistry of the reactions.
- Propose a reaction pathway for the conversion of cellulose
- Evaluate the potential of raw and pre-treated corn cob and spelt husk feedstocks for conversion to HMF and furfural.

6.2 Effect of pre-treatment on cellulose properties

To study the effect of pre-treatment on cellulose properties, model cellulose (α-cellulose) was pre-treated with ozone (O), ultrasound (U) and a combination of both ozone and ultrasound (OU). The SEM images (Fig 6.1) shows that pre-treatment with U resulted in a randomly disorganised broken fibre due to the vibrational effect of ultrasound while pre-treatment with O and OU led to formation of thin strips of cellulose fibres due to breakdown of the hydrogen bonds leading to reduction in particle size when compared to broad flat fibres in the untreated

α-cellulose. Image J software used to analyse particle size distribution confirmed that a change in particle size occurred from 17.5µm for untreated α-cellulose to 13.5µm, 15.2µm and 16.4µm for pre-treatment with OU, O and U respectively. The decrease in particle size with ultrasound likely occurs as a result of surface erosion due to collision between the particles and cavitation bubbles (Zhang et al., 2013a). Hence, the synergistic effect of the combined ozone and ultrasound pre-treatment led to a more pronounced effect on the cellulose surface and particle size. According to Strunk, (2012), cellulose reactivity can be improved by disrupting the fibrillar aggregation, reducing crystallinity, increasing accessible surface and widening pore structure as a result of breaking the inter- and intra-molecular hydrogen bonds of cellulose thus increasing the available hydroxyl groups needed for the reaction. Hence, the decrease in particle size and broken cellulose fibres obtained from this work would be beneficial for further processing of cellulose to platform chemicals. Similarly, SEM images revealed that ozone pre-treatment (ozone concentration of 4.5mg L^{-1}) of jute fibres led to thinning of closely packed cellulose fibres compared to the arrangement in bundles for untreated jute fibre (Maqsood et al., 2017), although the particle size wasn't reported. Also, ozonation of cotton fibre led to fibrillation and increased surface area of pre-treated cellulose when compared to the more dense bundled structure of untreated cotton fibre (Gashti et al., 2013). In addition, Zhang et al., (2013a) reported a decrease in particle size of microcrystalline cellulose (Avicel PH 105) from 38µm to 0.4µm at a sonication frequency of 20 kHz for 15 mins (Zhang et al., 2013a).

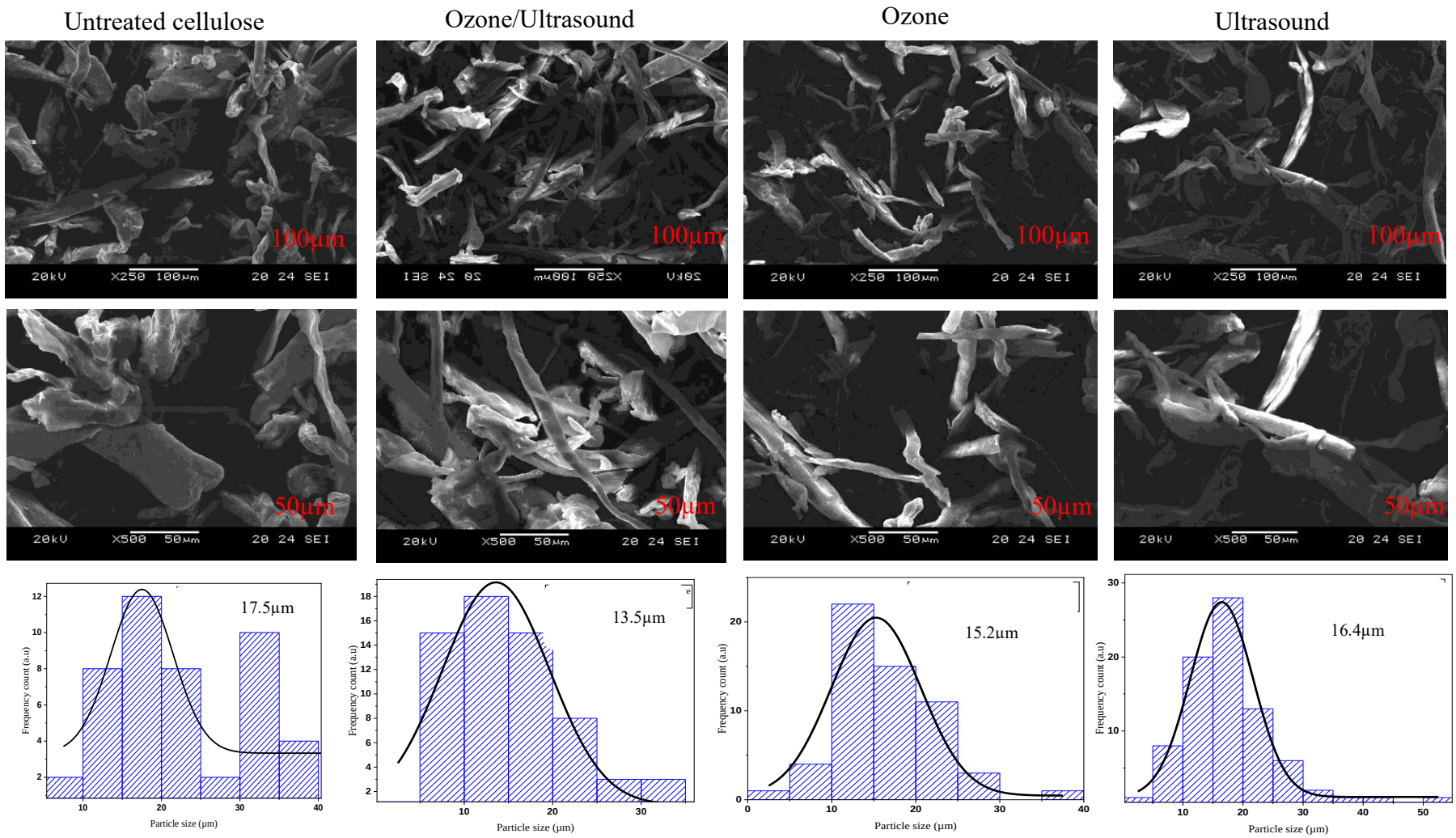

Fig 6.1: SEM images (at 50 and 100 µm) and particle size distribution of untreated and pre-treated (ozone, ultrasound and ozone + ultrasound) cellulose.

The XRD spectra (Fig 6.2) for the untreated and pre-treated cellulose show that the crystallinity index increased from 70% for untreated cellulose to 88.8%, 79.4% and 80.5% for pre-treatment with OU, O and U respectively. Hydrogen ions from water molecules present during pre-treatment led to degradation of the amorphous region of the cellulose thus reducing the fibre size (Jin et al., 2021). As the fibre sizes are reduced, the neighbouring cellulose chains are close to each other and lead to transformation between amorphous and crystalline portions (Wan et al., 2015) hence the slight increase in crystallinity index.

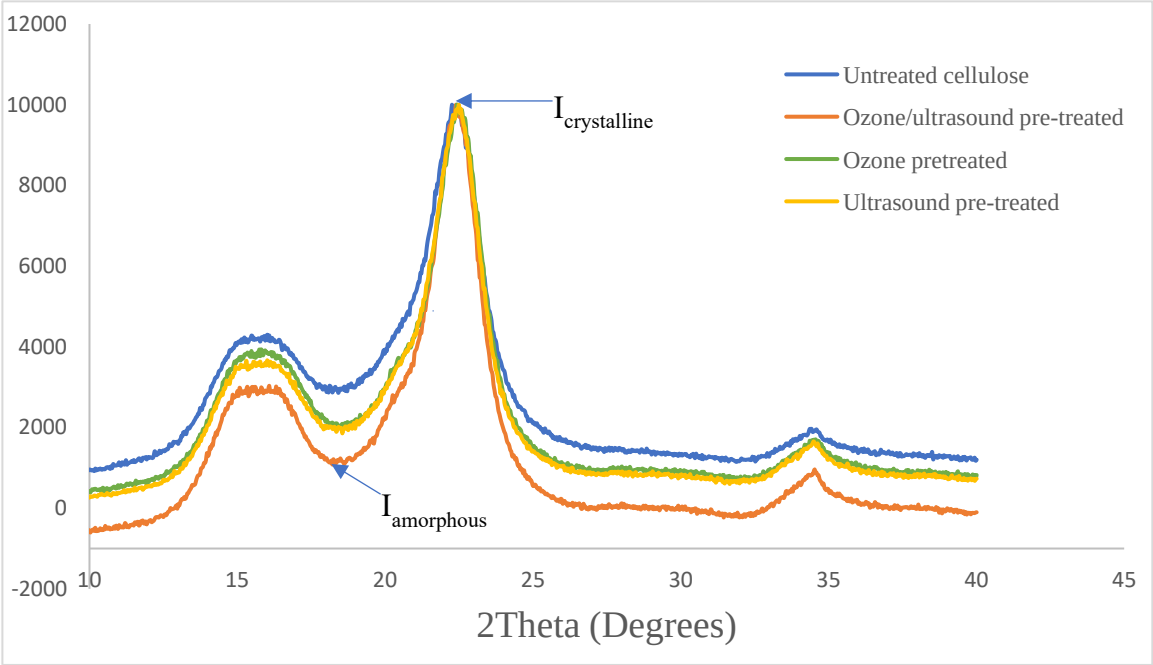

Fig 6.2: XRD spectra of untreated and pre-treated (ozone, ultrasound and ozone + ultrasound) cellulose.

Similarly, ozone pre-treatment of jute fibres showed a slight increase in crystallinity index from 68.5% for untreated fibre, to 70.1% for ozone pre-treated fibres. However, Gashti et al., (2013) observed no change in crystallinity when cotton (cellulose) was pre-treated with ozone, only a change in surface properties was observed. In addition, Zhang et al., (2013) pre-treated microcrystalline cellulose (Avicel PH 105) with ultrasound at a frequency of 20 kHz for 15 mins and found a slight decrease in CRI from 78.4% to 66.3% and concluded that sonication does not significantly affect the molecular structure of cellulose. Unlike in the case of a ball

milling pre-treatment (physical reduction in particle size) where particle size of cellulose was decreased from 56.4 to 28.3µm due to destruction of the rigid structure of cellulose hence significantly decreasing the CRI from 77.1% to 48.1% (Shen et al., 2020). Hence, it can be concluded that ozone and ultrasound pre-treatment only modify the surface of cellulose but have an insignificant effect on the crystallinity (molecular structure).

Subsequently, the average viscometric degree of polymerisation (DPv) carried out using Cuen (Cupriethylenediamine) solution (Table 6.1) shows that the degree of polymerisation decreased from 584 for untreated cellulose to 207, 235 and 443 for pre-treatments with OU, O and U respectively due to hydrolysis of cellulose. It should be noted that the DPv of OU and O were much lower than U pre-treatments as they produce very reactive species such as ozone and hydroxyl radicals (Section 5.7, Chapter 5) that depolymerise cellulose as opposed to the breakdown of cellulose by ultrasonic vibration. Ultrasonic vibration causes generation of microbubbles by ultrasonic waves which collapse causing decomposition of water molecule to hydroxyl radicals that is then able to react with the cellulose (Bussemaker and Zhang, 2013). Hence pre-treatment with OU and O led to a faster rate of cellulose degradation leading to more cellulose chain ends available for subsequent reactions. Similarly, Puri, (1984) reported that ozone pre-treated bagasse and wheat straw decreased cellulose crystallinity from 925 and 1045 to 800 and 908 respectively. Likewise, Sun and Tomkinson, (2005) pre-treated wheat straw with ultrasound for 30 min and observed a decrease in the DP_v from 1666.4 to 1605.

Table 6.1. Crystallinity index and viscometric degree of polymerisation of untreated and pre-treated cellulose

Sample	**CRI (%)**	**Degree of Polymerisation (DPv)**
Untreated cellulose	70.0	584
Ozone/ultrasound pre-treated	88.8	207
Ozone pre-treated	79.4	235
Ultrasound pre-treated	80.5	443

.

To optimise reaction conditions to test the effect of cellulose properties on further conversion to HMF, furfural etc., untreated α-cellulose was treated with different reaction conditions (temperature: 120 - 180^{o}C, time: 2-20min and various catalysts such as $AlCl_3$, $CrCl_3$, $CuCl_2$) to obtain the optimum product yields. DMSO was used as the reaction solvent due to its efficiency in the conversion of cellulose to HMF, furfural and its ability to inhibit undesired side reactions such as rehydration and reduce the formation of by-products (Choudhary et al., 2013, Jia et al., 2014b).

All reactions were carried out in a microwave digestion system. Microwave irradiation is increasingly gaining attention in recent years for its rapid heating, high efficiency (faster start up and shut down times) and easy operation as compared to conventional heating such as oil bath or hot plates. Microwave enhances dissolution of cellulose thereby increasing HMF and furfural yield by reducing the reaction time. It provides more rapid and efficient thermal energy that penetrates the centre of reactants and generate uniform heat throughout the volume than conventional heating that relies on the diffusion of heat from the heating surface to the reactant, hence microwave heating provides energy savings of up to 85-fold (Yu et al., 2017). Only a few researchers have used this technology for HMF and furfural production. Li et al., (2009) used microwave irradiation at 400W for 1 min to convert cellulose with 3.6% $CrCl_3$ in [C4MIM]Cl at 100^{o}C and achieved 60% HMF yield, In contrast, the above reaction with the same conditions was carried out using an oil bath at 100^{o}C for 60 min and 17% yield of HMF was achieved. It was noted that the high yield resulting from using microwave heating was due to rapid thermal energy transfer achieving 60% HMF yield at 1 min compared to 17% HMF yield at 60 min.

6.3 Effects of operating conditions on HMF and Furfural yield from cellulose.

6.3.1 Effect of Lewis acids

Lewis acids such as $AlCl_3$, $CrCl_3$, $CuCl_2$ etc. have been used by researchers to increase the selective formation of HMF from glucose (Mansilla et al., 1998, De et al., 2011). The chloride ion in the metal-halide catalyst promotes the isomerisation of glucose through the 1,2-hydride shift pathway to fructose and increases the dehydration of fructose to HMF (Li et al., 2018c, Mittal et al., 2020). Here the feasibility of conversion of α-cellulose to HMF was studied using $AlCl_3$, $CaCl_2$, $CuCl_2$, $FeCl_3$, $MnCl_2$. No HMF was detected when only a Lewis acid was used, this was due to the inefficient hydrolysis of cellulose to glucose due to lack of H^+ present. To

attain efficient hydrolysis of cellulose to glucose and its further conversion to HMF, the addition of a Bronsted acid was used. HCl and H_2SO_4 are Bronsted acids widely used with HCl achieving a higher yield of HMF and furfural due to its stronger acidic properties (Zhang et al., 2013b). Therefore, different Lewis acids in combination with HCl (Bronsted acid) were used as catalysts for cellulose conversion to HMF and furfural. The $AlCl_3$ catalyst had the highest HMF (17.9mg g^{-1}) and furfural (206.2 mg g^{-1}) yield (Table 6.2) due to its efficient interaction with glucose likely due to its small atomic radii amongst the acid catalysts evaluated. The trend observed from this work was $AlCl_3$ > $FeCl_3$ > $MnCl_2$ > $CaCl_2$ > $CuCl_2$ (Table 6.2). Pagán-Torres et al., (2012) found out that Lewis acids with a smaller ionic radius display stronger electrostatic interactions with sugars thereby catalysing the conversion of glucose more efficiently, they observed an decrease in HMF (68% to 44% yield) with a trend of $AlCl_3$ > $SnCl_4$ > $GaCl_3$ > $InCl_3$ > $YbCl_3$ > $LaCl_3$. Ishida and Seri, (1996) also observed that lanthanide ions with smaller atomic number showed a fast-initial rate of HMF generation when they studied the effects of lanthanide (III) salts on glucose dehydration to HMF. Hence a combination of $AlCl_3$ and HCl catalyst was used for subsequent experiments in this work.

Table 6.2. HMF and Furfural yields from different Lewis acid catalysts with HCl.

S/N	**Lewis Catalyst**	**Cellulose conversion (%)**	**Yield (mg g^{-1})**	
			HMF	**Furfural**
1.	$CaCl_2$	35	2.66	130.8
2.	$CuCl_2$	24	1.78	140.3
3.	$FeCl_3$	44	8.25	216.5
4	$MnCl_2$	35	4.75	200.1
5	$AlCl_3$	48	17.90	206.2
6	HCl alone	31	3.47	156.9

Reaction conditions: 5 wt% cellulose in DMSO, 1 wt% HCl, 0.1 wt% Lewis acid, at 170°C, for 10mins in a microwave.

6.3.2 Effect of $AlCl_3$ and HCl concentrations

Untreated α-cellulose was reacted in a microwave digestion system at 170°C for 5min with varying concentrations of $AlCl_3$ and HCl to determine the optimum $AlCl_3$ and HCl concentrations. At constant 0.1wt% $AlCl_3$, increasing HCl concentration from 0.5wt% to 1wt% increased both HMF and furfural yields from 12.7 and 175.9 mg g^{-1} to 19.8 and 218.7 mg g^{-1} respectively. A further increase in HCl above 1 wt% led to a decrease in HMF and furfural yields due to the rehydration to Levulinic acid and degradation reactions (Fig 6.3). Likewise, when HCl concentration (1 wt%) was kept constant, increasing $AlCl_3$ concentration to 0.1 wt% increased HMF and furfural yields by 7.07 and 6 mg g^{-1} respectively. A further increase in $AlCl_3$ above 0.1 wt% decreased both HMF and furfural yield due to rehydration to Levulinic acid and degradation reactions. Furthermore, the benefits of combining both Lewis and Bronsted acids were observed when a control experiment was done with HCl or $AlCl_3$ alone. Using HCl alone gave rise to very low HMF yield (3.80 mg g^{-1}) while furfural yield of 156 mg g^{-1} (similar to when $AlCl_3$ and HCl were used) was obtained which shows that HCl alone was sufficient for reaction to furfural. Furthermore, no product was obtained when $AlCl_3$ was used alone. This is because HCl is responsible for the hydrolysis of cellulose to glucose monomers while, $AlCl_3$ is mainly responsible for isomerisation of glucose to fructose before subsequent rehydration to HMF and furfural (Guo et al., 2020).

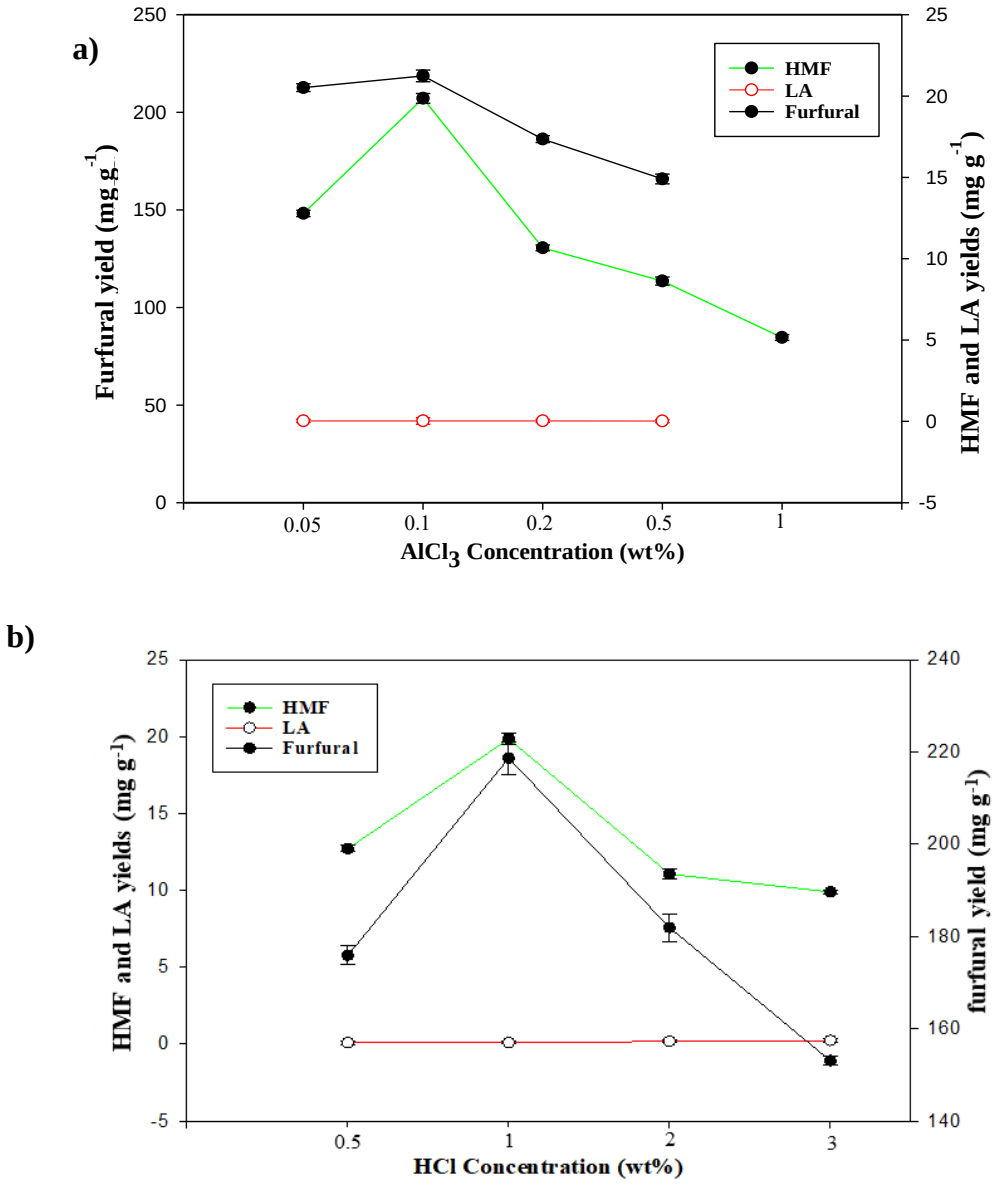

Fig 6.3: HMF, Furfural and Levulinic acid (LA) yields at varying concentrations of; (a) $AlCl_3$ at constant HCl of 1 % by weight and (b) HCl at constant $AlCl_3$ of 0.1. Reaction conditions: 5wt% cellulose in DMSO, 170°C, for 5 mins in a microwave.

6.3.3 Effects of reaction temperature and time

Experiments were performed with untreated α-cellulose at different temperature and times to optimise HMF and Furfural production. Temperatures of 160°C - 180°C and reaction times from 2 to 20 min were utilised for this study. Test experiments below 160°C showed a low furfural production (94 and 109 mg g^{-1} at 130°C and 150°C respectively) with no HMF formation. High temperature (>150^{o}C) is needed to overcome the high activation energy needed for HMF formation (Okano et al., 2013, Zhou et al., 2017, Moreau et al., 2006). HMF yields reached a maximum (19.9 mg g^{-1}) at 170°C for 5mins (Fig 6.4a) and then decreased with prolonged reaction time due to rehydration to Levulinic acid and cross-polymerisation between HMF and glucose forming humins (Jadhav et al, 2014). Shi et al., (2013) reported that cellulose hydrolysis to glucose is the rate determining step in the production of HMF as the activation energy for hydrolysis of cellulose (180 kJ mol^{-1}) is higher than the activation energy of glucose conversion to HMF (135 kJ mol^{-1}). Therefore, high temperature (> 150^{o}C) is needed to overcome the high activation energy (180 kJ mol^{-1}) of cellulose hydrolysis to its sugar monomers before further dehydration to HMF (da Silva Lacerda et al., 2015). Levulinic acid (LA) was observed to increase with reaction time for all temperatures (Fig 6.4c) as it is obtained from the subsequent rehydration of HMF. Although, very low LA yields were observed with the highest at 0.06 mg g^{-1} of cellulose suggesting the effective suppression of HMF rehydration as a result of using DMSO as solvent through inhibition of acyclic reactions that leads to undesirable reactions (De et al., 2011, Choudhary et al., 2013). At 180^{o}C, HMF yield was observed to decrease drastically likely due to its degradation and the formation of humins as LA yields at 180°C were relatively constant.

At any given reaction temperature, furfural yields were highest with shorter reaction times i.e. 5min. An increase in reaction time led to a steady decrease in furfural yield likely due to furfural degradation. Hence, optimum temperature and time chosen for subsequent reactions in this work were 170°C and 5 min.

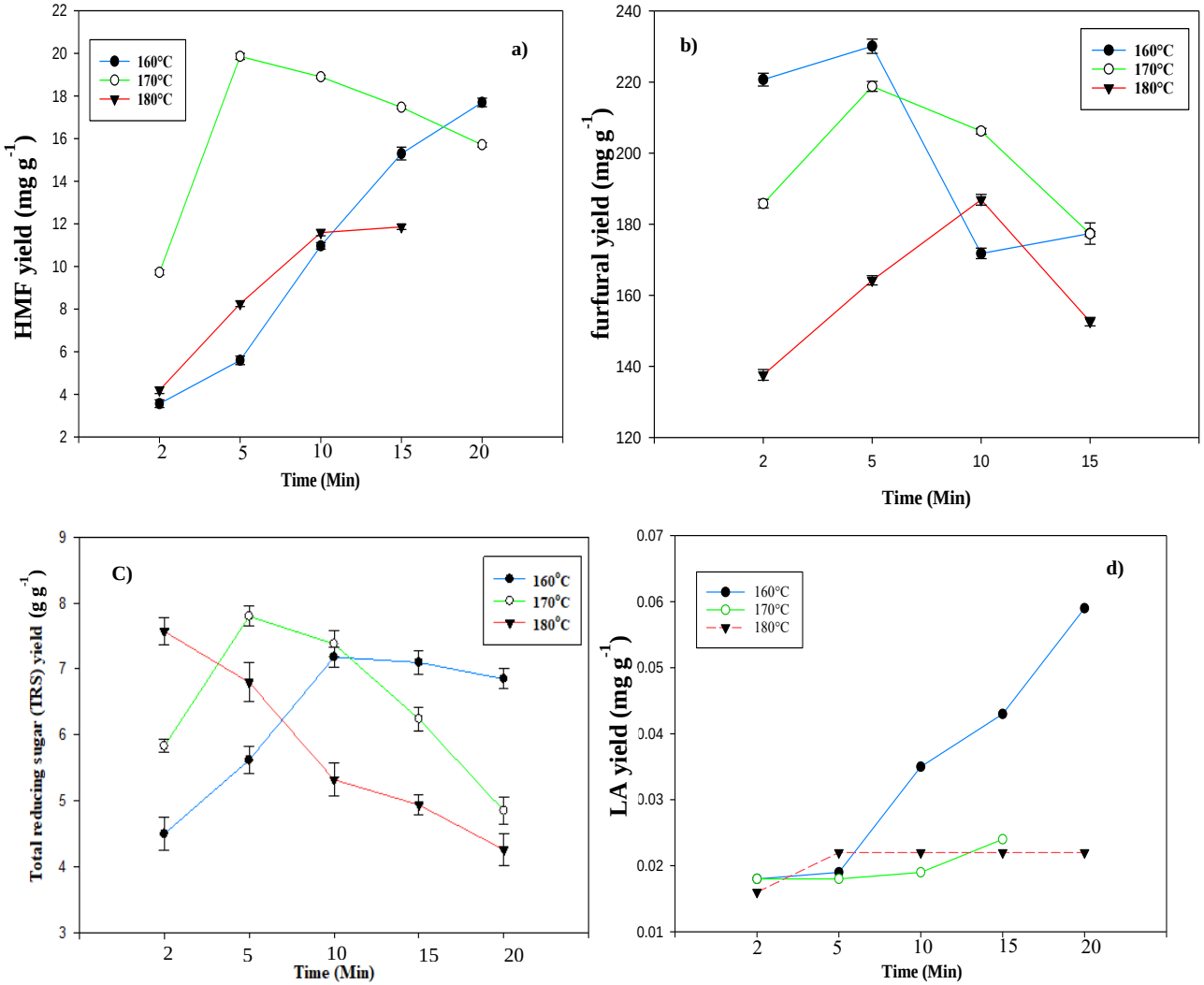

Fig. 6.4: Effect of reaction temperature and time on; (a) HMF, (b) Furfural, (c) TRS and (d) Levulinic acid (LA) yields. Reaction condition: 5wt% cellulose, 1 wt% HCl, 0.1 wt% $AlCl_3$, DMSO

6.3.4 Effect of cellulose concentration.

A range of cellulose concentrations (5-20 wt%) were tested, and results shows that increasing the cellulose concentration from 5 to 10 wt% increased the HMF yields from 18.2 to 26.6 mg g^{-1} with a subsequent decrease as cellulose concentration was increased beyond 10 wt%. while a decrease in furfural yield was observed with increasing cellulose concentration. Approximately 40% of cellulose was converted at 5 and 10 wt% cellulose concentration while a 30% conversion was achieved for 20wt% cellulose concentration due to its partial solubility in DMSO. The decrease in HMF and furfural yields with increasing cellulose concentration can be attributed to side reactions due to cross-polymerisation between excess cellulose or glucose and HMF or furfural as reported in previous studies (Qi et al., 2014, Wang et al., 2016, Zhou et al., 2017).

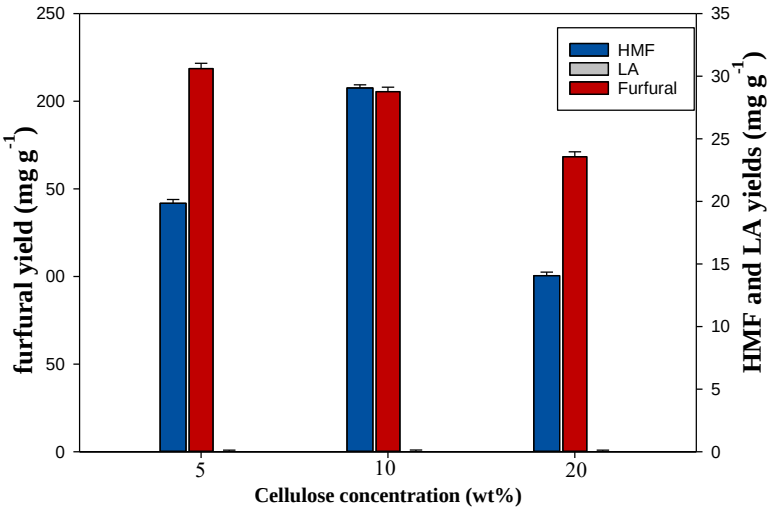

Fig 6.5. Effect of cellulose concentration on HMF, furfural and levulinic acid (LA) yields. Reaction condition: 5 – 20 wt% cellulose, 1 wt% HCl, 0.1 wt% $AlCl_3$, 20mL DMSO at 170ºC for 5 mins.

6.3.5 Effect of water addition to the reaction system.

Moving to economic and green solvent media, minimising solvent use is highly necessary (Mittal et al., 2020). A combination of polar aprotic solvent – water media has been proven to be effective solvent for substrate solvation and target product (Jin et al., 2021). As cellulose hydrolysis to glucose is the rate determining step to production of HMF and furfural, addition

of water is necessary to improve hydrolysis of cellulose to glucose before further conversion to HMF or furfural (Hu et al., 2012). The optimum amount of water needs to be determined as excessive amounts of water have a negative effect on HMF yield (da Silva Lacerda et al., 2015). High water dosage leads to the abundance of H^+ ions which promotes the rehydration of HMF to LA (Shi et al., 2013). Hence, the optimum water content was determined as well as its influence on product yield.

Addition of water led to an increase in HMF and furfural yield (Fig 6.6a). In the absence of water, cellulose was depolymerised partially to glucose yielding a total reducing sugar (TRS) of 7.8 g g^{-1} (Fig 6.6b) with low yields of HMF 29.3 mg g^{-1} (3 mol%) and furfural 243.8 mg g^{-1} (36.5mol%). Addition of water to obtain a DMSO-water ratio of 8:2 (vol/vol) showed an increase in TRS to 20.7 g g^{-1} which in turn increased HMF and furfural yields to 45.2 mg g^{-1} (5.4mol%) and 317.8 mg g^{-1} (55 mol%) respectively. The addition of water shifted the equilibrium of the reaction towards promoting cellulose hydrolysis which in turn led to the availability of more glucose which can then be converted to HMF and furfural (da Silva Lacerda *et al.*, 2015). However, the addition of more water to obtain a DMSO-water ratio of 6:4 (vol/vol) led to a slight increase in HMF and furfural yields by 5 and 69 mg g^{-1} respectively. A notable increase in LA yield of 0.73 mg g^{-1} (Fig 6.6a) was observed which was due to an abundance of H^+ ions rehydrating HMF to LA. Hence, an optimum DMSO-water ratio of 8:2 (vol/vol) was used for subsequent experiments. Furthermore, increase in HMF and furfural yields can be attributed to increase in isomerisation of glucose to fructose in the presence of $[Al(HO)_2]^+$ formed from $AlCl_3$ dissociation in water (Mittal et al., 2020). Various researchers have shown that a DMSO-water media optimises the stability and selectivity of HMF and furfural. Tsilomelekis et al., (2016) studied the origin of HMF stability in DMSO-water and showed that DMSO favourably solvated HMF with water content below 0.4 molar in a DMSO-water media. Similarly, Kimura et al., (2013) found that the D-Cellobiose conversion in DMSO-water media (8:2 vol/vol) yielded 70mol% HMF as compared to 45 mol% yield in DMSO or 40 mol% yield in water media at 170^{o}C for 26h using conventional heating. Jin et al., (2021) also observed a higher yield of HMF (51.6 mol%) in DMSO-water media (4:1 vol/vol) from cellulose-formate (a cellulose derivative) as compared to 11.2 mol% yield in water media at 160^{o}C for 20 min in a microwave reactor.

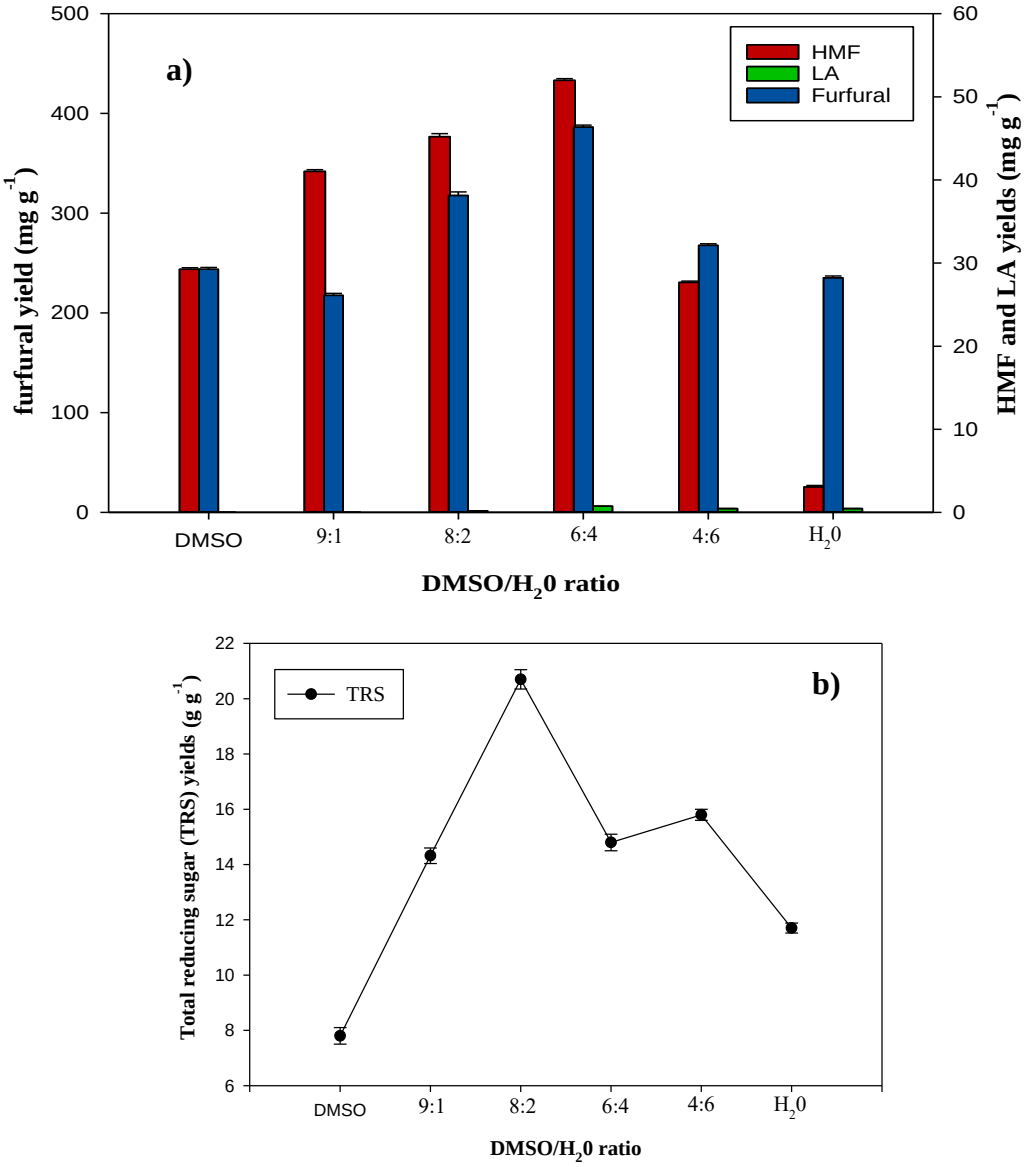

Fig 6.6: Effect of water addition on: (a) HMF, Furfural, Levulinic acid (LA) and (b) total reducing sugar (TRS) yield. Reaction conditions: 10 wt% cellulose, 1 wt% HCl, 0.1wt% AlCl3, 20mL solvent (DMSO: H2O).

Formation of humins (a brownish black solid residue) was observed as a sediment from the liquid filtrate of the reaction media with the DMSO-water mixture (8:2) (Fig 6.7). While no sediment was obtained for the DMSO only reaction. However, a darker coloured solution was obtained for the DMSO only reaction media probably due to solubility of Humins in DMSO as reported by several studies (Sumerskii et al., 2010, Alonso et al., 2013). Quantification of the amount of humins was difficult due to some of it being present in the residual cellulose and the rest in the filtrate (obtained after sedimentation).

Humins are products formed from the condensation reactions between HMF and sugars and intermediate during dehydration of carbohydrates (Van Zandvoort et al., 2013). The applications for humins are currently limited to the generation of heat through burning (Mija et al., 2017). It also has a potential of being used to produce biobased thermoset resins and adhesives (Sevilla and Fuertes, 2009) as well as feedstock for the production of synthesis gas and hydrogen due to its high carbon content of approximately 60 wt% (Hoang et al., 2015). Van Zandvoort et al., (2013) proposed a structure for humin as a furan ring connected through alkylene moieties. To confirm that the solid precipitate was humins, FTIR spectra was compared against cellulose (Fig 6.7). The FTIR spectra showed a peak at 2250 cm^{-1} corresponding to C-C triple bonds which arise from condensation reaction between HMF, sugars and intermediates (Mija et al., 2017). Peaks at 1020, 800 and 750 cm^{-1} corresponding to C-O and C-H bend of substituted furans, shows that humins were mainly derived from HMF (Sevilla and Fuertes, 2009, Patil et al., 2012). Absence of a peak at 3300 cm^{-1} (which correspond to O-H bonds) suggested removal of water arising from the condensation reaction.

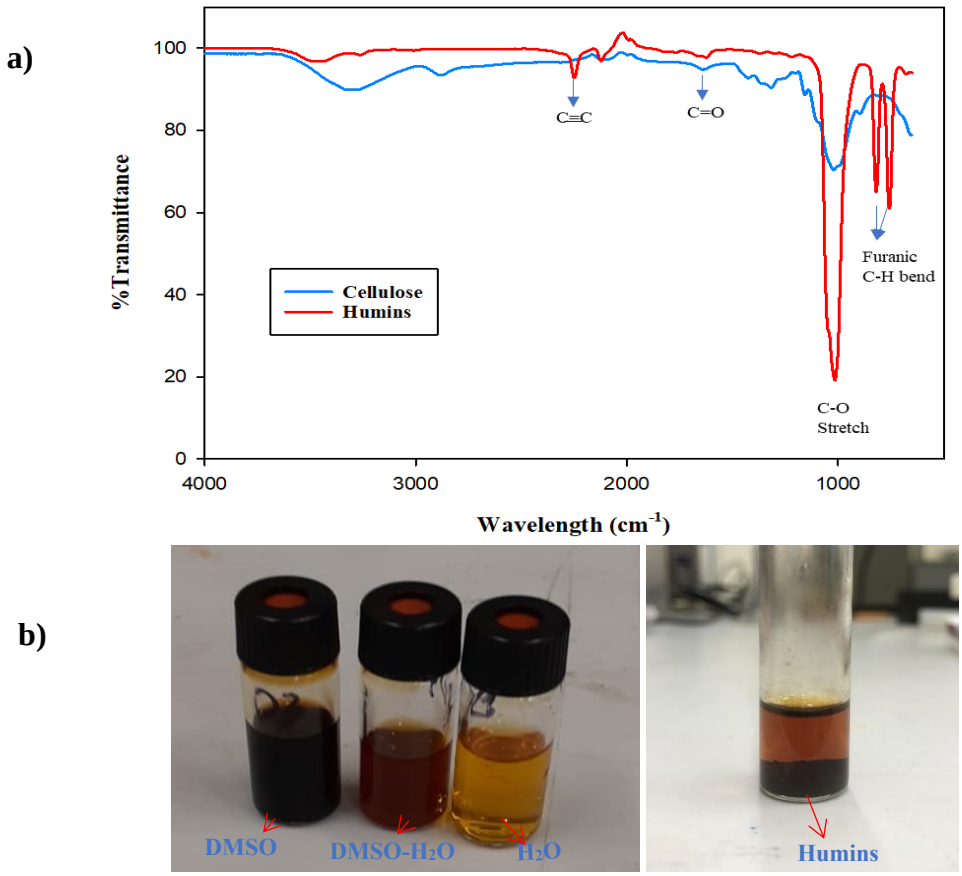

Fig. 6.7: FTIR spectra of (a) humins and (b) pictures of humins in different solvents.

Several reaction pathways for the formation of HMF and Furfural have been described in the literature (Shen and Gu, 2009, Guo et al., 2020, Shi et al., 2013). Therefore, from the products obtained in this work, the reaction pathway to which cellulose is converted to HMF and Furfural is described (Fig 6.8). Cellulose undergoes hydrolysis in the presence of H^+ (from HCl and H_2O) by cleavage of the glycosidic bond ring on the cellulose to glucose, producing a glucose molecule with an aldehyde on one of its carbons. Removal of the aldehyde in the presence of H^+ yields an intermediate which then undergoes subsequent dehydration to form furfural (De et al., 2011). Furfural can be formed from the decomposition of HMF through dehydromethylation of the furan ring yielding furfural and formaldehyde (Shafizadeh et al., 1971, Guo et al., 2020). However, since formaldehyde wasn't detected in this work, it is believed that furfural formation didn't occur through HMF decomposition. Furthermore, the glucose obtained from cellulose hydrolysis isomerises in the presence of Al^{3+} and $[Al(HO)_2]^+$ (formed from dissociation of $AlCl_3$) to fructose then undergoes subsequent dehydration by the removal of three water molecules to form HMF which in the presence of excess water undergoes hydration to form levulinic and formic acids. In addition, condensation reactions between, HMF, furfural, sugars and intermediates occur to form other by-products such as humins, oligomers etc. This proposed reaction scheme is similar to the reaction scheme proposed by Shi et al., (2013) for reacting cellulose in the presence of catalyst ($NaHSO_4$ and $ZnSO_4$) in THF: H_2O (10:1vol/vol) media at 160^{o}C for 60 min.

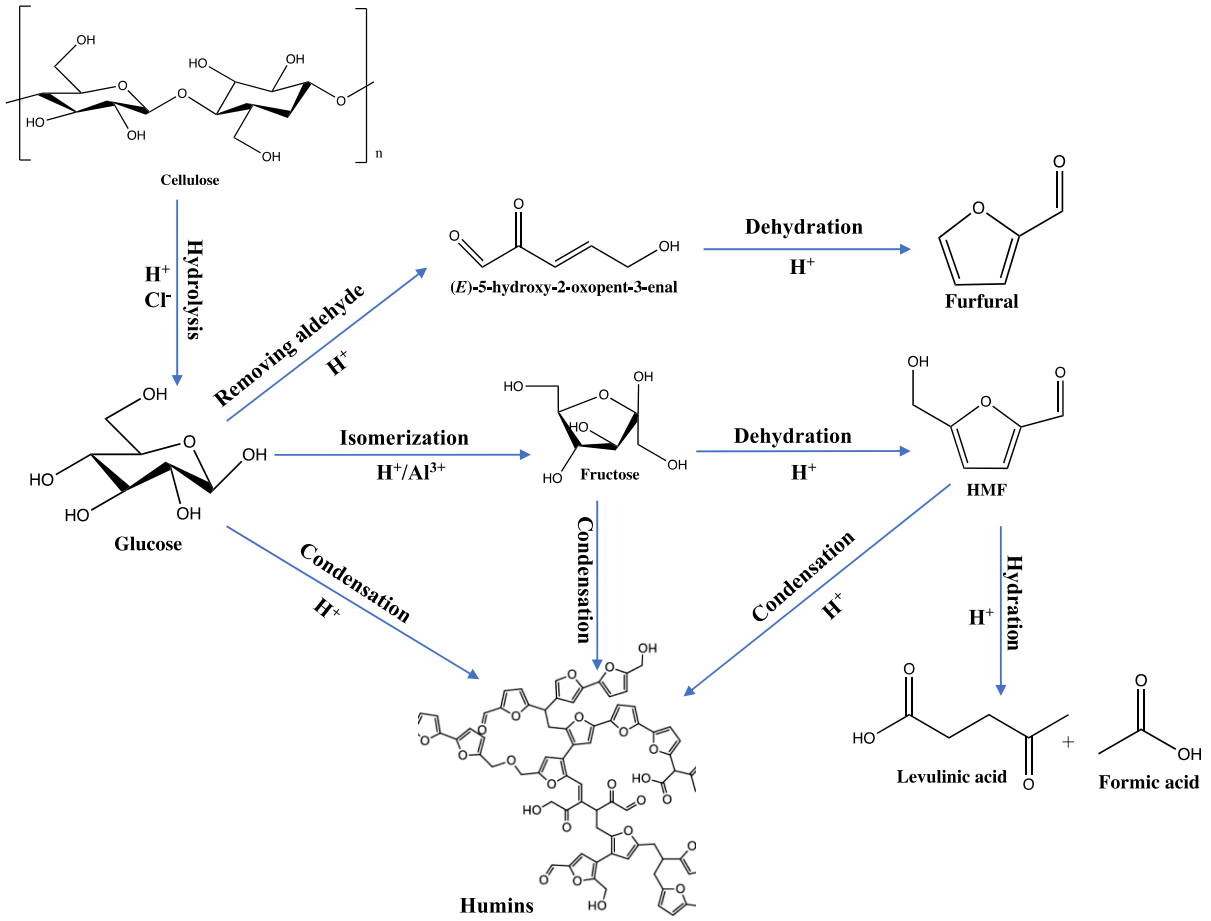

Fig 6.8: Proposed reaction scheme for the conversion of cellulose to HMF, furfural and other side products**.**

6.4 Effect of pre-treated modelled cellulose (α-cellulose) properties on conversion to HMF and furfural.

Untreated and pre-treated cellulose were converted to HMF and Furfural under the following conditions: 10 wt% cellulose, 1% HCl, 0.1% $AlCl_3$, DMSO:water (8:2 vol/vol) at 170°C for 5min. Pre-treated cellulose showed a higher yield of HMF and Furfural compared to untreated cellulose. Combined ozone and ultrasound pre-treatment of cellulose showed the highest yield of HMF (34.3 and 51.4 mg g^{-1}) and Fufural (523 and 257.3 mg g^{-1}) in both DMSO and DMSO-water media respectively as compared to HMF (29.2 and 45.2 mg g^{-1}) and furfural (243.8 and 317.6 mg g^{-1}) in DMSO and DMSO-water media respectively for untreated cellulose (Fig 6.9). As described in Section 6.2, pre-treatment led to a slight increase in % crystallinity (10 - 18%) and a decrease in particle size and degree of polymerisation. The slight increase in crystallinity was likely due to degradation of the amorphous region as an increase in crystallinity is

proportional to the extent of degradation during pre-treatment (Puri, 1984) as evident here by the decrease in the degree of polymerisation. Therefore, the degraded components of cellulose (monomers) after pre-treatment were retained in the pre-treated samples leading to increase in the availability of glucose at the start of the conversion process (Fig 6.9c) which in turn led to increased HMF and furfural yields. In addition, the rate of conversion of pre-treated cellulose likely increased due to the availability of more cellulose chain ends resulting from depolymerisation as well as increased surface area due to reduction in particle size as described (Section 6.2, Chapter 6). In addition cellulose conversion was increased from 40% to 50%. Mittal et al., (2020) studied the effect of crystallinity on HMF and furfural yield from alpha-cellulose with varying degree of crystallinity (59%, 45%, 35%, 17%) in a dioxane: water (3:1) media at 200^{o}C in the presence of $AlCl_3$/HCl catalyst and observed similar yields of 51% leading to a conclusion that cellulose crystallinity had no effect on HMF and furfural yield.

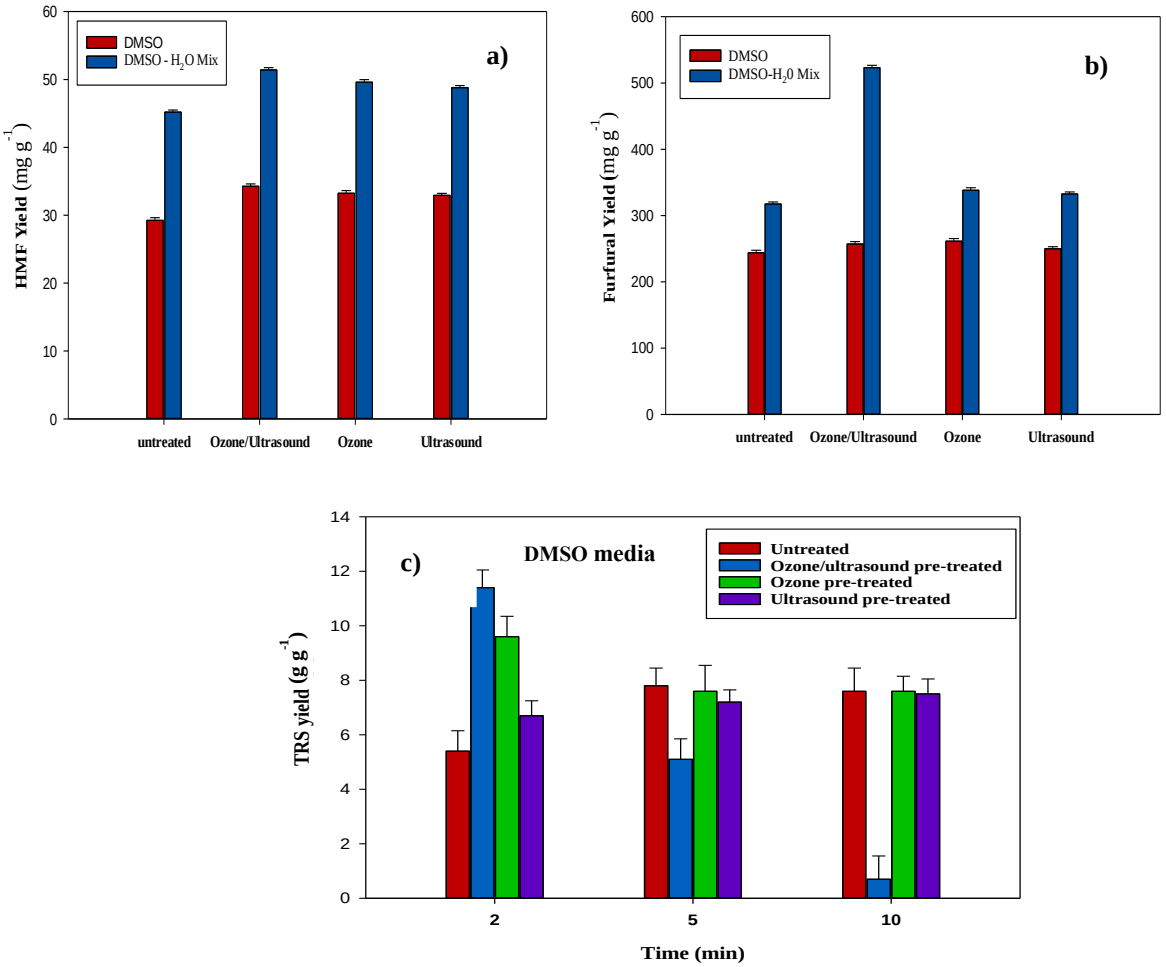

Fig 6.9**:** Effect of pre-treatment in DMSO and DMSO:water (8:2 vol/vol) on: (a) HMF, (b) furfural and (c) total reducing sugar (TRS) yields at 2 – 10 mins.

6.5 Effect of pre-treated and fractionated lignocellulosic cellulose properties on its conversion to HMF and furfural.

Untreated and pre-treated (non-fractionated) corn cob and spelt husk (as described in Chapter 5) were converted to HMF and furfural. HMF yields were highest in the ozone + ultrasound pre-treated feedstock (33.5 and 43.1 mg g^{-1}) followed by ozone (20.7 and 31.6 mg g^{-1}) and then untreated feedstock (15.9 and 11.8 mg g^{-1}) respectively. Similarly, furfural yields were highest for ozone + ultrasound pre-treated feedstock (1050 and 303.9 mg g^{-1}) followed by ozone pre-treated (978.1 and 245.7 mg g^{-1}) and then untreated feedstocks (884.2 and 103.3 mg g^{-1}) respectively. This is as a result of increased surface area caused by dis-organised morphology of cellulose and decrease in degree of polymerisation as described in Section 5.7. Although, a slight decrease in the % crystallinity (10% decrease) of pre-treated feedstock was observed due to increased disorder and amorphisation resulting from the removal of lignin (Section 5.5).

Comparing untreated corn cob and spelt husk (Fig 6.10), it was observed that HMF and especially Furfural yield of corn cob (15.9 and 884 mg g^{-1}) were higher than spelt husk (11.8 and 103.3 mg g^{-1}) due the lower lignin (5 vs 16 wt%) and higher carbohydrate content (81 vs 60.9 wt%) Section 3.3. In addition, another influencing factor was the difference in their morphology as corn cob was more porous with a loosely packed fibrous structure when compared to the more densely packed spelt husk (Fig 5.3, Section 5.2.3). Hence, a small difference of 17.5 mg g^{-1} in HMF yield was observed between untreated and OU pre-treated corn cob while, a greater difference of 31.2 mg g^{-1} in HMF yield was observed between untreated and ozone pre-treated spelt husk. A similar HMF yields was observed for both pre-treated (fractionated) and pre-treated feedstocks (unfractionated). The major difference with fractionated and unfractionated feedstock is that the lignin obtained for the fractionated process is of high purity (>95%) while for unfractionated process is of low purity and requires extra cost to separate from cellulose hydrolysis products.

The literature survey shows that studies on biomass pre-treatment and further conversion to HMF and furfural are very scarce. Recently, Kumar et al., (2021) pre-treated rice straw by grinding in liquid nitrogen and observed a significant decrease in particle size and disruption of its internal structure leading to HMF and furfural yield of 18 and 62 mg g^{-1} respectively using oxalic acid dihydrate, $AlCl_3$, HCl and activated charcoal as catalysts and DMSO, MIBK:2-butanol as solvents at 130^{o}C under reflux for 6 hours. Using the same reaction conditions, no HMF and furfural were detected using untreated rice straw feedstock due to its

high recalcitrant nature. Nis and Kaya Ozsel, (2020) reacted untreated corn straw and sorghum with amberlyst-15 catalyst in THF/water (3:1) media at 180^{o}C for 30 min and obtained HMF yield of 5 and 4 mg g^{-1} respectively. Although, high levulinic acid yields of 43.3 and 94.3 mg g^{-1} were obtained as a result of efficient dehydration of HMF to levulinic acid and humins. Furthermore, Nis and Kaya Ozsel, (2021) reacted untreated sorghum in ionic liquid – water ([BMIM]HSO_4 : H_2O) media 1:5 at 180^{o}C for 30 min and obtained 117.4 mg g^{-1} levulinic acid, 11.8 mg g^{-1} HMF and 9.4 mg g^{-1} furfural. The high yield of levulinic acid was attributed to the efficient dehydration of HMF due to the acidic nature of the ionic liquid. Therefore, results from this work shows that ultrasound-assisted ozone pre-treatment of feedstocks prior to hydrolysis significantly increase the HMF and furfural yield and selectivity.

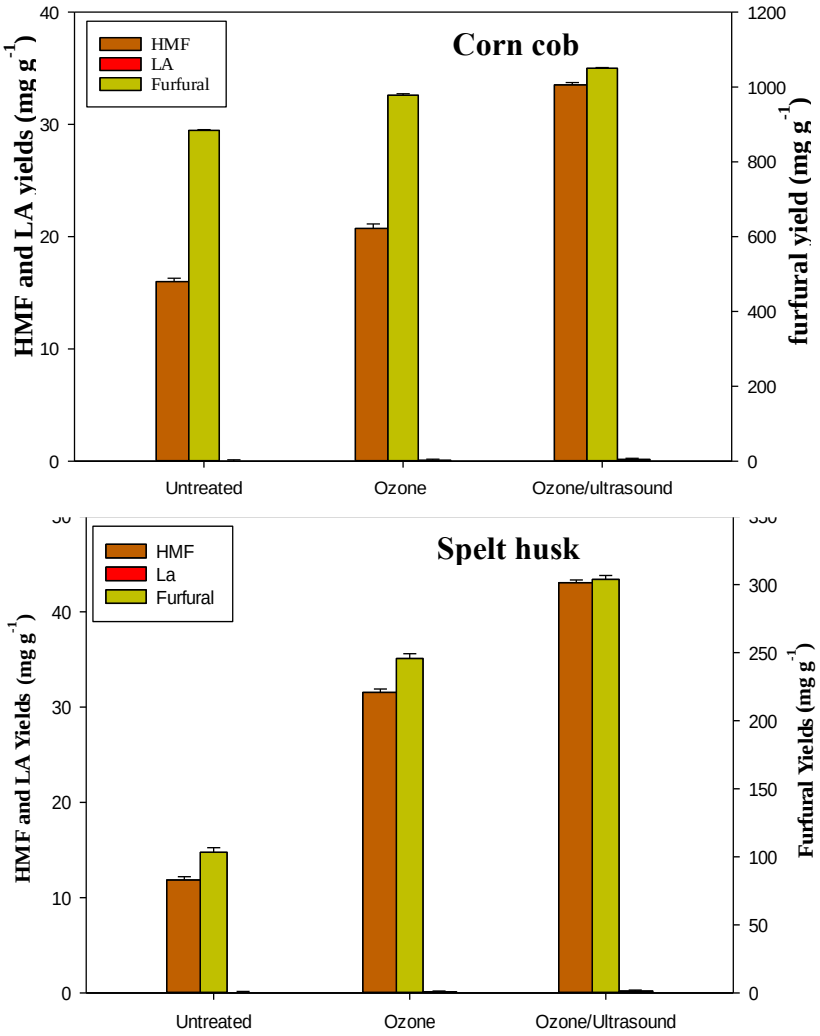

Fig 6.10**:** HMF and furfural yields from untreated and pre-treated corn cob and spelt husk. Reaction conditions: 10 wt% cellulose, 1 wt% HCl, 0.1wt% AlCl3, 20mL solvent (DMSO: H_2O) at 170ºC for 5 mins.

6.6 Summary

In a microwave reactor, corn cob and spelt husk (untreated and pre-treated) were reacted in DMSO-H_2O media to produce HMF and furfural. HMF and furfural yields of untreated corn cob were higher than those from spelt husk due to differences in their morphology as untreated corn cob was more porous than spelt husk allowing easier access to cellulose. Pre-treatment led to a 58% increase in HMF yield and 74% increase for corn cob and spelt husk respectively, while a 10% and 66.7% increase in furfural for corn cob and spelt husk were observed respectively. Reacting fractionated cellulose from corn cob and spelt husk produced a similar HMF yield of 40 mg g^{-1}. Overall, HMF and furfural yields were influenced by change in cellulose properties such as fibre size, surface area, degree of polymerisation achieved through cellulose pre-treatment, and lignin content all of which can be influenced by pre-treatment. Ozone pre-treatment had a more pronounced effect on cellulose properties obtained from biomass feedstock compared to the model cellulose due to the selective reaction with lignin which is 10^6 times faster than for the reaction of ozone with carbohydrates (Travaini et al., 2016).

Chapter 7: Techno-economic analysis of the co-production of HMF, furfural and lignin from spelt husk.

This chapter describes the techno-economic potential and competitiveness of the conversion process for large scale co-production of 5-hydroxymethyl furfural (HMF), furfural and lignin from spelt husk (scenario A). The proposed approach was compared with scenario B, where HMF and furfural are co-produced without lignin. A plant capacity of 100 tonnes per day of wet spelt husk (with 11 wt% moisture content) was considered for 320 effective working days of operation per year and 35 days of plant maintenance per year.

7.2 Process overview

The process utilises ultrasound-assisted ozone technology to pre-treat spelt husk (described in Chapter 5). The ozone used for pre-treatment was generated *in-situ* via a cold plasma ozone generator (Chapter 4) for both scenarios A & B. For scenario A, the pre-treated feedstock was then fractionated with ethanol/water into lignin and holocellulose (cellulose and hemicellulose). The holocellulose then undergoes acid hydrolysis before subsequent conversion to HMF and furfural. The simplified process design (Fig 7.1) consists of eight (8) areas, including feedstock handling, product separation and purification, wastewater treatment, ethanol recycling, product storage and utilities for scenario A while scenario B follows the same process with the exception of the fractionation and lignin recovery area (Area 300).

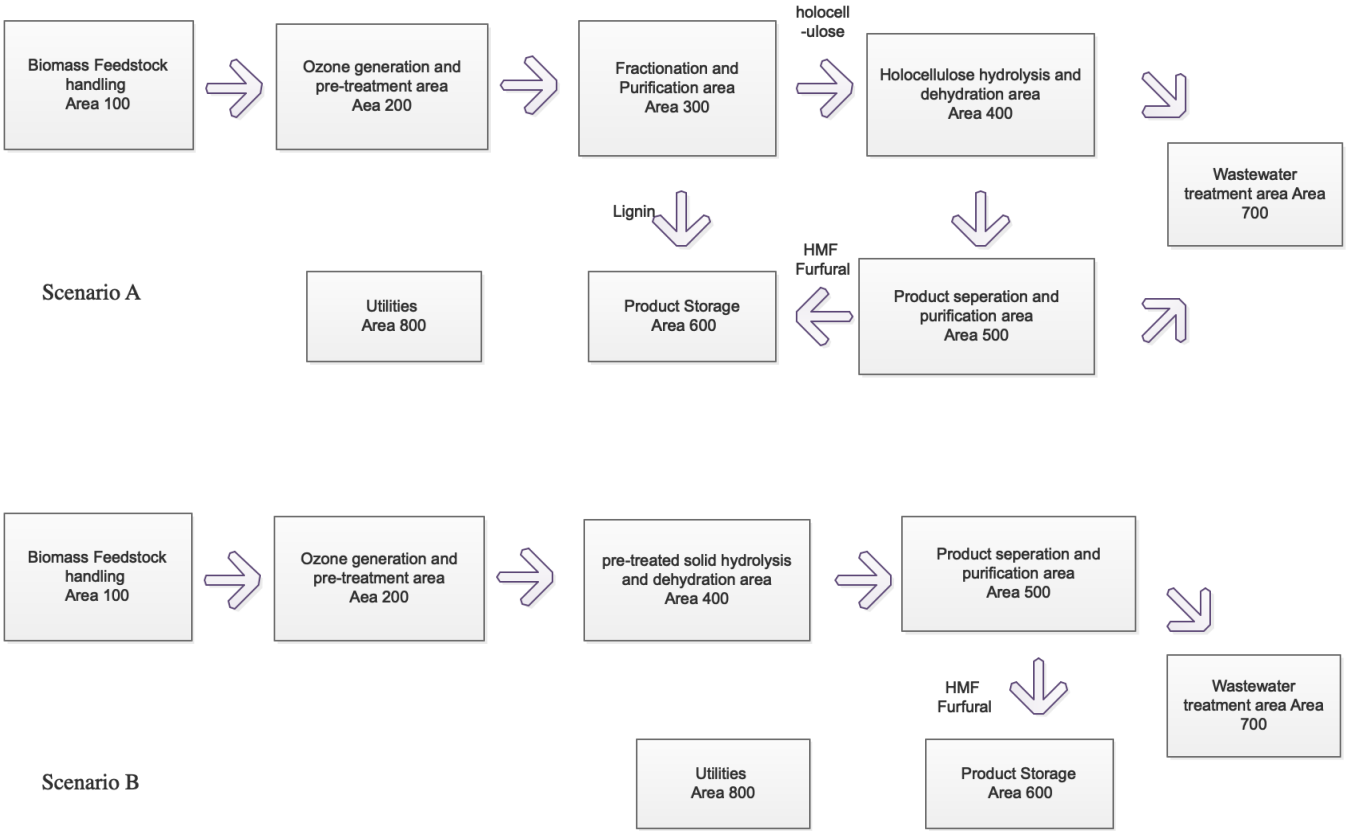

Fig 7.1: A simplified process flow diagram for Scenarios A and B.

AREA 100: Feedstock handling and size reduction.

The biomass feedstock (spelt husk) is delivered to this area of the plant via a truck and piled in a storage room. Before pre-treatment, the feedstocks are screened for unwanted materials such as metals via a magnetic separator, from there the feedstock passes to a hammer mill (stream 1), for size reduction to 1.0mm (optimum size for increase surface reaction between ozone and feedstock) (Schultz-Jensen et al., 2013). A hammer mill capable of processing 3.9 tonnes h^{-1} was used, and the ground spelt husk was collected in batches for the next stage. 100 tonnes of ground spelt husk with 11 % moisture content was transferred into stainless steel pre-treatment tank (stream 2). Stainless-steel was chosen for the pre-treatment tank to avoid corrosion with ozone (Ben'ko et al., 2013, Panneerselvam et al., 2013b, Li et al., 2015a, García-Cubero et al., 2009). As 40% moisture content was found to be the optimum for efficient ozone pre-treatment of spelt husk (Chapter 5, Section 5.2.3), 29,000 litres of water were added to 100 tonnes of spelt husk to increase the moisture content from 11 to 40 %. Hence, there was no need for drying of the feedstock.

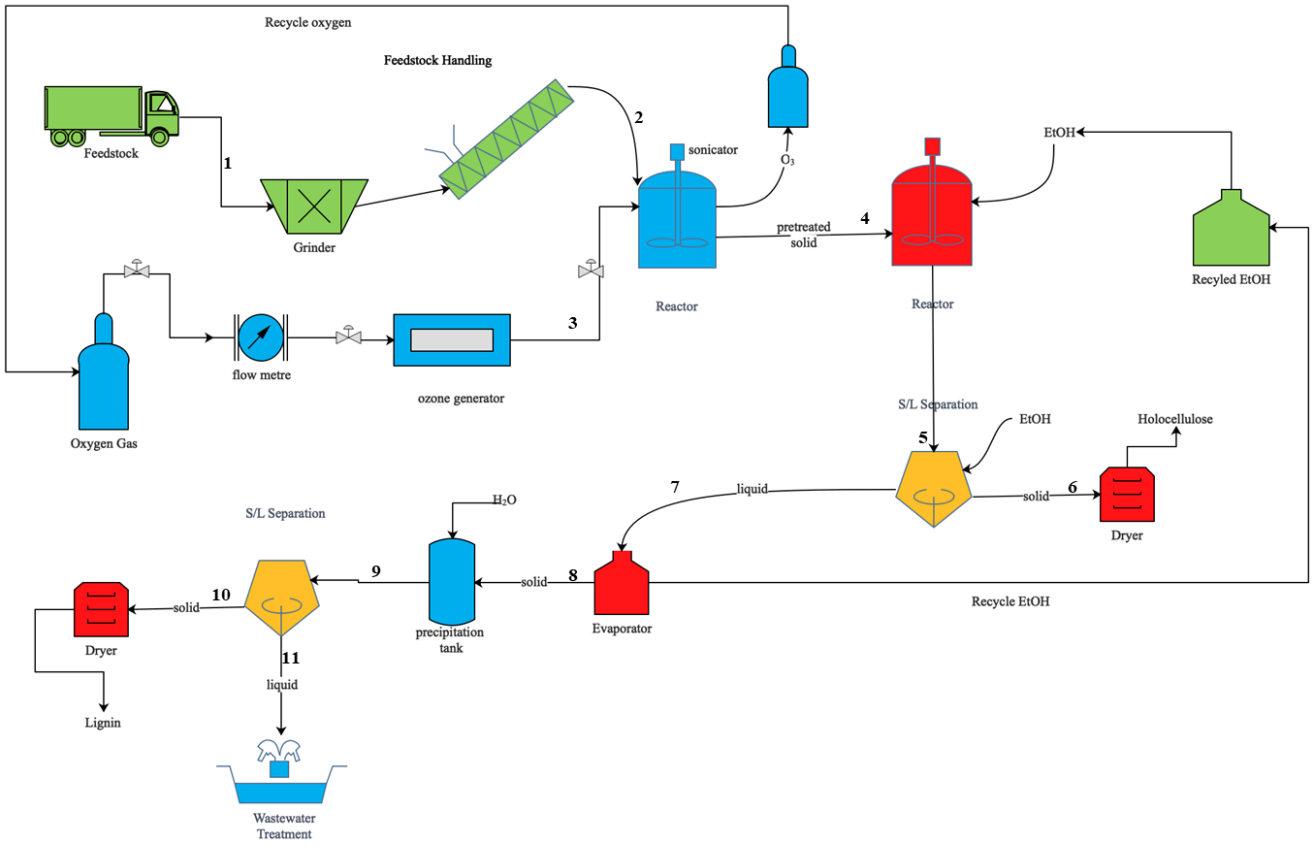

Fig 7.2: A detailed process flow diagram of Areas 100, 200 and 300 (i.e. feedstock handling, pre-treatment and fractionation areas).

Area 200: Ozone generation and pre-treatment area.

An ultrasonic horn (ultrasonic transducer of 3cm diameter at a frequency of 40kHz with a power amplifier of 50 W) (Wierschem et al., 2017) was placed above the stainless steel pre-treatment tank containing spelt husk from area 100 to improve the mass transfer of ozone (stream 3) to biomass and ozone consumption (Fig 7.2). It was assumed that one transducer connected to one power amplifier impinge a volume of $5m^3$ with 50W of power would achieve a power output of 10 W m^{-3} (Chapter 5) Therefore, for this process, 20 transducers and power amplifier are used to produce the ultrasound needed for pre-treating a volume of 100 m^3. A stainless-steel tank capacity of $100m^3$ was used for pre-treatment as no temperature and pressure regulator was required (Ben'ko et al., 2013, Panneerselvam et al., 2013, Li et al., 2015, García-Cubero et al., 2009). Pre-treatment was carried out in 2 batches at room temperature and atmospheric pressure consecutively for 30 min each. Two batches were used to enhance pre-treatment efficiency as one batch might not be adequate considering the quantity of

ultrasound used per m^3. Ozone gas was generated *in-situ* using an energy-efficient (11 kWh kg^{-1} O_3) designed cold plasma generator (Chapter 4). From experimental data obtained (Chapter 5, Section 5.2.1), 0.39g of ozone was consumed per gram of spelt husk. Therefore, for a plant size of 100 tonnes day^{-1}, 39 tonnes day^{-1} of ozone is required for pre-treatment to obtain 91 tonnes of pre-treated solid and 9 tonnes of liquid containing various carboxylic acids such as oxalic acid, acetic acid etc. obtained from the breakdown of lignin molecules and hydrolysed carbohydrate (Fig 5.2, Section 5.2.3). No washing was required after pre-treatment as the pre-treated feedstocks were transferred to Area 300 for fractionation and purification.

Area 300: Fractionation and purification area.

The pre-treated solid (spelt husk) from area 200 was transferred (Stream 4) to a $1000m^3$ stainless-steel jacketed reactor with agitation operated at 80ºC, atmospheric pressure and a residence time of 2 hours. This type of reactor was needed in the section as proper mixing of solvent with solid was required for efficient fractionation and maintenance of temperature at 80°C (Matsakas et al., 2019). From experimental data obtained in Chapter 5, Section 5.3, 728,000 litres of the solvent containing 432,430 litres of ethanol, 288,280 litres of water (60:40 v/v) and 7280 litres of hydrochloric acid was pumped into the reactor to give a solid to liquid ratio of 1:8 and the mixture refluxed for 2 hours. After the reaction, the mixture was transferred (Stream 5) to a vacuum belt filter and ethanol was pumped into the filter to wash off the remaining lignin from the solid. A vacuum belt filter was used as it is estimated to recover 95% of sugars using a cake washing process due to its high unit capacity, speed and low cost (Sievers et al., 2014). An output of 70.5 tonnes of solid was obtained from the filter containing the bulk of cellulose and hemicellulose, transferred (Stream 6) to a rotary vacuum dryer with a moisture content of zero and then stored in a storage tank in Area 600. After that, the filtrate (20 tonnes day^{-1}) from the vacuum belt filter containing a mixture of lignin, water, ethanol and water-soluble sugars (obtained from solubilisation of hemicellulose, extractives and lignin degradation products) (Stream 7) was passed to the distillator operated at 50ºC (Jiang et al., 2020) and vaporised ethanol collected using a condenser and transferred into an ethanol recycling tank for storage. The solid from the evaporator was transferred (Stream 8) to a precipitation tank and water was added to precipitate lignin and pass through a vacuum belt filter (Stream 9) where 11.5 tonnes day^{-1} of lignin was collected as solid and passed to the vacuum drum dryer (Stream 10) for drying (Jiang et al., 2020). The liquid containing water, carboxylic acid and sugars was passed to the distillation column. Solid from the distillation

column was sent to the combustor/boiler (Area 800) and water was transferred to the waste-water treatment area (Stream 11) (Area 700).

Area 400: Holocellulose hydrolysis and dehydration area

Dried hollocellulose (70.5 tonnes) obtained from area 300 was transferred to a microwave reactor (Stream 12) and 1 wt% HCl, 0.1 wt% $AlCl_3$, water and DMSO (20:80) (Stream 13) were added to form a solid-liquid ratio of 1:8 (Chapter 6, Section 6.3). The microwave reactor was operated at 170°C for 5mins. A microwave reactor capacity of 1000kg of solid per cycle was assumed for this work as large-scale microwave reactors (having limitation of penetration depth of microwave irradiation for large scale vessels) are currently unavailable due to the technology being in the development stage with no subsequent costs and technical management data available for large-scale plants (Shao et al., 2019, Wang et al., 2015a), leading to 70.5 cycles per 10 min each. The mixture was passed through a vacuum belt filter (Stream 14) where unreacted holocellulose was separated and recycled while the liquid was passed through a decanter (Stream 15) to separate the aqueous and organic layers (Fig 7.3). The aqueous layer was passed (Stream 16) to the waste-water treatment area (Area 700), while the organic layer was transferred (Stream 17) to the product separation and purification area (Area 500).

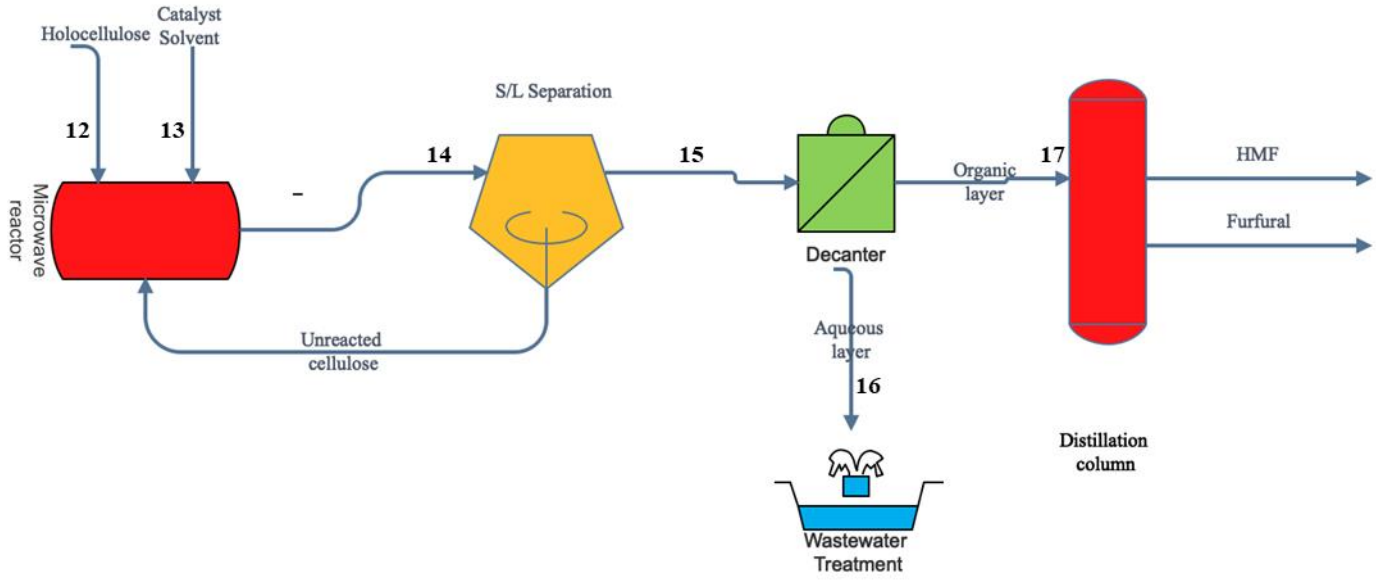

Fig 7.3: A process flow diagram of areas 400 and 500 (Hydrolysis and product separation areas).

Area 500: Product separation and purification area.

The liquid from the organic layer was passed to the distillation column to separate 3.5 tonnes day^{-1} of HMF and 25.1 tonnes day^{-1} of Furfural (Fig 7.3) at the top of the distillation column (Kim et al., 2021) while the solids (humins etc.) recovered at the bottom of the distillation column were transferred to the boiler for combustion (Area 800) while the solvent (DMSO) was recycled.

Area 600: Product storage area.

This area is where all the bulk storage of chemicals used in the process were stored. Also, products such as lignin, holocellulose, HMF and Furfural obtained from the process were stored in tanks prior to use.

Area 700: Waste-water treatment area.

The waste-water streams were treated by microbial digestion to obtain a biogas which is high in methane. At the same time, the treated water was recycled in the plant process (pre-treatment, fractionation, and hydrolysis) thereby reducing the amount of fresh water needed for the process (Ntimbani et al., 2021).

Area 800: Utilities.

The area includes cooling water systems, power systems and boilers. The solids from the distillation column and lignin having a higher heating value (HHV) of 18.35 kJ g^{-1} (Demirbaş, 2001b) were transferred to the boiler, producing steam converted to electricity for plant use (Tao et al., 2011). A boiler efficiency of 80% was assumed for this process (Humbird et al., 2011).

7.3 Mass balance of the process.

Mass balance for the complete process for a plant size of 100 tonnes day^{-1} spelt husk as obtained from the experimental data is described in Fig 7.4. A total of 11,560 kg day^{-1} of lignin, 3,560 kg day^{-1} of HMF and 25,090 kg day^{-1} of furfural was obtained.

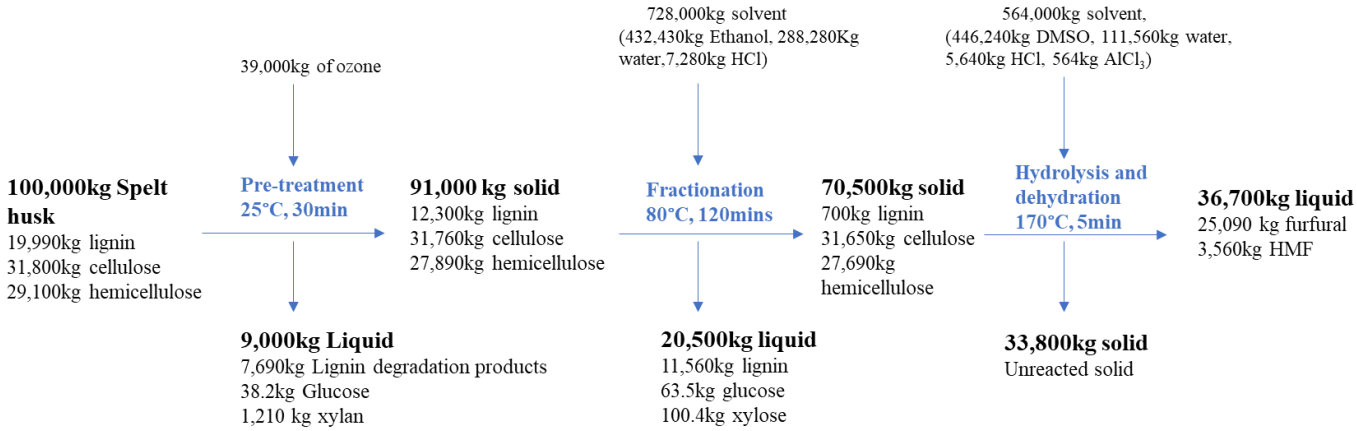

Fig 7.4: Mass balance for the conversion of 100 tonnes of spelt husk to HMF and furfural.

7.4 Energy consumption of the process.

The energy consumption of equipment in various process units is described in Table 7.1. The energy use of each piece of equipment was calculated from formulas (Section 3.5, Chapter 3) taken from the literature. The total energy consumption per day was estimated as 437,875.6 kW and estimated at 140,120,194 kW per year (320 days of plant activity) for scenario A while 139,703,436 kW per year of energy consumed for scenario B. Although in Scenario B, lignin was collected at the end of the hydrolysis process and used as boiler fuel to generate electricity (with lignin HHV of 18.35 kJ g^{-1} (Demirbaş, 2001b) and boiler efficiency of 80%), but the overall difference in energy consumption of Scenarios A & B was minimal as the ozone generator accounted for 97% of the total plant energy. The ozone generator equipment used for the pre-treatment process has an energy efficiency of 11 kw h kg^{-1} of ozone (Chapter 4) and consumes 429,000 kWh of energy per day for generation of 39,000 kg of ozone. Considering an electricity cost of \$0.06 kwh^{-1}, the electricity cost of our ozone generator was \$0.66 kg^{-1} O_3 which is lower than \$1.76 kg^{-1} as reported for ozone pre-treatment of 1tonne day^{-1} of brewer's spent grass (BSG) (Fernández-Delgado et al., 2019). In addition, the Environmental Protection Agency reported an electricity cost of \$1.49 kg^{-1} of ozone for a 45.35 kg O_3 day^{-1} plant at an ozone generation efficiency of 24.9 kwh kg^{-1} O_3 (Coca et al., 2016).

Table 7.1: Energy consumption for equipment in various process units.

Item	**Description**	**Scenario A Power consumption per day (kWh)**	**Scenario A Power consumption per year (kWh)**	**Scenario B Power consumption per year (kWh)**
Ozone generator	Pre-treatment	429,000[a]	137,280,000[a]	137,280,000
Ultrasonic probe		1.0×10^{-4} [b]	3.2×10^{-3}[b]	3.2×10^{-3}
Pumps	Solvent/recycle pump	12.74[c]	4076.8[c]	4076.8
Reactor	Fractionation	740.5*	236,960*	-
Microwave reactor	Hydrolysis/dehydration	170[d]	54,400[d]	54,400
Distillation column	HMF/Furfural separation and purification (Reboiler) (Condenser)	 2019.7[e] 4920.6[e]	 646,304[e] 1,574,592[e]	 646,304 1,574,592
Evaporator	Lignin recovery	337*	107,840*	-
Rotary vacuum dryer	Solid drying	592.6*	189,632*	126,421
Vacuum belt filter	Solid-liquid separation	82[c]	26,240[c]	17,493
Hammer mill	Particle size reduction	0.467[f]	149.44[f]	149.44
Total power consumption (kWh)		437,875.6	140,120,194	139,703,436

a = Calculated from energy efficiency of 11 kWh kg^{-1} obtained from Chapter 4 of this thesis.

b = Formula taken from Wierschem et al., (2017)

c = Taken from Sievers et al., (2014)

d = Formula taken from Shao et al., (2019)

e = Formula taken from Mehra, (2021)

f = Taken from Yancey et al., (2019)

* = Calculated using the heat energy equation $Q=MC_p\Delta T$

7.5 Economic analysis of the process.

For a plant capacity of 100 metric tonnes day^{-1} of spelt husk, 11.5 tonnes of lignin, 25 tonnes of furfural and 3.5 tonnes of HMF are co-produced. In addition, levulinic acid was also produced as a by-product at concentrations too low to be recovered and therefore is included in the waste-water stream. Two scenarios were considered for the biorefinery process. Scenario A involved pre-treatment, lignin fractionation and holocellulose hydrolysis to HMF and Furfural. While, scenario B involved pre-treatment and then direct holocellulose hydrolysis to HMF and furfural, excluding the fractionation stage. However, there was no difference in the yield of HMF and furfural from the two scenarios (experimental data obtained in chapter 6). The difference between the two strategies was that scenario A isolated pure lignin (98% purity) with a high market value and with the potential to be converted to high value platform chemicals. In contrast, non-pure/un-isolated lignin was obtained in scenario B which has relatively very low economic value and is treated as waste or boiler fuel.

The main equipment cost, including the auxiliary equipment cost of scenario A and B plants, is shown in Table 7.2. The equipment costs were obtained from several sources including vendors such as www.matches.com and the literature (Table 7.2) and converted to the current year cost (Chapter 3, Equation 3.13 & 3.14). The ozone generator cost was assumed considering the low-cost of materials (stainless steel mesh, quartz glass, plastic container etc.) used for construction. Scenario B had 16.5% lower total equipment cost than scenario A ($3,575,445 vs $4,284,246) due to the absence of fractionation and lignin recovery equipment such as the fractionation reactor, evaporator, precipitation tank, storage tank and condenser. The distillation column had the highest equipment cost accounting for 28% of the total equipment cost for scenario A and 33% for scenario B due to high temperatures needed for distillation leading to a higher number of distillation stages and column required as well as high demand for a significant amount of DMSO solvent.

Table 7.2: Main process equipment costs and capacity for 100 tonne day^{-1} plant size for scenario A (with fractionation) and B (without fractionation).

S/N	Equipment	Capacity	Scenario A Price $ (Year 2020)	Scenario B Price $ (Year 2020)
1.	Hammer mill	3.9 tonnes h^{-1}	140,406[a]	140,406
2.	Pre-treatment tank	100 m^3 (2 batches)	155,192[b]	155,192
3.	Ultrasonic probe	20 pieces of transducer and power amplifier	14,620[c]	14,620
4.	Ozone generator	39,000kg	800,000[d]	800,000
5.	Fractionation reactor	500 m^3	346,667[b]	-
6.	Solid-liquid separator	100 m^2	699, 671[b]	699,671
7.	Vacuum belt dryer	100 m^2	162,026[b]	162,026
8.	Evaporator	20.5 tonnes	82,877[e]	-
9.	Precipitation tank	30 m^3	56,576[b]	-
9.	Distillation column (Reboiler + condenser)	36,700 kg	1,091,987[f]	1,091,987
10.	Microwave reactor	1000 kg	129,469[g]	129,469
11.	Decanter	100 m^3	18,631[g]	18,631
12.	Storage tanks	50 m^3 (4 pieces)	42,246[b]	25,500
13.	Condenser	20.5 tonnes	122,340[e]	-
14.	Solvent pumps	12900 (2 pieces)	32,057[b]	12,900
	Total equipment cost (TEC)		**3,894,770**	**3,250,405**
	Total main + auxillary	TEC × 1.1	**4,284,246**	**3,575,445**

a = Yancey et al., (2018)
b = www.matches.com
c = Gholami et al., (2021)
d = Estimated
e = Jiang et al., (2020)
f = Kim et al., (2020)
g = Davies et al., (2020)

The total capital investment (TCI) of the process consisting of total direct costs including equipment cost, project capital and total operating costs was $21,382,672 for scenario A and $17,845,046 for scenario B (Table 7.3). While the production costs, including manufacturing and general expenses, was $22,322,252 and $19,946,468 for scenarios A and B, respectively (Table 7.4). The total production cost of scenario B was 10.6% lower than Scenario A due to a decrease in total raw material cost (absence of fractionation solvents such as ethanol, acetone and reduction in the total amount of water and HCl), decrease in labour units (fewer processing steps) and utilities (lower energy consumption due to absence of fractionation equipment).

The utility cost consisting of electricity and waste-water treatment contributed the highest (39.4% vs 42.8%) to the total production cost for both scenarios A and B respectively due to high annual energy demand (140,120,194 vs 139,703,436 kWh) of the process equipment (Table 7.1). Of which the fractionation equipment was only a small part (0.24%) of the energy consumption and the total production costs.

In as much as the energy demand of our designed ozone generator was reduced to 11 kWh kg^{-1} O_3 (40% reduced) as compared to commercial ozone generators, the operating cost of the ozone generation still dominates for the two scenarios. Hence, for this technology to compete with other pre-treatment technologies, there is a need to design an ozone generator where power consumption is minimal.

Furthermore, the raw material costs contributed the second highest (12.1 vs 11.9%) to the total production cost for scenarios A and B, of which DMSO contributed 27% vs 31%, respectively due to the large amount needed for holocellulose (10% solid loading) hydrolysis and the high price of DMSO at \$1480 $tonne^{-1}$ (Table 7.5).

Table 7.3: Total capital investment cost

S/N	ITEM	%	Scenario A ($)	Scenario B ($)
	Total fixed capital investment TFCI (Direct + indirect cost)		18,593,628	15,517,431
A	**Direct costs**	1 to 9	13,195,478	11,012,371
1.	Purchased equipment cost + auxillary equipment	100	4,284,246	3,575,445
2.	Purchased equipment installation	39	1,670,855	1,394,423
3.	Instrumentation and control	26	1,113,903	929,615
4.	Piping	31	1,328,116	1,108,387
5.	Electrical systems	10	428,424	357,544
6.	Building including services	29	1,242,431	1,036,879
7.	Yard improvement	12	514,109	429,053
8.	Sservice facilities	55	2,356,335	1,966,494
9.	Land	6	257,054	214,526
B	**Indirect costs**	10 to 14	5,398,149	4,505,060
10.	Engineering and supervision	32	1,370,958	1,144,142
11.	Construction expenses	34	1,456,643	1,215,651
12.	Legal expenses	4	171,369	143,017
13.	Contractor fees	19	814,006	679,334
14.	Contigency	37	1,585,171	1,322,914
C	**Working capital (WC)**	15% of TFCI	2,789,044	2,327,614
	Total capital investment	TFCI + WC	**21,382,672**	**17,845,046**

Table 7.4: Total annual production cost for a plant size of 100 tonnes day^{-1}.

S/N	ITEM	SUM	Scenario A ($)	Scenario B ($)
D	**Manufacturing cost. (direct + indirect production cost + overhead cost)**		18,914,223	16,936,210
D1	**Direct production cost**	1 to 8	14,988,634	13,732,603
1.	Raw materials (calculated)		2,719,633	2,375,482
2.	Labour (calculated)		1,216,512	912,384
3.	Direct supervisory and clerical labour (17.5% of operating labour)		212,889	159,667
4.	Utilities (calculated)		8,797,676	8,549,333
5.	Maintenance and repairs (6% of fixed capital)		1,115,617	931,045
6.	Operating supplies (15% of maintenance costs and repairs)		167,342	139,656
7.	Laboratory charges (15% of operating labour)		182,476	136,857
8.	Patent and royalties (4% of 4 to 10)		576,485	528,177
D2	**Indirect production costs**	9 to 11	2,398,578	2,001,748
9.	Depreciation (10% of fixed capital investment)		1,859,362	1,551,743
10.	Local taxes (2.5% of fixed capital investment)		464,840	387,935
11.	Insurance (0.4% of fixed capital investment)		74,374	62,069
D3	**Plant Overhead costs (60% of 2+3+5)**		1,527,011	1,201,858
E	**General expenses**	12 to 14	3,408,028	3,010,258
12.	Administrative cost (15% of 2+3+5)		381,752	300,464
13.	Distribution and selling costs (11% of manufacturing cost)		2,080,564	1,862,983
14.	Research and development costs (5% of manufacturing cost)		945,711	846,810
	Total production cost (Manufacturing cost + general expenses)	D+E	22,322,252	19,946,468

Table 7.5: Chemical prices

S/N	Raw Material	Price	Reference
1.	Spelt husk	\$50 $tonne^{-1}$	www.Alibaba.com
2.	Oxygen gas	\$0.18 m^{-3}	Kim et al., 2020
3.	Manganese dioxide	\$10.5 kg^{-1}	www.Alibaba.com
4.	Ethanol	\$512 $tonne^{-1}$	Jiang et al., 2020
5.	Water	\$0.30 $tonne^{-1}$	Zang et al., 2020
6.	HCl	\$17 $tonne^{-1}$	Yan et al., 2020
7.	Acetone	\$1370 $tonne^{-1}$	Jiang et al., 2020
8.	DMSO	\$1480 $tonne^{-1}$	www.Alibaba.com
9.	$AlCl_3$	\$186 $tonne^{-1}$	Yan et al., 2020

7.6 Revenue and profitability of Scenarios A and B.

The revenue calculated was higher for scenario A than scenario B due to additional sales obtained from the fractionated lignin (Table 7.6). In as much as scenario A had a higher production cost due to the extra processing step required for lignin fractionation, scenario A was economically superior to scenario B with an annual profit of $213,657 higher than scenario B (Table 7.6), meaning fractionation of lignin had a positive effect on the process economics than its alternative utilisation for heat or boiler fuel. Both scenarios were economically feasible with annual profits of $6,432,180 and $6,218,523 for scenarios A and B respectively. A technical modification of the process would be needed to ensure a higher production rate of HMF and Furfural through improved holocellulose conversion (currently 50% conversion). In addition, the substitution of DMSO solvent with a cheaper and low boiling point solvent will increase the profit of the plant as DMSO presently accounts for 27% of raw material cost and distillation column equipment (28% of equipment costs) because of complexity in separation and recycling of high boiling DMSO.

Table 7.6: Annual revenue and profitability of scenarios A and B.

S/N	Product	Production (tonnes yr^{-1})	Price ($ ton^{-1})	Scenario A Revenue ($ yr^{-1})	Scenario B Revenue ($ yr^{-1})
1.	Furfural	8028.8	1840[a]	14,772,992	14,772,992
2.	HMF	1139.2	10,000[b]	11,392,000	11,392,000
3.	Lignin	3699.2	700[c]	2,589,440	0
4.	Total Revenue			28,754,432	26,164,992
5.	Profit (Revenue – total costs)			6,432,180	6,218,523

a = Kuznetsov et al., (2020)
b = Krishna et al., (2018)
c = Kim et al., (2021)

7.7 Minimum fuel selling price (MFSP) of products.

The minimum fuel selling price of furfural and HMF for both scenarios were determined based on their capital and operating costs using equation 3-20 from Chapter 3. The sum of annualised capital costs and total production costs was divided by the total number of products for each scenario before further division with individual annualised product yields. The MFSP for furfural for Scenarios A and B were 997 and $1331 $tonne^{-1}$ respectively, while MFSP for HMF were 7032 and $9381 $tonne^{-1}$ for scenarios A & B respectively. A 25% reduction in MFSP of

both furfural and HMF were achieved for scenario A due to a decrease in total production cost as a result of co-production with lignin.

The MFSP for furfural in scenario A and B is lower than those reported in the literature from several processes. These are all below the current market value of furfural at \$1840 tonne^{-1} (Kuznetsov et al., 2020) and \$2200 tonne^{-1} (Ntimbani et al., 2021). Hossain et al., (2019) reported a furfural price of \$1700 tonne^{-1} from co-production with bioethanol through biochemical pre-treatment of corn stover (658,201 tonnes yr^{-1}) with corn stover priced at \$46.8 tonne^{-1}. Gómez Millán et al., (2021) obtained a furfural MFSP of \$1830 tonne^{-1} for a 5 k ton yr^{-1} furfural production capacity from birch hydrolysate in a biphasic system. The birch pre-treatment technology wasn't stated as it was assumed that the lignin removal occurred in a commercial pulp mill or biorefinery. Halder, (2020) obtained a furfural MFSP of \$1151 tonne^{-1} via ionic liquid pre-treatment with 1-butyl-3-methylimidazolium chloride integrated with pyrolysis co-producing furfural, levoglucosenone and lignin from a plant capacity of 15,120 tonne yr^{-1} of sugarcane straw.

The MFSP obtained for HMF of \$7032 tonne^{-1} and \$9381 tonne^{-1} for scenario A & B respectively were higher than the current market price of \$6000 tonne^{-1} (van Putten et al., 2013) for HMF. This might be due to the low yield of HMF obtained in this work as well as the low (50%) cellulose conversion. Santiago and Guirardello, (2020), obtained an HMF MFSP of \$4006 tonne^{-1} from sugarcane bagasse (17,640 tonne yr^{-1}) directly reacted in a biphasic system containing MIBK and 2-butanol with the acid (H_2SO_4) pre-treatment and hydrolysis carried out in one pot. The results suggested that production of HMF was not economically feasible as the HMF price was higher than the target to enter the polyethylene terephthalate (PEF) market to substitute PEF (\$1027 tonne^{-1}) and the process needed an improvement with cellulose hydrolysis and glucose-HMF yield. It is important to note that most MFSP of HMF (\$1,200 - \$1,800 tonne^{-1}) presented in the literature from several studies (Parshetti et al., 2015, Mukherjee et al., 2015, Yan et al., 2020, Motagamwala et al., 2019) were obtained from fructose as the starting material. However, it was identified as still too expensive to be used as a replacement for petroleum derived products such as terephthalic acid (\$800 tonne^{-1}) (Kazi et al., 2011)

7.8 Sensitivity analysis

The sensitivity analysis was carried out to identify the impact of some economic parameters such as feedstock price, variable operating costs, furfural yield, total capital investment and DMSO price on the MFSP of furfural. The MFSP of furfural was measured for a 20% change in the value of critical parameters while keeping other variables constant (Fig 7.5).

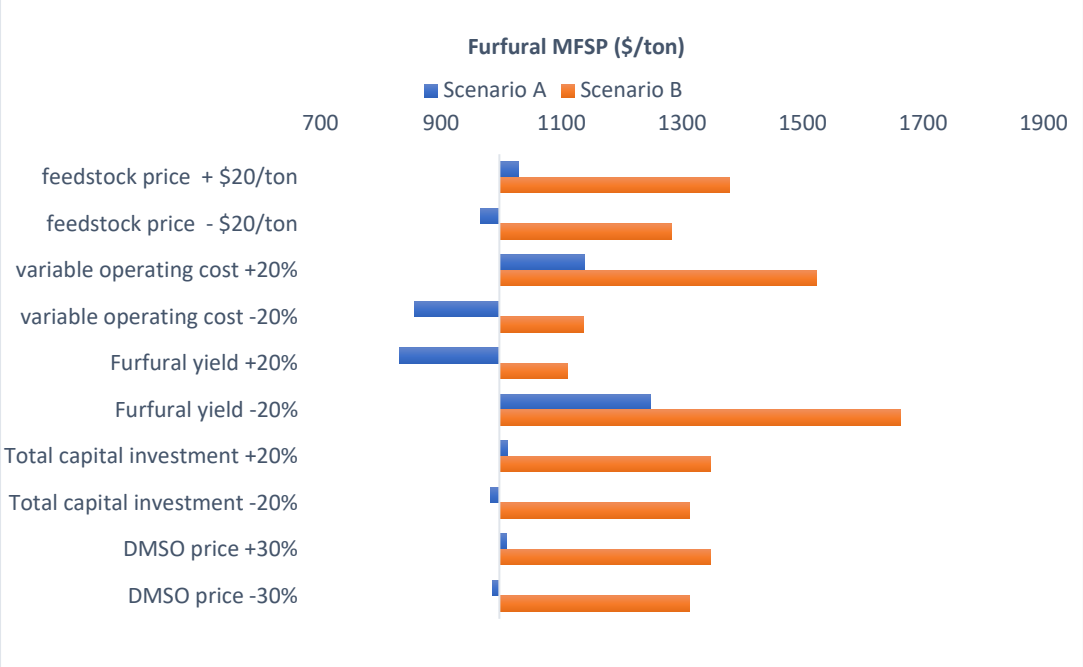

Fig 7.5: Effect of sensitivity analysis on minimum furfural price based on a 20% change in the value of critical parameters.

The furfural yield and variable operating cost are the most significant parameters affecting furfural MFSP. A 20% increase in furfural yield led to a 16.2% decrease in furfural MFSP. The major factor affecting the furfural yield is the low conversion (50%) achieved during holocellulose hydrolysis. An improvement could be achieved by developing a more efficient catalyst to improve hydrolysis and hence selectivity of furfural. Likewise, a lignocellulose feedstock with a high holocellulose content can improve the furfural yield.

The variable operating cost is the second most significant factor affecting furfural MFSP. A decrease in the variable operating cost by 20% led to a 14% decrease in the MFSP of furfural. The variable operating cost consists of raw material cost, operating labour and utilities, of which utilities constitute 69% of the variable operating cost. Decrease in feedstock price of

spelt husk from \$50 tonne^{-1} to \$30 tonne^{-1} had a very minimal impact (3.2% decrease) on the MFSP of furfural. This is because spelt husk used is a very cheap feedstock for the process.

7.9 Summary

This chapter describes the techno-economic potential and competitiveness of the conversion process for large scale co-production of HMF, Furfural and lignin from spelt husk (Scenario A). The proposed approach was compared with scenario B, where HMF and furfural are co-produced without lignin. Scenario B had a 16.5% lower total capital cost and 10.6% lower total production cost than scenario A due to the reduced processing stage of lignin fractionation. Scenario A was economically superior to scenario B, with a profit of \$213,657 higher than scenario B due to extra revenue obtained from lignin sales, meaning fractionation of lignin had a positive effect on the process economics than its utilisation for heat or boiler fuel.

The MFSP of furfural and HMF for scenario A were 25% lower than for scenario B due to reduction in total cost of production in scenario A as more products were obtained from the process. The process was economically feasible for furfural production for both scenarios A & B as the MFSP for both scenarios was lower than the current market value of furfural \$1840 tonne^{-1} (Kuznetsov et al., 2020). While the two scenarios were not very economically feasible for HMF production as the HMF MFSP were both higher than the current market value of HMF at \$6000 tonne^{-1} (van Putten et al., 2013) but the result suggests potential as HMF is co-produced with other products resulting in profitability of the entire process.

In as much as the energy demand of our designed ozone generator was reduced to 11 kWh kg^{-1} O_3 as compared to literature value of 24.9 kwh kg^{-1} O_3 generated for waste-water treatments, the utilities of the process contributed to the highest (39.4 vs 42.8%) total production cost for both scenarios A and B respectively. A comparison of its effect on the overall process with other studies could not be achieved due to limited literature on the techno-economic analysis of ozone pre-treatment of biomass to biofuels or chemical platforms.

Chapter 8: General Discussion

The quest for a green, cost effective and sustainable alternative to fossil fuel derived energy has led to increased utilisation of biomass as a renewable feedstock. Globally, about 140Gt of biomass wastes are produced annually with 66% derived from cereal crops but direct utilisation of these residues to value added products is not possible due to the recalcitrant nature of biomass. Pre-treatment is a crucial step in the utilisation of these residues as it reduces the recalcitrant nature but it accounts for about 30% of the total production costs in a biorefinery (Panneerselvam et al., 2013). Agricultural residues like rice husk, corn cobs etc have clear potential as feedstocks for energy generation due to their widespread abundance and no need for collection. To be competitive with fossil fuel derived platform chemicals, costs of production need to be low. Bio-industries can combine their material flow (residue from one bio-industry becomes a starting material for another) to achieve a complete utilisation of the biomass thereby creating opportunities for several small-scale businesses (Cherubini *et. al*, 2008).

Several pre-treatment technologies are in use commercially and have been evaluated in the literature with ozone offering clear potential due to several advantages it offers. Limitation with utilisation of ozone for pre-treatment lies with the high costs of ozone generation. This study designed a novel ozone generator consisting of two zone surface plasma comparable to commercial ozone generator but with 30-40% lower power consumption hence reducing the general electricity cost of ozone generation from \$1.49 kg^{-1} of O_3 to \$0.66 kg^{-1} of O_3. In addition, the ozone generator was made from materials such as stainless-steel mesh, quartz tube which is cheap, readily available, thus making commercial ozone generator fabrication relatively inexpensive. General concerns with utilisation of agricultural residue as a fuels and chemicals due to high moisture content is reduced as moisture is needed for the ozone pre-treatment thereby eliminating the high costs needed for drying the feedstocks.

Current pre-treatment technologies such as steam explosion that are relatively well established, (especially in the cellulosic ethanol industry) have demonstrated an increase in enzymatic hydrolysis yield due to increased surface area and porosity. However, utilisation of this pre-treatment for platform chemicals is not favourable as it demonstrates low acid hydrolysis yields (Steinbach et al., 2020, Carrasco et al., 1994). An increase in crystallinity has been observed in many studies that utilised steam explosion pre-treatment due to extensive degradation of the amorphous portion of cellulose. As such, a decrease in acid hydrolysis rate from 0.034 min^{-1}

for untreated wheat straw to 0.024 min^{-1} for steam exploded wheat straw using dilute sulfuric acid at 180ºC was observed due to increase in crystallinity index for steam exploded wheat straw from 58% to 76.55% (Carrasco et al., 1994). Increased crystallinity of cellulose is associated with strong hydrogen bonds which can only be broken by very high temperature (Steinbach et al., 2020). Cellulose obtained after ozone pre-treatment (this current study) showed defilbration of the microfibres, decreased degree of polymerisation and decreased crystallinity observed for ozone pre-treated corn cob (CI 45% to 36%) and spelt husk (CI 30% to 28%). This supports increased acid hydrolysis at mild temperatures as more cellulose chain ends are available leading to penetration of the acids into the crystalline structure of the cellulose. In addition, high solid recovery of 86% was observed due to selective reaction of ozone with lignin, without affecting cellulose and hemicellulose fraction. This high solid recovery is advantageous for further acid hydrolysis to platform chemicals as it provides high lignocellulose input for the conversion process. Unlike other pre-treatment methods such as steam explosion, hydrogen peroxide and alkaline where about 30- 40% solid is lost during pre-treatment due to extensive hemicellulose degradation decomposing it to lower molecular weight compounds or converted to pseudo-lignin (condensation product from hemicellulose and lignin). Reduced solid recovery is favourable for enzymatic hydrolysis as low enzyme loadings are needed for the conversion process thus reducing the overall process cost with increased yields. However, high solid recovery is needed for acid hydrolysis as more cellulose chain ends are needed for interaction with the acid. Hence ozone pre-treatment offers great potential when the downstream process is to platform chemicals.

To date, bio-refineries and pre-treatment technologies have largely focused on utilisation of the carbohydrate fraction of lignocellulosic biomass to biofuel/chemical platforms leaving low purity lignin as a residue which is often used for heat and power generation due to its high heating value (Xu et al., 2014, Ragauskas et al., 2014). As lignin is an abundant source of aromatic compounds, its conversion into high-value platform chemicals will increase the profitability and sustainability of the biorefinery process. However, to achieve complete utilisation of the lignin, it must be of high purity and lack extensive modifications.

Pre-treatment practices such as steam explosion and ionic liquids produce lignin molecules which are extensively modified due to their harsh operating conditions (Parsell et al., 2013) and produce pseudo-lignins (condensation products from reaction between hemicellulose and lignin) which are inert solids that are not easily degraded to phenolic compounds. Evidence of pseudo-lignin production from the above pre-treatment were observed as lignin mass after pre-

treatment was higher than the original lignin content of the biomass (Matsakas *et al.*, 2019, Steinbach et al., 2020). The current study demonstrated a potential for lignin valorisation as high purity (95%) lignin was fractionated alongside holocellulose from corn cob and spelt husk as a co-product using a mixture of ethanol and water at a mild temperature of 80^{o}C. ^{1}HNMR spectra showed a decreased intensity at the aromatic region of lignin confirming its reaction with ozone while other structural components remained unchanged as it was fractionated at a relatively mild temperature of 80^{o}C. Thus, lignin obtained in this study provides a useful source of phenolic compounds such as vanilin, syringaldehyde, hydroxybenzoic acid etc. Current commercial sources of lignin are obtained from paper and pulp industry via lignin sulfonation and alkaline depolymerisation reactions, generally yielding low purity lignin contaminated with sulfur and carbohydrates. These impurities and poor processability hinders the value of this lignin for composite products limiting its application for cement additives, dust supression and drilling fluids for oil recovery (Lora, 2008). In 2010, the paper and pulp industry produced 50 metric tonnes of lignin, of which only 2% was used in the binding sector while the remainder was used as a low value boiler fuel (Strassberger et al., 2014).

The techno-economic assessment in this work showed that co-production of lignin with HMF and furfural yielded a higher profit and 25% decrease in the minimum fuel selling price (MFSP) of HMF and furfural as compared to a plant that produces just HMF and furfural without lignin. Current commercial production of furfural from agricultural residue (sugarcane bagasse) from the Dominican Republic and South Africa produce 35,000 Tonnes of furfural per year (Mariscal et al., 2016). Although its current price still remains a clear bottleneck for industrial applications (Mariscal et al., 2016). For example, producing maleic anhydride (a commercial petrochemical) from furfural costing \$1500 tonne^{-1} requires a decrease in price to \$600 tonne^{-1} to become economically competitive to the petrochemical route for maleic anhydride production (Lin et al., 2012). The current furfural market is unstable and volatile, with a shortage of furfural in 2011 causing a significant rise in the market value to \$2000 tonne^{-1} (Marcotullio, 2011), Producing furfural at a much cheaper price (\$997 tonne^{-1} in this study) with the potential for large-scale production will provide a suitable and sustainable starting material for furfural based biorefineries resulting in a reduction in cost of the furfural derived products.

Furthermore, the techno-economic assessment showed that the MFSP of HMF (\$7032 tonne^{-1}) obtained in this study was lower than the current market value of HMF (\$10,000 tonne^{-1}) (Krishna et al., 2018). Although, as described by Thoma et al., (2020), the current price of

HMF ($10,000 tonne^{-1}) is still too high to be used in synthesing polyethlene 2,5-furandicarboxylate (PEF) as a replacement for polyethylene terephthalate (PET) currently derived from petroleum. This high price of HMF has led to no commercial large scale HMF plants running currently (Thoma et al., 2020). The current commercial scale HMF plant in Switzerland only produces 300 ton/yr annually. The sensitivity analysis in this study showed that a 20% increase in furfural yield would result in a 16.2% decrease in furfural MFSP. This shows that a substantial technological breakthrough is still needed to further decrease the price of furfural and HMF. Therefore, there is still a need to improve cellulose hydrolysis (currently 50% conversion in this study) through developing a more efficient catalyst and solvent system to completely dissolve cellulose as well as increase hydrolysis yield and subsequent dehydration to HMF and furfural as well as inhibit by-product formation.

Overall, the co-production of HMF, furfural and lignin from agricultural residues via optimised ozone pre-treatment technology is still relatively new but shows a clear economic potential for a biorefinery producing multi-products at low cost from a single feedstock (agricultural residue) through complete utilisation of all feedstock components. National reliance on imported fossil fuels will be reduced as biomass is readily available in many countries (Cherubini *et. al*, 2008). Therefore, the substitution of fossil fuel derived component by biomass will lead to reduced greenhouse gas emission thereby reducing global warming and reducing health related problems.

Chapter 9: Conclusions and Recommendation.

This chapter provides the major conclusions obtained from this study and recommendations for future studies.

9.1 Conclusions

In conclusion, higher ozone concentration and amount (2.5 times) was achieved using a two-zone compared with a single- zone plasma reactor. A maximum ozone concentration of 140 g m^{-3} and 90 g kW^{-1} h^{-1} productivity were obtained from the two-zone system, which is comparable to commercial ozone generators but with 30 – 40% lower power consumption (11 kWh kg^{-1} O_3). Cooling of the generator led to a decrease in gas temperature in the reactor leading to an increase in ozone concentration at low power input hence mitigating the drawbacks of the high cost of ozone generation for industrial applications.

The designed two-zone ozone generator was subsequently used for biomass pre-treatment. Intensification of the ozone pre-treatment (increase carbohydrate production via increased lignin separation) was achieved by incorporating ultrasound. Including ultrasound in the ozone pre-treatment of corn cobs enhanced the mixing between biomass and ozone, and resulting in an increase in ozone consumption from 0.24g O_3 g^{-1} corn cob to 0.39g O_3 g^{-1} with a 38.5% decrease in the acid insoluble lignin concentration from 52 to 32 mg g^{-1} compared to using ozone only. Moisture content was found to be the parameter most influencing ozone pre-treatment with each biomass feedstock having an optimum moisture content for efficient pre-treatment. Optimum moisture content of 66% and 40% were achieved for corn cob and spelt husk respectively. Leading to decrease in acid insoluble lignin content from 51 to 14 mg g^{-1} and 160 to 55.2 mg g^{-1} for corn cob and spelt husk respectively. About 90% and 94% of lignin with high purity (95%) were recovered for corn cob and spelt husk. In addition, cellulose pulp of 83.6% and 85.2% with 78% purity were recovered for corn cob and spelt husk respectively with a 19% decrease in cellulose crystallinity and 17% decrease in degree of polymerisation (DP).

Ozone pre-treatment was compared with an alternative oxidative pre-treatment method i.e. hydrogen peroxide and its effect on the carbohydrate content examined. It was found out that carbohydrate recovery for ozone pre-treatment (>83%) was higher than hydrogen peroxide pre-treatment (>54%) due to selective reaction of ozone with lignin. Mass loss after ozone pre-treatment was 5% and 7% for corn cob and spelt husk respectively compared to 31% and 68% for corn cob and spelt husk respectively after hydrogen peroxide pre-treatment.

Subsequently, the carbohydrate obtained after ozone pre-treatment was reacted in a DMSO-H_2O media to produce HMF and furfural in a microwave reactor. Pre-treatment led to a 58% increase in HMF yield and 74% increase for corn cob and spelt husk respectively, while a 10% and 66.7% increase in furfural for corn cob and spelt husk were observed respectively. Reacting fractionated cellulose from corn cob and spelt husk yielded a similar HMF yield of 40 mg g^{-1} irrespective of the biomass. HMF and furfural yields were influenced by change in cellulose properties such as fibre size, increased surface area, decrease in degree of polymerisation achieved through cellulose pre-treatment. HMF and furfural yields of untreated corn cob were higher than those from spelt husk due to a difference in their morphology as untreated corn cob was more porous than spelt husk allowing easy access to cellulose.

The economic efficiency and competitiveness of the conversion process for large scale co-production of HMF, furfural and lignin from spelt husk (Scenario A) was determined. The proposed approach was compared with process where HMF and furfural were co-produced without lignin (Scenario B). Co-production with lignin yielded a profit of $213,657 higher than without lignin for a plant size of 100 metric tonnes per day of spelt husk due to extra revenue obtained from lignin sales, meaning fractionation of lignin had a positive effect on the process economics than its utilisation for heat or boiler fuel. The MFSP of furfural and HMF for scenario A were 25% lower than for Scenario B due to reduction in total cost of production in scenario A as more products were obtained from the process. The sensitivity analysis showed that furfural yield and variable operating cost were the most significant parameter affecting furfural MFSP.

All objectives of this study stated in Chapter 1, section 1.3 was achieved. Below is the list of objectives and chapters in which each one was achieved:

1. Develop an energy-efficient ozone generator to reduce the costs associated with ozone generation (Chapter 4). A 40% more energy efficient ozone generator was achieved.
2. Optimise the pre-treatment of agricultural residues (corn cob and spelt husk) using ozone coupled with ultrasound (Chapter 5). Various pre-treatment conditions investigated and optimum condition for high lignin separation obtained.
3. Fractionate and recover lignin as a co-product in the process (Chapter 5). Lignin was successfully fractionated and recovered with high yield and purity.

4. Evaluate the effect of pre-treatment on cellulose structure and its effect on conversion yields to furfural and HMF (Chapter 6). Structural changes of cellulose as a result of pre-treatment and effect on furfural and HMF yields accessed.
5. Evaluate the techno-economic potential of the co-production of lignin, furfural and HMF (Chapter 7). Feasibility and profitability of the co-production process investigated.

9.2 Further work

The following are recommendations for further research;

- Valorisation of the fractionated lignin to chemicals and polymers should be explored as lignin obtained from this work is of high purity (>95%).
- Improve HMF and furfural yields by exploring solvents such as Deep Eutectic solvents (DES). DES solvents can be used as an alternative to ionic liquids as they have comparable characteristics but are cheaper to produce, are less toxic and biodegradable. In addition, they are solvents with low boiling point which will be beneficial for the process as it will reduce costs and separation difficulties encountered with the distillation of DMSO.
- Develop a more efficient solid acid catalyst capable of increasing HMF and furfural yields.
- Use of ASPEN plus to simulate the process for more accurate equipment sizing and electricity consumption calculations for a techno-economic analysis.
- Sensitivity analysis of technical parameters such as reaction temperature, time, solid loading, plant scale, plant life and operating hours should be evaluated.

Appendices

Appendix A1: Publication from thesis

A1.1: Ibrahim, H. H., Bilsborrow, P. E. & Phan, A. N. (2021). Intensification of pre-treatment and fractionation of agricultural residues. *Chemical Engineering and Processing - Process Intensification*, 159**,** 108231. https://doi.org/10.1016/j.cep.2020.108231

Appendix A2: Proximate analysis of moisture and ash contents (ASTM D3173 and D3174).

A 2.1: Moisture content (MC)

An empty crucible was weighed (mass M_1) and 1g of sample was added to the empty crucible and the weight recorded (mass M_2). Then oven dry the sample at 105C for 2-3 hrs. cool the crucible in a dessicator and reweigh (mass M_3) until a constant weight is achieved. The MC was calculated using Equation (A.1).

$$MC = \frac{M_2 - M_3}{M_2 - M_1} \times 100\% \qquad \text{Equation A.1}$$

A 2.2: Ash content (AC)

An empty crucible was weighed (mass M_1) and 1g of sample was added to the empty crucible and the weight recorded (mass M_2). The sample was heated in the absence of oxygen in a furnace at a 750C for 1hr. the residue (ash) was cooled to room temperature in a dessicator and the mass reweighed (mass M3). Ash content was calculated using Equation (A.2)

$$AC = \frac{M_2 - M_3}{M_2 - M_1} \times 100\% \qquad \text{Equation A.2}$$

Appendix A3: GC Calibration plots for (a) HMF, (b) furfural and (c) levulinic acid.

(a)

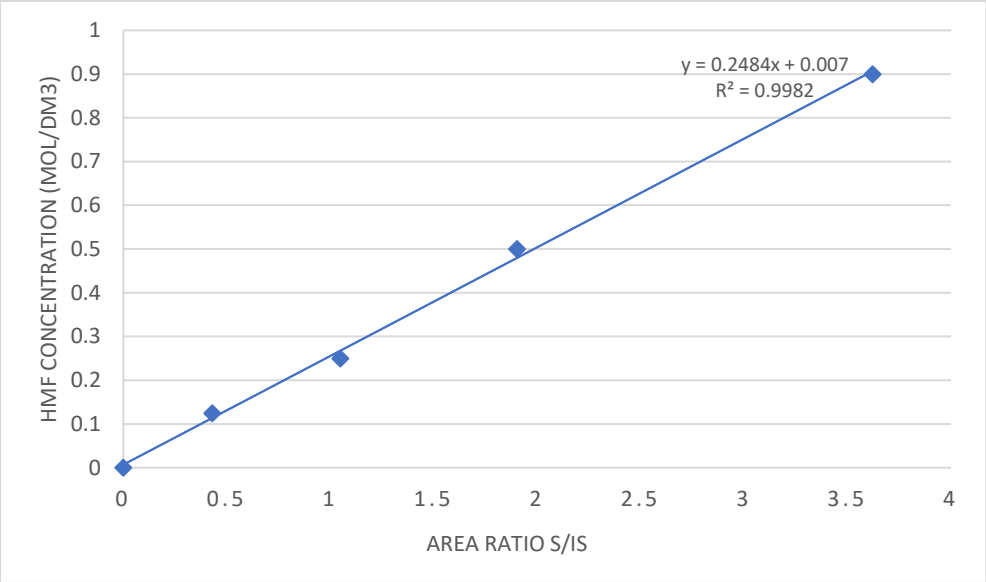

(b)

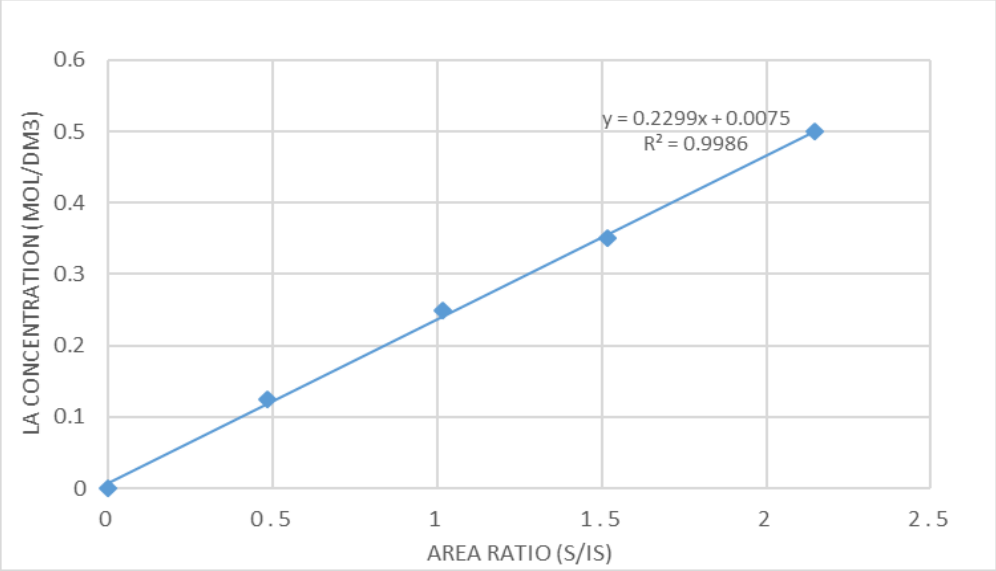

(c)

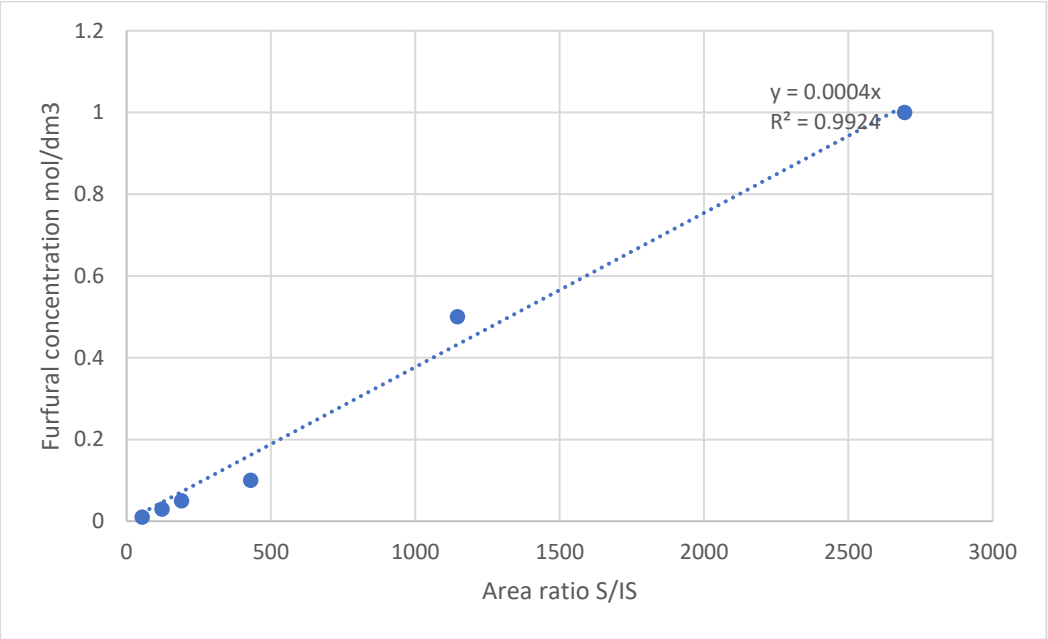
y = 0.0004x
R² = 0.9924
Furfural concentration mol/dm3
Area ratio S/IS
0
0.2
0.4
0.6
0.8
1
1.2
0
500
1000
1500
2000
2500
3000

Appendix A4: GC-MS analysis of HMF.

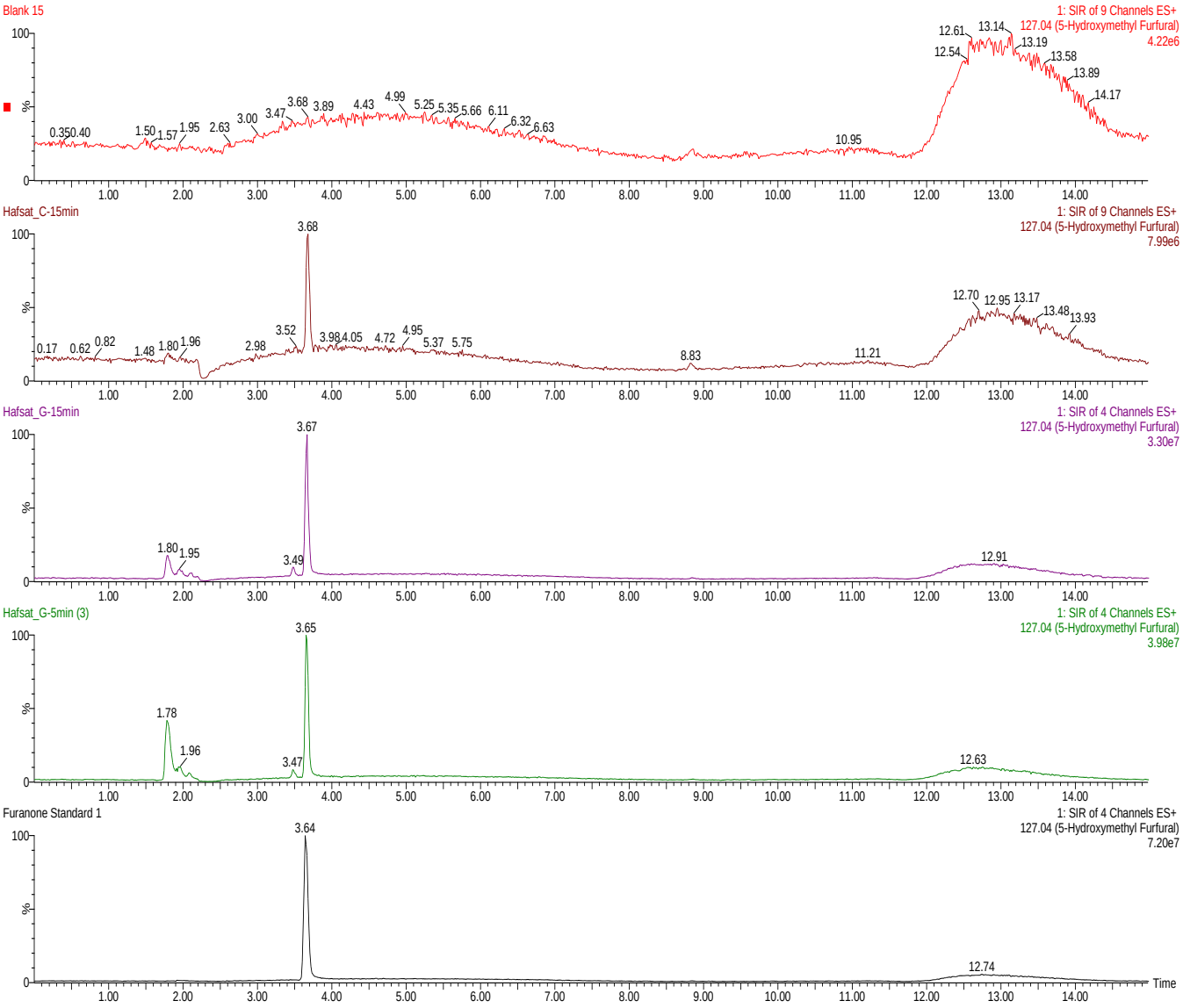

Appendix A5: HPLC calibration curves for lignin degradation products and water soluble fractions.

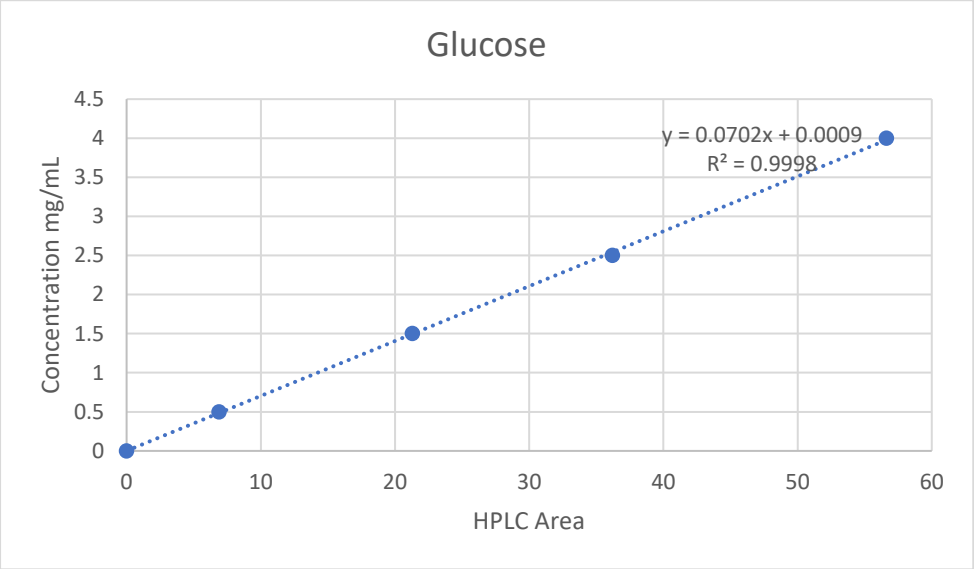

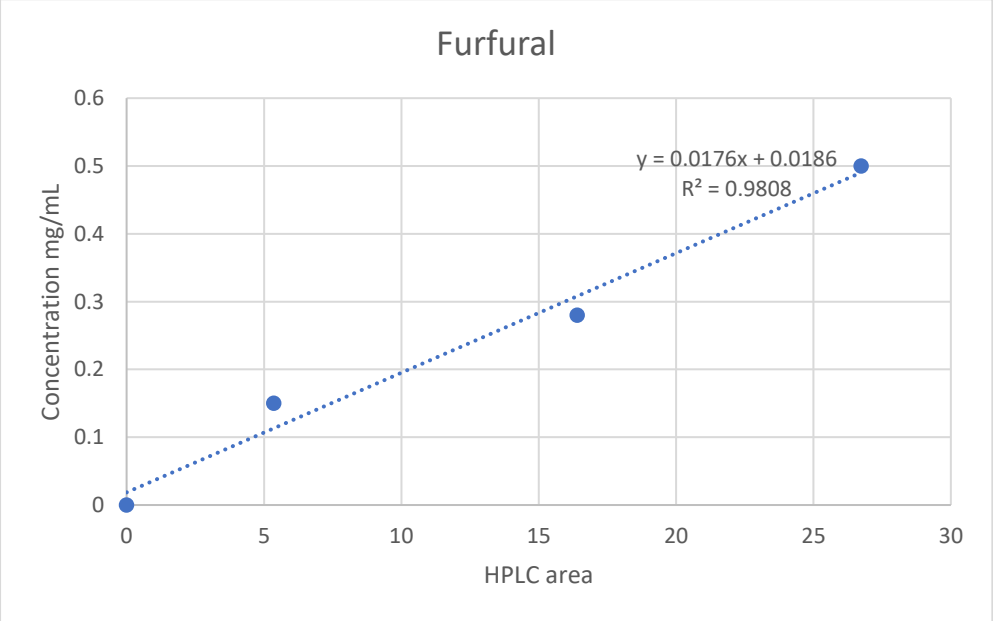

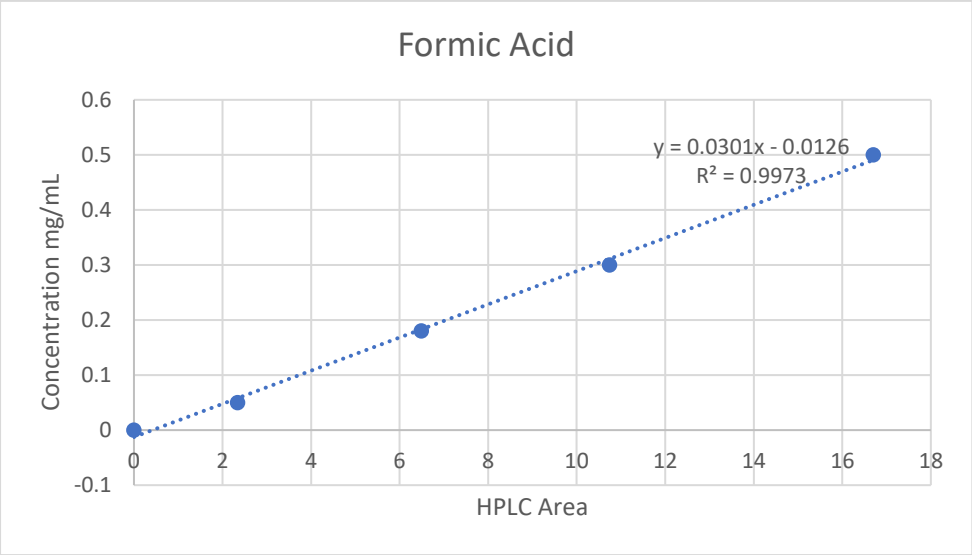
Formic Acid
y = 0.0301x - 0.0126
R² = 0.9973
Concentration mg/mL
HPLC Area
0.6
0.5
0.4
0.3
0.2
0.1
0
-0.1
0
2
4
6
8
10
12
14
16
18

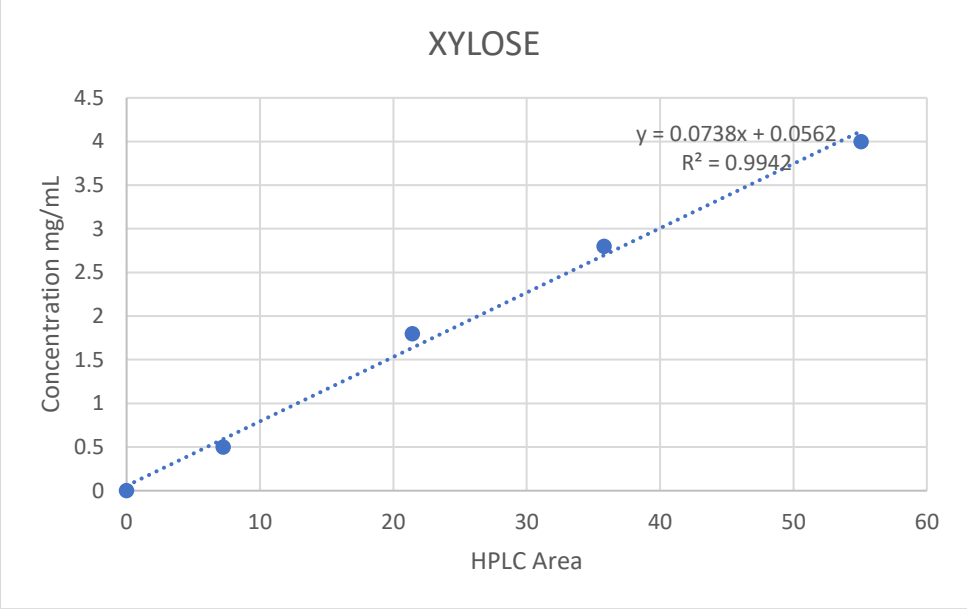
XYLOSE
y = 0.0738x + 0.0562
R² = 0.9942
Concentration mg/mL
HPLC Area
4.5
4
3.5
3
2.5
2
1.5
1
0.5
0
0
10
20
30
40
50
60

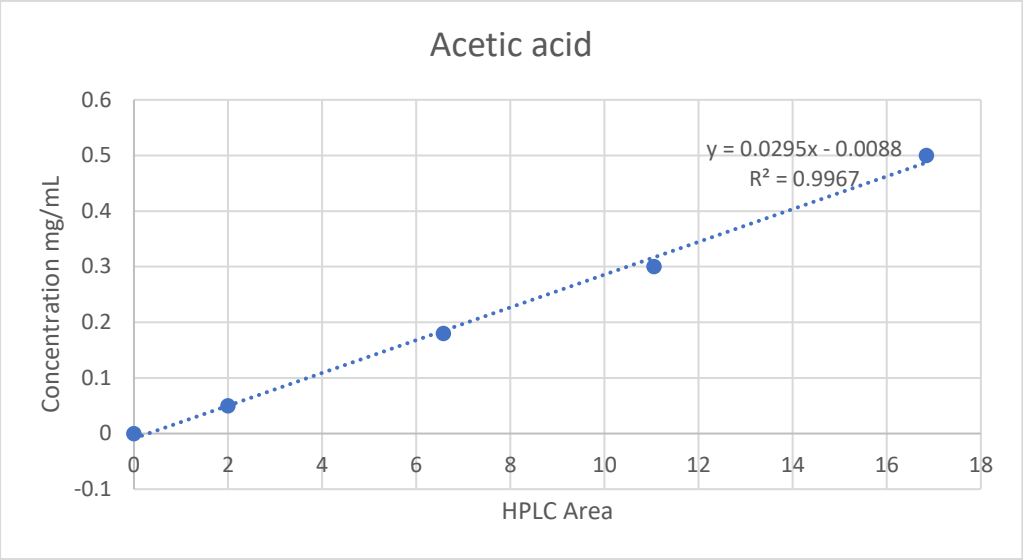
Acetic acid
y = 0.0295x - 0.0088
R² = 0.9967
Concentration mg/mL
HPLC Area
0.6
0.5
0.4
0.3
0.2
0.1
0
-0.1
0
2
4
6
8
10
12
14
16
18

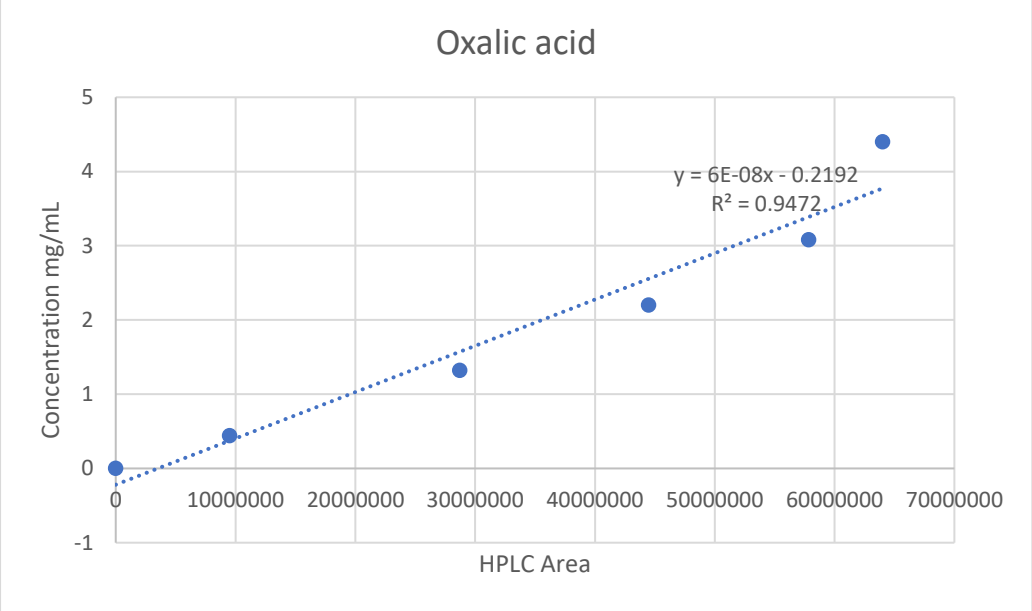
Oxalic acid
y = 6E-08x - 0.2192
R² = 0.9472
Concentration mg/mL
HPLC Area
5
4
3
2
1
0
-1
0
10000000
20000000
30000000
40000000
50000000
60000000
70000000

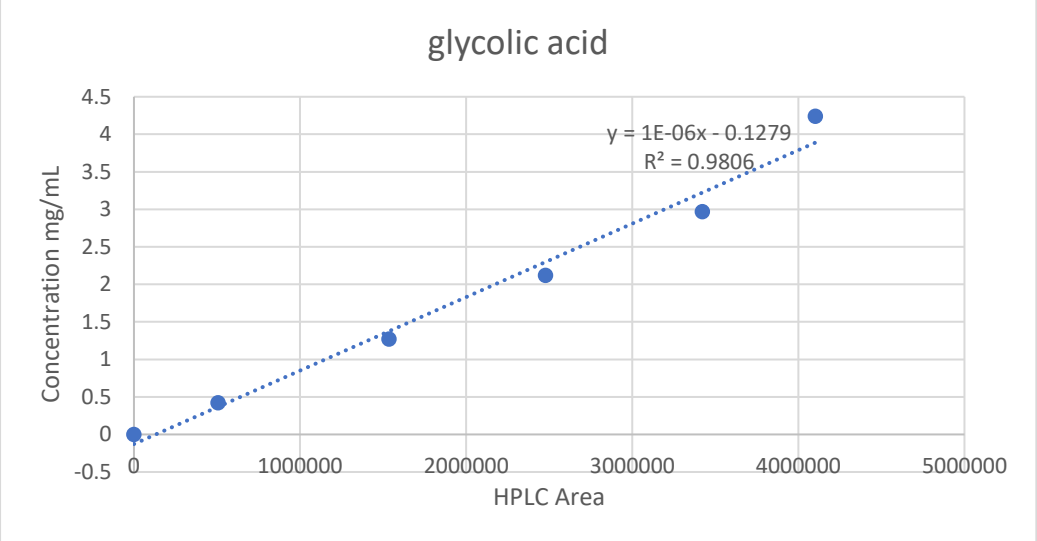
glycolic acid
y = 1E-06x - 0.1279
R² = 0.9806
Concentration mg/mL
HPLC Area
4.5
4
3.5
3
2.5
2
1.5
1
0.5
0
-0.5
0
1000000
2000000
3000000
4000000
5000000

Appendix A6: HPLC chromatograms of lignin degradation product peak area vs elution time. a) H_2O b) oxalic acid c) glucose d) fructose e) glycolic acid f) formic acid g) acetic acid.

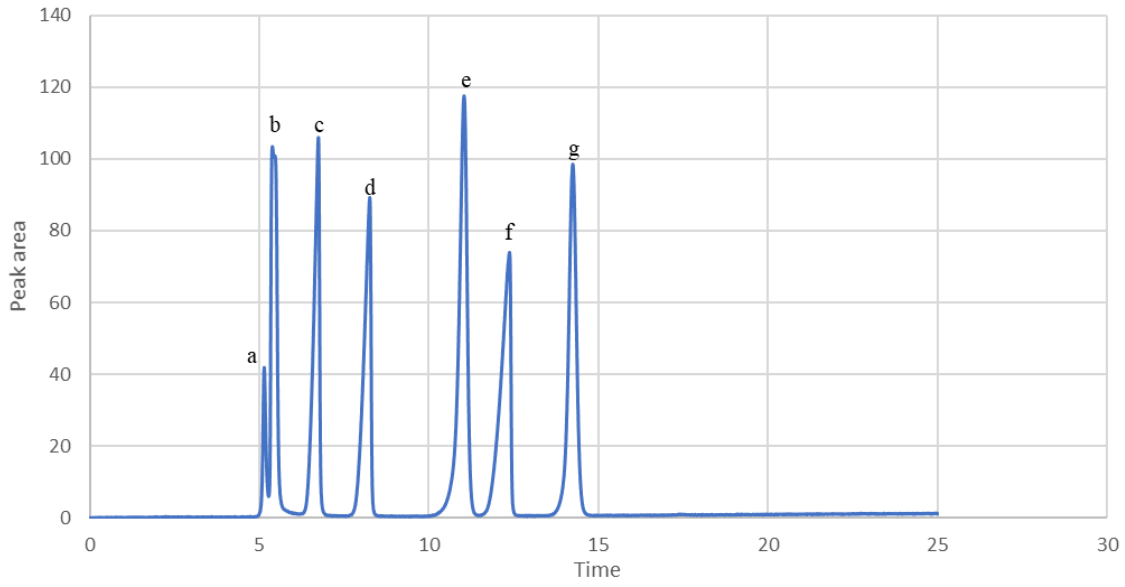

Appendix A7: UV -Vis TRS glucose calibration curve.

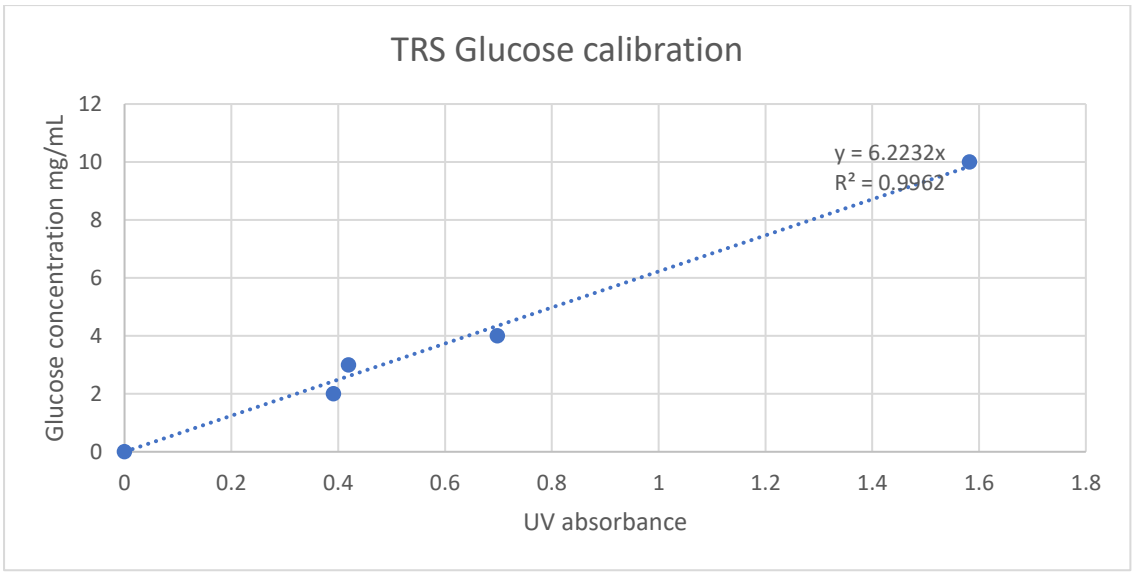

Appendix B: Structural comparison between cellulose obtained from ozone pre-treatment and hydrogen peroxide pre-treatment.

Appendix B1: DTG and TGA of corn cob and spelt husk of recovered cellulose from untreated ozone pre-treated and alkaline hydrogen peroxide pre-treated a) corn cob and b) spelt husk.

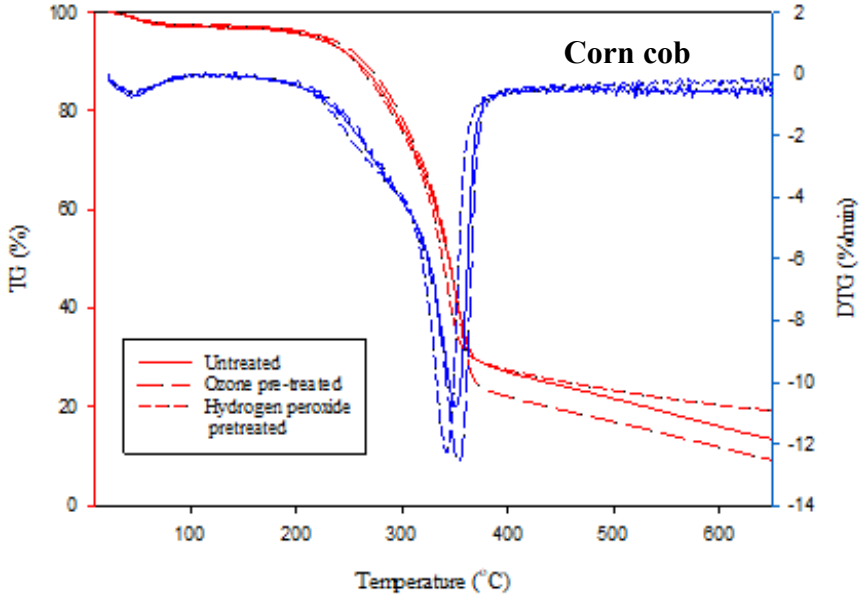

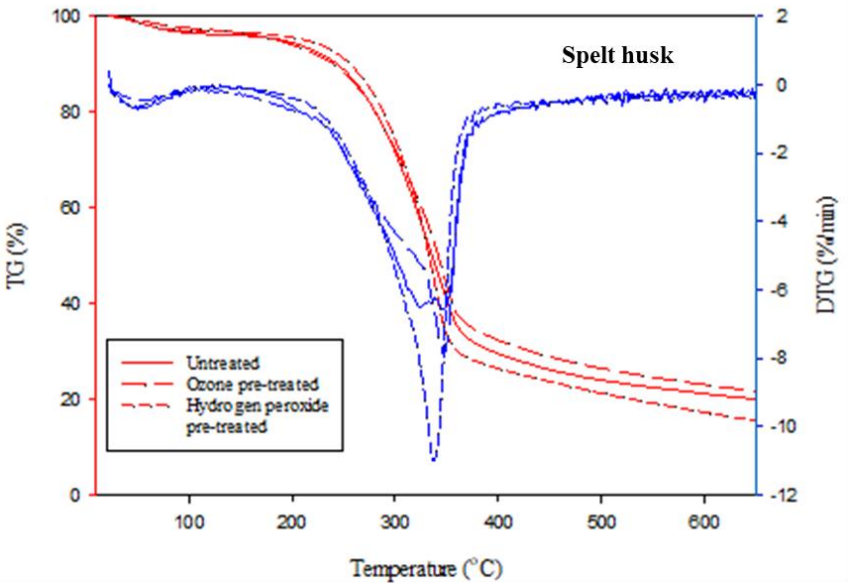

Appendix B2: XRD of corn cob and spelt husk of recovered cellulose from untreated ozone pre-treated and alkaline hydrogen peroxide pre-treated a) corn cob and b) spelt husk.

(a) Corn Cob

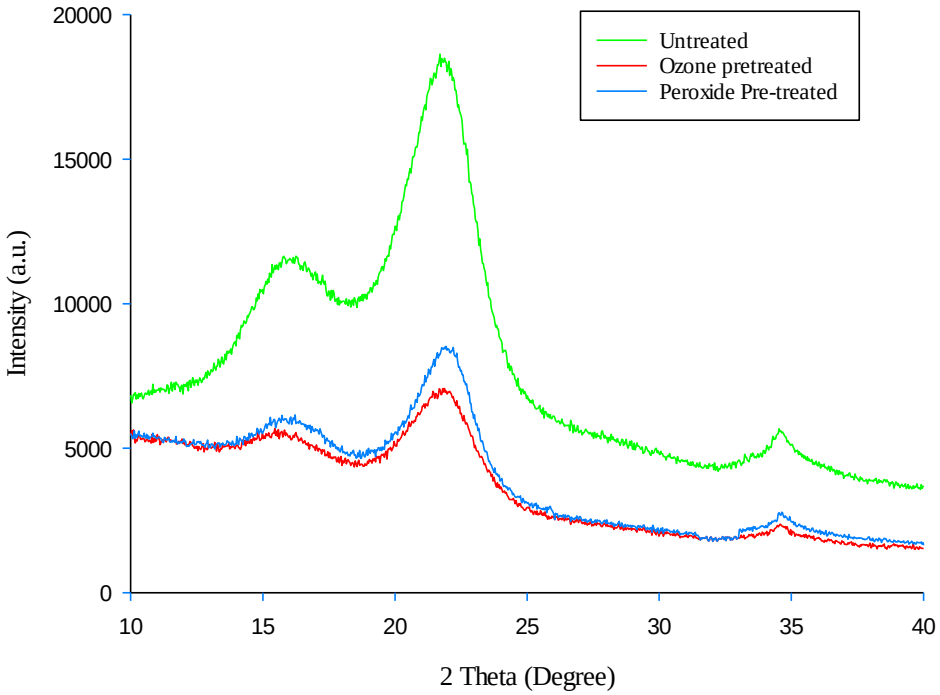

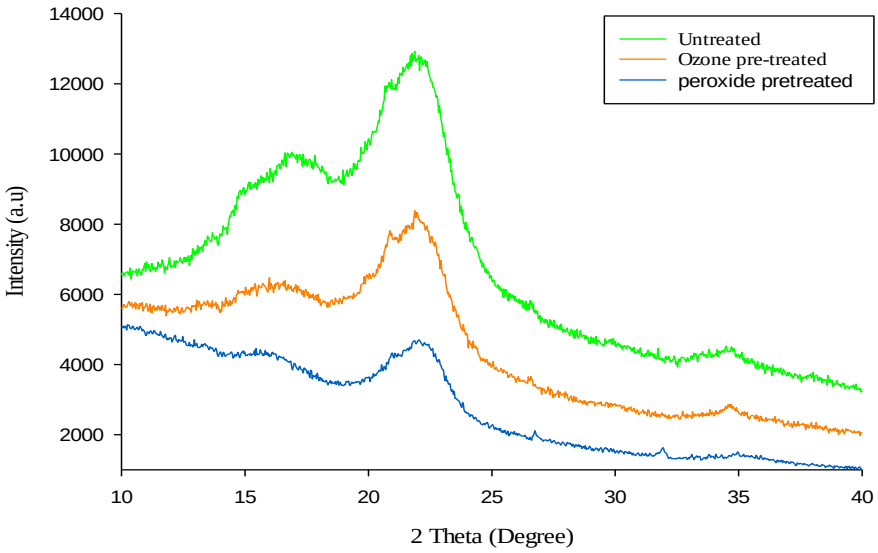

Appendix B3: SEM images of A) corn cob and B) spelt husk with different pre-treatments: i) raw/untreated ii) ultrasound assisted ozone and iii) alkaline hydrogen peroxide pre-treated.

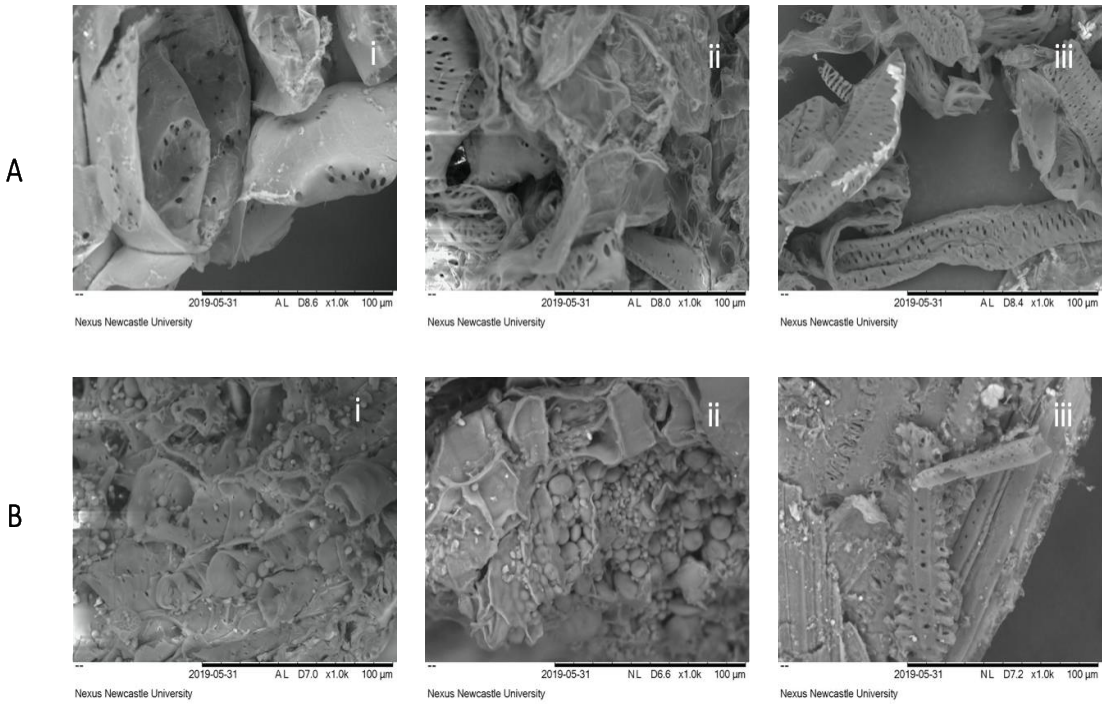

References

Ab Rasid, N. S., Shamjuddin, A., Abdul Rahmsan, A. Z. & Amin, N. A. S. 2021. Recent advances in green pre-treatment methods of lignocellulosic biomass for enhanced biofuel production. *Journal of Cleaner Production,* 321**,** 129038.

Ab Rasid, N. S., Zainol, M. M. & Amin, N. A. S. 2020. 14 - Pretreatment of agroindustry waste by ozonolysis for synthesis of biorefinery products. *In:* Kumar, R. P., Gnansounou, E., Raman, J. K. & Baskar, G. (eds.) *Refining Biomass Residues for Sustainable Energy and Bioproducts.* Academic Press.

Agbor, V. B., Cicek, N., Sparling, R., Berlin, A. & Levin, D. B. 2011. Biomass pretreatment: Fundamentals toward application. *Biotechnology Advances,* 29**,** 675-685.

Al-Abduly, A., Christensen, P. & Harvey, A. 2020. The characterization of a packed bed plasma reactor for ozone generation. *Plasma Sources Science and Technology,* 29**,** 035002.

Alonso, D. M., Wettstein, S. G., Mellmer, M. A., Gurbuz, E. I. & Dumesic, J. A. 2013. Integrated conversion of hemicellulose and cellulose from lignocellulosic biomass. s*Energy & Environmental Science,* 6**,** 76-80.

Arato, C., Pye, E. K. & Gjennestad, G. 2005. The lignol approach to biorefining of woody biomass to produce ethanol and chemicals. *Applied Biochemistry and Biotechnology,* 123**,** 871-882.

Arora, A., Nandal, P., Singh, J. & Verma, M. L. 2020. Nanobiotechnological advancements in lignocellulosic biomass pretreatment. *Materials Science for Energy Technologies,* 3**,** 308-318.

Au - Zijlstra, D. S., Au - De Santi, A., Au - Oldenburger, B., Au - De Vries, J., Au - Barta, K. & Au - Deuss, P. J. 2019. Extraction of Lignin with High β-O-4 Content by Mild Ethanol Extraction and Its Effect on the Depolymerization Yield. *JoVE,* e58575.

Baig, K. S., Wu, J., Turcotte, G. & Doan, H. D. 2015. Novel Ozonation Technique to Delignify Wheat Straw for Biofuel Production. *Energy & Environment,* 26**,** 303-318.

Baker, D. A. & Rials, T. G. 2013. Recent advances in low-cost carbon fiber manufacture from lignin. *Journal of Applied Polymer Science,* 130**,** 713-728.

Balakshin, M., Capanema, E., Gracz, H., Chang, H.-M. & Jameel, H. 2011. Quantification of lignin–carbohydrate linkages with high-resolution NMR spectroscopy. *Planta,* 233**,** 1097-1110.

Behera, S., Arora, R., Nandhagopal, N. & Kumar, S. 2014. Importance of chemical pretreatment for bioconversion of lignocellulosic biomass. *Renewable and Sustainable Energy Reviews,* 36**,** 91-106.

Ben'ko, E. M., Manisova, O. R., Murav'eva, G. P. & Lunin, V. V. 2013. Structural changes in wood during ozonation. *Russian Journal of Physical Chemistry A,* 87**,** 1097-1101.

Bi, S., Peng, L., Chen, K. & Zhu, Z. 2016. Enhanced enzymatic saccharification of sugarcane bagasse pretreated by combining O2 and NaOH. *Bioresource Technology,* 214**,** 692-699.

Binder, A., Pelloni, L. & Fiechter, A. 1980. Delignification of straw with ozone to enhance biodegradability. *European Journal of Applied Microbiology and Biotechnology,* 11**,** 1-5.

Bomtempo, J.-V., Chaves Alves, F. & De Almeida Oroski, F. 2017. Developing new platform chemicals: what is required for a new bio-based molecule to become a platform chemical in the bioeconomy? *Faraday Discussions,* 202**,** 213-225.

Bonafaccia, G., Galli, V., Francisci, R., Mair, V., Skrabanja, V. & Kreft, I. 2000. Characteristics of spelt wheat products and nutritional value of spelt wheat-based bread. *Food Chemistry,* 68**,** 437-441.

Boonduang, S., Limsuwan, S., Kongsri, W. & Limsuwan, P. 2012. Effect of Oxygen Pressure and Flow Rate on Electrical Characteristic and Ozone Concentration of a Cylinder-Cylinder DBD Ozone Generator. *Procedia Engineering,* 32**,** 936-942.

Bozell, J. J. 2010. Connecting Biomass and Petroleum Processing with a Chemical Bridge. *Science,* 329**,** 522-523.

Brandt-Talbot, A., Gschwend, F. J. V., Fennell, P. S., Lammens, T. M., Tan, B., Weale, J. & Hallett, J. P. 2017. An economically viable ionic liquid for the fractionation of lignocellulosic biomass. *Green Chemistry,* 19**,** 3078-3102.

Brémond, U., De Buyer, R., Steyer, J.-P., Bernet, N. & Carrere, H. 2018. Biological pretreatments of biomass for improving biogas production: an overview from lab scale to full-scale. *Renewable and Sustainable Energy Reviews,* 90**,** 583-604.

Brueggemann, N., Puehmeier, T., Fiekens, R., Richardt, F.-J. & Salvermoser, M. 2017. Cooling Conditions of Ozone Generators. *Ozone: Science & Engineering,* 39**,** 196-201.

Bule, M. V., Gao, A. H., Hiscox, B. & Chen, S. 2013. Structural Modification of Lignin and Characterization of Pretreated Wheat Straw by Ozonation. *Journal of Agricultural and Food Chemistry,* 61**,** 3916-3925.

Bussemaker, M. J. & Zhang, D. 2013. Effect of Ultrasound on Lignocellulosic Biomass as a Pretreatment for Biorefinery and Biofuel Applications. *Industrial & Engineering Chemistry Research,* 52**,** 3563-3580.

Carrasco, J. E., Sáiz, M. C., Navarro, A., Soriano, P., Sáez, F. & Martinez, J. M. 1994. Effects of dilute acid and steam explosion pretreatments on the cellulose structure and kinetics of cellulosic fraction hydrolysis by dilute acids in lignocellulosic materials. *Applied Biochemistry and Biotechnology,* 45**,** 23-34.

Cesaro, A. & Belgiorno, V. 2013. Sonolysis and ozonation as pretreatment for anaerobic digestion of solid organic waste. *Ultrasonics Sonochemistry,* 20**,** 931-936.

Chandra, R. P., Bura, R., Mabee, W. E., Berlin, A., Pan, X. & Saddler, J. N. 2007. Substrate pretreatment: The key to effective enzymatic hydrolysis of lignocellulosics? *Advances in Biochemical Engineering/Biotechnology.*

Chen, H. L., Lee, H. M., Chen, S. H. & Chang, M. B. 2008. Review of Packed-Bed Plasma Reactor for Ozone Generation and Air Pollution Control. *Industrial & Engineering Chemistry Research,* 47**,** 2122-2130.

Chen, W., He, H., Zhu, H., Cheng, M., Li, Y. & Wang, S. 2018. Thermo-Responsive Cellulose-Based Material with Switchable Wettability for Controllable Oil/Water Separation. *Polymers,* 10**,** 592.

Cheng, K., Winter, W. T. & Stipanovic, A. J. 2012. A modulated-TGA approach to the kinetics of lignocellulosic biomass pyrolysis/combustion. *Polymer Degradation and Stability,* 97**,** 1606-1615.

Choi, H., Lim, H. N., Kim, J., Hwang, T. M. & Kang, J. W. 2002. Transport characteristics of gas phase ozone in unsaturated porous media for in-situ chemical oxidation. *Journal of Contaminant Hydrology,* 57**,** 81-98.

Choudhary, V., Mushrif, S. H., Ho, C., Anderko, A., Nikolakis, V., Marinkovic, N. S., Frenkel, A. I., Sandler, S. I. & Vlachos, D. G. 2013. Insights into the Interplay of Lewis and Brønsted Acid Catalysts in Glucose and Fructose Conversion to 5-(Hydroxymethyl)furfural and Levulinic Acid in Aqueous Media. *Journal of the American Chemical Society,* 135**,** 3997-4006.

Coca, M., González-Benito, G. & García-Cubero, M. T. 2016. Chapter 18 - Chemical Oxidation With Ozone as an Efficient Pretreatment of Lignocellulosic Materials. *In:* MUSSATTO, S. I. (ed.) *Biomass Fractionation Technologies for a Lignocellulosic Feedstock Based Biorefinery.* Amsterdam: Elsevier.

Contescu, C. I., Adhikari, S. P., Gallego, N. C., Evans, N. D. & Biss, B. E. 2018. Activated Carbons derived from high-temperature pyrolysis of lignocellulose biomass. *Carbons,* 4,51.

Criegee, R. 1975. Mechanism of Ozonolysis. *Angewandte Chemie International Edition in English,* 14**,** 745-752.

Da Silva Lacerda, V., López-Sotelo, J. B., Correa-Guimarães, A., Hernández-Navarro, S., Sánchez-Bascones, M., Navas-Gracia, L. M., Martín-Ramos, P., Pérez-Lebeña, E. & Martín-Gil, J. 2015. A kinetic study on microwave-assisted conversion of cellulose and lignocellulosic waste into hydroxymethylfurfural/furfural. *Bioresource Technology,* 180**,** 88-96.

Dashtban, M., Gilbert, A. & Fatehi, P. 2012. Production of furfural: Overview and challenges. *J-FOR,* 2**,** 44-53.

Davies, E., Deutz, P. & Zein, S. H. 2020. Single-step extraction–esterification process to produce biodiesel from palm oil mill effluent (POME) using microwave heating: a circular economy approach to making use of a difficult waste product. *Biomass Conversion and Biorefinery*.

De, S., Dutta, S. & Saha, B. 2011. Microwave assisted conversion of carbohydrates and biopolymers to 5-hydroxymethylfurfural with aluminium chloride catalyst in water. *Green Chemistry,* 13**,** 2859-2868.

Demirbaş, A. 2001a. Biomass resource facilities and biomass conversion processing for fuels and chemicals. *Energy Conversion and Management,* 42**,** 1357-1378.

Demirbaş, A. 2001b. Relationships between lignin contents and heating values of biomass. *Energy Conversion and Management,* 42**,** 183-188.

Duff, S. J. B. & Murray, W. D. 1996. Bioconversion of forest products industry waste cellulosics to fuel ethanol: A review. *Bioresource Technology,* 55**,** 1-33.

Elgharbawy, A. A., Alam, M. Z., Moniruzzaman, M. & Goto, M. 2016. Ionic liquid pretreatment as emerging approaches for enhanced enzymatic hydrolysis of lignocellulosic biomass. *Biochemical Engineering Journal,* 109**,** 252-267.

Eliasson, B. & Kogelschatz, U. 1991. Nonequilibrium volume plasma chemical processing. *IEEE Transactions on Plasma Science,* 19**,** 1063-1077.

Fang, S., Wang, W., Tong, S., Zhang, C. & Liu, P. 2018. Evaluation of the Effects of Isolated Lignin on Cellulose Enzymatic Hydrolysis of Corn Stover Pretreatment by NaOH Combined with Ozone. *Molecules,* 23**,** 1495.

Fang, Z., Qiu, Y., Sun, Y., Wang, H. & Edmund, K. 2008. Experimental study on discharge characteristics and ozone generation of dielectric barrier discharge in a cylinder–cylinder reactor and a wire–cylinder reactor. *Journal of Electrostatics,* 66**,** 421-426.

Fernández-Delgado, M., Plaza, P. E., Coca, M., García-Cubero, M. T., González-Benito, G. & Lucas, S. 2019. Comparison of mild alkaline and oxidative pretreatment methods for biobutanol production from brewer's spent grains. *Industrial Crops and Products,* 130**,** 409-419.

Fridman, A. 2008. Plasma chemistsry textbook, Cambridge University Press, 382 – 390.

Furong, T., Huanling, S. & Lingjun, C. 2010. Hydrolysis of Cellulose by Using Catalytic Amounts of FeCl2 in Ionic Liquids. *ChemSusChem,* 3**,** 1298-1303.

Gallo, J. M. R., Alonso, D. M., Mellmer, M. A., Yeap, J. H., Wong, H. C. & Dumesic, J. A. 2013. Production of furfural from lignocellulosic biomass using beta zeolite and biomass-derived solvent. *Topics in Catalysis,* 56**,** 1775-1781.

García-Cubero, M. T., González-Benito, G., Indacoechea, I., Coca, M. & Bolado, S. 2009. Effect of ozonolysis pretreatment on enzymatic digestibility of wheat and rye straw. *Bioresource Technology,* 100**,** 1608-1613.

Gashti, M. P., Pournaserani, A., Ehsani, H. & Gashti, M. P. 2013. Surface oxidation of cellulose by ozone-gas in a vacuum cylinder to improve the functionality of fluoromonomer. *Vacuum,* 91**,** 7-13.

Gholami, A., Pourfayaz, F. & Maleki, A. 2021. Techno-economic assessment of biodiesel production from canola oil through ultrasonic cavitation. *Energy Reports,* 7**,** 266-277.

Gómez Millán, G., Bangalore Ashok, R. P., Oinas, P., Llorca, J. & Sixta, H. 2021. Furfural production from xylose and birch hydrolysate liquor in a biphasic system and techno-economic analysis. *Biomass Conversion and Biorefinery,* 11**,** 2095-2106.

Gould, J. M. 1984. Alkaline peroxide delignification of agricultural residues to enhance enzymatic saccharification. *Biotechnology and Bioengineering,* 26**,** 46-52.

Grasham, O., Dupont, V., Cockerill, T. & Camargo-Valero, M. A. 2022. Ammonia and Biogas from Anaerobic and Sewage Digestion for Novel Heat, Power and Transport Applications—A Techno-Economic and GHG Emissions Study for the United Kingdom. *Energies,* 15**,** 2174.

Guo, W., Heeres, H. J. & Yue, J. 2020. Continuous synthesis of 5-hydroxymethylfurfural from glucose using a combination of AlCl3 and HCl as catalyst in a biphasic slug flow capillary microreactor. *Chemical Engineering Journal,* 381**,** 122754.

Gürbüz, E. I., Gallo, J. M. R., Alonso, D. M., Wettstein, S. G., Lim, W. Y. & Dumesic, J. A. 2013. Conversion of hemicellulose into furfural using solid acid catalysts in γ-valerolactone. *Angewandte Chemie - International Edition,* 52**,** 1270-1274.

Halder, P. K. 2020. *Investigations on ionic liquid pre-treatment of lignocellulosic biomass for the production of biofuels and platform chemicals.*

Hendriks, A. C., Frederiks, B. J. M. & Verkerk, M. A. 2009. Het recht op autonomie in samenhang met goede zorg bezien. *Pro Vita Humana,* 16**,** 10-18.

Himmel, M. E., Ding, S.-Y., Johnson, D. K., Adney, W. S., Nimlos, M. R., Brady, J. W. & Foust, T. D. 2007. Biomass Recalcitrance: Engineering Plants and Enzymes for Biofuels Production. *Science,* 315**,** 804-807.

Hoang, T. M. C., Van Eck, E. R. H., Bula, W. P., Gardeniers, J. G. E., Lefferts, L. & Seshan, K. 2015. Humin based by-products from biomass processing as a potential carbonaceous source for synthesis gas production. *Green Chemistry,* 17**,** 959-972.

Holm, M. S., Saravanamurugan, S. & Taarning, E. 2010. Conversion of Sugars to Lactic Acid Derivatives Using Heterogeneous Zeotype Catalysts. *Science,* 328**,** 602-605.

Holzer, F., Kopinke, F. D. & Roland, U. 2005. Influence of Ferroelectric Materials and Catalysts on the Performance of Non-Thermal Plasma (NTP) for the Removal of Air Pollutants. *Plasma Chemistry and Plasma Processing,* 25**,** 595-611.

Hossain, M. S., Theodoropoulos, C. & Yousuf, A. 2019. Techno-economic evaluation of heat integrated second generation bioethanol and furfural coproduction. *Biochemical Engineering Journal,* 144**,** 89-103.

Hu, L., Sun, Y. & Lin, L. 2012. Efficient Conversion of Glucose into 5-Hydroxymethylfurfural by Chromium(III) Chloride in Inexpensive Ionic Liquid. *Industrial & Engineering Chemistry Research,* 51**,** 1099-1104.

Hudson, S. M. & Cuculo, J. A. 1980. The Solubility of Unmodified Cellulose: A Critique of the Literature. *Journal of Macromolecular Science, Part C,* 18**,** 1-82.

Hui, W., Zhou, Y., Dong, Y., Cao, Z.-J., He, F.-Q., Cai, M.-Z. & Tao, D.-J. 2019. Efficient hydrolysis of hemicellulose to furfural by novel superacid SO4H-functionalized ionic liquids. *Green Energy & Environment,* 4**,** 49-55.

Humbird, D., Davis, R., Tao, L., Kinchin, C., Hsu, D., Aden, A., Schoen, P., Lukas, J., Olthof, B., Worley, M., Sexton, D. & Dudgeon, D. 2011. Process Design and Economics for Biochemical Conversion of Lignocellulosic Biomass to Ethanol: Dilute-Acid Pretreatment and Enzymatic Hydrolysis of Corn Stover. United States.

Ibrahim, H. H., Bilsborrow, P. E. & Phan, A. N. 2021. Intensification of pre-treatment and fractionation of agricultural residues. *Chemical Engineering and Processing - Process Intensification,* 159**,** 108231.

Inone-Kauffmann, E. R. 2009. Arboform® - A lignin-based thermoplastic. *International Sugar Journal,* 111**,** 10-11.

Ishida, H. & Seri, K.-I. 1996. Catalytic activity of lanthanoide(III) ions for dehydration of d-glucose to 5-(hydroxymethyl) furfural. *Journal of Molecular Catalysis A: Chemical,* 112**,** L163-L165.

Jenei, I., Kis, P. & Kiss, E. 2007. The Development of Ozone Generators with the Analysis of the Field Distribution of the Electrode Arrangements. *Ozone: Science & Engineering,* 29**,** 215-220.

Jia, S., Xu, Z. & Zhang, Z. 2014a. Catalytic conversion of glucose in dimethylsulfoxide/water binary mix with chromium trichloride: Role of water on the product distribution. *Chemical Engineering Journal,* 254**,** 333-339.

Jia, S., Xu, Z. & Zhang, Z. C. 2014b. Catalytic conversion of glucose in dimethylsulfoxide/water binary mix with chromium trichloride: Role of water on the product distribution. *Chemical Engineering Journal,* 254**,** 333-339.

Jiang, X., Abbati De Assis, C., Kollman, M., Sun, R., Jameel, H., Chang, H.-M. & Gonzalez, R. 2020. Lignin fractionation from laboratory to commercialization: chemistry, scalability and techno-economic analysis. *Green Chemistry,* 22**,** 7448-7459.

Jin, C., Xiang, N., Zhu, X., E, S., Sheng, K. & Zhang, X. 2021. Selective 5-hydroxymethylfurfural production from cellulose formate in DMSO-H2O media. *Applied Catalysis B: Environmental,* 285**,** 119799.

Jodpimai, S., Boonduang, S. & Limsuwan, P. 2015. Dielectric barrier discharge ozone generator using aluminum granules electrodes. *Journal of Electrostatics,* 74**,** 108-114.

Kaur, U., Oberoi, H. S., Bhargav, V. K., Sharma-Shivappa, R. & Dhaliwal, S. S. 2012. Ethanol production from alkali- and ozone-treated cotton stalks using thermotolerant Pichia kudriavzevii HOP-1. *Industrial Crops and Products,* 37**,** 219-226.

Kazi, F. K., Patel, A. D., Serrano-Ruiz, J. C., Dumesic, J. A. & Anex, R. P. 2011. Techno-economic analysis of dimethylfuran (DMF) and hydroxymethylfurfural (HMF) production from pure fructose in catalytic processes. *Chemical Engineering Journal,* 169**,** 329-338.

Kennedy, J. F. & Hasamudin, W. H. W. 1995. Cellulose: structure, accessibility and reactivity, edited by H. A. Krassig. Gordon & Breach, Pennsylvania, 1993. Pp. xvi + 376, price £169.00, US$260.00. ISBN 2-88124-798-9. *Polymer International,* 36**,** 101-101.

Khanal, A., Manandhar, A., Adhikari, S. & Shah, A. 2021. Techno-economic analysis of novolac resin production by partial substitution of petroleum-derived phenol with bio-oil phenol. *Biofuels, Bioproducts and Biorefining,* 15, 1611-1620.

Kim, H., Choi, J., Park, J. & Won, W. 2020. Production of a sustainable and renewable biomass-derived monomer: conceptual process design and techno-economic analysis. *Green Chemistry,* 22**,** 7070-7079.

Kim, H., Lee, S., Lee, J. & Won, W. 2021. Simultaneous production of 1,6-hexanediol, furfural, and high-purity lignin from white birch: Process integration and techno-economic evaluation. *Bioresource Technology,* 331**,** 125009.

Kimura, H., Yoshida, K., Uosaki, Y. & Nakahara, M. 2013. Effect of Water Content on Conversion of d-Cellobiose into 5-Hydroxymethyl-2-furaldehyde in a Dimethyl Sulfoxide–Water Mixture. *The Journal of Physical Chemistry A,* 117**,** 10987-10996.

Kläusli, T. 2014. AVA Biochem: commercialising renewable platform chemical 5-HMF. *Green Processing and Synthesis.*

Kojima, Y. & Yoon, S.-L. 2008. Improved enzymatic hydrolysis of waste paper by ozone pretreatment. *Journal of Material Cycles and Waste Management,* 10**,** 134-139.

Kokossis, A. C. & Yang, A. 2010. On the use of systems technologies and a systematic approach for the synthesis and the design of future biorefineries. *Computers & Chemical Engineering,* 34**,** 1397-1405.

Kosyakov, D. S., Anikeenko, E. A., Ul'yanovskii, N. V., Khoroshev, O. Y., Shavrina, I. S. & Gorbova, N. S. 2018. Ionic liquid matrices for MALDI mass spectrometry of lignin. *Analytical and Bioanalytical Chemistry,* 410**,** 7429-7439.

Krishna, S. H., Huang, K., Barnett, K. J., He, J., Maravelias, C. T., Dumesic, J. A., Huber, G. W., De Bruyn, M. & Weckhuysen, B. M. 2018. Oxygenated commodity chemicals from chemo-catalytic conversion of biomass derived heterocycles. *AIChE Journal,* 64**,** 1910-1922.

Kumar, A., Chauhan, A. S., Bains, R. & Das, P. 2021. Rice straw (Oryza sativa L.) biomass conversion to furfural, 5-hydroxymethylfurfural, lignin and bio-char: A comprehensive solution. *Journal of Industrial and Engineering Chemistry,* 104**,** 286-294.

Kumar, S., Paritosh, K., Pareek, N., Chawade, A. & Vivekanand, V. 2018. De-construction of major Indian cereal crop residues through chemical pretreatment for improved biogas production: An overview. *Renewable and Sustainable Energy Reviews,* 90**,** 160-170.

Kuppens, T., Van Dael, M., Vanreppelen, K., Thewys, T., Yperman, J., Carleer, R., Schreurs, S. & Van Passel, S. 2015. Techno-economic assessment of fast pyrolysis for the valorization of short rotation coppice cultivated for phytoextraction. *Journal of Cleaner Production,* 88**,** 336-344.

Kuznetsov, A., Kumar, G., Ardagh, M. A., Tsapatsis, M., Zhang, Q. & Dauenhauer, P. J. 2020. On the Economics and Process Design of Renewable Butadiene from Biomass-Derived Furfural. *ACS Sustainable Chemistry & Engineering,* 8**,** 3273-3282.

Lange, J. P., Van Der Heide, E., Van Buijtenen, J. & Price, R. 2012. Furfural-A promising platform for lignocellulosic biofuels. *ChemSusChem,* 5**,** 150-166.

Lara-Serrano, M., Morales-Delarosa, S., Campos-Martín, J. M. & Fierro, J. L. G. 2019. Fractionation of Lignocellulosic Biomass by Selective Precipitation from Ionic Liquid Dissolution. *Applied Sciences*, 9**,** 1862.

Laxmikantádhepe, P. 2014. *RSC Adv.,* 4**,** 26215-26221.

Lee, J. M., Jameel, H. & Venditti, R. A. 2010. *Effect Of Ozone And Autohydrolysis Pretreatments On Enzymatic Digestibility Of Coastal Bermuda Grass*.

León, M., Silva, J., Carrasco, S. & Barrientos, N. 2020. Design, Cost Estimation and Sensitivity Analysis for a Production Process of Activated Carbon from Waste Nutshells by Physical Activation. *Processes,* 8**,** 945.

Li, C., Wang, L., Chen, Z., Li, Y., Wang, R., Luo, X., Cai, G., Li, Y., Yu, Q. & Lu, J. 2015a. Ozonolysis pretreatment of maize stover: The interactive effect of sample particle size and moisture on ozonolysis process. *Bioresource Technology,* 183**,** 240-247.

Li, C., Zhang, Z. & Zhao, Z. K. 2009. Direct conversion of glucose and cellulose to 5-hydroxymethylfurfural in ionic liquid under microwave irradiation. *Tetrahedron Letters,* 50**,** 5403-5405.

Li, H., Cai, X., Wang, Z. & Xu, C. 2020. Cost-effective production of organosolv lignin from woody biomass using ethanol-water mixed solvent at mild conditions. *The Journal of Supercritical Fluids*, 158**,** 104745.

Li, H., Ren, J., Zhong, L., Sun, R. & Liang, L. 2015b. Production of furfural from xylose, water-insoluble hemicelluloses and water-soluble fraction of corncob via a tin-loaded montmorillonite solid acid catalyst. *Bioresource Technology*, 176**,** 242-248.

Li, J., Ding, D. J., Xu, L. J., Guo, Q. X. & Fu, Y. 2014. The breakdown of reticent biomass to soluble components and their conversion to levulinic acid as a fuel precursor. *RSC Advances*, 4**,** 14985-14992.

Li, M., Yan, Y., Jin, Q., Liu, M., Zhu, B., Wang, L., Li, T., Tang, X.-J. & Zhu, Y.-M. 2018a. Experimental study on ozone generation from oxygen in double surface dielectric barrier discharge. *Vacuum*, 157**,** 249-258.

Li, W., Zhu, Y., Lu, Y., Liu, Q., Guan, S., Chang, H. M., Jameel, H. & Ma, L. 2017. Enhanced furfural production from raw corn stover employing a novel heterogeneous acid catalyst. *Bioresource Technology*, 245**,** 258-265.

Li, X., Peng, K., Xia, Q., Liu, X. & Wang, Y. 2018b. Efficient conversion of cellulose into 5-hydroxymethylfurfural over niobia/carbon composites. *Chemical Engineering Journal*, 332**,** 528-536.

Li, X., Zhang, Y., Xia, Q., Liu, X., Peng, K., Yang, S. & Wang, Y. 2018c. Acid-Free Conversion of Cellulose to 5-(Hydroxymethyl)furfural Catalyzed by Hot Seawater. *Industrial & Engineering Chemistry Research*, 57**,** 3545-3553.

Liang Chen, H., Ming Lee, H. & Been Chang, M. 2006. Enhancement of Energy Yield for Ozone Production via Packed-Bed Reactors. *Ozone: Science & Engineering*, 28**,** 111-118.

Lin, C. S. K., Luque, R., Clark, J. H., Webb, C. & Du, C. 2012. Wheat-based biorefining strategy for fermentative production and chemical transformations of succinic acid. *Biofuels, Bioproducts and Biorefining*, 6**,** 88-104.

Liu, Y., Xie, J., Wu, N., Ma, Y., Menon, C. & Tong, J. 2019. Characterization of natural cellulose fiber from corn stalk waste subjected to different surface treatments. *Cellulose*, 26**,** 4707-4719.

Long, J., Xu, Y., Wang, T., Shu, R., Zhang, Q., Zhang, X., Fu, J. & Ma, L. 2014. *Hydrothermal Depolymerization of Lignin: Understanding the Structural Evolution*.

Lora, J. 2008. Chapter 10 - Industrial Commercial Lignins: Sources, Properties and Applications. *In:* BELGACEM, M. N. & GANDINI, A. (eds.) *Monomers, Polymers and Composites from Renewable Resources.* Amsterdam: Elsevier.

Louwerse, M. J. & Rothenberg, G. 2012. Transferable basis sets of numerical atomic orbitals. *Physical Review B,* 85**,** 035108.

Lu, Y., Lu, Y.-C., Hu, H.-Q., Xie, F.-J., Wei, X.-Y. & Fan, X. 2017. Structural Characterization of Lignin and Its Degradation Products with Spectroscopic Methods. *Journal of Spectroscopy,* 2017**,** 8951658.

Lucia, L. A. 2008. Lignocellulosic Biomass: A Potential Feedstock To Replace Petroleum. *BioResources,* 3**,** 2.

Luo, Y., Li, Z., Li, X., Liu, X., Fan, J., Clark, J. H. & Hu, C. 2019. The production of furfural directly from hemicellulose in lignocellulosic biomass: A review. *Catalysis Today,* 319**,** 14-24.

Luo, Y., Li, Z., Zuo, Y., Su, Z. & Hu, C. 2017. A Simple Two-Step Method for the Selective Conversion of Hemicellulose in Pubescens to Furfural. *ACS Sustainable Chemistry and Engineering,* 5**,** 8137-8147.

Luterbacher, J. S., Martin Alonso, D. & Dumesic, J. A. 2014. Targeted chemical upgrading of lignocellulosic biomass to platform molecules. *Green Chemistry,* 16**,** 4816-4838.

Lynd, L. R. & Wang, M. Q. 2003. A Product-Nonspecific Framework for Evaluating the Potential of Biomass-Based Products to Displace Fossil Fuels. *Journal of Industrial Ecology,* 7**,** 17-32.

Mamleeva, N. A., Autlov, S. A., Bazarnova, N. G. & Lunin, V. V. 2009. Delignification of softwood by ozonation. *Pure and Applied Chemistry,* 81**,** 2081-2091.

Manning, T. J. 2000. Production Of Ozone in an Electrical Discharge Using Inert Gases as Catalysts. *Ozone: Science & Engineering,* 22**,** 53-64.

Mansilla, H. D., Baeza, J., Urzúa, S., Maturana, G., Villaseñor, J. & Durán, N. 1998. Acid-catalysed hydrolysis of rice hull: Evaluation of furfural production. *Bioresource Technology,* 66**,** 189-193.

Maqsood, H. S., Bashir, U., Wiener, J., Puchalski, M., Sztajnowski, S. & Militky, J. 2017. Ozone treatment of jute fibers. *Cellulose,* 24**,** 1543-1553.

Marcotullio, G. 2011. *The Chemistry and Technology of Furfural Production in Modern Lignocellulose-Feedstock Biorefineries.* Arkhé Edizioni - L'Aquila, Italy.

Marcotullio, G. & De Jong, W. 2010. Chloride ions enhance furfural formation from D-xylose in dilute aqueous acidic solutions. *Green Chemistry,* 12**,** 1739-1746.

Mariscal, R., Maireles-Torres, P., Ojeda, M., Sádaba, I. & López Granados, M. 2016. Furfural: a renewable and versatile platform molecule for the synthesis of chemicals and fuels. *Energy & Environmental Science,* 9**,** 1144-1189.

Masuda, S., Akutsu, K., Kuroda, M., Awatsu, Y. & Shibuya, Y. 1988. A ceramic-based ozonizer using high-frequency discharge. *IEEE Transactions on Industry Applications,* 24**,** 223-231.

Matsakas, L., Nitsos, C., Raghavendran, V., Yakimenko, O., Persson, G., Olsson, E., Rova, U., Olsson, L. & Christakopoulos, P. 2018. A novel hybrid organosolv: steam explosion method for the efficient fractionation and pretreatment of birch biomass. *Biotechnology for Biofuels,* 11**,** 160.

Matsakas, L., Raghavendran, V., Yakimenko, O., Persson, G., Olsson, E., Rova, U., Olsson, L. & Christakopoulos, P. 2019. Lignin-first biomass fractionation using a hybrid organosolv – Steam explosion pretreatment technology improves the saccharification and fermentability of spruce biomass. *Bioresource Technology,* 273**,** 521-528.

Medronho, B. & Lindman, B. 2015. Brief overview on cellulose dissolution/regeneration interactions and mechanisms. *Advances in Colloid and Interface Science,* 222**,** 502-508.

Mellmer, M. A., Sener, C., Gallo, J. M. R., Luterbacher, J. S., Alonso, D. M. & Dumesic, J. A. 2014. Solvent effects in acid-catalyzed biomass conversion reactions. *Angewandte Chemie - International Edition,* 53**,** 11872-11875.

Melro, E., Alves, L., Antunes, F. E. & Medronho, B. 2018. A brief overview on lignin dissolution. *Journal of Molecular Liquids,* 265**,** 578-584.

Miao, H. & Yun, G. 2011. The sterilization of Escherichia coli by dielectric-barrier discharge plasma at atmospheric pressure. *Applied Surface Science,* 257**,** 7065-7070.

Mija, A., Van Der Waal, J. C., Pin, J.-M., Guigo, N. & De Jong, E. 2017. Humins as promising material for producing sustainable carbohydrate-derived building materials. *Construction and Building Materials,* 139**,** 594-601.

Mikmekov, Aacute, Scaron, Aacute, Rka, Matsuda, K., Watanabe, K., Ikeno, S., Uuml, Llerov, Aacute, Ilona & Frank, L. 2011. Fib Induced Damage Examined With The Low Energy Sem. *Materials Transactions,* 52**,** 292-296.

Mishra, S., Manent, A.-S., Chabot, B. & Daneault, C. 2012. Production of nano-cellulose from native cellulose - Various options utilizing ultrasound. *Bioresources,* 7**,** 422-436.

Mittal, A., Pilath, H. M. & Johnson, D. K. 2020. Direct Conversion of Biomass Carbohydrates to Platform Chemicals: 5-Hydroxymethylfurfural (HMF) and Furfural. *Energy & Fuels,* 34**,** 3284-3293.

Möller, M., Harnisch, F. & Schröder, U. 2013. Hydrothermal liquefaction of cellulose in subcritical water-the role of crystallinity on the cellulose reactivity. *RSC Advances,* 3**,** 11035-11044.

Morales, G., Melero, J. A., Paniagua, M., Iglesias, J., Hernández, B. & Sanz, M. 2014. Sulfonic acid heterogeneous catalysts for dehydration of C6-monosaccharides to 5-hydroxymethylfurfural in dimethyl sulfoxide. *Cuihua Xuebao/Chinese Journal of Catalysis,* 35**,** 644-655.

Moreau, C., Finiels, A. & Vanoye, L. 2006. Dehydration of fructose and sucrose into 5-hydroxymethylfurfural in the presence of 1-H-3-methyl imidazolium chloride acting both as solvent and catalyst. *Journal of Molecular Catalysis A: Chemical,* 253**,** 165-169.

Morrison, C., Atkinson, A., Zamyadi, A., Kibuye, F., Mckie, M., Hogard, S., Mollica, P., Jasim, S. & Wert, E. C. 2021. Critical Review and Research Needs of Ozone Applications Related to Virus Inactivation: Potential Implications for SARS-CoV-2. *Ozone: Science & Engineering,* 43**,** 2-20.

Motagamwala, A. H., Huang, K., Maravelias, C. T. & Dumesic, J. A. 2019. Solvent system for effective near-term production of hydroxymethylfurfural (HMF) with potential for long-term process improvement. *Energy & Environmental Science,* 12**,** 2212-2222.

Mothé, C. G. & De Miranda, I. C. 2009. Characterization of sugarcane and coconut fibers by thermal analysis and FTIR. *Journal of Thermal Analysis and Calorimetry,* 97**,** 661.

Mountraki, A. D., Nikolakopoulos, A., Mlayah, B. B. & Kokossis, A. C. 2011. Biocore- A systems integration paradigm in the real-life development of a lignocellulosic biorefinery. *In:* PISTIKOPOULOS, E. N., GEORGIADIS, M. C. & KOKOSSIS, A. C. (eds.) *Computer Aided Chemical Engineering.* Elsevier.

Mukherjee, A., Dumont, M.-J. & Raghavan, V. 2015. Review: Sustainable production of hydroxymethylfurfural and levulinic acid: Challenges and opportunities. *Biomass and Bioenergy,* 72**,** 143-183.

Nandiwale, K. Y., Galande, N. D., Thakur, P., Sawant, S. D., Zambre, V. P. & Bokade, V. V. 2014. One-Pot Synthesis of 5-Hydroxymethylfurfural by Cellulose Hydrolysis over

Highly Active Bimodal Micro/Mesoporous H-ZSM-5 Catalyst. *ACS Sustainable Chemistry & Engineering,* 2**,** 1928-1932.

Nassour, K., Brahami, M., Nemmich, S., Hammadi, N., Zouzou, N. & Tilmatine, A. 2016. Comparative Experimental Study between Surface and Volume DBD Ozone Generator. *Ozone: Science & Engineering,* 38**,** 70-76.

Neely, W. C. 1984. Factors affecting the pretreatment of biomass with gaseous ozone. *Biotechnology and Bioengineering,* 26**,** 59-65.

Ng, K. S. & Martinez-Hernandez, E. 2020. 3 - Techno-economic assessment of an integrated bio-oil steam reforming and hydrodeoxygenation system for polygeneration of hydrogen, chemicals, and combined heat and power production. *In:* REN, J., WANG, Y. & HE, C. (eds.) *Towards Sustainable Chemical Processes.* Elsevier.

Nis, B. & Kaya Ozsel, B. 2020. A comprehensive experimental study on the production of key platform chemicals from raw biomass. *Fuel,* 280**,** 118674.

Nis, B. & Kaya Ozsel, B. 2021. Efficient direct conversion of lignocellulosic biomass into biobased platform chemicals in ionic liquid-water medium. *Renewable Energy,* 169**,** 1051-1057.

Nitsos, C., Rova, U. & Christakopoulos, P. 2018. Organosolv Fractionation of Softwood Biomass for Biofuel and Biorefinery Applications. *Energies,* 11**,** 50.

Nitsos, C., Stoklosa, R., Karnaouri, A., Vörös, D., Lange, H., Hodge, D., Crestini, C., Rova, U. & Christakopoulos, P. 2016. Isolation and Characterization of Organosolv and Alkaline Lignins from Hardwood and Softwood Biomass. *ACS Sustainable Chemistry & Engineering,* 4**,** 5181-5193.

Ntimbani, R. N., Farzad, S. & Görgens, J. F. 2021. Techno-economic assessment of one-stage furfural and cellulosic ethanol co-production from sugarcane bagasse and harvest residues feedstock mixture. *Industrial Crops and Products,* 162**,** 113272.

Offerhaus, B., Lackmann, J.-W., Kogelheide, F., Bracht, V., Smith, R., Bibinov, N., Stapelmann, K. & Awakowicz, P. 2017. Spatially resolved measurements of the physical plasma parameters and the chemical modifications in a twin surface dielectric barrier discharge for gas flow purification. *Plasma Processes and Polymers,* 14**,** 1600255.

Ogata, A., Shintani, N., Mizuno, K., Kushiyama, S. & Yamamoto, T. 1999. Decomposition of benzene using a nonthermal plasma reactor packed with ferroelectric pellets. *IEEE Transactions on Industry Applications,* 35**,** 753-759.

Okano, T., Qiao, K., Bao, Q., Tomida, D., Hagiwara, H. & Yokoyama, C. 2013. Dehydration of fructose to 5-hydroxymethylfurfural (HMF) in an aqueous acetonitrile biphasic system in the presence of acidic ionic liquids. *Applied Catalysis A: General,* 451**,** 1-5.

Ollegott, K., Wirth, P., Oberste-Beulmann, C., Awakowicz, P. & Muhler, M. 2020. Fundamental Properties and Applications of Dielectric Barrier Discharges in Plasma-Catalytic Processes at Atmospheric Pressure. *Chemie Ingenieur Technik,* 92**,** 1542-1558.

Otomo, R., Tatsumi, T. & Yokoi, T. 2015. Beta zeolite: a universally applicable catalyst for the conversion of various types of saccharides into furfurals. *Catalysis Science & Technology,* 5**,** 4001-4007.

Pagán-Torres, Y. J., Wang, T., Gallo, J. M. R., Shanks, B. H. & Dumesic, J. A. 2012. Production of 5-Hydroxymethylfurfural from Glucose Using a Combination of Lewis and Brønsted Acid Catalysts in Water in a Biphasic Reactor with an Alkylphenol Solvent. *ACS Catalysis,* 2**,** 930-934.

Palma, V., Cortese, M., Renda, S., Ruocco, C., Martino, M. & Meloni, E. 2020. A Review about the Recent Advances in Selected NonThermal Plasma Assisted Solid–Gas Phase Chemical Processes. *Nanomaterials,* 10**,** 1596.

Pan, X., Xie, D., Gilkes, N., Gregg, D. J. & Saddler, J. N. 2005. Strategies to enhance the enzymatic hydrolysis of pretreated softwood with high residual lignin content. *Appl Biochem Biotechnol,* 121-124**,** 1069-79.

Pandiselvam, R., Sunoj, S., Manikantan, M. R., Kothakota, A. & Hebbar, K. B. 2017. Application and Kinetics of Ozone in Food Preservation. *Ozone: Science & Engineering,* 39**,** 115-126.

Panneerselvam, A., Sharma-Shivappa, R. R., Kolar, P., Clare, D. A. & Ranney, T. 2013a. Hydrolysis of ozone pretreated energy grasses for optimal fermentable sugar production. *Bioresource Technology,* 148**,** 97-104.

Panneerselvam, A., Sharma-Shivappa, R. R., Kolar, P., Ranney, T. & Peretti, S. 2013b. Potential of ozonolysis as a pretreatment for energy grasses. *Bioresource Technology,* 148**,** 242-248.

Park, S., Baker, J. O., Himmel, M. E., Parilla, P. A. & Johnson, D. K. 2010. Cellulose crystallinity index: measurement techniques and their impact on interpreting cellulase performance. *Biotechnology for Biofuels,* 3**,** 10.

Parshetti, G. K., Suryadharma, M. S., Pham, T. P. T., Mahmood, R. & Balasubramanian, R. 2015. Heterogeneous catalyst-assisted thermochemical conversion of food waste biomass into 5-hydroxymethylfurfural. *Bioresource Technology,* 178**,** 19-27.

Patil, S. K. R., Heltzel, J. & Lund, C. R. F. 2012. Comparison of Structural Features of Humins Formed Catalytically from Glucose, Fructose, and 5-Hydroxymethylfurfuraldehyde. *Energy & Fuels,* 26**,** 5281-5293.

Pekárek, S. 2012. Experimental study of surface dielectric barrier discharge in air and its ozone production. *Journal of Physics D: Applied Physics,* 45**,** 075201.

Pekárek, S., Mikeš, J., Beshajová Pelikánová, I., Krčma, F. & Dzik, P. 2016. Effect of TiO2 on Various Regions of Active Electrode on Surface Dielectric Barrier Discharge in Air. *Plasma Chemistry and Plasma Processing,* 36**,** 1187-1200.

Perkowski, J., Kos, L. & Ledakowicz, S. 1996. Application of Ozone in Textile Wastewater Treatment. *Ozone: Science & Engineering,* 18**,** 73-85.

Perrone, O. M., Colombari, F. M., Rossi, J. S., Moretti, M. M. S., Bordignon, S. E., Nunes, C. D. C. C., Gomes, E., Boscolo, M. & Da-Silva, R. 2016. Ozonolysis combined with ultrasound as a pretreatment of sugarcane bagasse: Effect on the enzymatic saccharification and the physical and chemical characteristics of the substrate. *Bioresource Technology,* 218**,** 69-76.

Perrone, O. M., Moretti, M. M. D. S., Bordignon, S. E., Pereira, J. D. C., Da Silva, R., Gomes, E. & Boscolo, M. 2021. Improving cellulosic ethanol production using ozonolysis and acid as a sugarcane biomass pretreatment in mild conditions. *Bioresource Technology Reports,* 13**,** 100628.

Porto, E., Alves Filho, E. G., Silva, L. M. A., Fonteles, T. V., Do Nascimento, R. B. R., Fernandes, F. A. N., De Brito, E. S. & Rodrigues, S. 2020. Ozone and plasma processing effect on green coconut water. *Food Research International,* 131**,** 109000.

Puri, V. P. 1984. Effect of crystallinity and degree of polymerization of cellulose on enzymatic saccharification. *Biotechnology and Bioengineering,* 26**,** 1219-1222.

Qi, L., Mui, Y. F., Lo, S. W., Lui, M. Y., Akien, G. R. & Horváth, I. T. 2014. Catalytic Conversion of Fructose, Glucose, and Sucrose to 5-(Hydroxymethyl)furfural and Levulinic and Formic Acids in γ-Valerolactone As a Green Solvent. *ACS Catalysis,* 4**,** 1470-1477.

Ragauskas, A. J., Beckham, G. T., Biddy, M. J., Chandra, R., Chen, F., Davis, M. F., Davison, B. H., Dixon, R. A., Gilna, P., Keller, M., Langan, P., Naskar, A. K., Saddler, J. N.,

Tschaplinski, T. J., Tuskan, G. A. & Wyman, C. E. 2014. Lignin Valorization: Improving Lignin Processing in the Biorefinery. *Science,* 344**,** 1246843.

Román-Leshkov, Y. & Dumesic, J. A. 2009. Solvent effects on fructose dehydration to 5-hydroxymethylfurfural in biphasic systems saturated with inorganic salts. *Topics in Catalysis,* 52**,** 297-303.

Rout, P. K., Nannaware, A. D., Prakash, O., Kalra, A. & Rajasekharan, R. 2016. Synthesis of hydroxymethylfurfural from cellulose using green processes: A promising biochemical and biofuel feedstock. *Chemical Engineering Science,* 142**,** 318-346.

Roy Goswami, S., Dumont, M.-J. & Raghavan, V. 2016. Microwave Assisted Synthesis of 5-Hydroxymethylfurfural from Starch in AlCl3·6H2O/DMSO/[BMIM]Cl System. *Industrial & Engineering Chemistry Research,* 55**,** 4473-4481.

Saha, B. & Abu-Omar, M. M. 2014. Advances in 5-hydroxymethylfurfural production from biomass in biphasic solvents. *Green Chemistry,* 16**,** 24-38.

Saini, J. K., Patel, A. K., Adsul, M. & Singhania, R. R. 2016. Cellulase adsorption on lignin: A roadblock for economic hydrolysis of biomass. *Renewable Energy,* 98**,** 29-42.

Salam, Z., Facta, M., Amjad, M. & Buntat, Z. 2013. Design and implementation of a low cost, high yield dielectric barrier discharge ozone generator based on the single switch resonant converter. *IET Power Electronics,* 6**,** 1583-1591.

Saleem, F., Zhang, K. & Harvey, A. P. 2019. Decomposition of benzene as a tar analogue in CO2 and H2 carrier gases, using a non-thermal plasma. *Chemical Engineering Journal,* 360**,** 714-720.

Santiago, B. L. S. & Guirardello, R. 2020. 5-hydroxymethylfurfural Production in a Lignocellulosic Biorefinery: Techno-economic Analysis. *Chemical engineering transactions,* 80**,** 139-144.

Saritha, M., Arora, A. & Lata 2012. Biological Pretreatment of Lignocellulosic Substrates for Enhanced Delignification and Enzymatic Digestibility. *Indian Journal of Microbiology,* 52**,** 122-130.

Satari, B., Karimi, K. & Kumar, R. 2019. Cellulose solvent-based pretreatment for enhanced second-generation biofuel production: a review. *Sustainable Energy & Fuels,* 3**,** 11-62.

Schmidt-Szałowski, K., Borucka, A. & Jodzis, S. 1990. Catalytic activity of silica in ozone formation in electrical discharges. *Plasma Chemistry and Plasma Processing,* 10**,** 443-450.

Schoning, A. G. 1965. Absorptiometric determination of acid-soluble lignin in semichemical bisulfite pulp and in some woods and plants. *Svensk Papperstidn,* 68**,** 607-613.

Schultz-Jensen, N., Kádár, Z., Thomsen, A. B., Bindslev, H. & Leipold, F. 2011a. Plasma-Assisted Pretreatment of Wheat Straw for Ethanol Production. *Applied Biochemistry and Biotechnology,* 165**,** 1010-1023.

Schultz-Jensen, N., Leipold, F., Bindslev, H. & Thomsen, A. B. 2011b. Plasma-assisted pretreatment of wheat straw. *Applied Biochemistry and Biotechnology,* 163**,** 558-572.

Schultz-Jensen, N., Thygesen, A., Leipold, F., Thomsen, S. T., Roslander, C., Lilholt, H. & Bjerre, A. B. 2013. Pretreatment of the macroalgae Chaetomorpha linum for the production of bioethanol - Comparison of five pretreatment technologies. *Bioresource Technology,* 140**,** 36-42.

Seok, D. C., Jeong, H. Y., Jung, Y. H. & Lho, T. 2015. Optimizing Factors on High Concentration of Ozone Production with Dielectric Barrier Discharge. *Ozone: Science & Engineering,* 37**,** 221-226.

Sevilla, M. & Fuertes, A. B. 2009. The production of carbon materials by hydrothermal carbonization of cellulose. *Carbon,* 47**,** 2281-2289.

Shafizadeh, F., Philpot, C. W. & Ostojic, N. 1971. Thermal analysis of 1,6-anhydro-β-D-glucopyranose. *Carbohydrate Research,* 16**,** 279-287.

Shamjuddin, A., Ab Rasid, N. S., Michele Raissa, M. M., Abu Zarin, M. A., Wan Omar, W. N. N., Syahrom, A., Mohd Szali Januddi, M. A. F. & Saidina Amin, N. A. 2021. Kinetic and dynamic analysis of ozonolysis pre-treatment of empty fruit bunch in a well-mixed reactor for sugar production. *Energy Conversion and Management,* 244**,** 114526.

Shao, Y., Long, Y., Zhou, Y., Jin, Z., Zhou, D. & Shen, D. 2019. 5-Hydroxymethylfurfural production from watermelon peel by microwave hydrothermal liquefaction. *Energy,* 174**,** 198-205.

Shen, D. K. & Gu, S. 2009. The mechanism for thermal decomposition of cellulose and its main products. *Bioresource Technology,* 100**,** 6496-6504.

Shen, F., Sun, S., Zhang, X., Yang, J., Qiu, M. & Qi, X. 2020. Mechanochemical-assisted production of 5-hydroxymethylfurfural from high concentration of cellulose. *Cellulose,* 27**,** 3013-3023.

Shi, F., Xiang, H. & Li, Y. 2015. Combined pretreatment using ozonolysis and ball milling to improve enzymatic saccharification of corn straw. *Bioresource Technology,* 179**,** 444-451.

Shi, N., Liu, Q., Zhang, Q., Wang, T. & Ma, L. 2013. High yield production of 5-hydroxymethylfurfural from cellulose by high concentration of sulfates in biphasic system. *Green Chemistry,* 15**,** 1967-1974.

Shui, T., Feng, S., Yuan, Z., Kuboki, T. & Xu, C. 2016. Highly efficient organosolv fractionation of cornstalk into cellulose and lignin in organic acids. *Bioresource Technology,* 218**,** 953-961.

Siemens, W. 1857. Ueber die elektrostatische Induction und die Verzögerung des Stroms in Flaschendrähten. *Annalen der Physik,* 178**,** 66-122.

Sievers, D. A., Tao, L. & Schell, D. J. 2014. Performance and techno-economic assessment of several solid–liquid separation technologies for processing dilute-acid pretreated corn stover. *Bioresource Technology,* 167**,** 291-296.

Silverstein, R. A., Chen, Y., Sharma-Shivappa, R. R., Boyette, M. D. & Osborne, J. 2007. A comparison of chemical pretreatment methods for improving saccharification of cotton stalks. *Bioresource Technology,* 98**,** 3000-3011.

Sixma, F. & Wibaut, J. 2010. The mechanism of the reaction between ozone and aromatic bonds. A reply to G. M. Badger. *Recueil des Travaux Chimiques des Pays-Bas,* 71.

Slak, J., Pomeroy, B., Kostyniuk, A., Grilc, M. & Likozar, B. 2022. A review of bio-refining process intensification in catalytic conversion reactions, separations and purifications of hydroxymethylfurfural (HMF) and furfural. *Chemical Engineering Journal,* 429**,** 132325.

Smil, V. 1999. Nitrogen in crop production: An account of global flows. *Global Biogeochemical Cycles,* 13**,** 647-662.

Souza-Corrêa, J. A., Oliveira, C., Wolf, L. D., Nascimento, V. M., Rocha, G. J. M. & Amorim, J. 2013. Atmospheric pressure plasma pretreatment of sugarcane bagasse: The influence of moisture in the ozonation process. *Applied Biochemistry and Biotechnology,* 171**,** 104-116.

Steinbach, D., Kruse, A., Sauer, J. & Storz, J. 2020. Is Steam Explosion a Promising Pretreatment for Acid Hydrolysis of Lignocellulosic Biomass? *Processes,* 8**,** 1626.

Strassberger, Z., Tanase, S. & Rothenberg, G. 2014. The pros and cons of lignin valorisation in an integrated biorefinery. *RSC Advances,* 4**,** 25310-25318.

Strunk, P. 2012. *Characterization of cellulose pulps and the influence of their properties on the process and production of viscose and cellulose ethers.* Doctoral thesis, comprehensive summary, Umeå Universitet.

Su, Y., Brown, H. M., Huang, X., Zhou, X.-D., Amonette, J. E. & Zhang, Z. C. 2009. Single-step conversion of cellulose to 5-hydroxymethylfurfural (HMF), a versatile platform chemical. *Applied Catalysis A: General,* 361**,** 117-122.

Su, Y., Du, R., Guo, H., Cao, M., Wu, Q., Su, R., Qi, W. & He, Z. 2015. Fractional pretreatment of lignocellulose by alkaline hydrogen peroxide: Characterization of its major components. *Food and Bioproducts Processing,* 94**,** 322-330.

Sugimoto, T., Magara, K., Hosoya, S., Oosawa, S., Shimoda, T. & Nishibori, K. 2009. Ozone pretreatment of lignocellulosic materials for ethanol production: Improvement of enzymatic susceptibility of softwood. *Holzforschung,* 63**,** 537-543.

Sulfahri, Mushlihah, S., Langford, A. & Tassakka, A. C. M. A. R. 2020. Ozonolysis as an Effective Pretreatment Strategy for Bioethanol Production from Marine Algae. *BioEnergy Research,* 13**,** 1269-1279.

Sumerskii, I. V., Krutov, S. M. & Zarubin, M. Y. 2010. Humin-like substances formed under the conditions of industrial hydrolysis of wood. *Russian Journal of Applied Chemistry,* 83**,** 320-327.

Sun, J., Yuan, X., Shen, Y., Yi, Y., Wang, B., Xu, F. & Sun, R. 2015. Conversion of bamboo fiber into 5-hydroxymethylfurfural catalyzed by sulfamic acid with microwave assistance in biphasic system. *Industrial Crops and Products,* 70**,** 266-271.

Sun, R. & Tomkinson, J. 2005. Separation and Characterization of Cellulose from Wheat Straw. *Separation Science and Technology,* 39**,** 391-411.

Taherzadeh, M. J. & Karimi, K. 2008. Pretreatment of Lignocellulosic Wastes to Improve Ethanol and Biogas Production: A Review. *International Journal of Molecular Sciences,* 9**,** 1621-1651.

Takkellapati, S., Li, T. & Gonzalez, M. A. 2018. An overview of biorefinery-derived platform chemicals from a cellulose and hemicellulose biorefinery. *Clean Technologies and Environmental Policy,* 20**,** 1615-1630.

Tao, L., Aden, A., Elander, R. T., Pallapolu, V. R., Lee, Y. Y., Garlock, R. J., Balan, V., Dale, B. E., Kim, Y., Mosier, N. S., Ladisch, M. R., Falls, M., Holtzapple, M. T., Sierra, R., Shi, J., Ebrik, M. A., Redmond, T., Yang, B., Wyman, C. E., Hames, B., Thomas, S. & Warner, R. E. 2011. Process and technoeconomic analysis of leading pretreatment technologies for lignocellulosic ethanol production using switchgrass. *Bioresource Technology,* 102**,** 11105-11114.

Thoma, C., Konnerth, J., Sailer-Kronlachner, W., Solt, P., Rosenau, T. & Van Herwijnen, H. W. G. 2020. Current Situation of the Challenging Scale-Up Development of Hydroxymethylfurfural Production. *ChemSusChem,* 13**,** 3544-3564.

Tilman, D., Hill, J. & Lehman, C. 2006. Carbon-Negative Biofuels from Low-Input High-Diversity Grassland Biomass. *Science,* 314**,** 1598-1600.

Travaini, R., Martín-Juárez, J., Lorenzo-Hernando, A. & Bolado-Rodríguez, S. 2016. Ozonolysis: An advantageous pretreatment for lignocellulosic biomass revisited. *Bioresource Technology,* 199**,** 2-12.

Travaini, R., Otero, M. D. M., Coca, M., Da-Silva, R. & Bolado, S. 2013. Sugarcane bagasse ozonolysis pretreatment: Effect on enzymatic digestibility and inhibitory compound formation. *Bioresource Technology,* 133**,** 332-339.

Tripathi, N., Hills, C. D., Singh, R. S. & Atkinson, C. J. 2019. Biomass waste utilisation in low-carbon products: harnessing a major potential resource. *npj Climate and Atmospheric Science,* 2**,** 35.

Tsilomelekis, G., Orella, M. J., Lin, Z., Cheng, Z., Zheng, W., Nikolakis, V. & Vlachos, D. G. 2016. Molecular structure, morphology and growth mechanisms and rates of 5-hydroxymethyl furfural (HMF) derived humins. *Green Chemistry,* 18**,** 1983-1993.

Tuma, R. S. P. 2003. Maldi-Tof Mass Spectrometry: Getting a Feel for How It Works. *Oncology Times,* 25**,** 26.

Ueda, C., Takashima, Y., Ishiguri, F., Iizuka, K., Yoshizawa, N. & Yokota, S. 2014. Ozone oxidation pretreatment for enzymatic saccharification of spent culture media after Lentinula edodes cultivation. *Journal of Wood Science,* 61**,** 65-69.

Usmani, Z., Sharma, M., Gupta, P., Karpichev, Y., Gathergood, N., Bhat, R. & Gupta, V. K. 2020. Ionic liquid based pretreatment of lignocellulosic biomass for enhanced bioconversion. *Bioresource Technology,* 304**,** 123003.

Van Putten, R.-J., Van Der Waal, J. C., De Jong, E., Rasrendra, C. B., Heeres, H. J. & De Vries, J. G. 2013. Hydroxymethylfurfural, A Versatile Platform Chemical Made from Renewable Resources. *Chemical Reviews,* 113**,** 1499-1597.

Van Zandvoort, I., Wang, Y., Rasrendra, C. B., Van Eck, E. R. H., Bruijnincx, P. C. A., Heeres, H. J. & Weckhuysen, B. M. 2013. Formation, Molecular Structure, and Morphology of Humins in Biomass Conversion: Influence of Feedstock and Processing Conditions. *ChemSusChem,* 6**,** 1745-1758.

Verdía, P., Brandt, A., Hallett, J. P., Ray, M. J. & Welton, T. 2014. Fractionation of lignocellulosic biomass with the ionic liquid 1-butylimidazolium hydrogen sulfate. *Green Chemistry,* 16**,** 1617-1627.

Vidal, P. F. & Molinier, J. 1988a. Ozonolysis of lignin - Improvement of in vitro digestibility of poplar sawdust. *Biomass,* 16**,** 1-17.

Vidal, P. F. & Molinier, J. 1988b. Ozonolysis of lignin — Improvement of in vitro digestibility of poplar sawdust. *Biomass,* 16**,** 1-17.

Wan, J., Lian, J., Wang, Y. & Ma, Y. 2015. Investigation of cellulose supramolecular structure changes during conversion of waste paper in near-critical water on producing 5-hydroxymethyl furfural. *Renewable Energy,* 80**,** 132-139.

Wan Omar, W. N. N. & Amin, N. A. S. 2016. Multi response optimization of oil palm frond pretreatment by ozonolysis. *Industrial Crops and Products,* 85**,** 389-402.

Wang, L., Lei, H. & Ruan, R. 2015a. Techno-Economic Analysis of Microwave-Assisted Pyrolysis for Production of Biofuels. *In:* FANG, Z., SMITH, J. R. L. & QI, X. (eds.) *Production of Biofuels and Chemicals with Microwave.* Dordrecht: Springer Netherlands.

Wang, P., Ren, L., Lu, Q. & Huang, Y. 2016. Dehydration of Glucose to 5-Hydroxymethylfurfural Using Combined Catalysts in Ionic Liquid by Microwave Heating. *Chemical Engineering Communications,* 203**,** 1507-1514.

Wang, S., Gao, W., Xiao, L.-P., Shi, J., Sun, R.-C. & Song, G. 2019. Hydrogenolysis of biorefinery corncob lignin into aromatic phenols over activated carbon-supported nickel. *Sustainable Energy & Fuels,* 3**,** 401-408.

Wang, S., Lin, H., Chen, J., Zhao, Y., Ru, B., Qiu, K. & Zhou, J. 2015b. Conversion of carbohydrates into 5-hydroxymethylfurfural in an advanced single-phase reaction system consisting of water and 1,2-dimethoxyethane. *RSC Advances,* 5**,** 84014-84021.

Wang, T., Li, K., Liu, Q., Zhang, Q., Qiu, S., Long, J., Chen, L., Ma, L. & Zhang, Q. 2014. Aviation fuel synthesis by catalytic conversion of biomass hydrolysate in aqueous phase. *Applied Energy,* 136**,** 775-780.

Wang, W., Ren, J., Li, H., Deng, A. & Sun, R. 2015c. Direct transformation of xylan-type hemicelluloses to furfural via SnCl4 catalysts in aqueous and biphasic systems. *Bioresource Technology,* 183**,** 188-194.

Wang, Y.-H. & Chen, Q.-Y. 2013. Anodic Materials for Electrocatalytic Ozone Generation. *International Journal of Electrochemistry,* 2013**,** 128248.

Wei, L., Deng, Q. & Zhang, Y. 2020. Ozone generation enhanced by silica catalyst in oxygen-fed dielectric barrier discharge. *Vacuum,* 173**,** 109145.

Wei, Z., Li, Y., Thushara, D., Liu, Y. & Ren, Q. 2011. Novel dehydration of carbohydrates to 5-hydroxymethylfurfural catalyzed by Ir and Au chlorides in ionic liquids. *Journal of the Taiwan Institute of Chemical Engineers,* 42**,** 363-370.

Wierschem, M., Skiborowski, M., Górak, A., Schmuhl, R. & Kiss, A. A. 2017. Techno-economic evaluation of an ultrasound-assisted Enzymatic Reactive Distillation process. *Computers & Chemical Engineering,* 105**,** 123-131.

Wildschut, J., Smit, A. T., Reith, J. H. & Huijgen, W. J. J. 2013. Ethanol-based organosolv fractionation of wheat straw for the production of lignin and enzymatically digestible cellulose. *Bioresource Technology,* 135**,** 58-66.

Yan, P., Xia, M., Chen, S., Han, W., Wang, H. & Zhu, W. 2020. Unlocking biomass energy: continuous high-yield production of 5-hydroxymethylfurfural in water. *Green Chemistry,* 22**,** 5274-5284.

Yan, P., Xu, Z., Zhang, C., Liu, X., Xu, W. & Zhang, Z. C. 2015. Fractionation of lignin from eucalyptus bark using amine-sulfonate functionalized ionic liquids. *Green Chemistry,* 17**,** 4913-4920.

Yang, B., Boussaid, A., Mansfield, S. D., Gregg, D. J. & Saddler, J. N. 2002. Fast and efficient alkaline peroxide treatment to enhance the enzymatic digestibility of steam-exploded softwood substrates. *Biotechnology and Bioengineering,* 77**,** 678-684.

Yang, T., Zhou, Y. H., Zhu, S. Z., Pan, H. & Huang, Y. B. 2017. Insight into Aluminum Sulfate-Catalyzed Xylan Conversion into Furfural in a Γ-Valerolactone/Water Biphasic Solvent under Microwave Conditions. *ChemSusChem,* 10**,** 4066-4079.

Yang, Y., Hayashi, Y., Fujii, Y., Nagano, T., Kita, Y., Ohshima, T., Okuda, J. & Mashima, K. 2012. Efficient cyclic carbonate synthesis catalyzed by zinc cluster systems under mild conditions. *Catalysis Science and Technology,* 2**,** 509-513.

Yin, S., Pan, Y. & Tan, Z. 2011. Hydrothermal conversion of cellulose to 5-hydroxymethyl furfural. *International Journal of Green Energy,* 8**,** 234-247.

Yu, I. K. M. & Tsang, D. C. W. 2017. Conversion of biomass to hydroxymethylfurfural: A review of catalytic systems and underlying mechanisms. *Bioresource Technology,* 238**,** 716-732.

Yu, I. K. M., Tsang, D. C. W., Yip, A. C. K., Chen, S. S., Wang, L., Ok, Y. S. & Poon, C. S. 2017. Catalytic valorization of starch-rich food waste into hydroxymethylfurfural

(HMF): Controlling relative kinetics for high productivity. *Bioresource Technology,* 237**,** 222-230.

Yu, Z., Jameel, H., Chang, H. M. & Park, S. 2011. The effect of delignification of forest biomass on enzymatic hydrolysis. *Bioresource Technology,* 102**,** 9083-9089.

Yuan, T.-Q., Xu, F. & Sun, R.-C. 2013. Role of lignin in a biorefinery: separation characterization and valorization. *Journal of Chemical Technology & Biotechnology,* 88**,** 346-352.

Yulianto, E., Restiwijaya, M., Sasmita, E., Arianto, F., Kinandana, A. W. & Nur, M. 2019. Power analysis of ozone generator for high capacity production. *Journal of Physics: Conference Series,* 1170**,** 012013.

Zang, G., Shah, A. & Wan, C. 2020. Techno-economic analysis of an integrated biorefinery strategy based on one-pot biomass fractionation and furfural production. *Journal of Cleaner Production,* 260**,** 120837.

Zhang, K., Pei, Z. & Wang, D. 2016a. Organic solvent pretreatment of lignocellulosic biomass for biofuels and biochemicals: A review. *Bioresource Technology,* 199**,** 21-33.

Zhang, L., Xi, G., Chen, Z., Qi, Z. & Wang, X. 2017a. Enhanced formation of 5-HMF from glucose using a highly selective and stable SAPO-34 catalyst. *Chemical Engineering Journal,* 307**,** 877-883.

Zhang, L., Xi, G., Zhang, J., Yu, H. & Wang, X. 2017b. Efficient catalytic system for the direct transformation of lignocellulosic biomass to furfural and 5-hydroxymethylfurfural. *Bioresource Technology,* 224**,** 656-661.

Zhang, Q., Benoit, M., De Oliveira Vigier, K., Barrault, J., Jégou, G., Philippe, M. & Jérôme, F. 2013a. Pretreatment of microcrystalline cellulose by ultrasounds: effect of particle size in the heterogeneously-catalyzed hydrolysis of cellulose to glucose. *Green Chemistry,* 15**,** 963-969.

Zhang, T., Kumar, R. & Wyman, C. E. 2013b. Enhanced yields of furfural and other products by simultaneous solvent extraction during thermochemical treatment of cellulosic biomass. *RSC Advances,* 3**,** 9809-9819.

Zhang, Y.-R., Li, N., Li, M.-F. & Fan, Y.-M. 2016b. Highly efficient conversion of microcrystalline cellulose to 5-hydroxymethyl furfural in a homogeneous reaction system. *RSC Advances,* 6**,** 21347-21351.

Zhao, H., Holladay, J. E., Brown, H. & Zhang, Z. C. 2007. Metal Chlorides in Ionic Liquid Solvents Convert Sugars to 5-Hydroxymethylfurfural. *Science,* 316**,** 1597-1600.

Zheng, Y., Yanful, E. K. & Bassi, A. S. 2005. A Review of Plastic Waste Biodegradation. *Critical Reviews in Biotechnology,* 25**,** 243-250.

Zheng, Y., Zhao, J., Xu, F. & Li, Y. 2014. Pretreatment of lignocellulosic biomass for enhanced biogas production. *Progress in Energy and Combustion Science,* 42**,** 35-53.

Zhou, C., Zhao, J., Yagoub, A. E. A., Ma, H., Yu, X., Hu, J., Bao, X. & Liu, S. 2017. Conversion of glucose into 5-hydroxymethylfurfural in different solvents and catalysts: Reaction kinetics and mechanism. *Egyptian Journal of Petroleum,* 26**,** 477-487.

Zhou, L., Liang, R., Ma, Z., Wu, T. & Wu, Y. 2013. Conversion of cellulose to HMF in ionic liquid catalyzed by bifunctional ionic liquids. *Bioresource Technology,* 129**,** 450-455.

Zhu, S., Wu, Y., Yu, Z., Liao, J. & Zhang, Y. 2005. Pretreatment by microwave/alkali of rice straw and its enzymic hydrolysis. *Process Biochemistry,* 40**,** 3082-3086.

Zhu, W., Zhu, J. Y., Gleisner, R. & Pan, X. J. 2010. On energy consumption for size-reduction and yields from subsequent enzymatic saccharification of pretreated lodgepole pine. *Bioresource Technology,* 101**,** 2782-2792.